Investigation of the *in vivo* Lysosomal Proteome Changes in Different Starvation Periods

Dissertation

zur

Erlangung des Doktorgrades (Dr. rer. nat.)

der

Mathematisch-Naturwissenschaftlichen Fakultät

der

Rheinischen Friedrich-Wilhelms-Universität Bonn

vorgelegt von

Edgar Kaade

aus

Aleppo, Syrien

Bonn, 2021

Angefertigt mit Genehmigung der Mathematisch-Naturwissenschaftlichen
Fakultät der Rheinischen Friedrich-Wilhelms-Universität Bonn

1. Gutachter: Prof. Dr. Volkmar Gieselmann

2. Gutachter: Prof. Dr. Walter Witke

Tag der Promotion: 30.03.2021

Erscheinungsjahr: 2021

Table of Contents

Abbreviations

°C	degree celsius
µl	microliter
µm	micrometer
2-AAA	2-aminoadipic acid
2-ABA	2-aminobutyric acid
4E-BP	eukaryotic translation initiation factor 4E-binding protein
AA	amino acid
AC	acylcarnitine
ACN	acetonitrile
AGC	automatic gain control
ALR	autophagic lysosome reformation
APS	ammonium persulfate
ATF4	activating transcription factor 4
ATG	autophagy-related protein
ATP	adenosine triphosphate
BCAA	branched-chain amino acid
Beta-HB	beta-hydroxybutyrate
BORC	BLOC-1-related complex
BSA	bovine serum albumin
CACT	carnitine acylcarnitine translocase
cDNA	complementary DNA
CID	collision induced dissociation
cm	centimeter
Comm	copper metabolism gene MURR1
Conc.	concentration
CPT	carnitine O-palmitoyltransferase
cRAP	common repository adventitious proteins
Ct	cycle threshold
C-terminal	carboxy-terminal
ctrl.	control
Da	dalton
DB	digestion buffer
DC	detergent compatible
DEPTOR	DEP-domain-containing mTOR-interacting protein
Dim	dimension
DMSO	dimethyl sulfoxide
DNA	deoxyribonucleic acid
dNTPs	deoxynucleoside triphosphates
DPBS	dulbecco’s phosphate-buffered saline
dsDNA	double stranded DNA
dT	deoxythymine
DTT	dithiothreitol
ECL	enhanced chemiluminescence
EDTA	ethylenediaminetetraacetic acid
eIF4E	eukaryotic translation initiation factor 4E

ESI	electrospray ionization
FA	formic acid
FASP	filter aided sample preparation
FCS	fetal calf serum
FDR	false discovery rate
FFA	free fatty acid
FIP200	FAK family kinase-interacting protein of 200 kDa
Fnip	folliculin-interacting protein
for	forward
g	gram
GAP	GTPase activating protein
GAPDH	glyceraldehyde-3-phosphate dehydrogenase
GATOR	GAP activity towards the Rags
GDP	guanosine diphosphate
GEF	guanine nucleotide exchange factor
GLUT	glucose transporter
GO	gene ontology
GOI	gene of interest
GTP	guanosine triphosphate
GYS2	glycogen synthase
h	hours
HCD	higher-energy collisional dissociation
HLB	hydrophilic-lipophilic balance
HMGCS2	3-hydroxymethylglutaryl-CoA synthase
HPLC	high pressure liquid chromatography
HRP	horseradish peroxidase
IgG (H+L)	immunoglobulin G (heavy + light chains)
IP	intraperitoneal
IS	internal standard
iTRAQ	isobaric tags for relative and absolute quantification
kDa	kilodalton
KEGG	kyoto encyclopedia of genes and genomes
KO	knockout
KOR	South Korea
l	liter
LAMP	lysosome-associated membrane glycoprotein
LAMTOR	Late endosomal/lysosomal adaptor and MAPK and MTOR activator
LC	liquid chromatography
LC3	microtubule associated proteins 1A/1B light chain 3
LC-MS/MS	liquid chromatography-tandem mass spectrometry
log10	logarithm with base 10
log2	binary logarithm
LONP2	lon protease homolog 2
LTQ	linear trap quadrupole
LYNUS	lysosomal nutrient sensing machinery
LysoIP	lysosome immunoprecipitation
M	molar (mol/l)

M/L	mitochondria/lysosomes layer
m/z	mass-to-charge
mA	milliamper
MALDI	matrix assisted laser desorption/ionization
min	minutes
ml	milliliter
mLST8	mammalian lethal with Sec13 protein 8
mM	millimolar (mmol/l)
mRNA	messenger ribonucleic acid
ms	millisecond
MS	mass spectrometry
MS1	precursor ion analysis
MS2	reporter ion analysis
MS3	reporter ion quantification
MTHFD2	methylenetetrahydrofolate dehydrogenase 2
mTORC1	mechanistic target of rapamycin complex 1
N/A	not available
n.s.	not significant
NC	nitrocellulose
NDUFB	NADH dehydrogenase [ubiquinone] 1 beta subcomplex
NEAA	non-essential amino acid
nmol	nanomole
NPRL2	nitrogen permease regulator 2-like protein
N-terminal	amino-terminal
NUDT12	NADH pyrophosphatase
PBS	phosphate-buffered saline
PCA	principal component analysis
PCK1	phosphoenolpyruvate carboxykinase
PCR	polymerase chain reaction
PD	proteome discoverer
pH	power of hydrogen
phospho	phosphorylation
pI	isoelectric point
PNS	post-nuclear supernatant
PPARα	proliferator-activated receptor alpha
ppm	parts per million
PRAS40	proline-rich AKT substrate 40 kDa
PSMA	proteasome subunit alpha
PSMB	proteasome subunit beta
PSMs	peptide spectrum matches
PVDF	polyvinylidene fluoride
PYGL	glycogen phosphorylase
qPCR	quantitative real-time polymerase chain reaction
Rag	ras-related GTP-binding protein
Raptor	regulatory-associated protein of mTOR
Rep	replicate
rev	reverse
Rheb	ras homolog enriched in brain

RNA	ribonucleic acid
RT	room temperature
S240/244	serine at amino acid position 240, 244
S6	40S ribosomal protein S6
S6K	p70 S6 kinase
SDC	sodium deoxycholate
SDS	sodium dodecyl sulfate
SDS-PAGE	sodium dodecyl sulfate polyacrylamide gel electrophoresis
sec	seconds
SEM	standard error of the mean
SILAC	stable isotope labeling by/with amino acids in cell culture
SLC38A9	sodium-coupled neutral amino acid transporter 9
SNARE	soluble *N*-ethylmaleimide-sensitive factor-attachment protein receptor
SPE	solid phase extraction
SPIONs	superparamagnetic iron oxide nanoparticles
SREBP	sterol regulatory element binding protein
StageTips	stop-and-go-extraction tips
T37/46	threonine at amino acid position 37, 46
TBC1D7	TBC1 domain family member 7
TBS	tris-buffered saline
TCA	tricarboxylic acid cycle
TEAB	triethylammonium bicarbonate
TEMED	N,N,N’,N’-Tetramethyl ethylenediamine
TFA	trifluoroacetic acid
TFEB	transcription factor EB
TMT	tandem mass tag
TPP1	tripeptidyl-peptidase 1
Tris	tris(hydroxymethyl)aminomethane
TSC	tuberous sclerosis complex
U	unit
UK	United Kingdom
ULK1	unc-51 like autophagy activating kinase 1
USA	United States of America
V	volt
v/v	volume per volume
VDAC	voltage-dependent anion-selective channel protein
VPS	vacuolar protein sorting-associated protein
VSN	variance stabilizing normalization
w/v	weight per volume
WASH	Wiskott-Aldrich syndrome protein and scar homolog
WB	western blot
wt	wild-type
x g	earth’s gravitational acceleration
µg	microgram
ρ	density

Abstract

Nutrient deprivation is a type of stress that can change the stability, activity and subcellular localization of a protein. The cellular response to starvation includes lysosomal response mechanisms composed of the autophagy/lysosomal degradation pathway and the nutrient signaling pathway via the mechanistic target of rapamycin complex 1 (mTORC1) as the regulator of cell growth. The current study investigates the impact of *in vivo* starvation on the lysosomal proteome and on cellular metabolism. Before analyzing the lysosomal proteome, the activity of mTORC1 was defined at various time periods. The protein complex displayed different activity patterns in three key mouse metabolic organs. It was deactivated/reactivated after short/prolonged starvation periods, respectively, in the liver, gradually deactivated in the skeletal muscle, and continuously activated in the brain.

In the second part of this study, the two selected starvation periods with distinct molecular effects in the liver had different impacts on the body metabolism after measuring the levels of essential metabolites in blood serum. Glucose levels were stable at 6 hours of starvation, while the ketogenesis started to occur as shown by a 2.04-fold increase in beta-hydroxybutyrate (β-HB) concentrations. Furthermore, the 2.1-fold decrease in glucose levels after 24 hours of starvation was accompanied by a significant increase in β-HB and in the relative expression of ketogenesis-related genes as examined by enzyme assay and real-time PCR, respectively. Besides ketogenesis, the levels of long-, but not short-, chain acylcarnitines significantly increased after prolonged starvation as a marker of potential fatty acid beta-oxidation. In addition, the increased levels of muscle protein breakdown biomarkers indicated an activation of gluconeogenesis. These results suggest alternative energy sources during starvation.

The last part of the thesis focused on the analysis of starvation-induced changes in liver lysosomal/non-lysosomal protein amounts by large-scale quantitative mass spectrometry of enriched lysosomes using tandem mass tag (TMT) labeling approach. The proteomic analysis quantified 1725 proteins. From 233 quantified lysosomal proteins, 4 out of 11 and 8 out of 17 downregulated proteins after 6

and 24 hours, respectively, were linked to the mTOR signaling pathway. Western blot analysis of the lysosomal fractions depicted a decreased abundance of mTORC1 and Rag complex after short starvation and an increase after 24 hours of starvation, while a continuous decrease in LAMTOR complex levels was monitored after short and prolonged starvation, suggesting a Ragulator-independent mTORC1 reactivation. However, the specific activator is not yet defined. Moreover, 162 and 283 differentially regulated non-lysosomal proteins were quantified after 6 and 24 hours of starvation, respectively. The selected non-lysosomal proteins for further validation included biomarkers of glycogen metabolism and gluconeogenesis. In addition, the data depicted a persistent decreased levels of the endosomal WASH complex in the lysosomal fraction during starvation. Moreover, the results showed a significant upregulation in 12 proteasome subunits after 6 and 24 hours of starvation indicating a continuously induced proteaphagy. In contrast, starvation-induced autophagy displayed a significant upregulation of 12 peroxisomal proteins and 54 mitochondrial proteins after short and prolonged starvation, respectively, hypothesizing an early pexophagy and a late mitophagy, and therefore an ordered organelle degradation. This thesis provides a thorough analysis and insights into the lysosomal proteome changes in mouse liver during different starvation periods and the associated cellular metabolic alterations.

1 Introduction

1.1 Metabolism

The human body consists of about 37 trillion cells (Bianconi et al. 2013) that are classified into more than 200 types of tissues forming the different organs. These cells need to use energy to function, survive and reproduce (Eknoyan 1999). This energy is the result of a variety of biochemical reactions involved in anabolic and catabolic processes (DeBerardinis and Thompson 2012). The breakdown and synthesis of large macromolecules like proteins, lipids and carbohydrates are critical mechanisms that regulate energy metabolism throughout the whole body and coordinate the metabolic interactions among the organs to reach a fuel homeostasis (Curi et al. 2016). Brain, liver, heart and skeletal muscle oxidize most of the metabolites, mainly glucose, lactate and fatty acids consuming more than 70 % of the body's total oxygen (Hall 2006; Kim et al. 2007). These metabolites are the product of a large number of metabolic pathways mainly glycolysis, acetyl-CoA oxidation, fatty acid β-oxidation, oxidative phosphorylation, urea cycle and gluconeogenesis (Schultz 2005). The consumption of specific metabolites for energy production may differ depending on the body's physiological state. At rest, during normal activities or endurance training, lipids are the major source of energy. Under intense exercise, the main fuel source shifts to carbohydrates, which provide more than two thirds of the required energy (Melzer 2011). In the case of prolonged starvation, fatty acids and ketone bodies become the primary source to spare the body's remaining glucose supply (Watford 2015). In addition, while the contributions of lipids and carbohydrates to energy metabolism are relatively high compared to proteins, specific amino acids such as glutamine are crucial for both glucose synthesis and the nitrogen transport in the liver (Stumvoll et al. 1999; Chaudhry et al. 2002).

1.1.1 Metabolic profile of key organ systems

The metabolic characteristics of each organ are related to its function and biochemical reactions (Figure 1.1) (Cahill 2006). Briefly, liver and adipose tissue store nutrients that are digested and taken up into the blood stream via the

intestines. Glucose produced in the liver will be distributed to other body organs and will be mainly consumed by the brain under rest conditions. During starvation, amino acid breakdown in the skeletal muscle provides most of the metabolites needed for gluconeogenesis. In parallel, the renal back filtration system avoids energy loss due to the reabsorption of soluble metabolites (Alberts et al. 2002).

As a major producer of ~ 95 % of blood glucose, the liver acts as a central hub for regulating metabolic homeostasis by the short storage of carbohydrates and the supply of glucose to several body organs such as the brain and also red blood cells (Han et al. 2016). Glucose production and its concentration in the blood is regulated by gluconeogenesis and glycogenolysis, where most of the glycolysis metabolites like lactate and pyruvate and half of the glycerol produced by lipolysis are taken up by the liver and used as precursors for glucose synthesis (Jelen et al. 2011; Sharabi et al. 2015; von Morze et al. 2017). The liver depends on the oxidation of free fatty acids (FFAs) for energy metabolism. The uptake of FFA increases during prolonged starvation and leads to the production of the ketone bodies acetoacetate, beta-hydroxybutyrate (most abundant) and acetone (least abundant) (Laffel 1999), which are used as an alternative energy source (Figure 1.1).

Even though adipose tissue is a massive triacylglycerol fuel storage, its major metabolic energy is supplied by glucose. Adipose tissue is not only known to be a fat reservoir for the body, but it is also a dynamic organ, which can regulate several homeostatic reactions. During periods of starvation, adipose tissue releases FFA through lipolysis to supply energy to other organs such as the liver and skeletal muscle (Coelho et al. 2013).

In the brain, more than half of the produced blood glucose, which is considered to be the primary source of energy metabolism under normal nutrient circumstances, is consumed (Figure 1.1). The cerebral glucose level remains stable due to the constant supply mediated by the glucose transporter type 3 (GLUT3) (Simpson et al. 2008). To adapt to nutrient deprivation, ketone bodies partially replace glucose as a fuel source, as fatty acids are not able to cross the blood-brain barrier and thus cannot serve as an energy source for the brain (Puchalska and Crawford 2017).

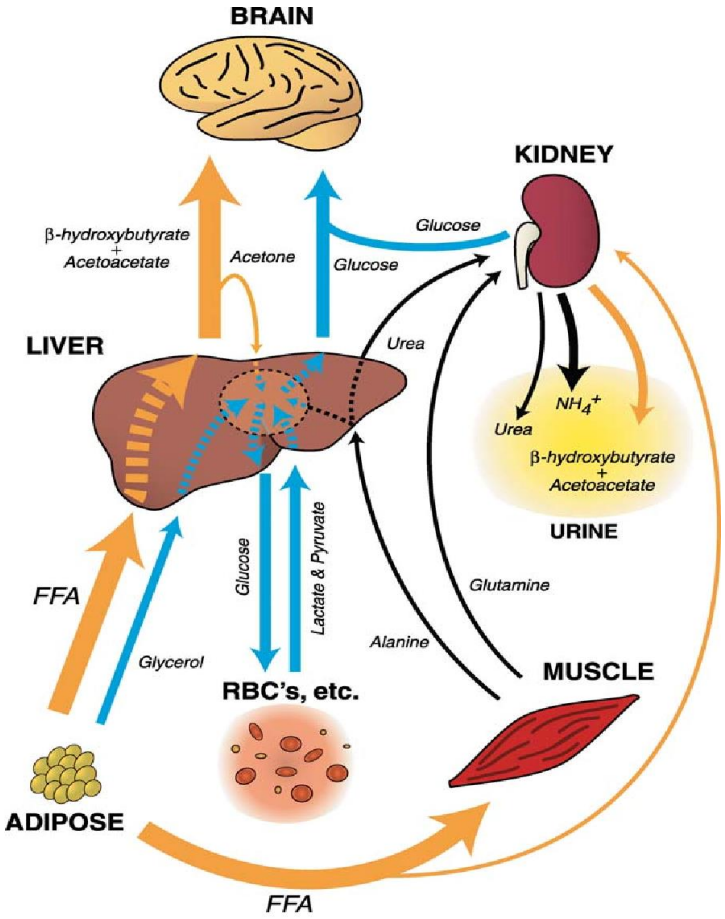

Figure 1.1: Starvation fuel metabolism
Schematic view of the main metabolic organs and their chemical reactions during starvation (Cahill 2006).

The skeletal muscle uses FFA at rest for its energy metabolism, which covers most of its energy needs. During exercise and starvation, alanine and glutamine represent more than half of the amino acids released by the skeletal muscle, with alanine being taken up by the liver and used as a substrate for gluconeogenesis (Felig 1973).

The kidney's main function is to produce urine as a way to secrete any remains created by metabolic reactions. After several filtration cycles, various water soluble ions and molecules such as glucose are reabsorbed to avoid energy loss and to supply the brain with metabolic fuel (Figure 1.1). As a response to starvation, the kidney increases the metabolism of glutamine, resulting in the production of ammonium ions, and the remaining glutamine carbon is used in the gluconeogenesis pathway (Goodman et al. 1966). Renal reabsorption of ketone

bodies is also increased, retaining a high concentration of circulating ketone bodies (Sapir and Owen 1975).

1.1.2 Cellular metabolism (Beta-oxidation and ketogenesis)

All metabolites produced and consumed by key metabolic organs are the products of cellular biochemical processes that are highly influenced by the amount and sort of food intake (Woods and Ramsay 2011). After the mechanical and chemical breakdown of nutrients within the digestive system, the absorbed molecules by the cell are either transported into the cytosol and take part in some biochemical pathways for example glycolysis, fatty acid biosynthesis and gluconeogenesis (Berg et al. 2003), or to the mitochondria where other reactions such as fatty acid β-oxidation, ketogenesis and branched-chain amino acid (BCAA) catabolism occur completely or partially (Demine et al. 2014).

Mitochondrial fatty acid (FA) β-oxidation is a major catabolic mechanism that provides ATP to the body's organs and guarantees a continuous energy supply (Houten and Wanders 2010). It begins with converting FAs to acyl-CoA esters through the acyl-CoA synthase (Figure 1.2) (Xiong 2018). This conversion facilitates the transport of FAs from the cytosol into the mitochondria, which is mediated by the carnitine acylcarnitine translocase system also known as the carnitine shuttle (Foster 2004). Carnitine palmitoyltransferase 1 (CPT1), mainly known by its liver isoform CPT1a, is localized in the outer mitochondrial membrane and converts acyl-CoA esters into acylcarnitines (Ramsay et al. 2001). After reaching the mitochondria via the inner membrane transporter carnitine acylcarnitine translocase (CACT), the CPT2 enzyme converts acylcarnitines back to their former CoA esters (Bonnefont et al. 2004) (Figure 1.2). Peroxisome proliferator-activated receptor alpha (PPARα) plays an essential role as a regulator of the acylcarnitine metabolism, especially in response to starvation (van Vlies et al. 2007). The carnitine shuttle is used to transfer long-chain fatty acids (> C8), while short-chain fatty acids are carnitine-independent (Schönfeld and Wojtczak 2016). In the mitochondria, the process of dehydrogenation, hydration, oxidation and thiolysis results in the production of a two carbons shorter acyl-CoA ester (Bartlett and Eaton 2004).

Formed acetyl-CoA can either enter the tricarboxylic acid cycle (TCA) or be involved in starvation-related metabolic pathways such as mitochondrial ketogenesis via 3-hydroxymethylglutaryl-CoA synthase (HMGCS2) (Figure 1.2) (Nicholson et al. 1999). The catalyzed acetyl-CoA generates HMG-CoA that is cleaved and produces acetyl-CoA and acetoacetate (first ketone body). Acetoacetate, in turn, is later reduced to beta-hydroxybutyrate (second ketone body) and also decarboxylated to acetone (third ketone body) (Dedkova and Blatter 2014). The generated ketone bodies are ready to be transported outside the liver to supply energy to other tissues within the body.

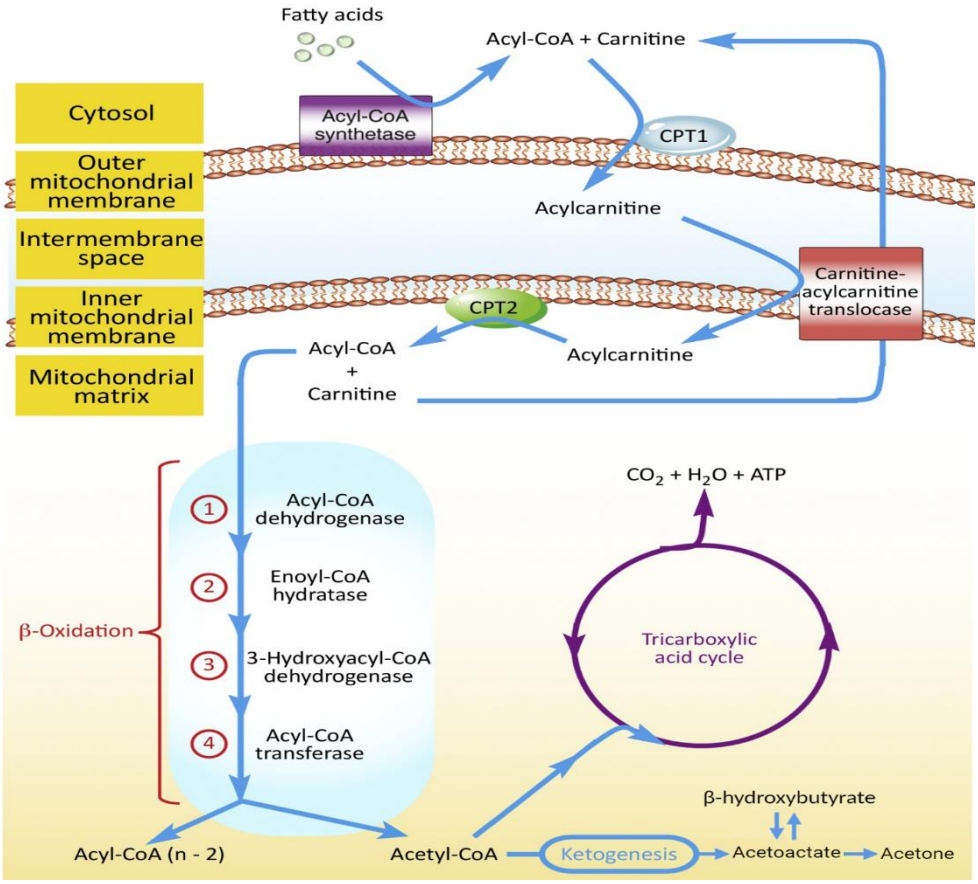

Figure 1.2: Metabolic roles of acyl-CoA
Schematic presentation of fatty acid transport through carnitine shuttle system, and acyl-CoA function in energy production or ketone body formation via fatty acid beta-oxidation, adapted from Xiong (Xiong 2018).

Beta-oxidation and ketogenesis are part of several important mitochondrial-controlled biochemical processes for the production of cellular energy. In addition, mitochondria can connect with other cellular organelles such as lysosomes, to coordinate their metabolic functions by setting the transfer of

metabolites through their contact sites (Todkar et al. 2017; Wong et al. 2019). As a mitochondrial-interacting organelle, lysosome degradation and nutrient signaling pathways play an important role in mitochondrial energy production.

1.2 Lysosomes

Lysosomes were first discovered and described by Christian de Duve as the main degradative organelles of eukaryotic cells (de Duve et al. 1955). These membrane-bound organelles, which are in average 0.1-2 µm in diameter (Novikoff et al. 1956), are enclosed by a lipid-bilayer and have an acidic lumen (pH 4.5-5). The acidification, which is regulated by a vacuolar H^+-ATPase that pumps protons into the lumen (Finbow and Harrison 1997), maintains a high activity of at least 60 different soluble lysosomal hydrolases (Lübke et al. 2009) that are involved in the breakdown of polysaccharides, proteins, lipids and other macromolecules (Luzio et al. 2007). Deficiencies in the lysosomal enzymes can lead to numerous lysosomal storage diseases (Ballabio and Gieselmann 2009). More than 100 highly glycosylated membrane proteins are directly involved in lysosomal functions by maintaining the lysosomal membrane integrity, regulating the transport of metabolites across the lysosomal membrane as well as modulating lysosomal motility and fusion capability (Saftig 2005; Huynh et al. 2007; Ruivo et al. 2009; Schwake et al. 2013). Along with lysosomal membrane proteins, lipids protect the integrity of the membrane to prevent the release of hydrolases into the cytosol, which may lead to lysosomal-dependent cell death (Wang et al. 2018). Lysosomes are also involved in biological and physiological functions such as plasma membrane repair (Pu et al. 2016), production of inflammatory cytokines (Ge et al. 2015) and osteoclastogenesis (Erkhembaatar et al. 2017).

1.2.1 Lysosomal adaptation in response to nutrient status

Lysosomes are dynamic organelles, which can adapt to alterations in nutrient availability via changes in their size, number, enzyme activity and positioning (Reviewed by Settembre and Ballabio 2014). Apart from the lysosomal luminal enzymes, the solute transporters and the motility proteins, the lysosome has a

set of membrane-associated complexes that can respond to the changes in nutrient status, primarily via the master regulator of cell growth and metabolism, the mechanistic target of rapamycin (mTOR) as part of mTOR complex 1 (mTORC1) (Sancak et al. 2010). In addition to the 289-kDa serine/threonine protein kinase, the signaling complex consists of four components: the regulatory-associated protein of mTOR (RAPTOR); the proline-rich AKT substrate 40 kDa (PRAS40); the DEP-domain-containing mTOR-interacting protein (DEPTOR); and the mammalian lethal with Sec13 protein 8 (mLST8) (Sengupta et al. 2010b) as shown in figure 1.3. Moreover, mTOR is a catalytic subunit of a distinct mTORC2 complex (Reviewed by Liu and Sabatini 2020).

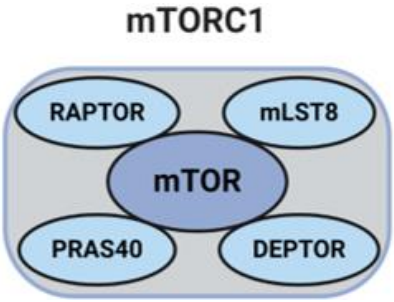

Figure 1.3: Components of the mTORC1 complex
Cartoon illustrating the structure of mTORC1 complex. mTORC1 is composed of five know protein components: mTOR, RAPTOR, mLST8, PRAS40 and DEPTOR.

In the presence of nutrients, mTORC1 is localized on the lysosomal surface and can sense the availability of the nutrient components like amino acids. During starvation, the inactive complex dissociates into the cytosol as part of a well-known adaptive mechanism to nutrient deprivation (Kim et al. 2013). Inactivation of mTORC1 enables autophagy initiation and nuclear translocation of the transcription factor EB (TFEB) to activate lysosomal biogenesis (Settembre et al. 2012; Roczniak-Ferguson et al. 2012). Lysosomes are relocated in order to fuse with the newly formed autophagosomes. This process is mediated by several autophagy-related (ATG) proteins such as phosphatidylethanolamine-conjugated LC3-II, which is associated with the inner and outer membrane of the autophagosome throughout the autophagy process (Korolchuk and Rubinsztein 2011; Ktistakis and Tooze 2016; Nguyen et al. 2016). Higher acidification in the lysosomal lumen leads to an increase in the degradation of macromolecules and the cytosolic release of amino acids to enable the reactivation of mTORC1 after

a prolonged starvation (Yu et al. 2010). The number of lysosomes is finally adapted via lysosomal biogenesis and autophagic lysosome reformation (ALR) (Shen and Mizushima 2014).

1.2.2 The molecular mechanisms of nutrient signaling at the lysosome

Lysosomes play a crucial role as a cellular signaling hub, regulating different metabolic pathways like cell growth (Sancak et al. 2008). In nutrient-rich conditions, mTORC1 activation and lysosomal positioning are controlled by several proteins mainly the arginine-regulated transporter SLC38A9 (Wang et al. 2015) and the lysosomal nutrient sensing machinery (LYNUS), consisting of vacuolar H^+-ATPase, Rag GTPases, Rag GAPs and Ragulator complex (Settembre et al. 2013; Wolfson and Sabatini 2017) (Figure 1.4).

SLC38A9, a positive regulator of mTORC1, senses the arginine in the lysosome and activates the Ragulator complex. The active pentameric complex consisting of LAMTOR1-5 functions as guanine nucleotide exchange factor (GEF) for Rag GTPases heterodimers converting them into their active forms with GTP bound-RagA/B and GDP bound-RagC/D (Sancak et al. 2010; Bar-Peled et al. 2012). Active Rags then recruit and bind mTORC1 at the lysosomal surface (Figure 1.4). Another essential activator of mTORC1 is the small GTPase Rheb, ras homolog enriched in brain, which directly activates it through a strong interaction (Saito et al. 2005; Buerger et al. 2006). This interaction is negatively regulated by the tuberous sclerosis complex (TSC) consisting of TSC1, TSC2 and TBC1 domain family member 7 (TBC1D7) (Dibble et al. 2012). TSC's strong GTPase activating protein (GAP) can convert Rheb into its GDP-bound inactive form and thus inhibits it. As regulators of Rag GTPases, Folliculin and its bound proteins FNIP1/2 have a GAP activity against RagC/D (Tsun et al. 2013). At the same time, the GAP activity towards the Rags 1 complex (GATOR1) consisting of DEPDC5, NPRL2 and NPRL3, as well as its partner GATOR2 complex consisting of WDR59, WDR24, MIOS, SEH1L and SEC13 can regulate RagA/B by their GAP activity (Bar-Peled et al. 2013).

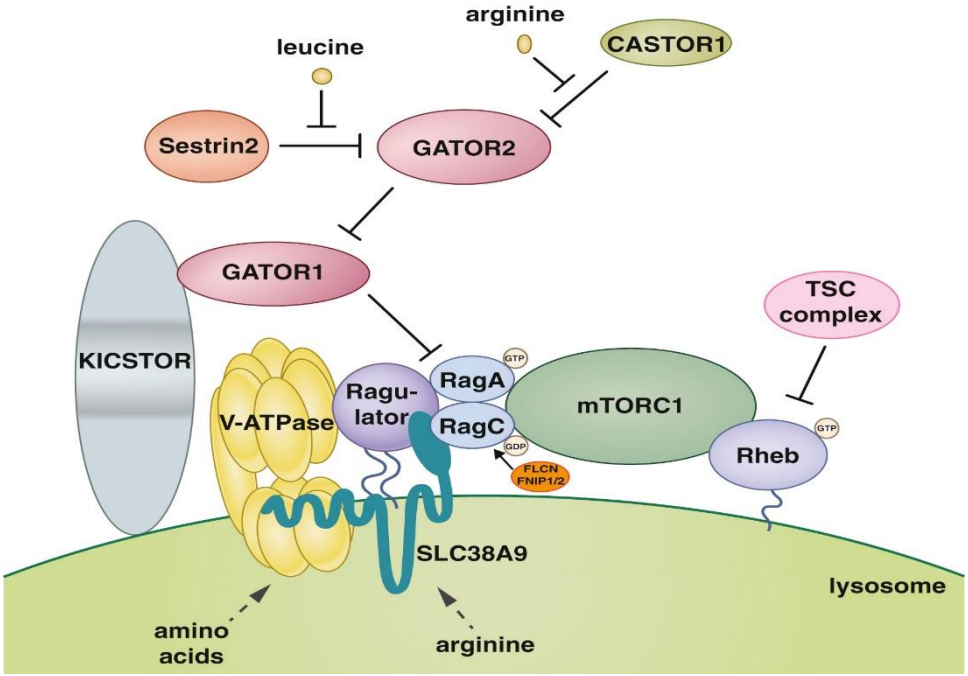

Figure 1.4: mTORC1 upstream nutrient signaling pathway
Schematic describing the nutrient sensing pathway upstream of mTORC1 and its key molecular components (Wolfson and Sabatini 2017).

GATOR1 and GATOR2 have recently being identified to be recruited to the lysosomal surface by the KICSTOR complex which is composed of KPTN, ITFG2, C12orf66 and SZT2 (Figure 1.4). The vacuolar H^+-ATPase pump is suggested to sense the amino acids in the lysosome and send a signal to Rag GTPases via the Ragulator complex (Figure 1.4) (Zoncu et al. 2011).

1.2.3 Downstream targets and functions of lysosomal mTORC1

Several anabolic and catabolic reactions need to be regulated for normal cell growth and division (Kuo et al. 1992). When nutrient and energy are abundant, activated mTORC1 triggers a variety of cellular processes such as protein, lipid and nucleotide synthesis, along with suppressing autophagy and thus lysosome biogenesis by phosphorylation of distinct substrates (Figure 1.5) (Reviewed by Liu and Sabatini 2020).

mTORC1 stimulates protein synthesis by phosphorylating p70S6 Kinase 1 (S6K1) and eIF4E Binding Protein 1 (4EBP1) (Figure 1.5). Direct phosphorylation of S6K1 promotes mRNA translation initiation and leads to the activation of several substrates. S6K1 phosphorylates the S6 protein, a ribosomal 40S subunit that is claimed to be involved in the transcription of ribosomal genes (Chauvin et

al. 2014). 4EBP1 inhibits translation by binding the eukaryotic translation initiation factor 4E (eIF4E) and thus prevents the assembly of eIF4F complex. mTORC1 phosphorylates 4EBP1 and dissociates it from eIF4E and allows a 5′ cap-dependent mRNA translation (Pause et al. 1994; Brunn et al. 1997; Hara et al. 1997; Gingras et al. 1999).

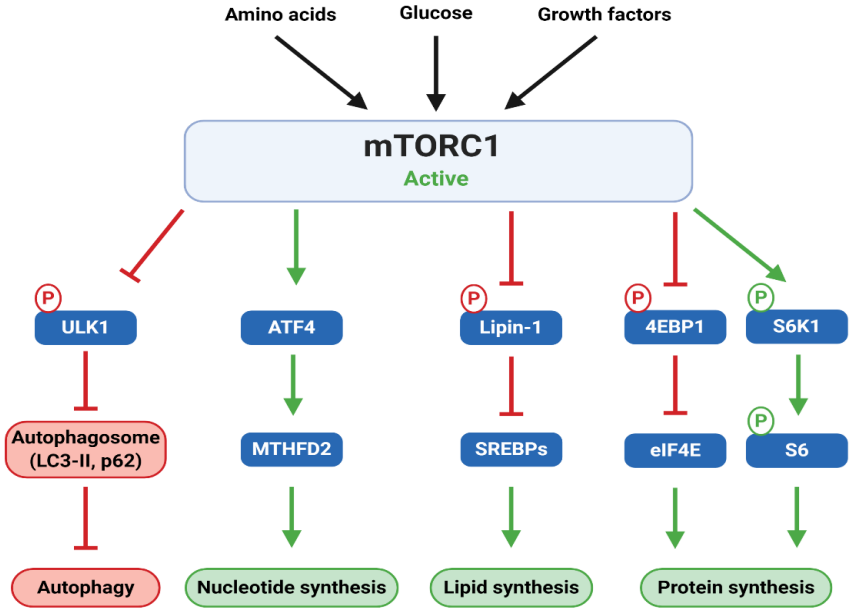

Figure 1.5: mTORC1 downstream signaling targets
Schematic representation of mTORC1 activation and the initiation of anabolic processes that stimulate the production of proteins, lipids and nucleotides as well as the inhibition of catabolic programs such as autophagy.

For a balanced cell membrane expansion, mTORC1 promotes lipid synthesis through the transcription factors sterol regulatory element binding protein 1/2 (SREBP1/2) (Porstmann et al. 2008), which is activated by S6K-dependent mechanisms or lipin-1. Lipin-1 gets inhibited by mTORC1 phosphorylation (Düvel et al. 2010; Peterson et al. 2011).

mTORC1 also regulates DNA replication and nucleotide synthesis by stimulating ATF4 transcription factor and the mitochondrial tetrahydrofolate cycle enzyme methylenetetrahydrofolate dehydrogenase 2 (MTHFD2) associated with purine synthesis (Ben-Sahra et al. 2016).

Besides the anabolic reactions, mTORC1 controls cell growth by suppressing catabolic processes such as autophagy. In the presence of nutrients, mTORC1 inhibits autophagy via the phosphorylation of Unc-51 like autophagy activating kinase 1 (ULK1) (Figure 1.5). As a result, phosphorylated ULK1 is prevented from

activating AMPK and thus the initiation of autophagosome formation is inhibited (Zhao and Goldberg 2016).

1.3 Mass spectrometry (MS)-based proteomics

Each cell contains an entire set of expressed proteins called proteome. The cellular proteome consists of subcellular protein groups, that refer to the proteome of different organelles such as mitochondria, Golgi apparatus and lysosomes (Bernhardt 2005). The organelle proteome undergoes several changes based on the environmental conditions, internal stimuli, stress factors as well as several other aspects (Anderson and Anderson 1998; Anderson et al. 2016).

Mass spectrometry (MS) is a method frequently used to analyze protein samples of a proteome, by either measuring intact proteins through so called ‘top-down proteomics’ or peptide products of proteolytic cleavage via ‘bottom-up proteomics’ (Aebersold and Mann 2003; Chait 2006). A mass spectrometer consists of an ion source, a mass analyzer and a detector (Zhang et al. 2013). In the bottom-up approach, peptides are commonly ionized by the electrospray ionization technique (ESI) or the matrix assisted laser desorption/ionization (MALDI) method (Tanaka et al. 1988; Fenn et al. 1989) to be detectable in the gas-phase during the MS measurement (Awad et al. 2015). After peptide ionization, the mass analyzer measures the mass-to-charge (m/z) ratio of the generated precursor ions and the selected ions are fragmented in a tandem mass spectrometry into product ions by collision. Later on, the detector defines the ratios and intensities of each ion (Awad et al. 2015). Finally, during the processing step, the generated MS data are compared to reliable databases using specific software, which identify the peptides and thus the proteins detected in the sample (Aebersold and Mann 2016). Recently, following the development of label-free and label-based methods, mass spectrometry is considered not only a qualitative but also a quantitative technique (Smith et al. 2019). Label-free method relies on the peptide spectral counts or the precursor ion peak intensities for a relative comparison of two peptides (Cox et al. 2014). Stable isotope labeling by/with amino acids in cell culture (SILAC), stable isotope dimethyl labeling, tandem

mass tags (TMT) and isobaric tags for relative and absolute quantification (iTRAQ) (Ong et al. 2002; Thompson et al. 2003; Hsu et al. 2003; Wiese et al. 2007), are some of the label-based methods that utilize isotopic/isobaric labels integrated into peptides to compare their abundances.

2 Aim of the Project

The goal of this study is to obtain a detailed understanding of the lysosomal proteome changes and to define the impact of starvation on the cellular metabolic status after short and prolonged starvation periods.

To analyze the lysosomal proteome during starvation and define the starvation time periods, mTORC1 activation/deactivation is monitored in different metabolic organs for various starvation periods by quantifying the phosphorylation of its downstream targets and the cellular autophagy status using western blot.

Subsequently, in order to examine the impact of starvation on cellular metabolism, serum metabolites are investigated using different approaches at two starvation periods with distinct effects on mTORC1 activity. For this purpose, the blood glucose levels and the concentrations of amino acids and acylcarnitines are measured. In addition, the production of essential metabolites such as ketone bodies are analyzed by real-time PCR along with a colorimetric enzyme assay.

Furthermore, due to the lack of *in vivo* proteomic data analyzing starvation-induced changes in lysosome-specific proteins, our aim is to characterize changes in the liver lysosomal proteome at the same two starvation periods by large-scale quantitative mass spectrometry approach. Moreover, as the possible interaction of several non-lysosomal proteins with the lysosome is not yet fully understood, the shift in their abundances depending on the starvation duration are investigated in this thesis. Based on a comparative bioinformatics analysis, the *in vivo* regulation of candidate lysosomal/non-lysosomal proteins are further evaluated by western blot.

3 Materials and Methods

3.1 Materials

3.1.1 Consumables

Table 3.1: List of used consumables

Consumable	Provider
10 kDa cut off spin filter	VWR international (Radnor, USA)
Axygen pipette tips maximum recovery	Corning (Corning, USA)
Axygen reaction tubes maximum recovery 1.5 ml	Corning (Corning, USA)
C18 empore extraction-membrane	Merck KGaA (Darmstadt, Germany)
Centrifuge tubes (polypropylene)	Beckman Coulter (Brea, USA)
Centrifuge tubes (Ultra-clear™)	Beckman Coulter (Brea, USA)
Conical plastic tubes 15 ml, 50 ml	Sarstedt (Nümbrecht, Germany)
Disposable scalpels	Feather® Safety Razor (Osaka, Japan)
Filter papers	Whatman™ (Maidstone, UK)
Filtropur V50	Sarstedt (Nümbrecht, Germany)
Folded filter papers	Whatman™ (Maidstone, UK)
Glassware (beakers, bottles, graduated cylinders)	Carl Roth (Karlsruhe, Germany)
Microplate 96-well	BD Falcon (Heidelberg, Germany)
Nitrocellulose membrane	GE Healthcare (Little Chalfont, UK)
Oasis HLB cartridges	Waters (Eschborn, Germany)
Pipette tips	Greiner (Frickenhausen, Germany)
Plastic dishes	Sarstedt (Nümbrecht, Germany)
Polyethersulfone membrane	Pall Filtersystems (Crailsheim, Germany)
Polyvinylidene fluoride membrane	GE Healthcare (Little Chalfont, UK)
qPCR adhesive film	Applied Biosystems (Foster City, USA)
qPCR microplate 96-well	Applied Biosystems (Foster City, USA)
Reaction tubes 1.5 ml, 2 ml	Sarstedt (Nümbrecht, Germany)
Syringes, micro-fine+ 29G 1 ml	Becton Dickinson (Franklin Lakes, USA)

3.1.2 Equipment

Table 3.2: List of used equipment

Equipment	Model	Manufacturer
Analytical balance	A 200S	Sartorius (Göttingen, Germany)
Basic power supply	Power Pac 200	Bio-Rad (Hercules, USA)

Centrifuge	5702, 5425	Eppendorf (Hamburg, Germany)
Centrifuge benchtop	Allegra X-15R	Beckman Coulter (Brea, USA)
Dounce homogenizer	1 ml	Wheaton (Millville, USA)
Dounce homogenizer	5 ml	Sigma-Aldrich (St. Louis, USA)
Electronic pipette controller	Easypet 3	Eppendorf (Hamburg, Germany)
Electrophoresis system	Mini-PROTEAN® Tetra Cell	Bio-Rad (Hercules, USA)
Electrotransfer system	Trans-Blot® Cell	Bio-Rad (Hercules, USA)
Fridge 4 °C	Pentan	Bosch (Gerlingen, Germany)
Glucose meter	Accu-Chek® Guide	F. Hoffmann-La Roche (Basel, Switzerland)
HPLC column	ReproSil-Pur 120 C18-AQ	Dr. Maisch (Ammerbuch-Entringen, Germany)
Ice machine		Ziegra (Isernhagen, Germany)
Incubator	Forma™ Series II 3110	Thermo Fisher Scientific (Waltham, US)
Laboratory rocker	Rotamax 120	Heidolph (Schwabach, Germany)
Magnetic stirrer	RH basic	IKA Werke (Staufen, Germany)
Magnetic stirrer	RCT classic	IKA Werke (Staufen, Germany)
Mass spectrometer	Orbitrap Fusion Lumos	Thermo Fisher Scientific (Waltham, USA)
Micro scale	CP 124-OCE	Sartorius (Göttingen, Germany)
Microcentrifuge	Galaxy MiniStar	VWR (Darmstadt, Germany)
Micropipettes	Research Plus	Eppendorf (Hamburg, Germany)
Microplate reader	GENios	Tecan (Männedorf, Switzerland)
Microplate reader	Infinite 200 Pro	Tecan (Männedorf, Switzerland)
Multisteppipette		Eppendorf (Hamburg, Germany)
Nano HPLC system	Ultimate 3000 RSLC	Dionex (Idstein, Germany)
Offgel fractionator	3100	Agilent Technologies (Waldbronn, Germany)
pH electrode	WTW SenTix 50	Xylem (Weilheim, Germany)
pH-meter	Calimatic 761	Knick (Berlin, Germany)
Pinsette	5 extra	Dumont (Montignez, Switzerland)
Real-Time PCR System	7300	Applied Biosystems (Foster City, USA)
Refrigerated centrifuge	5810 R, 5417 R	Eppendorf (Hamburg, Germany)
Refrigerator -20 °C	Comfort	Liebherr (Bulle, Switzerland)
Refrigerator -80 °C	Sanyo™ MDF-U55V	Fischer Scientific (Dublin, Ireland)
Roller mixer	RS-TR05	Carl Roth (Karlsruhe, Germany)
Rotor	Ti-50	Beckman Coulter (Brea, USA)

Rotor	SW41	Beckman Coulter (Brea, USA)
Scale	PC4400 DeltaRange	Mettler Toledo (Columbus, USA)
Spectrophotometer	NanoDrop 2000	PeQlab (Ehrlangen, Germany)
Fume hood	EN 14175	ARGE (Wathlingen, Germany)
Thermomixer	Comfort	Eppendorf (Hamburg, Germany)
Tissue homogenizer	HOMGEN	Schütt Labortechnik (Göttingen, Germany)
Ultra Thurrax	T 10 basic	IKA Werke (Staufen, Germany)
Ultracentrifuge	Optima L-80 XP	Beckman Coulter (Brea, USA)
Ultrapure water system	Arium® Pro	Sartorius (Göttingen, Germany)
Ultrasonic bath	2510	Branson (Danbury, USA)
Vacuum centrifuge	ScanSpeed 40	ScanVac (Lynge, Denmark)
Vortex mixer	UNIMAG ZX3	UniEquip (Leipzig, Germany)
Vortex mixer	Vortex Genie	Scientific Industries (Bohemia, USA)
Water bath	ED	Julabo (Seelbach, Germany)
Western blot imaging system	Fusion Solo	Vilbert Lourmat (Collégien, France)

3.1.3 Chemicals

All MS-related chemicals were either HPLC or MS grade.

Table 3.3: List of used chemicals

Chemical	Provider
2-Mercaptoethanol	Sigma-Aldrich (St. Louis, USA)
Acetic acid	Biosolve (Valkenswaard, Netherlands)
Acetonitrile	Biosolve (Valkenswaard, Netherlands)
Acrylamide	Merck KGaA (Darmstadt, Germany)
Ammonium persulfate (APS)	Carl Roth (Karlsruhe, Germany)
Bovine serum albumin (BSA)	Carl Roth (Karlsruhe, Germany)
Bromophenol blue	Merck KGaA (Darmstadt, Germany)
Dimethyl sulfoxide (DMSO)	Sigma-Aldrich (St. Louis, USA)
Dithiothreitol (DTT)	Sigma-Aldrich (St. Louis, USA)
Deoxynucleoside triphosphates (dNTPs)	Thermo Fisher Scientific (Waltham, USA)
Ethanol	AppliChem (Darmstadt, Germany)
Ethyl acetate	AppliChem (Darmstadt, Germany)
Ethylenediaminetetraacetic acid (EDTA)	Sigma-Aldrich (St. Louis, USA)
Formic acid (FA)	Biosolve (Valkenswaard, Netherlands)
Glycine	Merck KGaA (Darmstadt, Germany)
Halt™ phosphatase inhibitor cocktail	Thermo Fisher Scientific (Waltham, USA)

Hydrochloric acid	Carl Roth (Karlsruhe, Germany)
Hydroxylamine	Sigma-Aldrich (St. Louis, USA)
Isopropanol	Merck KGaA (Darmstadt, Germany)
Methanol	Merck KGaA (Darmstadt, Germany)
Milk powder	Carl Roth (Karlsruhe, Germany)
N,N,N`,N`-Tetramethylethylenediamine (TEMED)	Carl Roth (Karlsruhe, Germany)
Nuclease-free distilled water	Thermo Fisher Scientific (Waltham, USA)
Pageruler™ prestained protein ladder	Thermo Fisher Scientific (Waltham, USA)
PonceauS	AppliChem (Darmstadt, Germany)
Protease inhibitor cocktail cOmplete™	F. Hoffmann-La Roche (Basel, Switzerland)
RevertAid Reverse Transcriptase	Thermo Fisher Scientific (Waltham, USA)
RiboLock RNAse Inhibitor	Thermo Fisher Scientific (Waltham, USA)
Sequencing grade modified trypsin, porcine	Promega (Madison, USA)
Sodium chloride	Carl Roth (Karlsruhe, Germany)
Sodium dodecyl sulfate (SDS)	Bio-Rad (Hercules, USA)
Sodium deoxycholate (SDC)	Thermo Fisher Scientific (Waltham, USA)
Spectra™ multicolor high range protein ladder	Thermo Fisher Scientific (Waltham, USA)
Sucrose	Carl Roth (Karlsruhe, Germany)
SYBR © Select Master Mix	Applied Biosystems (Foster City, USA)
TMT10plex reagents	Thermo Fisher Scientific (Waltham, USA)
triethylammonium bicarbonate (TEAB)	Thermo Fisher Scientific (Waltham, USA)
Trifluoroacetic acid (TFA)	Biosolve (Valkenswaard, Netherlands)
Tris(hydroxymethyl)aminomethane	Carl Roth (Karlsruhe, Germany)
Triton WR1339 (tyloxapol bioXtra)	Sigma-Aldrich (St. Louis, USA)
Triton X-100	Fluka Chemie (Buchs, Switzerland)
TRIzol® reagent	Thermo Fisher Scientific (Waltham, USA)
Tween-20	Sigma-Aldrich (St. Louis, USA)
Water	Biosolve (Valkenswaard, Netherlands)

3.1.4 Buffers, media and solutions

As far as not otherwise mentioned, all buffers, media and solutions were prepared in ddH2O. MS-related buffers and solutions were either HPLC or MS grade.

Table 3.4: List of used buffers, media and solutions

Name	Components
10x SDS-running buffer (3.2.2.6 SDS-PAGE)	3.02 % (w/v) Tris-base 14.4 % (w/v) Glycin 1 % (w/v) SDS

10x TBS, pH 7.4 (3.2.2.8 WB stripping)	1.21 % (w/v) Tris-HCl 8.76 % (w/v) NaCl
4x Laemmli buffer, pH 6.8 (Laemmli 1970) (3.2.2.6 SDS-PAGE)	250 mM Tris-HCl 8 % (w/v) SDS 40 % (v/v) Glycerol 10 % (v/v) Mercaptoethanol 0.004 % (w/v) Bromophenol blue
4x Running gel buffer, pH 8.8 (3.2.2.6 SDS-PAGE)	1.5 M Tris-HCl
4x Stacking gel buffer, pH 6.8 (3.2.2.6 SDS-PAGE)	0.5 M Tris-HCl
Blocking buffer (3.2.2.7 WB analysis)	1x TBS 0.1 % (v/v) Tween-20 5 % (w/v) Milk powder or 5 % (w/v) Bovine serum albumin
Blotting buffer (3.2.2.7 WB analysis)	48 mM Tris-base 39 mM Glycin 0.037 % (w/v) SDS 20 % (v/v) Methanol
Digestion buffer (DB) (3.2.4.1 FASP)	20 mM TEAB 0.5 % (w/v) SDC
Running gel solution 12.5 % (3.2.2.6 SDS-PAGE)	12.5 % (v/v) Acrylamide 25 % (v/v) Running gel buffer 0.1 % (w/v) SDS 0.1 % (w/v) APS 0.1 % (v/v) TEMED
Running gel solution 7.5 % (3.2.2.6 SDS-PAGE)	7.5 % (v/v) Acrylamide 25 % (v/v) Running gel buffer 0.1 % (w/v) SDS 0.1 % (w/v) APS 0.1 % (v/v) TEMED
Solvent B (3.2.4.6 MS instrumental analysis)	90 % (v/v) Acetonitrile 0.1 % (v/v) Formic acid 5 % (v/v) DMSO
Stacking gel solution 5 % (3.2.2.6 SDS-PAGE)	5 % (v/v) Acrylamide 25 % (v/v) Stacking gel buffer 0.1 % (w/v) SDS 0.1 % (w/v) APS 0.2 % (v/v) TEMED

Sucrose gradient solutions (3.2.2.3 Tritosome enrichment)	ρ 1.21 Sucrose solution (26.98 g + 33.02 g dH2O) ρ 1.15 Sucrose solution (20.09 g + 39.91 g dH2O) ρ 1.14 Sucrose solution (18.88 g + 41.12 g dH2O) ρ 1.06 Sucrose solution (8.59 g + 51.40 g dH2O)
Tissue homogenization buffer, pH 7.4 (3.2.2.1 Tissue homogenate preparation)	10 mM Tris-HCl 250 mM Sucrose 1 mM EDTA 1x Protease inhibitor cocktail 1x Phosphatase inhibitor cocktail
Washing buffer (3.2.2.7 WB analysis)	1x TBS 0.1 % (v/v) Tween-20

3.1.5 Kits and assays

Table 3.5: List of used kits and assays

Name	Provider
Beta-Hydroxybutyrate (beta-HB) Assay Kit	Abcam (Cambridge, UK)
Bio-Rad DC™ Protein Assay	Bio-Rad (Hercules, USA)
Clarity™ Western Blotting ECL Substrate Kit	Bio-Rad (Hercules, USA)
RevertAid™ H Minus First Strand cDNA Synthesis Kit	Thermo Fisher Scientific (Waltham, USA)

3.1.6 Mouse strains

All mice were obtained from our animal facility at Bonn University Hospital and housed in accordance with the institutional guidelines. The wild-type mice used in all experiments had a C57BL/6 genetic background and supplied either from Janvier Labs (Le Genest-Saint-Isle, France) or Charles River Laboratories (Massachusetts, USA). The experimental procedures were carried out in correspondence with the instructions approved by the local and state authorities regarding animal welfare.

3.1.7 Antibodies

3.1.7.1 Primary antibodies

Table 3.6: List of used primary antibodies

Antigen	Host	Dilution in WB*	Manufacturer/Order number
4E-BP1	Rabbit	1:1000	Cell Signaling Technology (Danvers, USA); Order Number: 9644S
CPT2	Rabbit	1:1000	Proteintech (Manchester, UK); Order Number: 26555-1-AP
GAPDH	Rabbit	1:2000	Santa Cruz (Dallas, USA); Order Number: sc-25778
GYS2	Rabbit	1:1000	Proteintech (Manchester, UK); Order Number: 22371-1-AP
LAMP-1	Rat	1:1000	Developmental Studies Hybridoma Bank (DSHB) (Iowa, USA); Order Number: 1D4B
LAMTOR1	Rabbit	1:1000	Sigma-Aldrich (St. Louis, USA); Order Number: HPA002997
LAMTOR2	Rabbit	1:1000	Cell Signaling Technology (Danvers, USA); Order Number: 8145S
LAMTOR5	Rabbit	1:1000	Cell Signaling Technology (Danvers, USA); Order Number: 14633S
LC3B	Rabbit	1:1000	Cell Signaling Technology (Danvers, USA); Order Number: 2775S
LONP2	Rabbit	1:1000	Proteintech (Manchester, UK); Order Number: 18035-1-AP
NDUFB11	Rabbit	1:1000	Proteintech (Manchester, UK); Order Number: 16720-1-AP
NDUFB7	Rabbit	1:1000	Proteintech (Manchester, UK); Order Number: 14912-1-AP
NPRL2	Rabbit	1:1000	Cell Signaling Technology (Danvers, USA); Order Number: 37344S
NUDT12	Rabbit	1:1000	Proteintech (Manchester, UK); Order Number: 17487-1-AP
p-4E-BP1 (T37/36)	Rabbit	1:1000	Cell Signaling Technology (Danvers, USA); Order Number: 2855S
PCK1	Rabbit	1:1000	Proteintech (Manchester, UK); Order Number: 16754-1-AP
PRAS40	Rabbit	1:1000	Cell Signaling Technology (Danvers, USA); Order Number: 2691S
p-S6 ribosomal protein (S240/244)	Rabbit	1:1000	Cell Signaling Technology (Danvers, USA); Order Number: 2215S
PSMA7	Rabbit	1:1000	Proteintech (Manchester, UK); Order Number: 15219-1-AP

PSMB5	Rabbit	1:1000	Cell Signaling Technology (Danvers, USA); Order Number: 12919S
PYGL	Rabbit	1:1000	Proteintech (Manchester, UK); Order Number: 15851-1-AP
RagA	Rabbit	1:1000	Cell Signaling Technology (Danvers, USA); Order Number: 4357S
RagC	Rabbit	1:1000	Cell Signaling Technology (Danvers, USA); Order Number: 9480S
Raptor	Rabbit	1:1000	Cell Signaling Technology (Danvers, USA); Order Number: 2280S
S6 Ribosomal Protein	Rabbit	1:1000	Cell Signaling Technology (Danvers, USA); Order Number: 2217S
TPP1	Mouse	1:2000	Santa Cruz (Dallas, USA); Order Number: sc-393961
VDAC1	Rabbit	1:2000	Cell Signaling Technology (Danvers, USA); Order Number: 4866S
WASHC4	Rabbit	1:1000	Proteintech (Manchester, UK); Order Number: 51101-1-AP

*: Western Blot

3.1.7.2 Secondary antibodies

Table 3.7: List of used secondary antibodies

Antigen/Tag	Host	Dilution in WB*	Manufacturer
Mouse IgG (H+L)/HRP	Goat	1:5000	Dianova (Hamburg, Germany); Order Number: 115-035-044
Rabbit IgG (H+L)/HRP	Goat	1:5000	Dianova (Hamburg, Germany); Order Number: 111-035-003
Rat IgG (H+L)/HRP	Goat	1:5000	Dianova (Hamburg, Germany); Order Number: 112-035-167

*: Western Blot

3.1.8 Primers

Table 3.8: List of used primers

Primer	Sequence 5'-3'	Temperature °C
Actin for	TCCATCATGAAGTGTGACGT	48
Actin rev	GAGCAATGATCTTGATCTTCAT	48
CPT1a for	CCATGAAGCCCTCAAACAGATC	55
CPT1a rev	ATCACACCCACCACCACGATA	55
HMGCS2 for	ATACCACCAACGCCTGTTATGG	55
HMGCS2 rev	CAATGTCACCACAGACCACCAG	55
PPARA for	AGAGCCCCATCTGTCCTCTC	52
PPARA rev	ACTGGTAGTCTGCAAAACCAAA	51

3.1.9 Software

Table 3.9: List of used software

Software	Provider
7300 System SDS RQ Study 1.4	Thermo Fisher Scientific (Waltham, USA)
BioRender 2020	www.biorender.com
CorelDRAW X6	Corel Corporation (Ottawa, Canada)
g:Profiler 2020	https://biit.cs.ut.ee/gprofiler/gost
FusionCapt Advance Solo 4	Vilber Lourmat (Collégien, France)
GraphPad Prism 6.01	GraphPad Software Inc. (San Diego, USA)
Gene Ontology (GO)	http://geneontology.org/
i-control™ (Infinite 200 Pro)	Tecan (Männedorf, Switzerland)
Mascot server 2.6.1	Matrix Science Ltd (London, UK)
Office Professional Plus 2016	Microsoft Corporation (Redmond, USA)
Proteome discoverer 2.3	Thermo Fisher Scientific (Waltham, USA)
R 3.5.1	R Core Team 2018 (Vienna, Austria)
Thermo Xcalibur 2.2	Thermo Fisher Scientific (Waltham, USA)
UniProt	www.uniprot.org
Venny 2.1	https://www.stefanjol.nl/venny
Xfluor4 (GENios)	Tecan (Männedorf, Switzerland)

3.2 Methods

3.2.1 Molecular biology methods

3.2.1.1 RNA isolation

All RNA isolation steps were performed on ice and mice liver tissues were placed on dry ice, unless stated differently. To enable cDNA synthesis, RNA was isolated from liver tissues of control and starved mice. Samples were resuspended in 500 µl TRIzol reagent (Chomczynski and Sacchi 1987) and homogenized at low speed using Ultra Thurrax T 10 basic. After 5 min incubation at room temperature (RT), 100 µl chloroform was added and the samples were vortexed for 15 seconds. Samples were again incubated under the same conditions as described above and then centrifuged for 15 min at 16000 x g at 4 °C, creating three phases within each sample. The upper transparent phase containing the mRNA was carefully transferred to a new 1.5 ml reaction tube and both the lower TRIzol/chloroform phase and the thin white protein interphase were discarded. After adding 500 µl of isopropanol, samples were incubated for 15 min at RT and

centrifuged again for 15 min at 16000 x g at 4 °C. The resulting pellet was washed with 700 µl of 70 % ethanol and the samples were recentrifuged. Following this, the remaining ethanol was removed and the pellets were dried at RT and resuspended in 40 µl nuclease-free water. Samples were stored overnight at -80 °C and the concentration and purity of isolated RNA were measured using a spectrophotometer.

3.2.1.2 Spectrophotometric analysis of nucleic acids

NanoDrop 2000 spectrophotometer was used to determine the concentration and purity of RNA and DNA using wavelengths of 230, 260 and 280 nm absorbance and calculated ratios of 260/280 and 260/230. The measured absorbance was proportional to the nucleic acid amount of 50 ng/µl dsDNA or 40 ng/µl RNA. 1 µl of DNA or RNA sample was used for every measurement and 1 absorbance unit = 1 cm light path.

3.2.1.3 Reverse transcription (First strand cDNA synthesis)

To perform a cDNA synthesis, RevertAid™ H Minus First Strand cDNA Synthesis Kit was carried out as described in the manufacturer's instructions. Briefly, 5 µg of isolated RNA was diluted to a final volume of 10 µl using nuclease-free water. The sample was pipetted to a PCR reaction tube along with 1 µl of oligo $(dT)_{18}$ primer and the volume was filled to a total volume of 12 µl using nuclease-free water. The first strand cDNA master mix (Table 3.10) was added to the sample and incubated for 60 min at 42 °C and the reaction was stopped by heating up to 70 °C for 5 min. The 250 ng/µl synthesized cDNA was then diluted to a final concentration of 25 ng/µl and stored at -20 °C for future qPCR experiments.

Table 3.10: First strand cDNA master mix composition

Component	Volume
Reaction buffer (5x)	4 µl
RiboLock RNase inhibitor (20 U/µl)	1 µl
dNTP mix (10 mM)	2 µl
RevertAid H Minus M-MuLV reverse transcriptase (200 U/µl)	1 µl

3.2.1.4 Quantitative real-time polymerase chain reaction (qPCR)

To amplify the gene of interest (GOI), appropriate forward and reverse primers were selected and a primer test PCR was performed. To perform the quantitative

real-time PCR, SYBR© Select Master Mix was used to detect the amplified gene by increased fluorescence intensities using The SYBR GreenER™ dye. As recommended by the manufacturer, 125 ng cDNA was pipetted in triplicates into a 96-well microplate together with the reaction mixture (Table 3.11). The reaction was conducted by the 7300 Real-Time PCR System using the thermocycling program mentioned below (Table 3.12). Data analysis was performed by 7300 System SDS RQ Study 1.4 software, and the $2^{-\Delta\Delta Ct}$ method (Livak and Schmittgen 2001) was used to analyze the changes and relative gene expression. Together with each target gene reaction, an internal control such as actin as well as water control reactions were performed in triplicates.

Table 3.11: Reaction mixture

Component	Volume
Forward primer	1 µl
Reverse primer	1 µl
SYBR© Select Master Mix	10 µl
Nuclease-free water	3 µl

Table 3.12: qPCR program

Stage	Cycles	Temperature	Time
1	1	50 °C	2 min
2	1	95 °C	2 min
3	40	95 °C	15 sec
4	40	60 °C	1 min

3.2.2 Protein-biochemistry methods

3.2.2.1 Tissue homogenate preparation

Removed mice tissues were weighed and homogenized in five volumes of ice-cold tissue homogenization buffer (Table 3.4). After douncing for 20 strokes using a 1 ml dounce homogenizer, 1 % (v/v) Triton X-100 was added to the homogenate and incubated for 1 h on ice. For a separation into soluble and insoluble Triton X-100 fractions, the mixture was centrifuged at 15.000 x g for 15 min at 4 °C using a refrigerated centrifuge. After centrifugation, the insoluble fraction (pellet) was discarded and the soluble fraction (supernatant) was transferred into a new 1.5 ml reaction tube for protein concentration determination or stored at -20 °C.

3.2.2.2 Protein concentration determination

Based on Lowry assay protocol (Lowry et al. 1951), the colorimetric determination of protein concentration was followed using detergent compatible Bio-Rad DC™ protein assay.

According to the manufacturer's manual, 20 µl of reagent S was added to 1 ml reagent A to prepare reagent A'. 5 µl of the protein sample and seven BSA standard dilutions, namely 2.0000, 1.0000, 0.5000, 0.2500, 0.1250, 0.0625, 0.0312 and 0.0000 µg/µl were loaded in triplicates into a 96-well microplate. 25 µl of working reagent A' and 200 µl of reagent B were added successively to the already loaded samples. The mixture was incubated for 15 min at RT and the absorption was measured at 750 nm wavelength using Tecan GENios microplate reader. The protein concentration of the sample was calculated with the help of the BSA standard.

3.2.2.3 Tritosome enrichment

Tritosomes are lysosomes isolated from mice liver using a sucrose gradient-based technique (Wattiaux et al. 1963) after an injection of Triton WR1339 solution (Tyloxapol) (Leighton et al. 1968). Their content corresponds to that of the lysosomes and thus are expected to show comparable catalytic reactions (Gersten et al. 1974).

Enrichment of tritosomes was performed as previously described (Markmann et al. 2017). Four days ahead of sacrifice, control and starved mice were intraperitoneally (IP) injected with 17 % (w/v) Triton WR1339 solution in 0.9 % (v/v) NaCl. 4 µl/g of bodyweight. In the case of starved mice, chow depletion was introduced prior to the experimental day in accordance with the time of starvation. On the experimental day, mice were sacrificed by a cervical dislocation and livers were removed. Mice livers were homogenized in five volumes of 250 mM ice-cold sucrose buffer. After douncing for three strokes using 5 ml dounce homogenizer, homogenates were centrifuged at 1000 x g for 10 min at 4 °C. The supernatant was transferred to a new 15 ml conical plastic tube, while the pellet was re-homogenized in 3.5 ml of 250 mM sucrose buffer followed by another similar centrifugation. Both post-nuclear supernatants (PNS) were pooled and ultra-centrifuged for 7 min at 56.500 x g at 4 °C using Ti-50 fixed angle rotor. After discarding the supernatant and resuspending the pellet in 10 ml of 250 mM sucrose buffer with a glass pestle, another ultra-centrifugation was performed under the same conditions. The resulting pellet, containing mitochondria and lysosomes, represents the M/L layer. In order to separate both organelles, a

discontinuous sucrose gradient using different sucrose density solutions was carried out (Table 3.4). The M/L pellet was resuspended in 3.5 ml sucrose solution of ρ 1.21 density, forming the first layer of a discontinuous sucrose gradient. Using a 1000 µl micropipette, the following 2.5 ml sucrose solution layers of ρ 1.15, 1.14 and 1.5 ml of ρ 1.06 density were carefully added. The density gradient was ultra-centrifuged at 110000 x g for 150 min at 4 °C, using SW41 swinging-bucket rotor. Subsequently, the resulting tritosome-enriched interphase fraction, located between ρ 1.14 and ρ 1.06 layers, was carefully collected and further prepared for western blot analysis and tandem mass tag (TMT) labeling or stored at -20 °C.

3.2.2.4 Mouse serum preparation

6-month-old male wild-type mice were sacrificed, and the thorax was opened. After collecting 400-1000 µl of whole blood samples from the chest region using a 1000 µl micropipette, coagulation at RT was performed for 30 min. Samples were centrifuged at 18000 x g for 10 min at 4 °C and the supernatant was transferred to a new 1.5 ml reaction tube. 50 µl of serum samples were sent to Dr. Eberhard & Partner medical care center (Dortmund, Germany) for the determination of amino acid and acylcarnitine concentrations by mass spectrometry.

3.2.2.5 Measurement of blood glucose levels

Accu-Chek® Guide instrument was used to test the blood glucose levels in control, 6 and 24 hours starved mice. To prevent blood clotting, samples were collected quickly and directly after the sacrifice. According to the manufacturer's manual, the test strip was inserted into the instrument and a fresh whole blood drop was carefully added to the edge of the strip. The test results were obtained in mg/dl and the mean out of three individual measurements was calculated.

3.2.2.6 Sodium dodecyl sulfate polyacrylamide gel electrophoresis (SDS-PAGE)

In a discontinuous sodium dodecyl sulfate polyacrylamide gel electrophoresis, negatively charged proteins are separated based on their molecular mass while migrating through a SDS polyacrylamide gel to the anode (Laemmli 1970).

Either 12.5 % or 7.5 % running gel was prepared, followed by a 5 % stacking gel (Table 3.4) and both mixtures were cast using a BioRad Mini-PROTEAN Tetra Cell Stand. The desired number and size of pockets formed in the stacking gel was decided using the appropriate comb. After polymerization, the gel was placed into an electrophoresis chamber filled with 1x SDS-running buffer (Table 3.4). Ahead of samples loading, 10-20 µg of protein samples were mixed with 1x laemmli buffer (Table 3.4) and incubated for 5 min at 95 °C. During this process, proteins will be denatured and negatively charged. In addition, 3 µl of Pageruler™ prestained protein ladder or 7.5 µl of Spectra™ multicolor high range protein ladder were loaded into the gel pocket. Gel electrophoresis was carried out at a constant 90 V for 2 h.

3.2.2.7 Western blot (WB) analysis

Western blot is an analytical method used for transferring previously separated SDS-PAGE proteins onto a protein-binding membrane. The protein of interest is then detected using specific antibodies. Antibodies are usually coupled to enzymes or chemical compounds to visualize the signal (Towbin et al. 1979).

For the immune detection, separated proteins were transferred onto a nitrocellulose (NC) or a methanol activated polyvinylidene fluoride (PVDF) membrane using Trans-Blot® Cell electrotransfer system. First, three thin Whatman papers were soaked in blotting buffer (Table 3.4). Subsequently, the membrane and the gel were submerged shortly into the blotting buffer and placed on top of it, followed by three additional presoaked Whatman papers. The semi-dry electrotransfer was carried out for 45 min at 300 mA.

After the electrotransfer, the membrane was blocked for 1 h by using 5 % (w/v) milk powder or 5 % (w/v) BSA blocking buffer (Table 3.4) to avoid unspecific binding of antibodies. Afterwards, the membrane was washed three times with a washing buffer (Table 3.4) and incubated with the diluted primary antibody in blocking buffer overnight at 4 °C. The appropriate horseradish peroxidase (HRP) conjugate secondary antibody was applied for 1 h at RT.

For a specific protein signal detection, additional three washes using the same washing buffer were completed. An equal amount of the enhanced chemiluminescence (ECL) substrates was mixed in a 1:1 ratio and poured over

the whole surface of the membrane. After 1 min, visualization was accomplished using Fusion Solo imaging system.

3.2.2.8 Western blot stripping

To investigate more than one protein on the same WB membrane, primary and secondary antibodies need to be removed before the detection with other antibodies. Therefore, a mild stripping protocol was used.

The dry membrane was equilibrated in 1x TBST for 5 min. Following this, the membrane was agitated thrice with an acidic stripping buffer (100 mM glycine, pH 2.0), while alternating with three washes of 1x TBS (Table 3.4) for 10 min each. Subsequently, the membrane was blocked again, if necessary, prior to the addition of primary and secondary antibodies.

3.2.2.9 Western blot quantification

Enhanced chemiluminescence (ECL) was developed and visualized protein signals were quantified using FusionCapt Advance Solo 4. The software displays the emitted light from each detected band in the form of a gray scaled signal. By choosing the appropriate exposure time, the detected protein signals below the saturation limit were further used for quantification purposes. After defining the boundary and subtracting the background intensities from the signal of interest, the quantity of the detected protein was determined by the sum of the pixel intensities in the selected area. For normalization, housekeeping proteins were utilized as a control. Band intensities originating from the protein of interest were divided by the corresponding housekeeping (control) protein band intensities, for example: Glyceraldehyde-3-phosphate dehydrogenase (GAPDH) for whole lysates or tripeptidyl-peptidase 1 (TPP1) for lysosomal fractions. Subsequently, the amounts of the normalized signals were compared to the control sample intensities which was set to 1. Values greater or less than 1 represent an increase or a decrease in the amount of protein in the treated sample compared to the control sample, respectively.

For a statistical analysis of the selected normalized signals, a two samples t-test (two-tailed distribution, unpaired) was performed, with a p-value <0.05 was defined as significant, a p-value <0.01 as highly significant and a p-value >0.05

as not significant. The standard deviation was determined using the n-1 method and the standard error of the mean was calculated using the following formula:
Standard error = standard deviation/square root of total number of samples

3.2.3 Beta-hydroxybutyrate enzymatic assay

While undergoing starvation, the body glucose levels drop and the liver responds by producing β-hydroxybutyrate as the most abundant ketone body in mammals, which is used as an alternative energy source for the body (Newman and Verdin 2017).

Beta-hydroxybutyrate (beta-HB) Assay Kit was used according to the manufacturer's protocol to determine the concentrations of beta-HB in control and starved mice serum samples. In brief, 2 µl enzyme mix and 2 µl substrate mix were added to 46 µl assay buffer to prepare the colorimetric reaction mix. 5 µl of serum samples were added in duplicates into a 96-well microplate and the total volume was adjusted to 50 µl using assay buffer. 50 µl of six prepared β-HB standard dilutions were also pipetted in duplicates, namely 10.0 8.0, 6.0, 4.0, 2.0 and 0.0 nmol/well. Following this, 50 µl of the colorimetric reaction mix was added into the already loaded samples. The mixture was then incubated in the dark for 30 min at RT and the absorption was measured at 450 nm wavelength using Tecan Infinite 200 Pro microplate reader. The protein concentration of the sample was calculated using the β-HB standard. A background reaction mix of 2 µl substrate mix added to 48 µl assay buffer was prepared then pipetted into new duplicates of serum samples and β-HB standard dilutions. Subsequently, the background readings were subtracted.

3.2.4 Techniques for mass spectrometry-based proteomics

3.2.4.1 In-solution digest by filter aided sample preparation (FASP)

To convert the proteins obtained from biological samples to peptides compatible for tandem mass tag (TMT) labeling, filter aided sample preparation method was used. In-solution digest by FASP utilize a molecular mass cut off spin filter, where passing through peptides get collected for mass spectrometry-based protein analysis (Manza et al. 2005; León et al. 2013).

A 10 kDa cut off spin filter was equilibrated by adding 300 µl digestion buffer (DB) (Table 3.4) and centrifuging for 5 min at 10000 x g. After adding 50 µg of protein sample to the filter, proteins were reduced using 20 mM dithiothreitol (DTT) in DB and incubated for 30 min at 55 °C. To wash the remaining DTT, the sample was centrifuged again using 300 µl DB. Thereafter, the sample was alkylated using DB containing 40 mM acrylamide and incubated in the dark for 30 min at RT. Two centrifugation steps using 100 µl DB were applied to remove the acrylamide residues. After adjusting the volume to 100 µl, the protein sample was trypsinized at a 1:100 mass ratio and incubated for 10 h at 37 °C. The next day, the incubated sample was centrifuged for 10 min at 10000 x g and the flow through containing peptides was transferred to a new reaction tube. The centrifugation procedure described above was repeated using 200 µl digestion buffer and both flow throughs were combined. An appropriate volume of trifluoroacetic acid (TFA) was added to the peptides to reach a final concentration of 2.5 % (v/v) TFA. TFA acidification led to the precipitation of sodium deoxycholate (SDC). The acidified peptide sample was centrifuged for 10 min at 10000 x g and the supernatant was carefully pipetted to a new reaction tube. Pelletized SDC was resuspended in 250 µl 0.1 % (v/v) TFA and centrifuged for 10 min at 14000 x g. After combining both supernatants, SDC remains were extracted by centrifuging the peptide sample twice in 500 µl ethyl acetate for 2 min at 10000 x g. Finally, the peptides were dried and concentrated in a vacuum centrifuge at 60 °C.

3.2.4.2 Tandem mass tag (TMT) labeling

Tandem mass tag (TMT) is an isobaric labeling method used for a relative protein quantification by mass spectrometry (Thompson et al. 2003). TMT10plex labeling uses ten different isobaric compounds with the same mass and chemical structure. It enables ten variable peptide samples to be labeled in parallel then mixed together for MS analysis.

Dried peptides were dissolved in 100 µl of 0.1 M triethylammonium bicarbonate (TEAB) and sonicated for 5 min. TMT10plex reagents were removed from the freezer and equilibrated to room temperature in a desiccator. After dissolving each reagent in 41 µl of acetonitrile (ACN), the reagent vials were incubated at RT for 5 min and centrifuged shortly for 30 sec. Each reagent solution was

carefully pipetted to a different 100 µl peptide sample and incubated in the dark for 1 h at RT. Later on, 10 µl 5 % (v/v) hydroxylamine was added, and the samples were vortexed for 20 sec. After 15 min incubation at RT, the peptide solutions were combined and ready for desalting through the solid phase extraction (SPE) method.

3.2.4.3 Peptide purification by solid phase extraction (SPE)

TMT labeled peptides were purified and desalted by the solid phase extraction (SPE) technique using Oasis® hydrophilic-lipophilic balance (HLB) cartridges. First, the columns were equilibrated with 1.5 ml ACN and washed using 5 ml 0.1 % (v/v) TFA. Afterwards, the peptide solutions were loaded and washed with 1 ml 0.1 % (v/v) TFA. Before the elution step, the columns were washed off ten times with 1 ml 0.1 % (v/v) TFA. Finally, the peptides were eluted in 1.5 ml 70 % (v/v) ACN in 0.1 % (v/v) TFA and dried in a vacuum centrifuge at 60 °C.

3.2.4.4 Peptide isoelectric fractionation (OFFGEL)

The peptide isoelectric fractionation step is important for a higher number of protein identifications and comprehensive MS analysis of complex samples. Agilent 3100 fractionator device was used to separate peptides in a pH gradient based on their isoelectric point (pI).

For a 12 fractions separation, dried peptides were dissolved in 1.9 ml of 0.2 % (v/v) IPG buffer, pH 3-10. After assembling the offgel apparatus and fixing the strip according to the manufacturer's instructions, 20 µl of IPG buffer was pipetted to each slot to rehydrate the strip. 150 µl of the sample was pipetted to each well after placing two wetted electrode pads at each protruding end of the strip. The mineral oil was pipetted onto anode and cathode, and then a high voltage (see offgel fractionation program, table 3.13) was applied to achieve an overnight separation of peptides. After the fractionation was finished, samples were transferred to separate reaction tubes. To collect the remaining peptides, each well was incubated in 200 µl of 0.1 % (v/v) FA for 15 min at RT and combined with the corresponding extract. The samples were dried in a vacuum centrifuge at 60 °C.

Table 3.13: Offgel fractionation program (12-well frame)

	Volt Hour (kVh)	Voltage (V)	Current (µA)	Power (mW)	Time (h:m)
Focusing	64	4500	50	200	100:00
Hold		500	20	50	

3.2.4.5 Peptide purification by stop and go extraction (STAGE) tips

Offgel fractionated peptides need to be purified and desalted prior to LC-MS measurement. For this purpose, small quantities of peptides were desalted using the stop and go extraction (STAGE) tips protocol (Rappsilber et al. 2007). Briefly, 6 small disks of Empore C18 material were pressed over each other into a 200 µl micropipette tips with the aid of a glass capillary tube. Afterwards, the micropipette tips together with a self-made holder were positioned into a 2 ml reaction tube forming so called a ‘column’.

To activate the C18 material, 20 µl of methanol was added and the stagetips were centrifuged for 1 min at 2500 x g. The column was washed and equilibrated by a subsequent addition of 20 µl 0.5 % (v/v) AcOH in 80 % (v/v) ACN and 20 µl 0.5 % (v/v) AcOH solutions with centrifugation in between for 1 min at 2500 x g. The dried peptides were dissolved in 20 µl 5 % (v/v) ACN 5 % (v/v) FA solution and resuspended in an ultrasonic bath for 5 min. To dilute the ACN amount, the reaction tube volume was filled up to 100 µl with water and applied to the column. After a centrifugation for 1 min at 2500 x g, stagetips were washed with 100 µl of 5 % (v/v) AcOH and transferred to the new 1.5 ml reaction tube in preparation for the elution step. Desalted peptides were eluted two times in 20 µl 0.5 % (v/v) AcOH in 80 % (v/v) ACN and centrifuged for 1 min at 2500 x g in between. The 40 µl eluted peptides were dried in a vacuum centrifuge at 60 °C. Shortly before the MS measurement, peptides were dissolved in 20 µl 5 % (v/v) ACN 5 % (v/v) FA solution and resuspended in an ultrasonic bath for 5 min. Resuspended samples were centrifuged for 15 min at 16000 x g and 5 µl were pipetted into a 96-well microplate.

3.2.4.6 Mass spectrometry instrumental analysis

Peptides were separated on a Dionex Ultimate 3000 RSLC nano HPLC system. Liquid chromatography (LC) separation was performed on an in-house C18 analytical column using a P-2000 laser puller and fused silica capillaries (200 mm

length, 75 µm inner diameter, ReproSil-Pur 120 C18-AQ, 1.9 µm). The autosampler was operated in µl-pickup mode with 3 µl per injection and peptides were dissolved in 10 µl of 0.1 % (v/v) formic acid (solvent A) before being loaded on the column. Peptides were separated at a flow rate of 300 nl/min during a 90 min linear gradient ranging from 1 % to 35 % solvent B (Table 3.4). The nano HPLC was connected online to an Orbitrap Fusion Lumos mass spectrometer. Peptide precursor ions between 330-1600 m/z were scanned every 3 seconds in the Orbitrap mass analyzer (resolution 120000, maximum injection time 50 ms, automatic gain control (AGC) target 4×10^5). Internal calibration with a typical mass error ≤1.5ppm was conducted using polysiloxane (445.12002 Da). Precursor ions were identified and isolated by collision induced dissociation (CID: 0.7 Da quadrupole isolation, threshold intensity 5000, normalized energy 35 %, charges 2-7) in the top speed mode. Fragments were analyzed in the linear ion trap using turbo mode with AGC target 10^4 and maximum injection time of 35 ms. The top 5 fragment ions were isolated with an isolation width of 2 Da and fragmented with a high-energy collision dissociation (HCD) represented by 65 % collision energy. For the detection of reporter ions, the MS2 spectra was processed in the Orbitrap detector (resolution 50000, maximum injection time 86 ms, AGC target 10^5). Fragmented precursor ions were excluded from repeated analysis for 20 sec.

3.2.4.7 Mass spectrometric data analysis

MS raw files were analyzed by the proteome discoverer software 2.3. For peptide identification, database searches were performed using an in-house made server (Mascot 2.6.1). Using the annotated protein sequences (SwissProt) and contaminants of the common repository adventitious proteins (cRAP) as reference databases, the MS data were searched against Mus musculus sequences. A maximum of two trypsin miss cleavages was accepted. The precursor mass tolerance was 10 ppm and the fragmentation tolerance (CID) was 0.5 Da. For a TMT10plex experiment, propionamide at cysteine was searched as static modification and oxidation at methionine was set as dynamic modification. The percolator algorithm (Käll et al. 2008) was applied to validate the mascot results. The algorithm performs a strict false discovery rate (FDR) of 0.01 based

on the q-value. Spectral identifications <0.01 were appointed to a second mascot database search (SwissProt). Semi-tryptic peptides with one miss cleavage were searched. Precursor and fragment mass tolerance parameters were kept the same. In addition to the previously mentioned dynamic modifications, acetylation at protein N-terminus was added. Quantified reporter ions were derived from the MS3 level. Peptide spectral matches (PSMs) were validated with a strict FDR of 0.01 and 'total peptide amount' was used as a normalization method.

3.2.4.8 Statistical analysis

Raw MS-data, processed by proteome discoverer 2.3, was subjected to a comparative statistical analysis. The entire (PSM-level) TMT dataset representing all the replicates of control, 6 and 24 hours starvation samples were statistically analyzed in an R environment (R 3.5.1) (R Core Team 2018) using an in-house developed workflow. The R-script was provided by Dr. Farhad Shakeri from the Core Unit for Bioinformatics Data Analysis of Bonn University Hospital. Prior to the statistical analysis, all low-quality data, namely unspecific peptides and single-hit proteins, were filtered out, and only fractions with a maximum average intensity per protein in all channels were selected. After applying the variance stabilizing normalization method (VSN 3.54.0) (Huber et al. 2002), the data were aggregated from the peptide-level to the protein-level using the robust Tukey's median polish process (Mosteller and Tukey 1977). In this statistical study, the R package Limma 3.40.0 was implemented to correct the p-values for multiple testing according to the Benjamini-Hochberg procedure (Ritchie et al. 2015).

The online software (g:Profiler) for functional enrichment analysis and conversions of gene lists was used to map genes on the Kyoto Encyclopedia of Genes and Genomes (KEGG) pathway (Raudvere et al. 2019).

Statistical graphs and diagrams were created using GraphPad Prism 6.01 (https://www.graphpad.com/), FactoMineR 1.42, ggplot2 3.2.0 and Venny 2.1 (https://github.com/benfred/venn.js) software (Oliveros 2007; Lê et al. 2008; Gu et al. 2016; Wickham 2016).

3.2.5 Metabolite analysis by mass spectrometry

The sample preparation and MS measurement of serum amino acid and acylcarnitine concentrations were carried out by Dr. Eberhard & Partner medical care center (Dortmund, Germany).

3.2.5.1 Serum sample preparation for acylcarnitine analysis

From control and starved mice, 50 µl of serum samples were mixed with 200 µl of methanol extraction buffer containing stable isotope-labeled acylcarnitines, which were used as an internal standard (IS). The mixture was centrifuged at 15.000 x g for 5 min at 4 °C using a refrigerated centrifuge. The collected supernatant was concentrated and dried under a nitrogen stream at 60°C for 20 min. Following this, acylcarnitines were derivatized to their butyl esters by adding 50 µl of an anhydrous n-butanol/HCl solution to the dried samples. After the derivatization step, the samples were concentrated and dried again under the same conditions as described above. Reconstituted samples in a 100 µl acetonitrile-based solution were then ready for ESI-MS/MS measurement.

3.2.5.2 Serum sample preparation for amino acid analysis

Before the injection into the mass spectrometer, 50 µl of control and starved mice serum samples were mixed with 200 µl of methanol extraction buffer. The extraction buffer contained stable isotope-labeled amino acids, which were used as an internal standard (IS). After the centrifugation at 15.000 x g for 5 min at 4 °C, 10 µl of the supernatant was mixed with 70 µl of borate buffer (pH 8.0) and 20 µl of 6-aminoquinolyl-n-hydroxysuccinimidyl carbamate solution leading to a substitution reaction at the primary and secondary amino groups. Processed samples were then ready for LC-MS/MS measurement.

3.2.5.3 Mass spectrometric analysis of serum acylcarnitines

After the sample preparation, the serum acylcaritine concentrations were measured using an ESI-MS/MS system. Briefly, 7 µl of the analyte mixture was directly injected into the MS ionization source without prior chromatographic separation. The ionization was conducted using a positive electrospray ionization (ESI +) mode (cone voltage 35 V, collision energy 25 V, capillary voltage 3000 V,

source temperature 120 °C). After setting the measurement mode to parent ion scan (PIS), ions within a mass range of 200-500 Da were scanned in MS1. The ions corresponding to the mass-to-charge (m/z) ratio of butylated acylcarnitines were isolated and fragmented in the collision cell containing argon gas. The characteristic fragment ion of m/z 85 Da was selected and transferred through MS2. A photomultiplier was used for the ion detection.

Since the isotope-labeled acylcarnitines from the internal standard (IS) were added in a known quantity, the concentrations of the analogous acylcarnitines (A) were calculated from the fragmentation ratios of the intensities following this formula:

$$\text{conc. acylcarnitine} = \frac{\text{Sample A}}{\text{Sample IS}} \text{ x conc. IS}$$

3.2.5.4 Mass spectrometric analysis of serum amino acids

The serum amino acid concentrations in the processed samples were measured using an LC-MS/MS system. Briefly, the liquid chromatography (LC) separation was carried out on a C18 analytical column and the autosampler was set to 1 µl per injection. The column was equilibrated using 0.1 % (v/v) formic acid. Molecules were separated at a flow rate of 0.4 ml/min during a 9 min linear gradient ranging from 1 % to 95 % using a solvent composed of 90 % (v/v) acetonitrile and 0.1 % (v/v) formic acid. The LC system was connected to a tandem mass spectrometer. The multiple reaction monitoring (MRM) mode was used for the detection of the amino acids (cone voltage 25 V, collision energy 20 V, capillary voltage 400 V, source temperature 150 °C), where only defined ions were scanned in MS1. After the fragmentation in the collision cell containing argon gas, the selected fragment ions were transferred through MS2. The internal standard (IS) was used to compensate potential effects caused by co-eluting matrix components such as the changes in the ionization and chromatographic response of target amino acids (Reviewed by Panuwet et al. 2016).

By calculating the peak area of the recorded chromatogram, the respective peaks provided quantitative information about the analyzed amino acids. The quantitative analysis was performed using a 7-point calibration standard and a blank. The calculation was based on a linear calibration function.

4 Results

4.1 Monitoring mTORC1 activity in different mouse tissues

Lysosomes can respond to changes in nutrient status via the key lysosome-associated protein mTORC1, which controls cell growth and metabolism. mTORC1 activity and localization change based on the nutrient availability in the cell, where the presence of nutrients leads to mTORC1 activation and thus to the phosphorylation of specific downstream substrates (Reviewed by Perera and Zoncu 2016; Lamming and Bar-Peled 2019). In order to monitor whether mTORC1 activity varies between the body organs upon starvation and to determine the starvation time frame in which mTORC1 is the least active, adult C57BL/6 mice were food starved for 6, 9, 12, 16 or 20 hours and control mice were fed *ad libitum* before sacrifice. From three biological replicates, the liver, skeletal muscle and brain were removed at each starvation period (Figure 4.1 A).

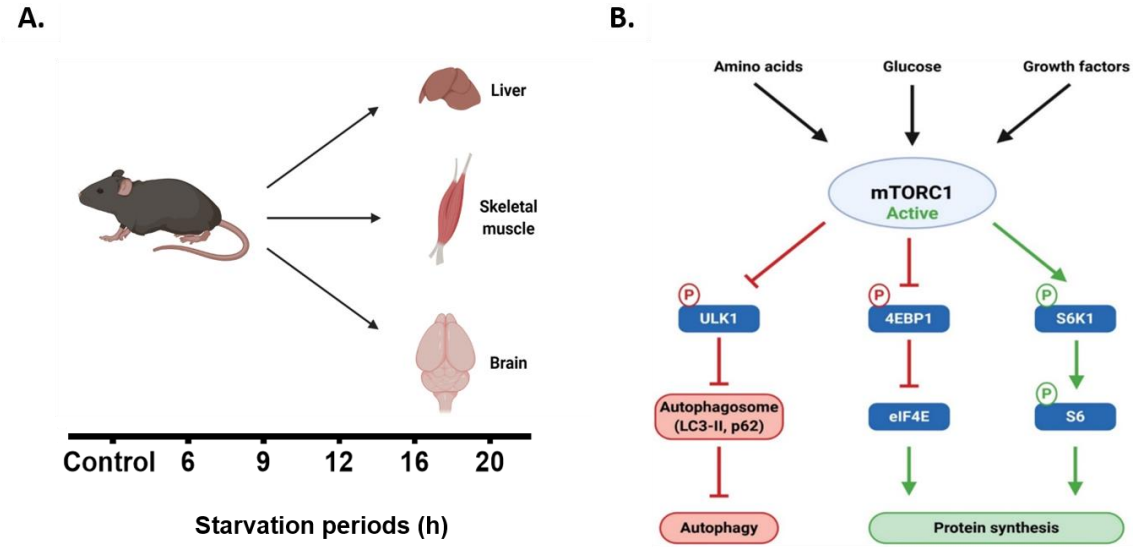

Figure 4.1: Monitoring mTORC1 activity in different mouse tissues
A. Experimental set-up of mice starvation and organ removal. Adult C57BL/6 mice were food starved for 6, 9, 12, 16 or 20 hours and control mice were fed *ad libitum* before sacrifice. The liver, skeletal muscle and brain were removed at each time period. **B.** Schematic of mTORC1 activity and its downstream targets in the presence of nutrients.

mTORC1 activity was determined by the phosphorylation of two of its downstream targets: 40S ribosomal protein S6 (S6) and eIF4E binding protein 1 (4EBP1) which are both involved in the protein synthesis pathway as well as by

the observation of autophagosome formation mediated by the microtubule-associated protein1 light chain 3 (LC3) (Figure 4.1 B).
The phosphorylation of mTORC1 downstream targets and autophagy monitoring were mainly investigated by western blotting of homogenated tissues (see 3.2.2.1 and 3.2.2.7) followed by the relative quantification of measured intensities.

4.1.1 Effect of starvation on mTORC1 activity in liver tissues

The activity of mTORC1 was first monitored in liver tissues of mice sacrificed by cervical dislocation. The liver of control and starved mice was homogenized and the proteins were separated using SDS-PAGE. Transferred proteins were examined for mTORC1 activity by antibody-based detection of the mTORC1 direct downstream target 4EBP1 phosphorylation sites T37/46, which play an important role in the protein synthesis, as well as the total 4EBP1 protein. 4EPB1 is a small 15 to 20 kDa-sized protein represented by 3 migrating isoforms named gamma, beta and alpha. Gamma (γ) is the uppermost phosphorylated isoform and alpha (α) is the lower and least phosphorylated isoform (Brunn et al. 1997). As a stable expressed protein in whole cell lysates of prokaryotic and eukaryotic samples as well as a well-known housekeeping protein (Wu et al. 2012), the detected 37 kDa Glyceraldehyde-3-phosphate dehydrogenase (GAPDH) served as a loading control. After densitometric quantification, the intensities of p-4EBP1 and total 4EBP1 within the different samples were normalized to the corresponding GAPDH signals. Figure 4.2 A shows the detected signals of p-4EBP1 and GAPDH of three biological replicates, starting from the control mice and ending with samples having starved for 20 hours. The mean GAPDH-normalized p-4EBP1 intensities and the standard error of the mean (SEM) detected in the starved sample group as well as the control are visualized in figure 4.2 B. The summed intensities of all isoforms within a sample were calculated and the control sample intensity was set to 1. Compared to control samples, the measured intensities showed a gradual decrease in the phosphorylation of 4EBP1 reaching a statistical significant decrease of 2.19- and 2.39-fold after 9 and 12 hours of starvation, respectively. Subsequently, the phosphorylation

increased after prolonged starvation with a significant 1.43- and 1.56-fold increase after 16 hours compared to 9 and 12 hours of starvation, respectively.

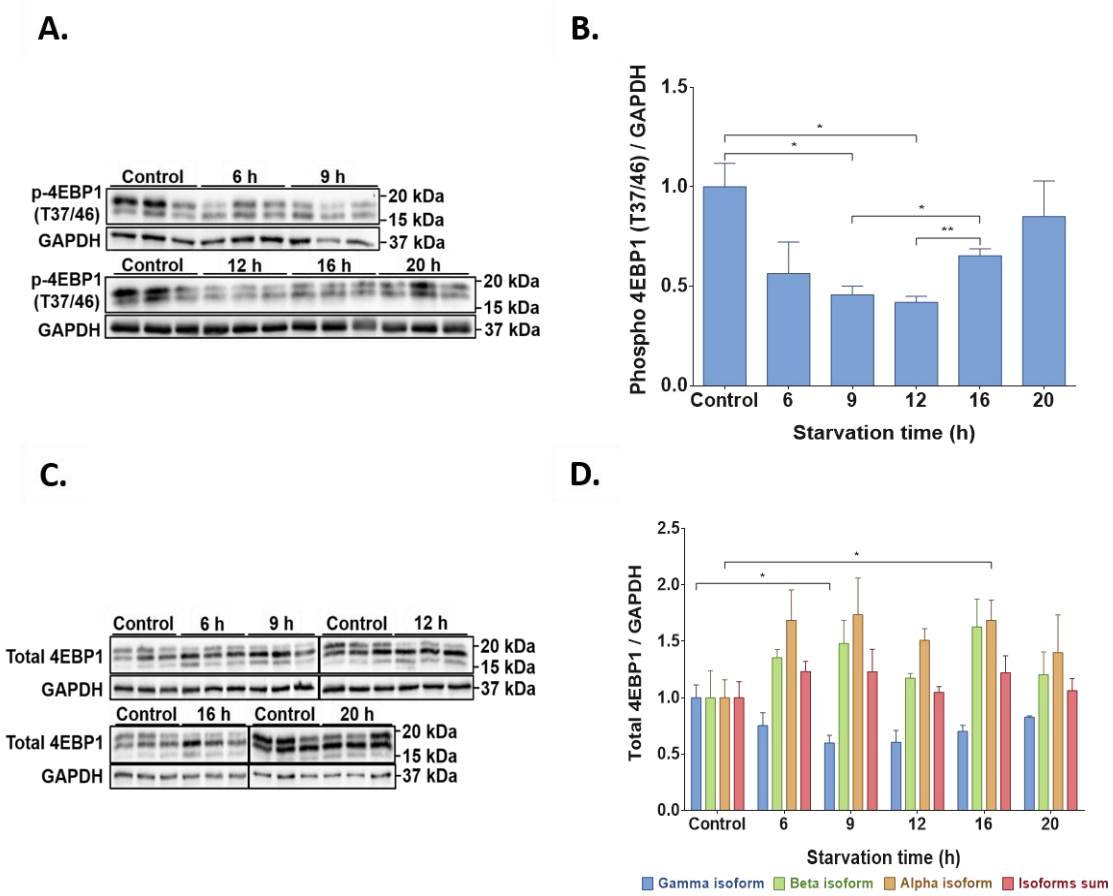

Figure 4.2: Investigation of mTORC1 activity in liver tissues by 4EBP1 immune detection
Adult C57BL/6 mice were starved for 6, 9, 12, 16 or 20 hours and control mice were fed *ad libitum* before sacrifice. After liver tissues were removed and lysed, 12 µg proteins were separated on a 12.5 % SDS-PAGE gel, transferred onto a nitrocellulose membrane and probed with antibodies. **A.** Membranes were incubated with p-4EBP1 (T37/46) as a readout of mTORC1 activity and GAPDH as a loading control. **B.** Densitometric quantified p-4EBP1 signals were normalized to the corresponding GAPDH intensity. **C.** Total 4EBP1 and GAPDH signals were visualized by immune detection. **D.** The relative protein amounts of all isoforms from control and starved sample groups are depicted as bar charts. Shown are mean + SEM; n=3 and the significance was calculated by unpaired student's t-test (*=p<0.05; **=p<0.01). Control samples were set to 1.

Figure 4.2 C displays the observed signals of total 4EBP1 and GAPDH for three biological replicates of control and starved samples, where all 4EBP1 isoforms are more prominent compared to p-4EBP1 blots. The relative quantities of total 4EBP1 were calculated as the ratio of total 4EBP1 and GAPDH signal intensities for the single replicates and the average of control and starved sample groups as well as SEM are depicted in figure 4.2 D. The summed intensities of all isoforms

as well as the single intensities of each isoform within a sample were calculated relative to total 4EBP1 intensity where the control was set to 1. The relative intensity of the uppermost phosphorylated isoform, gamma isoform, decreased after a short starvation period reaching a significant decrease of 1.67-fold after 9 hours of starvation, while its increase after prolonged starvation was not statistically significant. Furthermore, the relative intensities of the least phosphorylated isoform, alpha isoform, demonstrated no significant change except for a 1.68-fold increase relative to the control after 16 hours of starvation. In addition, the beta isoform intensities as well as the summed intensities of all isoforms displayed neither a notable pattern nor a statistically significant change for the entire starvation course.

As a second validation of mTORC1 activity in liver tissues, the 32 kDa phospho S6 ribosomal protein, an indirect downstream target, was detected by anti-phospho S6 antibody which detects the phosphorylation sites S240/244, in addition to the total S6 protein abundance. The intensities of p-S6 and total S6 were normalized to GAPDH as a loading control. The p-S6 and GAPDH signals for control and starved samples are displayed in figure 4.3 A. The mean of GAPDH-normalized p-S6 intensities and the standard error of the mean detected in all sample groups are depicted in figure 4.3 B. After comparing all starvation conditions, the unpaired student's t-test demonstrated a 4-fold decrease in S6 phosphorylation after 6 hours of starvation compared to control samples set to 1. Afterwards, the relative intensities depicted a continuous increase in the phosphorylation throughout the starvation time course, reaching its highest after 20 hours of starvation. Compared to 6 hours starved samples, phosphorylation signals at 16 and 20 hours showed a significant increase of 7.18- and 8.89-fold, respectively. Similarly, phosphorylation increased by 3.5-fold between 9 and 20 hours of starvation. In addition, a phosphorylation increase of 2.2-fold was monitored after 20 hours compared to the non-starved control samples.

After incubating the membranes with anti-S6 and anti-GAPDH antibodies (Figure 4.3 C), the plotted intensities with the standard error of the mean of normalized total S6 protein showed no significant change, except after 20 hours of starvation

with a phosphorylation increase of 1.29-, 1.34- and 1.24-fold relative to control, 12 and 16 hours starved samples, respectively (Figure 4.3 D).

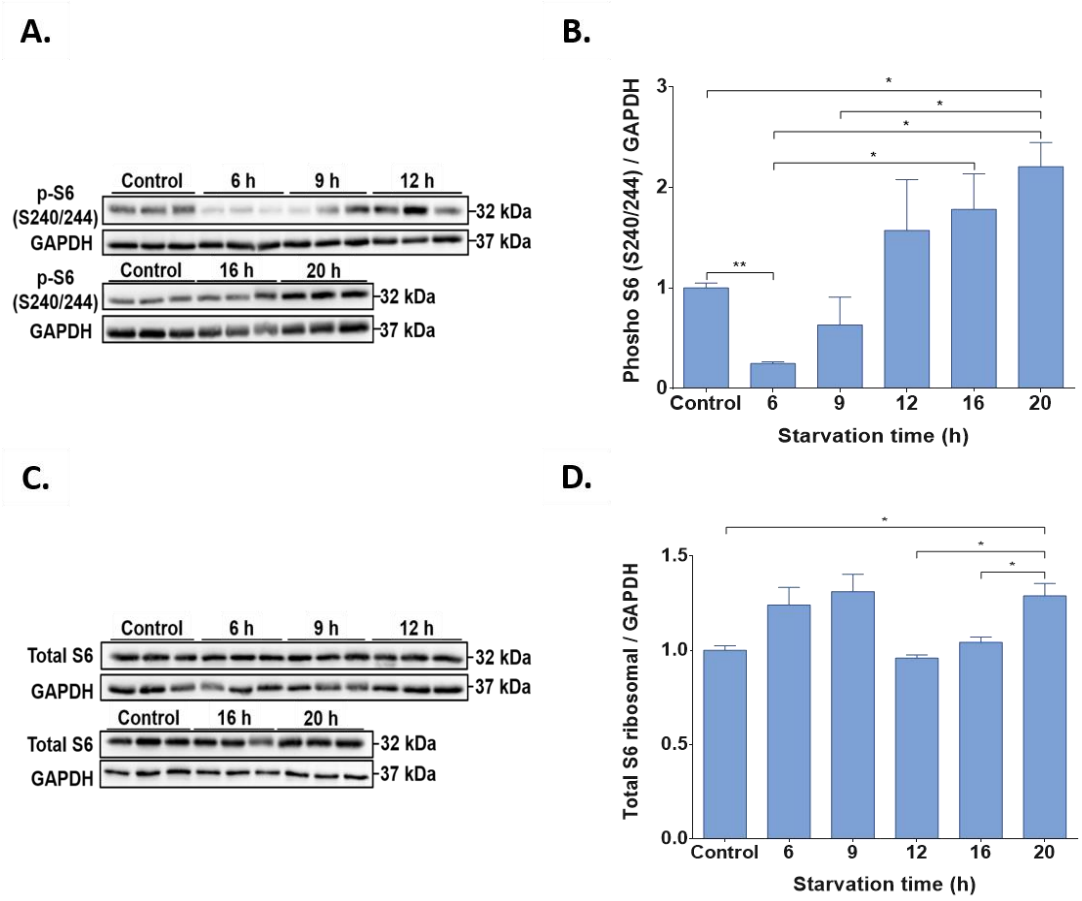

Figure 4.3: Investigation of mTORC1 activity in liver tissues by S6 immune detection
Adult C57BL/6 mice were starved for 6, 9, 12, 16 or 20 hours and control mice were fed *ad libitum* before sacrifice. After liver tissues were removed and lysed, 12 µg proteins were separated on a 12.5 % SDS-PAGE gel, transferred onto a PVDF membrane and probed with antibodies. **A.** Immune detection of p-S6 (S240/244) as a readout of mTORC1 activity and GAPDH as a loading control was performed by protein specific antibodies. **B.** The relative p-S6 intensities were depicted after normalization to the corresponding GAPDH intensities. **C.** After membrane incubation with total S6 and GAPDH antibodies, immune detected signals were visualized. **D.** For control and starved sample group, densitometric quantified total S6 signals were normalized according to their GAPDH intensities. Shown are mean + SEM; n=3 and the significance was determined by unpaired student's t-test (*=p<0.05; **=p<0.01). The control samples were set to 1.

After monitoring mTORC1 activity by the phosphorylation of S6 and 4EBP1 as two downstream targets, the results show a relevant loss in the phosphorylation levels reaching its lowest after 6 hours and a complete recovery after prolonged starvation.

4.1.2 Effect of starvation on mTORC1 activity in skeletal muscle tissues

Skeletal muscle is considered a key metabolic organ, especially during starvation (Baskin et al. 2015). Based on this fact and after showing mTORC1 activation pattern in the liver, the influence of starvation on mTORC1 in starved skeletal muscle tissues was examined. The investigation was performed in three biological replicates from control and starved mice by western blot analysis. For signal quantification, obtained intensities were normalized to GAPDH signals as a loading control. Obtained signals at 15-20 kDa and 37 kDa representing p-4EBP1 and GAPDH, respectively, are visualized in figure 4.4 A. Figure 4.4 B represents the normalized results of p-4EBP1 at each starvation period after setting the control sample to 1, with a decrease in the intensities appearing from the early starvation periods. The significance of the normalized intensities was measured using the unpaired student's t-test. By comparing the control sample to the starvation time periods, there is a gradual decrease of signal intensity until 12 hours of starvation. After 16 and 20 hours the signal increases slightly, but stays significantly below the control values. Compared to the fed state, 4EBP1 phosphorylation decreased by 1.60-, 7.85-, 4.58- and 2.41-fold after 9, 12, 16 and 20 hours of starvation, respectively. Compared to 9 hours starved samples, a 4.89- and 2.86-fold decrease was measured after 12 and 16 hours of starvation, respectively. In figure 4.4 C, samples were subjected to western blotting using antibodies directed against total 4EBP1 and GAPDH proteins. Figure 4.4 D depicts the quantification of immune detected signals relative to control samples which were set to 1. The amount of gamma isoform, the uppermost phosphorylated isoform, dropped starting from 12 hours in contrast to increased alpha isoform amount, showing a reduction in 4EBP1 phosphorylation. In parallel, the beta isoform levels were not affected by starvation. Statistical analysis was applied to gamma, beta and alpha isoforms as well as the sum of all isoforms at each starvation period, and demonstrated no statistical change in the intensities at the early starvation time periods. On average, the gamma isoform revealed a significant decrease of 3.4-, 2.78- and 2.73-fold compared to control, 6 and 9 hours, respectively, starting from 12 hours of starvation. In contrast, alpha isoform amounts increased substantially after 12 and 16 hours compared to control, 6

and 9 hours starved samples. The increase was by 3.13- and 2.76-fold (control), 2.62- and 2.33-fold (6 hours) as well as 3.1- and 2.75-fold (9 hours), all after 12 and 16 hours, respectively.

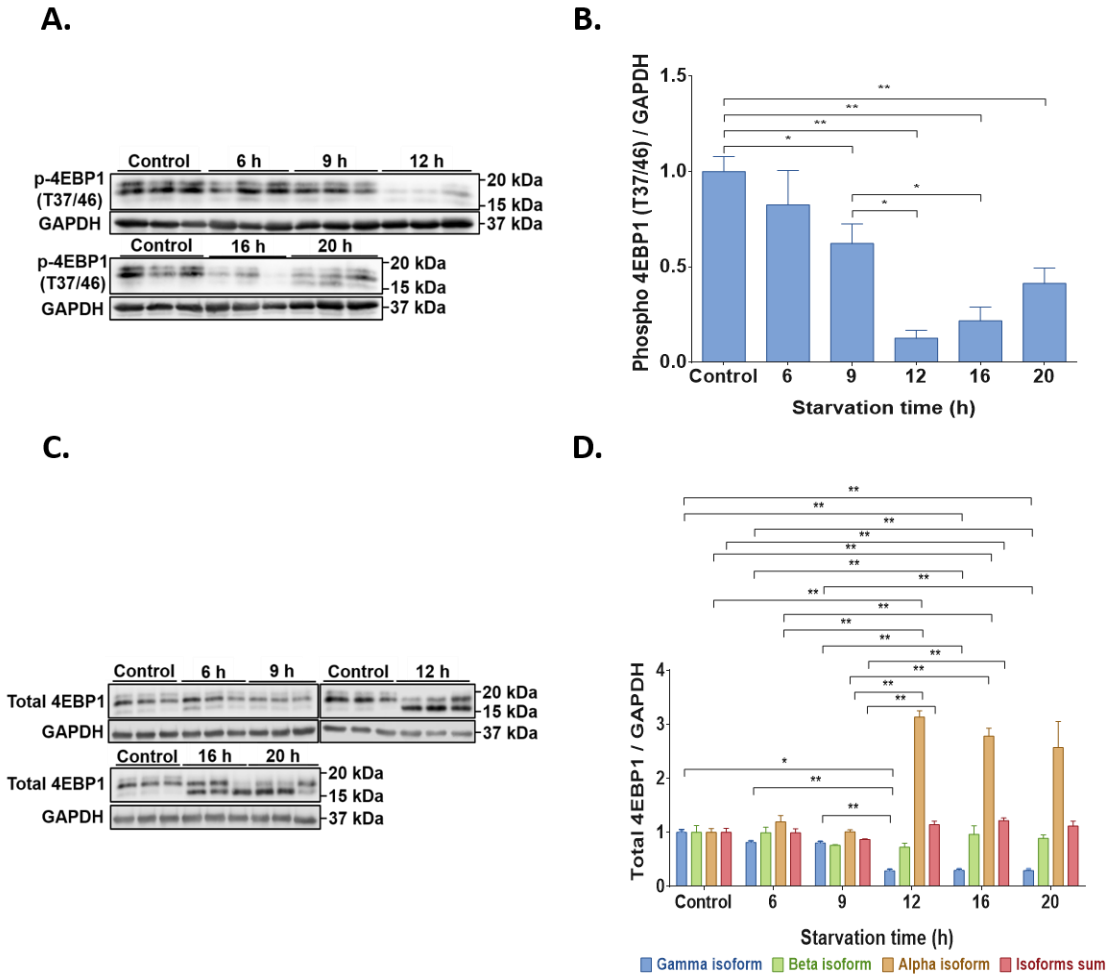

Figure 4.4: Investigation of mTORC1 activity in skeletal muscle tissues by 4EBP1 immune detection
Adult C57BL/6 mice were starved for 6, 9, 12, 16 or 20 hours and control mice were fed *ad libitum* before sacrifice. After skeletal muscle tissues were removed and lysed, 12 µg proteins were separated on a 12.5 % SDS-PAGE gel, transferred onto a nitrocellulose membrane and probed with antibodies. **A.** Obtained signals from p-4EBP1 (T37/46) and the loading control GAPDH were visualized. **B.** Densitometric quantified and normalized intensities are depicted as bar charts. **C.** Western blot signals of total 4EBP1 and GAPDH proteins were displayed. **D.** For all conditions and isoforms, intensities were normalized to GAPDH signals. Shown are mean + SEM; n=3 and the significance was determined by unpaired student's t-test (*=p<0.05; **=p<0.01). The control samples were set to 1.

The comparison of the sum of the isoforms under all conditions depicted no significant change except for an increase of 1.22-fold between the control and 16 hours starved samples. In addition, a 1.32- and 1.4-fold increase after 12 and 16 hours was calculated relative to 9 hours. As a measure of the mean distribution

of the samples, the standard error of the mean (SEM) was applied (Figure 4.4 B, D).

In addition to 4EBP1, signals of total S6 and p-S6 were detected by western blot and GAPDH-normalized intensities were subjected to the unpaired student's t-test. Figure 4.5 A shows the immune detected signals of p-S6 and the loading control GAPDH where low protein abundances were seen in all starvation periods relative to control samples except of 9 hours starved samples.

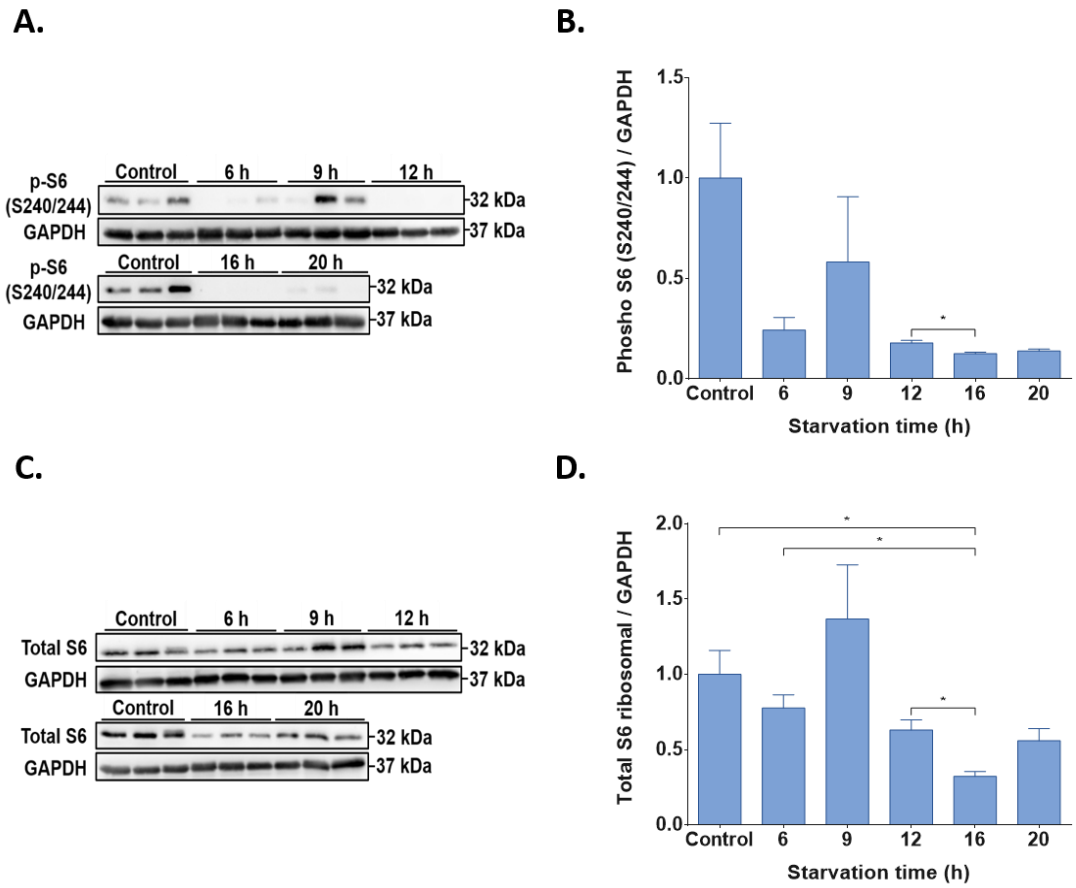

Figure 4.5: Investigation of mTORC1 activity in skeletal muscle tissues by S6 immune detection

Adult C57BL/6 mice were starved for 6, 9, 12, 16 or 20 hours and control mice were fed *ad libitum* before sacrifice. After skeletal muscle tissues were removed and lysed, 12 µg proteins were separated on a 12.5 % SDS-PAGE gel, transferred onto a nitrocellulose membrane and probed with antibodies. **A.** Western blotting of p-S6 (S240/244) and the loading control GAPDH. **B.** Quantified signals were normalized to the corresponding loading control intensities. **C.** Total S6 and GAPDH signals were detected in skeletal muscle samples of control and starved mice. **D.** The level of total S6 in each sample was normalized to the GAPDH level. Shown are mean + SEM; n=3 and the significance was determined by unpaired student's t-test (*=p<0.05). The control samples were set to 1.

After setting the control sample to 1, the average of normalized p-S6 with the SEM are depicted in figure 4.5 B, where S6 phosphorylation showed a statistical

decrease of 1.43-fold between 12 and 16 hours of starvation. Although p-S6 abundance showed a decrease up from 6 hours of starvation, however this decrease was not statistically significant. The second replicate of 9 hours starved mice, which showed a strong signal intensity, was considered an outlier and was excluded from the calculation of the mean abundance. Therefore, the unpaired student's test is not reliable at 9-hour starvation period.

As for p-S6, total S6 together with GAPDH signals are visualized in figure 4.5 C and the relative intensities as well as the standard error of the mean are shown in figure 4.5 D. The obtained signals showed a varying pattern throughout the time course of starvation. The unpaired student's t-test showed a statistical decrease of 3.11-, 2,41- and 1.96-fold after 16 hours in correlation with control, 6 and 12 hours starved samples, respectively.

Regarding the results obtained from the starved skeletal muscle tissues, phosphorylation of 4EBP1 and S6 indicates a gradually decreased level by increasing the duration of starvation.

4.1.3 Effect of starvation on mTORC1 activity in brain tissues

As one of the most active metabolic organs in the body, the brain is supplied with several fuel sources for cerebral metabolism under different nutrient conditions (Owen et al. 1967; Hasselbalch et al. 1994; Clarke and Sokoloff 1999). In addition to liver and skeletal muscle tissues, starvation-mediated changes in mTORC1 activity was examined in brain tissues from three biological replicates by western blot. To quantify the detected signals, probed samples with 4EBP1, S6 and their phospho forms-specific antibodies were normalized to GAPDH as a loading control. Control samples were set to 1 and the standard error of the mean was used to calculate the distribution of the sample.

Signals obtained from p-4EBP1 and GAPDH are shown in figure 4.6 A. The unpaired student's t-test of normalized signals depicted no significant changes in phosphorylation except for a 1.21-fold decrease between 9 and 16 hours of starvation (Figure 4.6 B).

Figure 4.6 C represents total 4EBP1 detected signals along with their corresponding loading control. Densitometric quantified signals of total 4EBP1

were normalized to GAPDH. The levels of gamma, beta and alpha isoforms were relatively stable during the starvation course, except for the alpha isoform at the starvation period of 12 hours (Figure 4.6 D). At this starvation period, alpha isoform normalization revealed a 1.48-, 1.29- and 1.6-fold increase compared to control, 6- and 9-hour starvation periods, respectively. In addition, a decrease of 1.23-fold was also measured between 12 and 16 hours of starvation by unpaired student's t-test.

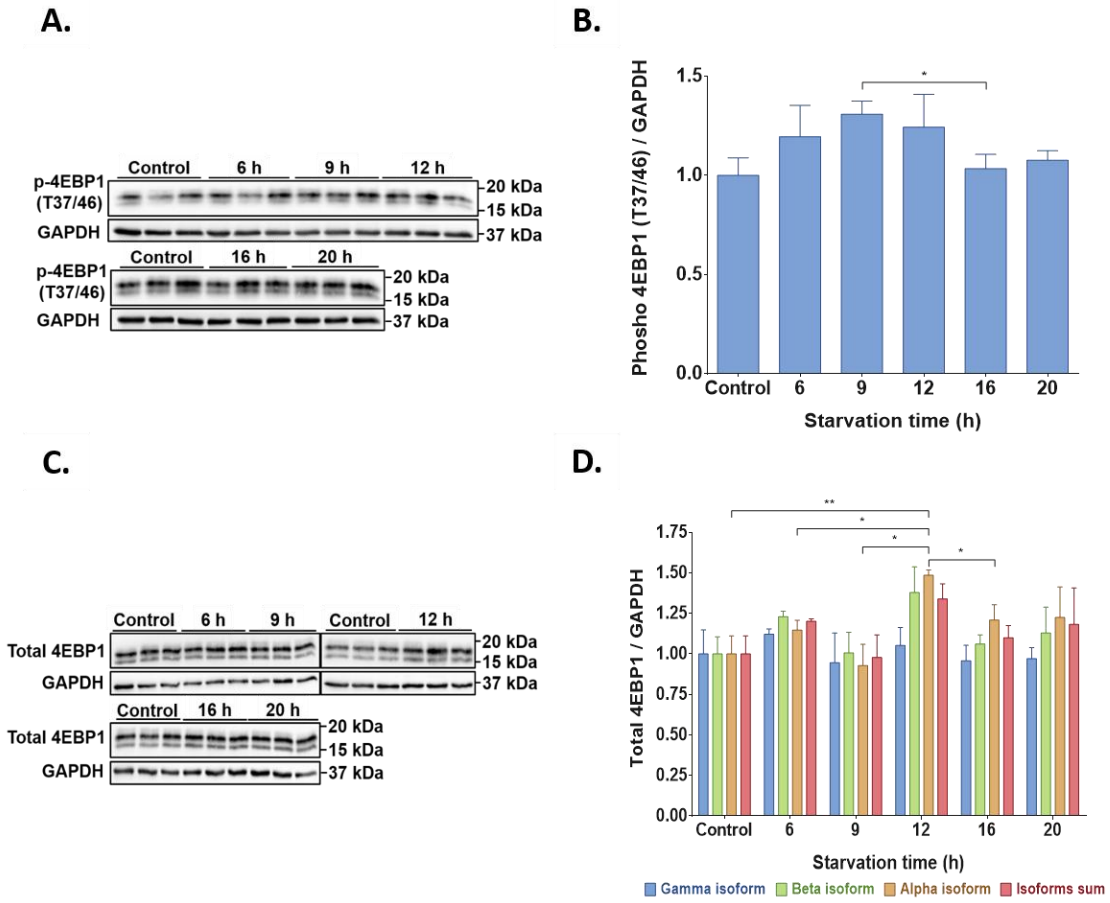

Figure 4.6: Investigation of mTORC1 activity in brain tissues by 4EBP1 immune detection

Adult C57BL/6 mice were starved for 6, 9, 12, 16 or 20 hours and control mice were fed *ad libitum* before sacrifice. After brain tissues were removed and lysed, 12 µg proteins were separated on a 12.5 % SDS-PAGE gel, transferred onto a nitrocellulose membrane and probed with antibodies. **A.** Signals of p-4EBP1 (T37/46) as a readout of mTORC1 activity and GAPDH as a loading control were detected by western blot. **B.** The protein abundance was densitometrically quantified and normalized to GAPDH. **C.** After probing the samples with protein-specific antibodies, total 4EBP1 and GAPDH signals were visualized. **D.** Relative abundances of different starvation periods were depicted after GAPDH normalization. Shown are mean + SEM; n=3 and the significance was determined by unpaired student's t-test (*=p<0.05; **=p<0.01). The control samples were set to 1.

As a second observed downstream target of mTORC1, phosphorylated S6 ribosomal protein signals were detected during the starvation experiment (Figure 4.7 A). The uniformity of GAPDH signals served as a loading control. The starvation periods analyzed showed no significant changes between the normalized samples during different starvation periods except for a 1.73-fold decrease between control and 12 hours of starvation (Figure 4.7 B). Figure 4.7 C depicts the signals observed after incubating the membrane with anti-total S6 and anti-GAPDH antibodies. Normalized total S6 intensities showed no significant differences in control or starved brain tissues (Figure 4.7 D).

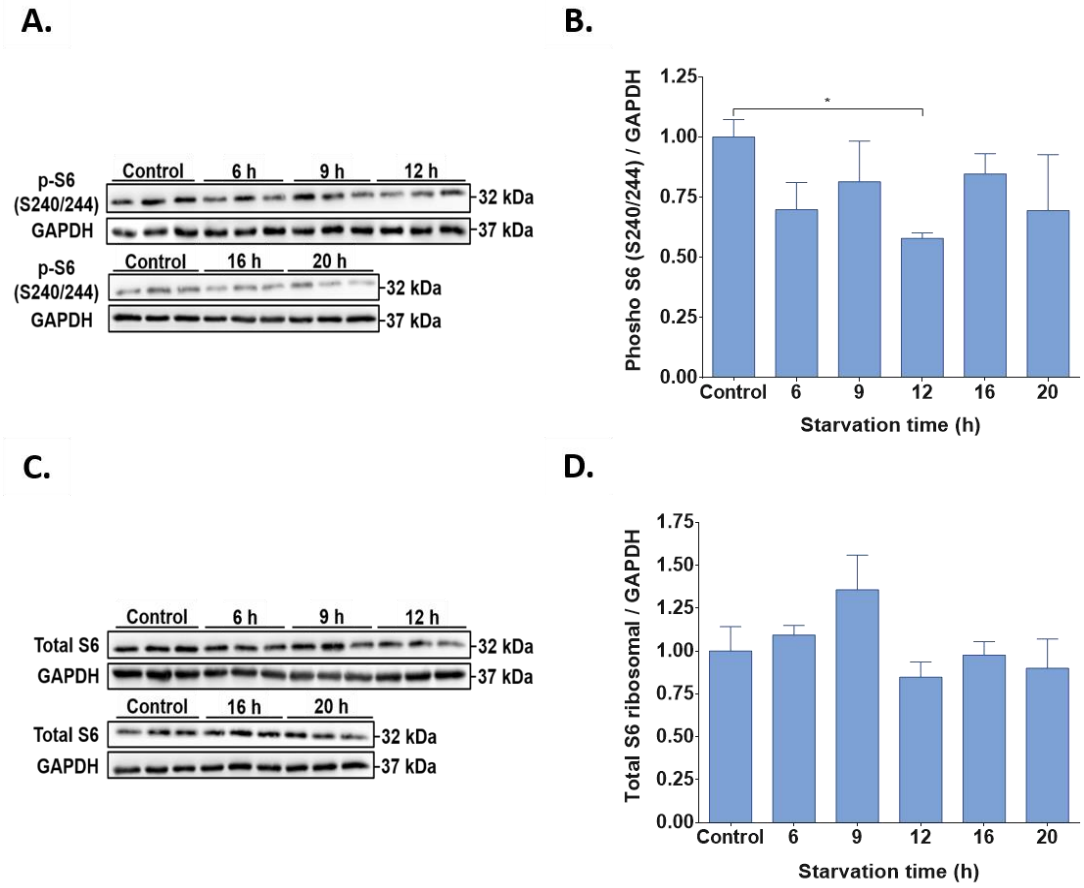

Figure 4.7: Investigation of mTORC1 activity in brain tissues by S6 immune detection

Adult C57BL/6 mice were starved for 6, 9, 12, 16 or 20 hours and control mice were fed *ad libitum* before sacrifice. After brain tissues were removed and lysed, 12 µg proteins were separated on a 12.5 % SDS-PAGE gel, transferred onto a nitrocellulose membrane and probed with specific antibodies. **A.** Brain homogenate analysis after incubation with p-S6 (S240/244) and GAPDH antibodies. **B.** Relative p-S6 quantification results normalized to the loading control are depicted as bar charts. **C.** Immune detection of total S6 and GAPDH signals. **D.** After densitometric quantification, the mean abundance values of total S6 normalized intensities are displayed. Shown are mean + SEM; n=3 and the significance was determined by unpaired student's t-test (*=p<0.05). The control samples were set to 1.

The results acquired from the starved brain tissues depict that the abundance levels of mTORC1 downstream targets and their phosphorylation show no relevant change during the 20 hours of starvation.

4.1.4 Autophagy induction in liver, skeletal muscle and brain tissues

Since autophagy activation is tightly regulated by mTORC1 and starvation-induced autophagy indicates mTORC1 inactivation (Kim et al. 2011), it was examined to monitor mTORC1 activity in different mouse tissues. The lysosome-mediated degradation of cytosolic material could be enhanced as a response to cellular damage and nutrient deprivation (Reviewed by Singh and Cuervo 2011; Reviewed by Yim and Mizushima 2020). Microtubule-associated protein 1 light chain 3 (LC3) is an indicator of autophagosome biogenesis via its conversion of a cytosolic LC3-I form to lipid bound LC3-II form, which binds to the autophagic membranes (Kabeya et al. 2000). LC3 has three isoforms, namely LC3A, B and C, with the first two being preserved in mice (Cann et al. 2008).

In this experiment, LC3B isoform was used as an autophagy marker. In the presence and absence of food intake, autophagy activation was monitored in liver, skeletal muscle and brain tissues via western blot. SDS-PAGE separated proteins were blotted and probed with LC3B and GAPDH antibodies. Since LC3B-II is bound to the autophagosomal membrane and is subject to lysosomal degradation, the detected signals of LC3B-II normalized to GAPDH correspond to the levels of autophagosomes (Reviewed by Klionsky et al. 2016). For a more informative picture of the cellular autophagic response, LC3B-II was normalized to LC3B-I and the ratio was measured (Kabeya et al. 2004; Tanida et al. 2005). At each starvation condition, three biological replicates were used. The distribution of the sample means was measured via the standard error of the mean (SEM) after setting the control samples to 1.

Figure 4.8 A shows the detected signals of the 16 kDa LC3B-I and the 14 kDa LC3B-II as well as GAPDH as a loading control in liver tissues. The GAPDH-normalized LC3B-II intensities depicted a gradual increase reaching their highest after 9 and 12 hours of starvation with a statistical significant increase of 3.68- and 3.64-fold, respectively, compared to control samples. A 1.82-fold increase

was also measured between the control and 16 hours starved samples. Subsequently, the intensities decreased by 2.02- and 2.84-fold after 16 and 20 hours compared to 9 hours of starvation, respectively. In addition, a decrease of 2.81-fold was monitored between 12 and 20 hours of starvation. In parallel, the measured LC3B-II/LC3B-I ratio in liver lysates showed a similar pattern with an increase of 1.51- and 1.58-fold after 9 and 12 hours of starvation, respectively, compared to control samples. The ratio then decreased by 2.6- and 2.73-fold after 20 hours compared to 9 and 12 hours, respectively.

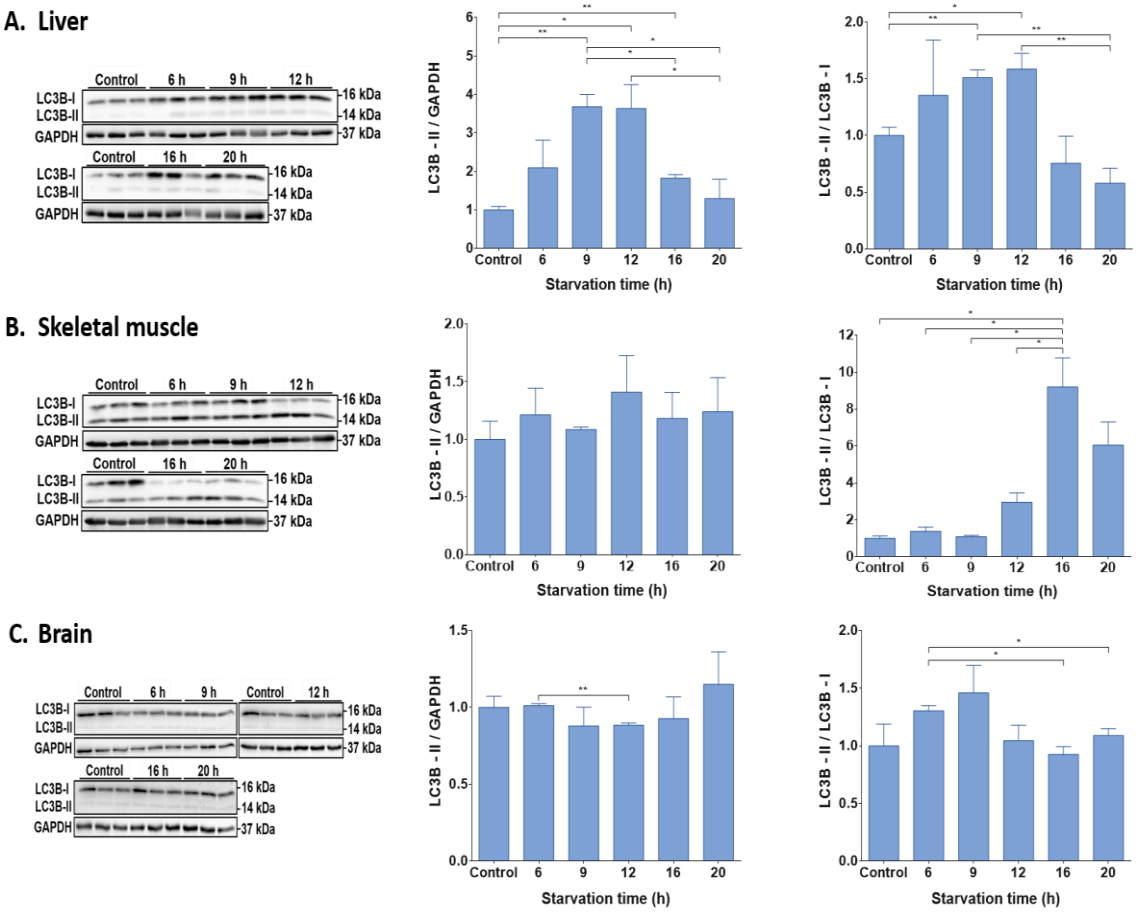

Figure 4.8: Levels of LC3B in different tissues of starved mice
Adult C57BL/6 mice were starved for 6, 9, 12, 16 or 20 hours and control mice were fed *ad libitum* before sacrifice. After liver, skeletal muscle and brain tissues were removed and lysed, 12 µg proteins were separated on a 12.5 % SDS-PAGE gel, transferred onto a nitrocellulose membrane and probed with LC3B as an autophagosome marker and GAPDH as a loading control. **A-C.** The protein abundance was densitometrically quantified and LC3B-II signals were normalized to GAPDH and LC3B-I intensities. The average relative intensities are shown as bar charts for the three different tissues. Shown are mean + SEM; n=3 and the significance was determined by unpaired student's t-test (*=p<0.05; **=p<0.01). The control samples were set to 1.

In skeletal muscle, figure 4.8 B displays the protein amounts of LC3B-I and -II together with GAPDH. The intensities of normalized LC3B-II demonstrated no statistical significant change throughout the starvation course. Meanwhile, the abundance of LC3B-II signals was getting more distinct than LC3B-I the longer the starvation occurs. This shift was also measured after applying the unpaired student's t-test to the LC3B-II/LC3B-I ratio. At the early starvation time periods, no change in the intensities was monitored. Next, after 16 hours, LC3B-II/LC3B-I ratio increased by 9.21-, 6.66-, 8.46- and 3.12-fold compared to control, 6, 9 and 12 hours starved samples, respectively.

In figure 4.8 C, brain homogenates were incubated with LC3B and GAPDH specific antibodies and a very low abundance of LC3B-II was observed. LC3B-II signals were normalized to GAPDH and no statistical significant change was measured except for a 1.14-fold decrease between 6 and 12 hours of starvation. At the same time, LC3B-II signals were normalized to LC3B-I and the intensities decreased by 1.41- and 1.2-fold after 16 and 20 hours, respectively, compared to 6 hours of starvation. No further significant change was recorded.

These findings suggest that autophagy takes place when mTORC1 is least active, consistent with previous observations of protein synthesis regulation by mTORC1.

4.2 Analysis of short- and long-term starvation and their impact on body metabolism in wild-type mice

Metabolism of the main energy sources glucose, fatty acids and amino acids can vary as a response to different starvation situations. Although starvation is usually accompanied by weight and energy loss, the body adapts by producing other fuel molecules such as ketone bodies (Berg et al. 2002a).

Findings of starvation experiments in key metabolic organs demonstrated interesting response mechanisms to short and prolonged nutrient deprivation on the molecular level. In liver tissues, phosphorylation of downstream targets by mTORC1 was decreased after short starvation and autophagy occurred. In contrast, prolonged starvation demonstrated a reactivation in downstream targets phosphorylation and a decline in starvation-mediated autophagy. Therefore, two

starvation periods with different molecular impacts, namely 6 and 24 hours, were selected and the effect of starvation on body and cellular metabolism was investigated.

From control, 6 and 24 hours starved mice for later lysosome enrichment experiment, the body weight and the whole blood glucose levels were tested too. In addition, the concentrations of ketone bodies, acylcarnitines, amino acids and their derivatives were also measured in the serum of the same sacrificed mice.

4.2.1 Investigation of body weight and blood glucose levels

Weight loss is strongly associated with the lack of energy intake and is often used as an indicator of starvation (Dokken and Tsao 2007). To evaluate the influence of short and long starvation periods on the body weight, control and starved mice were weighed using a lab animal scale with a dynamic weighing mode.

The documentation of body weight was performed for all mice that were included in this study and therefore in 18, 14 and 12 biological replicates representing control, 6 and 24 hours starved mice, respectively. The average weight of each condition and the standard error of the mean are represented in the bar chart as a percentage of the original body weight (Figure 4.9).

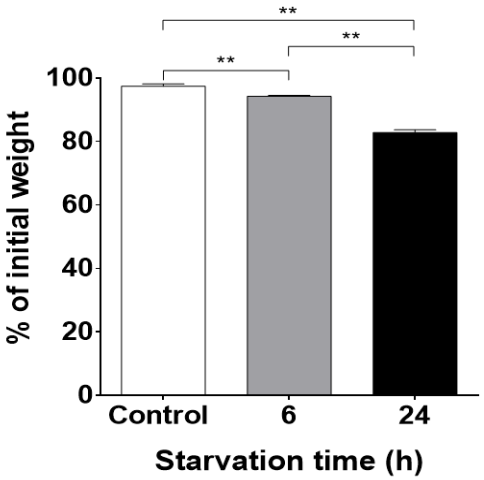

Figure 4.9: Weight changes induced by starvation in mice
6-month-old male wild-type mice were starved for 6 or 24 hours and control mice were fed *ad libitum* before the body weight was measured. Average weights are depicted as a percentage of the initial weight. Samples from control (n=18), 6 hours (n=14) and 24 hours (n=12) starved mice were statistically analyzed. Shown are mean + SEM and the significance was calculated by unpaired student's t-test (**=p<0.01).

Compared to control mice, the body weight decreased significantly by 3.18 % and 14.6 % after 6 and 24 hours of starvation, respectively. In parallel, a significant weight loss of 11.42 % was calculated between 6 and 24 hours starved mice (Figure 4.9).

As a simple carbohydrate involved in many metabolic processes, glucose oxidation is responsible for most of the energy produced at rest and its consumption is mainly spared for the brain during prolonged starvation (Unger et al. 1963; Brosnan 1999). Using a glucose meter, blood glucose levels were measured in control and starved mice after sacrifice (see 3.2.2.5).

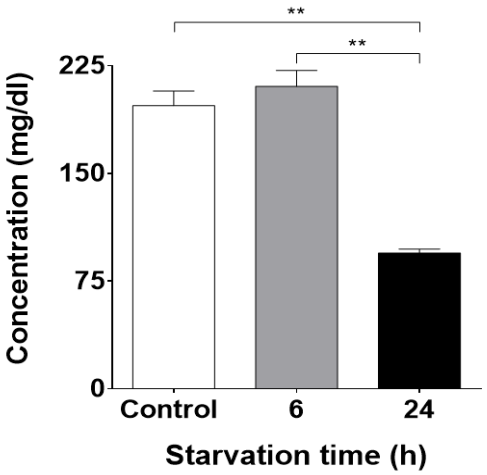

Figure 4.10: Monitoring blood glucose levels in starved mice
6-month-old male wild-type mice were starved for 6 or 24 hours and control mice were fed *ad libitum* before sacrifice. Blood glucose level was tested using a blood glucose meter. Average concentrations (mg/dl) were calculated to each group. Samples from control (n=12), 6 hours (n=8) and 24 hours (n=12) starved mice were statistically analyzed. Shown are mean + SEM and the significance was calculated by unpaired student's t-test (**=p<0.01).

The experiment was performed in 12, 8 and 12 biological replicates representing control, 6 and 24 hours starved mice, respectively. The average concentrations (mg/dl) of each group as well as the standard error of the mean are depicted in figure 4.10. Compared to control samples, no change was monitored after short period of starvation. In addition, after 24 hours of starvation, blood glucose levels showed a significant decrease of 2.1- and 2.23-fold compared to control and 6 hours starved mice, respectively.

Monitored body weight and circulating glucose concentrations after starvation show a drop mainly after prolonged starvation.

4.2.2 Investigation of ketone body metabolism

In physiological states where glucose supply is limited for example under prolonged starvation conditions, the three ketone bodies acetoacetate, beta-hydroxybutyrate and acetone are produced as a potential source of energy for peripheral tissues such as brain and skeletal muscles (Robinson and Williamson 1980; Newman and Verdin 2014). To verify this notion, concentrations of ketone bodies were monitored using a colorimetric beta-hydroxybutyrate assay. Furthermore, the relative expression of genes involved in the ketogenesis pathway was determined by quantitative real-time PCR (qPCR).

4.2.2.1 Verification of ketone body production by β-HB assay

After mice sacrifice, concentrations of beta-hydroxybutyrate (β-HB) in control and starved mice serum were measured by a colorimetric enzyme assay. The experiment was performed in 12, 8 and 12 biological replicates representing control, 6 and 24 hours starved mice, respectively. The average concentration (nmol/µl) and the standard error of the mean of each mouse group is depicted in figure 4.11. The data significance was examined by unpaired student's t-test. Compared to control mice, ketone body production increased by 2.04- and 5.01-fold after 6 and 24 hours of starvation, respectively. Moreover, a 2.46-fold increase between 6 and 24 hours starved mice was monitored (Figure 4.11).

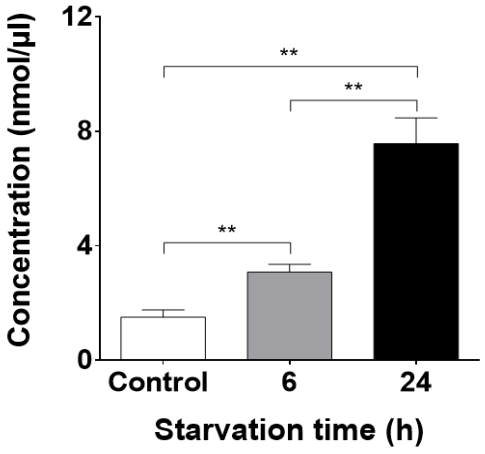

Figure 4.11: Serum concentration of ketone bodies in starved mice
6-month-old male wild-type mice were starved for 6 or 24 hours and control mice were fed *ad libitum* before sacrifice. Blood serum was collected from each group and the average concentrations of ketone bodies (nmol/µl) were measured by beta-hydroxybutyrate colorimetric assay. Samples from control (n=12), 6 hours (n=8) and 24 hours (n=12) starved mice were statistically analyzed. Shown are mean + SEM and the significance was calculated by unpaired student's t-test (**=p<0.01).

4.2.2.2 Analysis of ketogenesis-related gene expression by qPCR

Mitochondrial 3-hydroxy-3-methylglutaryl-COA synthase 2 (Hmgcs2), a key ketogenic enzyme, and carnitine palmitoyl transferase 1a (Cpt1a) are involved in fatty acid oxidation and ketogenesis. Both are regulated by peroxisome proliferator-activated receptor alpha (Pparα), which is activated under prolonged starvation conditions (Song et al. 2010; Newman and Verdin 2014).

As an additional method to analyze the production of ketone bodies, the expression of Pparα, Hmgcs2 and Cpt1a as three candidate genes involved in the synthesis of ketone bodies, was monitored in liver tissues of control and starved mice. After RNA isolation and cDNA synthesis, the gene expression was quantified by real-time PCR (see 3.2.1.4). Three biological replicates represented each condition, except for 24 hours with four biological replicates. Fold changes were analyzed by $2^{-\Delta\Delta Ct}$ method (Livak and Schmittgen 2001) and the average relative expression is depicted in figure 4.12.

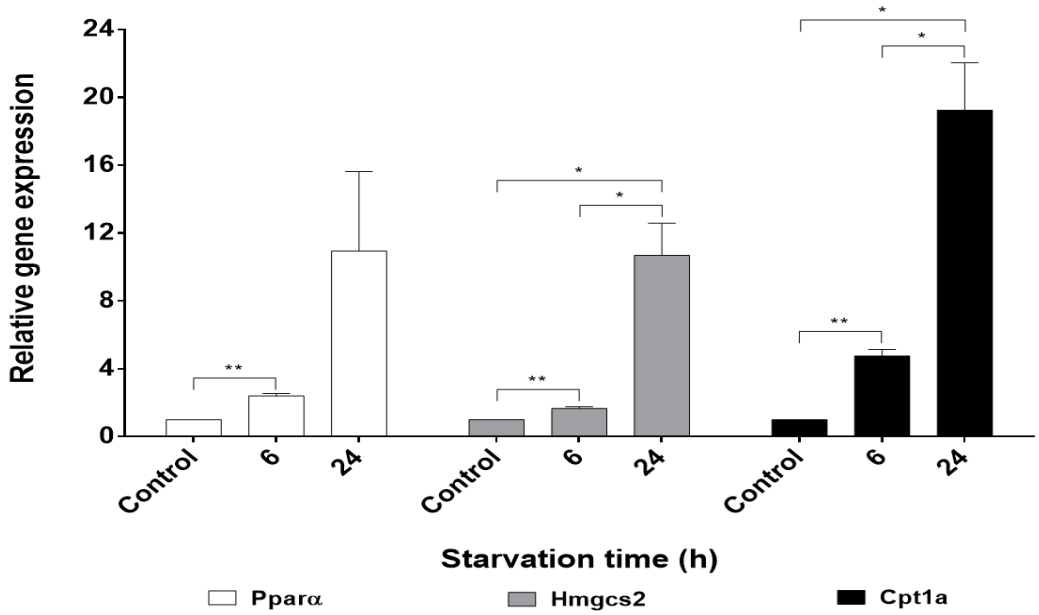

Figure 4.12: Relative expression of candidate genes in starved mice
6-month-old male wild-type mice were starved for 6 or 24 hours and control mice were fed *ad libitum* before RNA was isolated from liver tissues. After cDNA synthesis, 125 µg of cDNA and SYBR© Select Master Mix were used to quantify the gene expression by real-time PCR. Fold changes of ketogenesis-related genes (Pparα, Hmgcs2 and Cpt1a) were analyzed by $2^{-\Delta\Delta Ct}$ method. Samples from control (n=3), 6 hours (n=3) and 24 hours (n=4) starved mice were statistically analyzed. Shown are mean + SEM and the significance was calculated by unpaired student's t-test (*=p<0.05; **=p<0.01).

Relative expression of Pparα showed an increase after starvation. In comparison to control mice, a significant increase of 2.4-fold after 6 hours of starvation was measured, while the increase after 24 hours was not statistically significant (Figure 4.12).

Regarding Hmgcs2 relative expression to control mice, a significant increase was determined for both starvation time periods. The increase was by 1.66- and 10.68-fold after 6 and 24 hours, respectively. Subsequently, the expression values increased by 6.43-fold between 6 and 24 hours of starvation (Figure 4.12).

Finally, Cpt1a-expression values expressed a continuous increase after short and prolonged starvation. Relative to control samples, an increase of 4.76- and 19.24-fold after 6 and 24 hours of food deprivation, respectively, was measured. In addition, a 4.04-fold of significant increase in expression was monitored after 24 hours compared to 6 hours of starvation (Figure 4.12).

Based on the acquired data from beta-hydroxybutyrate concentrations and the relative expression of ketogenesis-related genes, a progressive increase in ketone body production throughout the starvation time course can be observed.

4.2.3 Investigation of acylcarnitine concentrations in whole blood serum

Acylcarnitines, esters of fatty acids and L-carnitines, are involved in long-chain fatty acid mitochondrial β-oxidation to produce cell-function energy (Kerner and Hoppel 2000). They differ between short, medium and long-chain acylcarnitines based on the acyl group length. To indicate the effect of short- and long starvation on fatty acid metabolism, whole blood serum of fed and starved mice was collected after sacrifice. After the derivatization of extracted acylcarnitines to their butyl esters, the concentrations were determined using ESI-MS/MS. The levels of 30 acylcarnitines were measured (Supplementary table 8.1), while significantly changed metabolites after starvation are shown in figure 4.13, 4.14 and 4.15. The experiment was performed in 12, 8 and 12 biological replicates representing control, 6 and 24 hours starved mice, respectively. Concentrations (µmol/l) and the SEMs of differentially long acylcarnitines are depicted as bar charts. Results were subjected to unpaired student’s t-test to examine the significant changes.

In figure 4.13, the concentrations of acylcarnitines (C0-C6) showed no significant change between control and 6 hours starved mice. In contrast, a significant decrease in the serum was monitored after prolonged starvation compared to control or 6 hours starved mice. After 24 hours, the concentrations of acylcarnitines C0, C2, C3, C4, C5 and C6 decreased by 1.82-, 1.41-, 1.96-, 3.76-, 2.19- and 3.74-fold compared to control mice, respectively. In a parallel comparison to 6-hour starvation period, C0, C2, C5 and C5OH acylcarnitines showed a decrease of 1.92-, 1.68-, 1.77- and 1.7-fold after 24 hours, respectively.

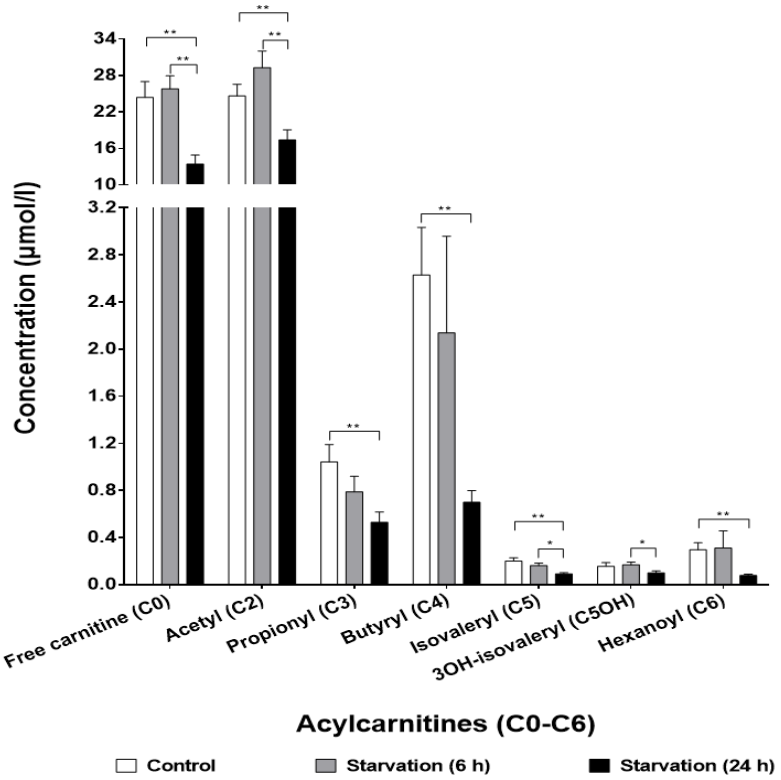

Figure 4.13: Acylcarnitine (C0-C6) concentrations in serum of starved mice
6-month-old male wild-type mice were starved for 6 or 24 hours and control mice were fed *ad libitum* before sacrifice. Blood serum was collected from each group and the average concentrations (µmol/l) of acylcarnitines (C0-C6) were measured using ESI-MS/MS. Samples from control (n=12), 6 hours (n=8) and 24 hours (n=12) starved mice were statistically analyzed. Shown are mean + SEM and the significance was calculated by unpaired student's t-test (*=p<0.05; **=p<0.01).

Acylcarnitines with longer chain lengths demonstrated no statistical significant change between control and 6 hours starved mice with the exception of a significant 1.72-fold increase of tetradecenoyl (C14:1). Subsequently, the concentrations increased significantly after prolonged starvation in mice serum (Figure 4.14 and 4.15). After the long starvation period, concentrations of C10,

C10:1, C12, C14, C14:1 and C14:2 acylcarnitines increased by 1.88-, 1.82-, 2.04-, 3.69-, 4.17- and 3.45-fold compared to fed mice, respectively. Equal to previous findings but in comparison to 6-hour starvation period, C10:1, C12, C14, C14:1 and C14:2 concentrations increased by 1.62-, 2.21-, 2.46-, 2.42- and 2.63-fold after 24 hours, respectively (Figure 4.14).

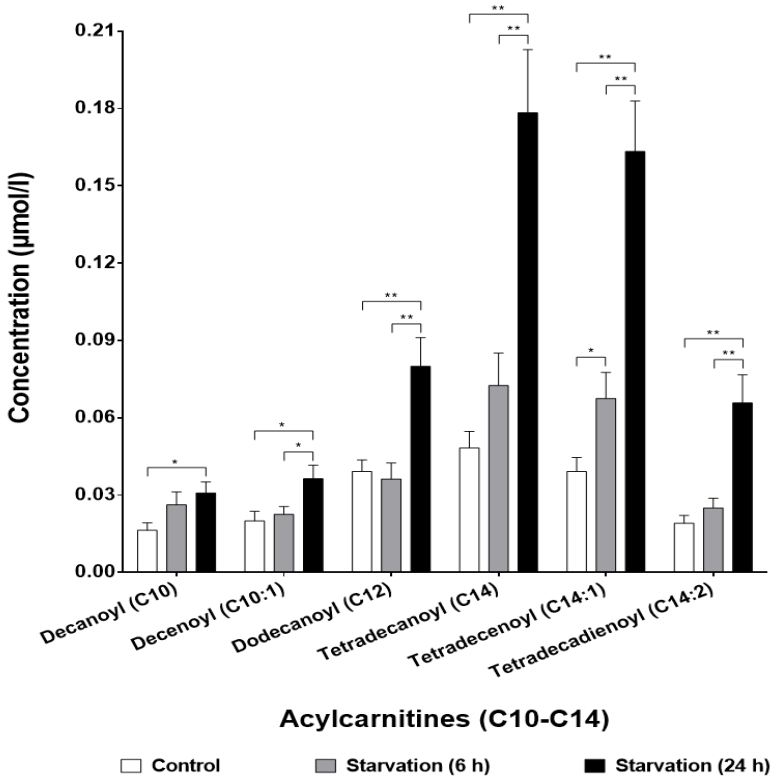

Figure 4.14: Acylcarnitine (C10-C14) concentrations in serum of starved mice
6-month-old male wild-type mice were starved for 6 or 24 hours and control mice were fed *ad libitum* before sacrifice. Blood serum was collected from each group and the average concentrations (µmol/l) of acylcarnitines (C10-C14) were measured using ESI-MS/MS. Samples from control (n=12), 6 hours (n=8) and 24 hours (n=12) starved mice were statistically analyzed. Shown are mean + SEM and the significance was calculated by unpaired student's t-test (*=p<0.05; **=p<0.01).

When evaluating acylcarnitine (C16-C18) concentrations in mouse serum after 24 hours of starvation, C16, C16:1, C16OH, C16:1OH, C18, C18:1, C18OH, C18:1OH and C18:2OH showed an increase of 3.41-, 3.3-, 3.92-, 4.92-, 8.6-, 7.48-, 2.9-, 6.67- and 4.15-fold compared to fed mice, respectively. The same tendency was monitored when comparing to 6 hours starved mice, where C16, C16:1, C16OH, C16:1OH, C18, C18:1, C18OH, C18:1OH and C18:2OH concentrations increased by 3.1-, 2.37-, 3.26-, 5.63-, 14.65-, 5.77-, 4.36-, 7.29- and 6-fold after 24 hours, respectively (Figure 4.15).

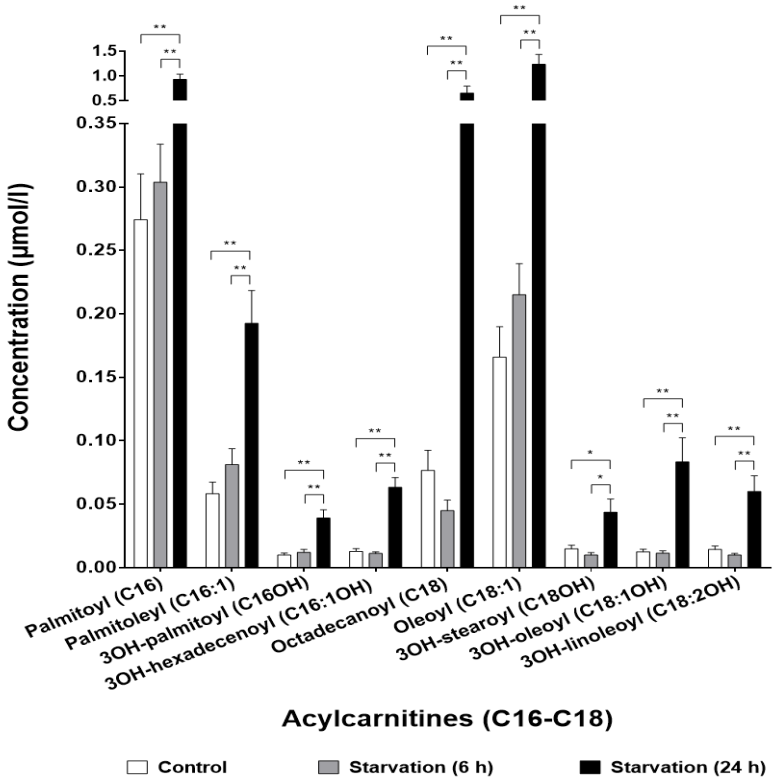

Figure 4.15: Acylcarnitine (C16-C18) concentrations in serum of starved mice
6-month-old male wild-type mice were starved for 6 or 24 hours and control mice were fed *ad libitum* before sacrifice. Blood serum was collected from each group and the average concentrations (µmol/l) of long-chain acylcarnitines (C16-C18) were measured using ESI-MS/MS. Samples from control (n=12), 6 hours (n=8) and 24 hours (n=12) starved mice were statistically analyzed. Shown are mean + SEM and the significance was calculated by unpaired student's t-test (*=p<0.05; **=p<0.01).

4.2.4 Investigation of serum amino acid and derivative concentrations

Amino acids have been described to be involved as intermediates for gluconeogenesis, energy sources for most cells and can affect the regulation of the amino acids sensor mTORC1 (Reviewed by Bröer and Bröer 2017). To examine the impact of starvation on amino acid metabolism, the whole blood serum was collected from the mice after sacrifice and the amino acids were extracted. After stabilizing the amino acids by a substitution reaction at the primary and secondary amino groups, the concentrations were measured by LC-MS/MS. Changes in the levels of 36 circulating amino acids and derivatives in control and starved mice were monitored (Supplementary table 8.1). In figure 4.16 and 4.17, significantly changed metabolites after starvation are depicted. The experimental procedures were conducted on 12, 8 and 12 biological

replicates representing control, 6 and 24 hours starved mice, respectively. mean concentrations (µmol/l) identified for each amino acid or derivative are shown as bar charts together with their standard error of the mean. Significance was verified by unpaired student's t-test.

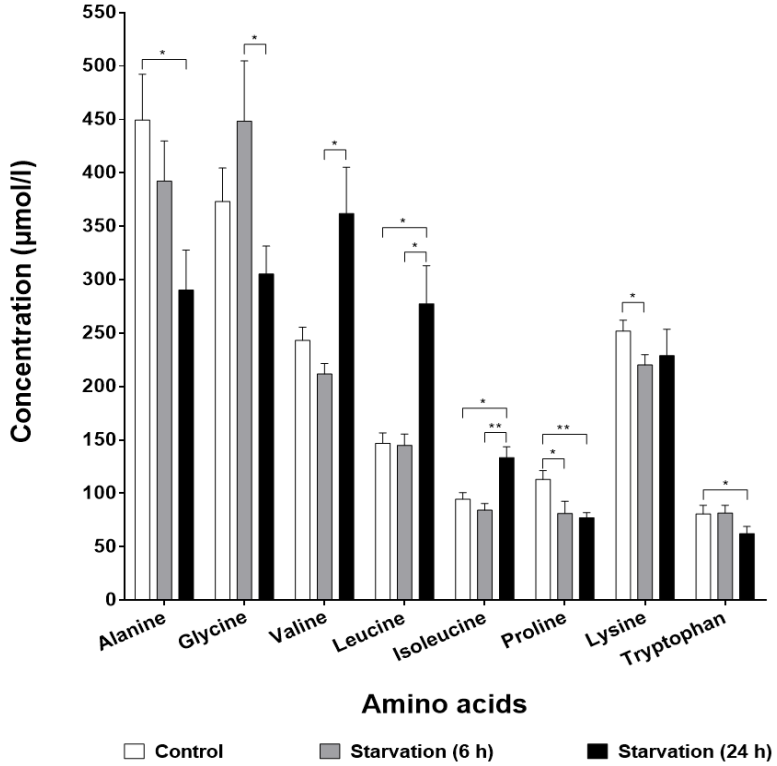

Figure 4.16: Circulating amino acid levels in starved mice
6-month-old male wild-type mice were starved for 6 or 24 hours and control mice were fed *ad libitum* before sacrifice. Blood serum was collected from each group and the mean concentrations (µmol/l) of amino acids were measured using LC-MS/MS. Samples from control (n=12), 6 hours (n=8) and 24 hours (n=12) starved mice were statistically analyzed. Shown are mean + SEM and the significance was calculated by unpaired student's t-test (*=$p<0.05$; **=$p<0.01$).

From the investigated amino acids, 5 showed a decrease in their levels after short or prolonged starvation, while the 3 branched-chain amino acids (BCAAs), namely valine, leucine and isoleucine, increased after long-term starvation.

After short starvation period, proline and lysine decreased by 1.39- and 1.14-fold in relation to recorded fed concentrations, respectively. After prolonged starvation, alanine, proline and tryptophan depicted a 1.55-, 1.46- and 1.29-fold decrease in their levels compared to fed mice, respectively. At the same time, glycine decreased by 1.47-fold between 6 and 24 hours of starvation. In contrast, leucine and isoleucine increased by 1.89- and 1.41, respectively, after comparing

fed to 24 hours starved mice. Compared to 6 hours of starvation time, valine, leucine and isoleucine raised by 1.71-, 1.91- and 1.58-fold after 24 hours, respectively (Figure 4.16).

Possible changes in the derivatives resulting from amino acid reactions were also investigated. By comparing control to 6 hours starved mice, no change in the circulating amino acid derivative levels was monitored. After 24 hours of starvation, two histidine derivatives, 1- and 3-methylhistidne, as well as 2-aminoadipic acid and 2-aminobutyric acid derivatives concentrations increased by 1.29-, 2.63-, 5.04- and 3.9-fold compared to control mice serum, respectively. The same propensity was recorded when comparing to the short starvation period, where 3-methylhistidine, 2-aminoadipic acid, 2-aminobutyric acid and methionine-derivative taurine increased by 2.07-, 6.4-, 4.12- and 1.43-fold after 24 hours, respectively.

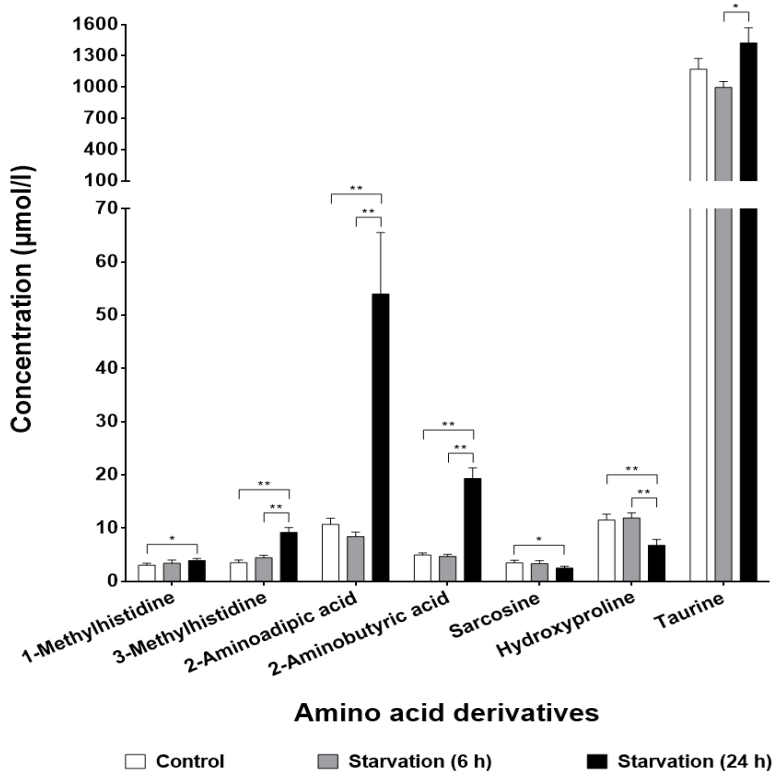

Figure 4.17: Circulating amino acid derivative levels in starved mice
6-month-old male wild-type mice were starved for 6 or 24 hours and control mice were fed *ad libitum* before sacrifice. Blood serum was collected from each group and the mean concentrations (µmol/l) of amino acid derivatives were measured using LC-MS/MS. Samples from control (n=12), 6 hours (n=8) and 24 hours (n=12) starved mice were statistically analyzed. Shown are mean + SEM and the significance was calculated by unpaired student's t-test (*=$p<0.05$; **=$p<0.01$).

In contrast, glycine-derivative sarcosine and proline-derivative hydroxyproline showed a 1.4- and 1.7-fold decrease, respectively, when comparing control to 24 hours starved samples. In parallel, the level of hydroxyproline decreased by 1.76-fold between 6 and 24 hours of starvation (Figure 4.17).

4.3 Proteomic study on lysosomes from starved mice

To study the differences in the proteome composition of lysosomes between control, short- and long-term starved mice, proteomic data to detect lysosomal protein changes, depending on the metabolic status, were required. Therefore, liver lysosomes were enriched from mice injected with Triton WR1339 and TMT labeled peptides were fractionated, desalted and analyzed on an Orbitrap Fusion Lumos mass spectrometer (Figure 4.18).

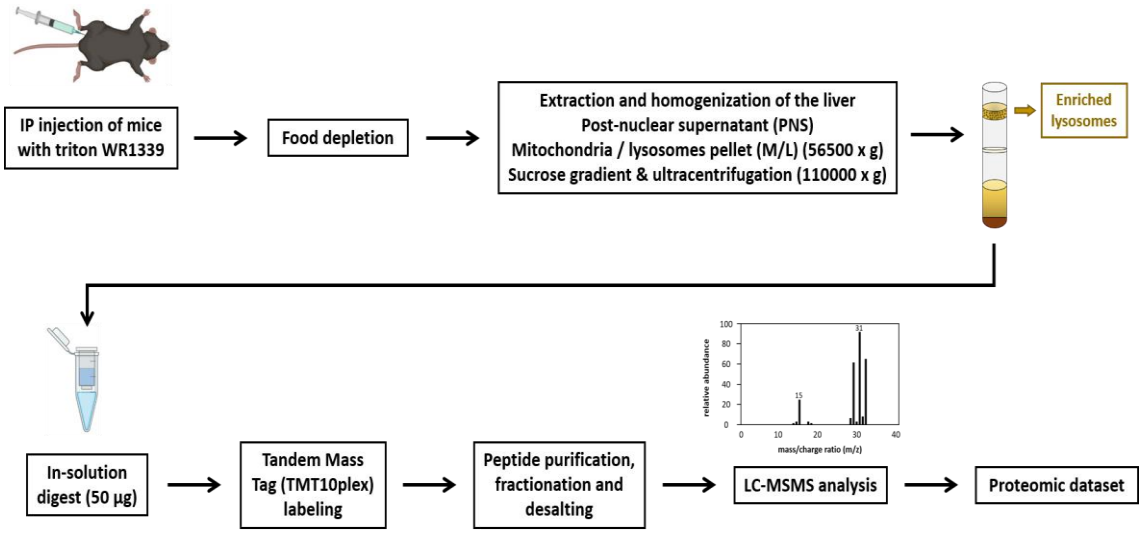

Figure 4.18: Experimental procedure of the proteomic study on lysosomes
Male wild-type mice were injected with Triton WR1339 at the age of 6 months. After liver isolation from control, 6 and 24 hours starved mice, lysosomes were enriched via sucrose gradient-based separation. 50 µg proteins were digested in solution and tryptic peptides were labeled with TMT10plex. Peptides were purified, OFFGEL fractionated and desalted via STAGE tips. Orbitrap Fusion Lumos mass spectrometer was used to analyze the sample and the proteomic dataset obtained was processed by proteome discoverer software 2.3.

4.3.1 Lysosome enrichment from mouse liver

In order to isolate and enrich lysosomes from liver tissues, wild-type mice were injected with Triton WR1339. The solution is taken up by liver hepatocytes leading to the accumulation of lipids in the lysosomes as a result of lipoprotein lipase

inhibition. This treatment induces a density shift in the ‘tritosomes’ compared to other organelles, mainly mitochondria (Wattiaux et al. 1963). Enrichment of tritosomes was carried out as described in 3.2.2.3. Briefly, the removed liver from control, 6 hours and 24 hours starved mice was homogenized and centrifuged. The resulting pellet of post-nuclear supernatant (PNS) ultra-centrifugation represents the mitochondria/lysosomes layer (M/L). Both organelles were separated by a discontinuous sucrose gradient using different sucrose density solutions. To verify the success of the lysosome ‘tritosome’ enrichment in fed and starved mice, equal protein amounts of liver, PNS, M/L and tritosome fractions collected during the experiment were analyzed by western blot. Enrichment efficiency was examined by antibody-based detection of lysosome-associated membrane glycoprotein-1 (LAMP-1). The 110 kDa-sized protein, one of the most abundant lysosomal membrane proteins, showed a gradual increase in the protein levels throughout the experiment steps, reaching the highest abundance in the tritosome fractions (Figure 4.19).

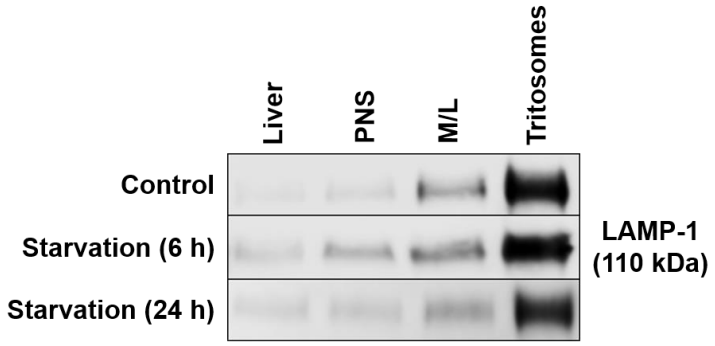

Figure 4.19: Verification of lysosome enrichment by LAMP-1 immune detection
Male wild-type mice were injected with Triton WR1339 at the age of 6 months. Liver was removed from control and starved mice and lysosomes were enriched via sucrose gradient-based separation. 20 µg proteins of crude liver lysate, post-nuclear supernatant (PNS), mitochondria/lysosomes layer (M/L) and lysosome ‘tritosome’ fraction were separated on a 12.5 % SDS-PAGE gel, transferred onto a nitrocellulose membrane and probed with LAMP-1 antibody.

4.3.2 Proteomic analysis of lysosomes from starved mice

Tryptic peptides of fed, 6 hours and 24 hours starved samples were labeled using a 10plex tandem mass tag isobaric reagents. Since TMT10plex labeled peptide of control and starved samples were mixed and measured together in Orbitrap Fusion Lumos mass spectrometer, proteomic analysis and quantification processes applied to all conditions are equal, including upcoming filtration and

normalization steps. The proteomic raw data were searched against Mus musculus databases by proteome discoverer (PD) software 2.3 and further subjected to a comparative statistical analysis. The proteomic dataset was represented by three biological replicates of fed and 6 hours starved mice, and by four biological replicates of 24 hours starved mice. Mass spectrometric analysis yielded 3417 identified proteins. After filtering low-quality data such as non-unique peptides and single-hit proteins from exported PD 2.3 raw files and accepting proteins with at least two unique peptides, 1725 proteins and consequently 9639 peptide-spectral-matches (PSMs) were suitable for quantification and further statistical analysis of labeled and pooled TMT fractions. From a total of 1725 proteins, 233 lysosomal proteins were detected out of 456 according to the protein center database in PD 2.3 (Supplementary table 8.2) and gene ontology (GO) analysis tool, which equals 13.5 % of all quantified proteins. To enhance the statistical analysis and to be able to proceed with the already measured and filtered proteins, quality control procedures were applied to investigate the sample distribution and the correlation between the replicates. The results were visualized by boxplots and principal component analysis plot (PCA).

First of all, it was necessary to remove possible technical bias between samples as well as the effect of heteroscedasticity. Therefore, proteomic dataset was log_2-transformed and calibrated by the variance stabilizing normalization method (VSN) (Huber et al. 2002). In figure 4.20, boxplots of normalized replicates at each condition showed the summarized protein abundances displaying a close-to-normal sample distribution. Outliers are given as colored dots according to the respective replicate color.

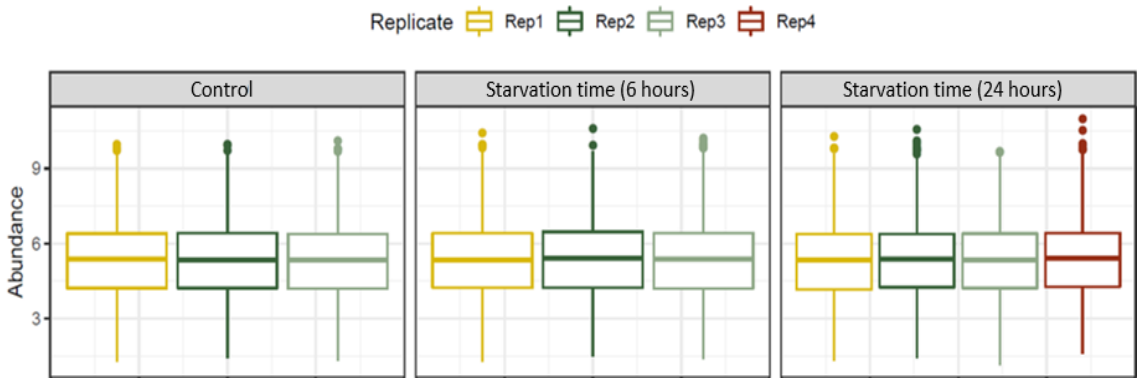

Figure 4.20: Distribution of replicates after normalization visualized by boxplots
Proteomic data were normalized by the variance stabilizing normalization method (VSN). Normalized values were used to display the boxplots by ggplot2 3.2.0 software. Boxplots represent every replicate of control (n=3), 6 (n=3) and 24 (n=4) hours starved mice. Summarized proteins of each replicate were represented by abundance values. Outliers are demonstrated as colored dots in relation with the appropriate replicate.

Next, to evaluate the correlation between replicates related to a particular condition, a principal component analysis (PCA) plot is displayed as shown in figure 4.21. Each replicate is depicted by a dot, where the color represents the treatment and the size reflects the contribution of each replicate to the variability explained by the first two principle components 'dimensions'. Dimension 1 and 2 represent 42 % and 27.2 % of the total variability, respectively. Clear distinctions were observed between the studied groups revealing high correlation between replicates belonging to the same treatment.

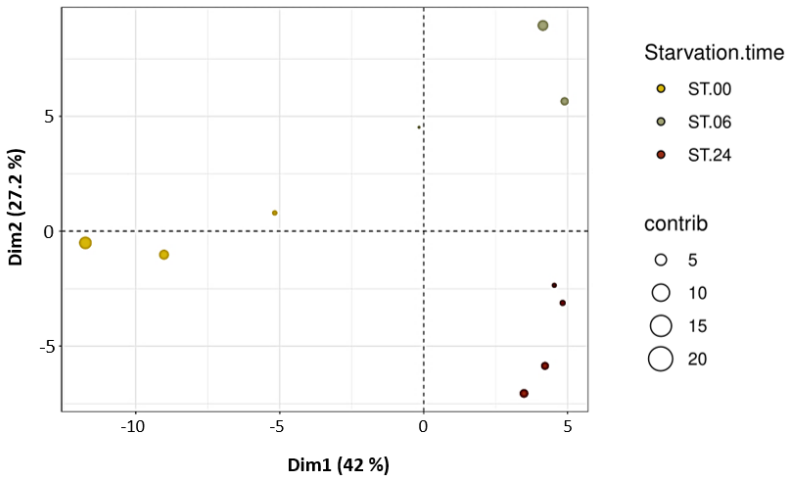

Figure 4.21: Clustering of similarly treated replicates visualized by PCA plot
The correlation between individual replicates belonging to control (n=3), 6 (n=3) and 24 (n=4) hours starved mice are shown through a principal component analysis plot using FactoMineR 1.42 software. Three groups of replicates demonstrating each condition are represented with a particular colored dot (Yellow: control group, green: 6 hours starved group, red: 24 hours starved group). Dot sizes diverse based on their contribution to each dimension (Dim1 and Dim2).

4.3.2.1 Identification of differentially regulated lysosomal proteins upon short- and long-term starvation in lysosome-enriched fractions

The proteomic dataset obtained from lysosome-enriched fractions of 6 and 24 hours starved mice was examined for changes in lysosomal proteome composition after low-quality data filtration and normalization as described above. The 233 quantified lysosomal proteins include classical lysosomal enzymes as well as lysosomal integral and lysosome-associated proteins. In this study, the term regulation was used to represent the protein abundances in the lysosomal fraction, meaning proteins with an increased or a decreased abundance are referred to as up- or downregulated, respectively. To determine the differentially regulated lysosomal proteins, the ratios of starved to control samples were calculated for three biological replicates of fed and 6 hours starved mice, except for 24 hours starved mice for four biological replicates. The p-values were corrected for multiple testing by the Benjamini-Hochberg method. A volcano plot was used to visualize the statistical analysis of protein abundance changes. In this type of scatter plot, the $-\log_{10}$ of the p-values are plotted on the Y-axis, while the $\log_2$ fold changes between starved and control mice are depicted on the X-axis. The adjusted p-value threshold of 0.05 was defined by a red horizontal solid line. Each dot represents one of the 233 quantified lysosomal proteins. The red dots indicate significantly regulated proteins, whereas black dots are non-significant proteins. All proteins with a corrected p-value <0.05 as well as an increased or decreased amounts by a $\log_2$ fold change of at least -0.75 or 0.75 according to their starvation/control ratios were considered to be differentially regulated. These proteins are located above the red horizontal solid line and before or after two black vertically dashed lines (Figure 4.22). After applying these criteria in the present dataset, direct analysis of the lysosomal proteins after 6 hours of starvation revealed a significant down- and upregulation of 11 and 1 lysosomal annotated proteins, respectively (Figure 4.22 A, table 4.1). Furthermore, 17 and 1 lysosomal annotated proteins were detected to be down- and upregulated after 24 hours of starvation, respectively (Figure 4.22 B, table 4.2). Both volcano plots showed an almost similar protein distribution of significantly regulated proteins (Figure 4.22).

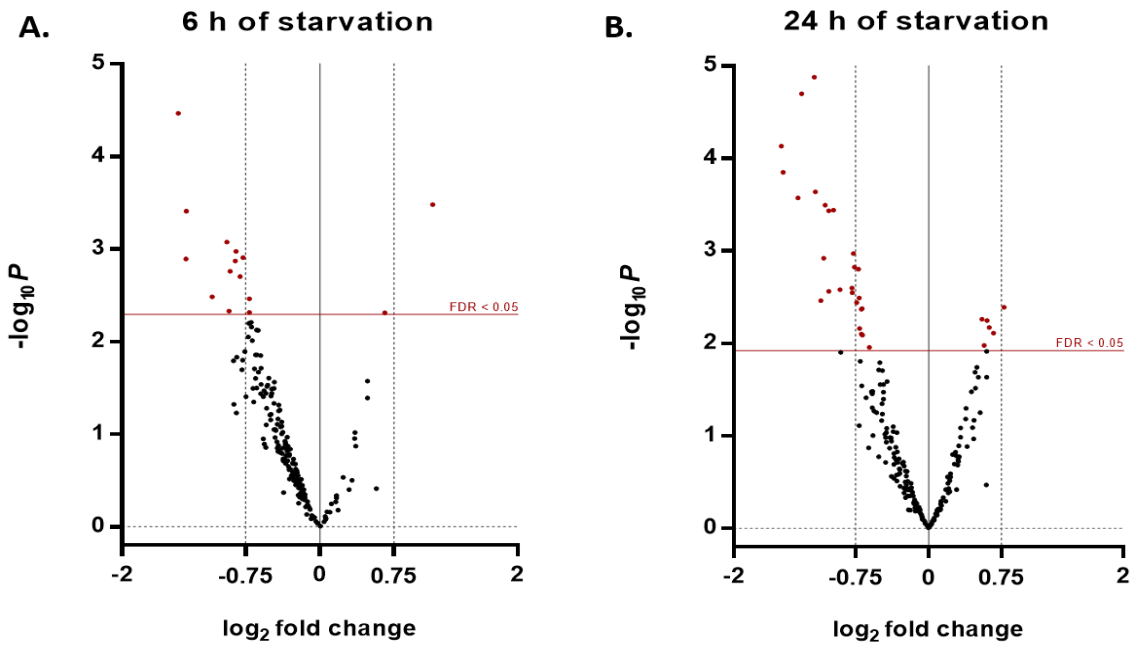

Figure 4.22: Volcano plots of quantified lysosomal proteins after 6 and 24 hours of starvation
Enriched lysosomal fractions from control (n=3), 6 (n=3) and 24 (n=4) hours starved mice were tryptic digested. TMT labeled peptides were mixed and fractionated prior to MS measurement. Raw data were searched by proteome discoverer 2.3. Normalized lysosomal proteins were statistically analyzed and p-values were corrected by the Benjamini-Hochberg method with a threshold of 0.05. **A** and **B.** The $-\log_{10}$ p-values were plotted against $\log_2$ fold change of starved/control. Lysosomal proteins with an adjusted p-value <0.05 are marked in red. Among those, proteins with a $\log_2$ fold change <-0.75 or >0.75 are considered differentially regulated. Others are marked in black.

After 6 hours of starvation, 4 out of 11 downregulated proteins are lysosome-associated proteins related to the mTOR signaling pathway, namely GATOR complex protein WDR59, Rag complex members (RagA, RagC) and the mammalian target of rapamycin (mTOR) (Table 4.1). Furthermore, 8 out of 17 downregulated proteins after 24 hours of starvation are lysosome-associated proteins involved in the mTOR signaling pathway, namely Ragulator complex components (LAMTOR1, 2, 3 and 5) and GATOR complex subunits (WDR59, MIOS, NPRL2 and DEPDC5) (Table 4.2). The only significantly upregulated protein identified after 6 and 24 hours of starvation is peroxiredoxin-6 (PRDX6) with 4 unique peptides. PRDX6 has a $\log_2$ fold change of 1.14 and 0.77 after 6 and 24 hours of starvation, respectively (Figure 4.22). In each table, the $\log_2$ fold change ratios of the lysosomal proteins at the starvation period of interest are marked in blue and depicted in a descending order.

Table 4.1: Downregulated lysosomal proteins upon 6 hours of starvation
List of the 11 downregulated lysosomal proteins identified after short-term starvation in the proteomic dataset. Shown are proteins with more than one unique peptide, p-value <0.05 and log_2 fold change ratios <-0.75. In addition, the log_2 fold change ratios after 24 hours as well as the log_2 fold change ratios of the difference between 6 and 24 hours of starvation are also shown in the table (#: number of unique peptides, blue: starvation period of interest).

Protein name	Gene name	Log_2FC (6h)	Log_2FC (24h)	Log_2FC (24-6h)	#
WD repeat-containing protein 81	Wdr81	-1.43	-1.06	0.37	2
Ganglioside-induced differentiation-associated protein 2	Gdap2	-1.35	-1.51	-0.16	9
Heme transporter HRG1	Slc48a1	-1.35	-0.24	1.11	2
Proprotein convertase subtilisin/kexin type 9	Pcsk9	-1.09	-1.49	-0.4	3
Ras-related GTP-binding protein C	Rragc	-0.94	-0.6	0.33	5
AP-3 complex subunit delta-1	Ap3d1	-0.92	-0.53	0.38	9
Serine/threonine-protein kinase mTOR	Mtor	-0.91	-0.68	0.23	2
Vesicle-associated membrane protein 7	Vamp7	-0.86	-0.71	0.14	2
GATOR complex protein WDR59	Wdr59	-0.85	-0.76	0.09	2
Transmembrane protein 106B	Tmem106b	-0.81	-0.23	0.57	5
Ras-related GTP-binding protein A	Rraga	-0.78	-0.47	0.3	2

Following the analysis of differentially regulated lysosomal proteins at each starvation period independently, a comparative study using Venn diagrams generated by Venny online software (Oliveros 2007) was conducted (Figure 4.23). Since only one lysosomal upregulated protein, PRDX6, was identified after both short and prolonged periods of starvation, the comparative study was applied for the downregulated proteins after 6 and 24 hours of starvation. Lysosomal downregulated proteins after 6 hours of starvation are marked in blue, whereas the orange color represents downregulated proteins in 24 hours starved samples. When comparing the downregulated proteins, 4 out of 11 and 17 downregulated proteins after 6 and 24 hours of starvation, respectively, are overlapping between both datasets (Figure 4.23). The overlapping proteins include the GATOR complex protein WDR59 (Table 4.3).

Table 4.2: Downregulated lysosomal proteins upon 24 hours of starvation
List of the 17 downregulated lysosomal proteins identified after long-term starvation in the proteomic dataset. Shown are proteins with more than one unique peptide, p-value <0.05 and log_2 fold change ratios <-0.75. In addition, the log_2 fold change ratios after 6 hours as well as the log_2 fold change ratios of the difference between 6 and 24 hours of starvation are also shown in the table (#: number of unique peptides, blue: starvation period of interest).

Protein name	Gene name	Log_2FC (6h)	Log_2FC (24h)	Log_2FC (24-6h)	#
Ganglioside-induced differentiation-associated protein 2	Gdap2	-1.35	-1.51	-0.16	9
Proprotein convertase subtilisin/kexin type 9	Pcsk9	-1.09	-1.49	-0.4	3
Rabankyrin-5	Ankfy1	-0.07	-1.34	-1.26	22
Vacuolar protein sorting-associated protein 26A	Vps26a	-0.17	-1.30	-1.13	7
Vacuolar protein sorting-associated protein 35	Vps35	-0.33	-1.17	-0.84	18
Ragulator complex protein LAMTOR2	Lamtor2	-0.26	-1.16	-0.9	3
Ragulator complex protein LAMTOR3	Lamtor3	-0.57	-1.11	-0.54	4
Ragulator complex protein LAMTOR5	Lamtor5	-0.78	-1.08	-0.3	3
WD repeat-containing protein 81	Wdr81	-1.43	-1.06	0.37	2
Ragulator complex protein LAMTOR1	Lamtor1	-0.84	-1.02	-0.18	5
GATOR complex protein NPRL2	Nprl2	-0.54	-1.02	-0.48	2
Apolipoprotein E	Apoe	0.17	-0.98	-1.15	13
ATP-binding cassette sub-family A member 2	Abca2	-0.08	-0.91	-0.83	3
GATOR complex protein MIOS	Mios	-0.68	-0.79	-0.1	10
Ras-related protein Rab-14	Rab14	-0.27	-0.78	-0.51	9
GATOR complex protein DEPDC5	Depdc5	-0.62	-0.77	-0.14	3
GATOR complex protein WDR59	Wdr59	-0.85	-0.76	0.09	2

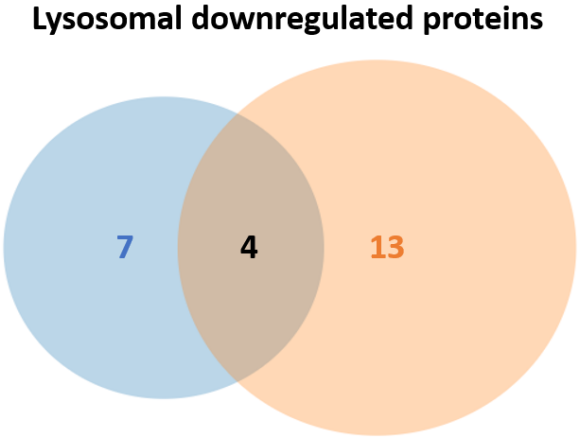

Figure 4.23: Comparative analysis of lysosomal downregulated proteins after 6 and 24 hours of starvation using a Venn diagram
Lysosomal downregulated proteins were subjected to a comparative analysis after short and prolonged starvation using Venny online software. Downregulated proteins of both starvation datasets were compared and the number of overlapping proteins is shown in black color. The blue color represents downregulated proteins after 6 hours of starvation, whereas downregulated proteins after 24 hours of starvation are shown in orange.

Table 4.3: Overlapping lysosomal downregulated proteins after 6 and 24 hours of starvation

List of the 4 overlapping lysosomal downregulated proteins identified after short- and long term starvation in the proteomic dataset. Shown are proteins with more than one unique peptide, p-value <0.05 and log_2 fold change ratios <-0.75. In addition, the log_2 fold change ratios of the difference between 6 and 24 hours of starvation are also shown in the table (#: number of unique peptides).

Protein name	Gene name	Log_2FC (6h)	Log_2FC (24h)	Log_2FC (24-6h)	#
WD repeat-containing protein 81	Wdr81	-1.43	-1.06	0.37	2
Ganglioside-induced differentiation-associated protein 2	Gdap2	-1.35	-1.51	-0.16	9
Proprotein convertase subtilisin/kexin type 9	Pcsk9	-1.09	-1.49	-0.4	3
GATOR complex protein WDR59	Wdr59	-0.85	-0.76	0.09	2

4.3.2.2 Starvation influence on the regulation of lysosomal candidate proteins based on the proteomic analysis

The above analyzed proteomic dataset showed a significant change in the abundance of several lysosomal proteins at the lysosomal level after 6 and 24 hours of starvation. A closer look and a manual investigation of the lysosomal regulated proteins revealed a change in the abundances of complexes associated with the lysosome and mTORC1 signaling pathway such as Ragulator complex proteins (LAMTOR1, 2, 3 and 5), two members of ras-related GTP-binding (Rag) complex (RagA and RagC), 4 components of GAP activity towards the Rags (GATOR) complex (WDR59, DEPDC5, MIOS and NPRL2) as well as a change in the regulation of the mechanistic target of rapamycin (mTOR) as part of mTOR complex 1 (Table 4.4).

The alteration in the regulation of the lysosomal complexes, shown in the MS results, was validated by further western blot experiments using protein members of each complex.

Table 4.4: List of the quantified proteins from the selected lysosomal complexes for subsequent validation experiments
Differentially regulated proteins after short and prolonged starvation in the proteomic dataset were analyzed and protein complexes related to the lysosome and mTORC1 signaling pathway were further investigated. The table displays the candidate complexes, their log_2 fold change ratios after 6 and 24 hours of starvation as well as the log_2 fold change ratios of the difference between 6 and 24 hours of starvation and the corresponding unique peptide number (#: number of unique peptides, *: not significant).

Protein name	Gene name	Log_2FC (6h)	Log_2FC (24h)	Log_2FC (24-6h)	#
Serine/threonine-protein kinase mTOR	Mtor	-0.91	-0.68	0.23	2
Ragulator complex protein LAMTOR1	Lamtor1	-0.84*	-1.02	-0.18	5
Ragulator complex protein LAMTOR2	Lamtor2	-0.26*	-1.16	-0.9	3
Ragulator complex protein LAMTOR3	Lamtor3	-0.57*	-1.11	-0.54	4
Ragulator complex protein LAMTOR5	Lamtor5	-0.78*	-1.08	-0.3	3
Ras-related GTP-binding protein A	Rraga	-0.78	-0.47*	0.3	2
Ras-related GTP-binding protein C	Rragc	-0.94	-0.6	0.33	5
GATOR complex protein WDR59	Wdr59	-0.85	-0.76	0.09	2
GATOR complex protein DEPDC5	Depdc5	-0.62*	-0.77	-0.14	3
GATOR complex protein MIOS	Mios	-0.68*	-0.79	-0.1	10
GATOR complex protein NPRL2	Nprl2	-0.54*	-1.02	-0.48	2

4.3.2.2.1 Validation of mTORC1 regulation after different starvation periods

Before confirming the findings of the proteomic analysis concerning the regulation of Ragulator-Rag complex and GATOR complex proteins under different starvation conditions, it was necessary to investigate the localization and thus the regulation of mTORC1 on the lysosomal surface. In addition to the core protein mTOR, mTORC1 consists of its two unique proteins RAPTOR and PRAS40 as well as two common proteins with mTORC2, namely DEPTOR and mLST8 (Reviewed by Liu and Sabatini 2020). In previous liver starvation experiments performed in this study, phosphorylation of mTORC1 downstream targets was decreased after short starvation and increased after prolonged starvation demonstrating a reactivation in their phosphorylation (Figure 4.2 and 4.3). Moreover, in the proteomic dataset (Table 4.4), significant log_2 fold change ratios demonstrated more downregulation of mTOR protein after 6 hours of starvation than after a longer starvation period. To clarify whether the alterations in the

abundances during starvation were consistent, a confirmation of these findings by western blot analysis was applied.

The experiment was performed in eight biological replicates from control and starved mice. Since the immune detection of the mTOR protein was not successful, size-separated proteins were probed with protein-specific antibodies against RAPTOR and PRAS40 proteins. The protein abundance was investigated at the levels of crude liver lysate and lysosome 'tritosome' fraction after 6 hours of starvation and a prolonged starvation period of 24 hours. For signal quantification, obtained intensities were normalized to loading controls. Control samples were set to 1 and the standard error of the mean (SEM) was used to calculate the distribution of the sample. A representative figure of four biological replicates is shown, while the statistical significance of all eight replicates was calculated by unpaired student's t-test.

Depending on the sample source, the selected loading control is either the housekeeping protein glyceraldehyde-3-phosphate dehydrogenase (GAPDH) or the lysosomal hydrolase tripeptidyl-peptidase 1 (TPP1). In this study, MS analysis of lysosome-enriched samples showed no change in the protein amount of the lysosomal hydrolase TPP1 after short- and long period of starvation compared to control samples. At the same time, cell culture experiments conducted by Wyant et al. demonstrated that TPP1 abundance in lysosomal fractions is stable when comparing control, nutrient-starved and mTOR inhibitor Torin1-treated human embryonic kidney (HEK) 293T cells (Wyant et al. 2018). Therefore, TPP1 was selected as a loading control for the western blot experiments in this research.

Figure 4.24 A shows the detected signals of the 150 kDa RAPTOR, 37 kDa GAPDH and 48 kDa TPP1 for control, 6 and 24 hours starved mice, as well as the average relative intensities of normalized liver lysate and lysosome samples. In liver whole lysates, no significant differences in RAPTOR amounts was observed. The lysosomal fractions depicted a decrease of 2.62-fold in the abundance after 6 hours of starvation whereas an increase of 2.49-fold was measured after 24 hours compared to 6 hours of starvation.

Furthermore, figure 4.24 B shows the detected signals of PRAS40. The normalized 40 kDa-sized protein depicted a decrease in the abundances after

prolonged starvation in liver tissues. Compared to the control and 6-hour starvation periods, PRAS40 amounts decreased significantly by 1.67- and 1.51-fold, respectively, after prolonged starvation. In the lysosome fraction, the decrease in the signal intensities after short starvation period and the increase after 24 hours was not statistically significant.

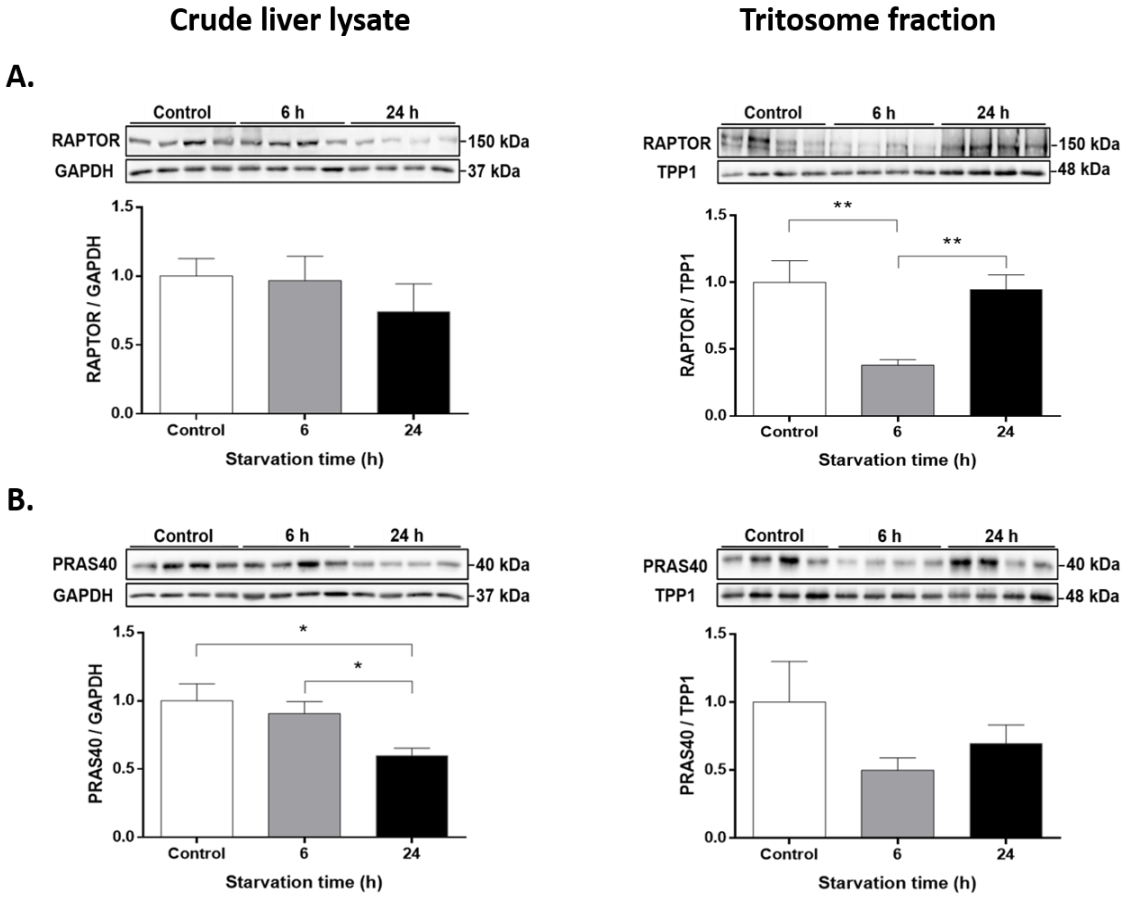

Figure 4.24: Abundances of mTORC1 subunits during starvation
Male wild-type mice were injected with Triton WR1339 at the age of 6 months. Following liver isolation from control, 6 and 24 hours starved mice, lysosomes were enriched via sucrose gradient-based separation. 10 µg proteins of crude liver lysate and lysosome 'tritosome' fraction were separated on a 7.5 % SDS-PAGE gel, transferred onto a PVDF membrane and probed with RAPTOR- and PRAS40-specific antibodies representing the mTORC1 unique subunits together with GAPDH and TPP1 as loading controls. **A** and **B.** After densitometric quantification, detected signals were normalized and the average relative intensities of RAPTOR and PRAS40 are shown as bar charts defining each condition. Protein signals represent four biological replicates out of eight. Shown are mean + SEM; n=8 and the significance was determined by unpaired student's t-test (*=p<0.05; **=p<0.01). The control samples were set to 1.

The validation experiments of mTORC1 unique subunits reveal that the protein levels of PRAS40 are continuously decreasing at the crude liver lysate level. In addition, RAPTOR levels at the lysosome show a relevant decrease after a short

starvation period of 6 hours and the abundance increases significantly after 24 hours of starvation.

4.3.2.2.2 Validation of Ragulator complex regulation after different starvation periods

The pentameric Ragulator complex plays an important role in mTORC1 activation and hence its positioning on the lysosomal surface (Reviewed by Kim and Guan 2019). In the proteomic results, the log_2 fold change ratios of LAMTOR1, 2, 3 and 5 demonstrated significant downregulation after 24 hours of starvation, while their downregulation after 6 hours was not statistically significant (Table 4.4). To clarify whether the decrease in the abundance after starvation was relevant, a validation of the findings by western blot analysis was applied. The immune detection was performed on crude liver lysate and lysosome 'tritosome' fraction of eight biological replicates and the protein abundances were detected by LAMTOR1-, 2- and 5-specific antibodies. For relative quantification, protein signals were normalized to GAPDH or the lysosomal hydrolase TPP1 as a loading control after setting control values to 1 and the standard error of the mean was calculated to measure the sample distribution. Shown here are the detected signals of four biological replicates, while the statistical significance of eight biological replicates was calculated and the relative intensities are depicted as bar charts.

Figure 4.25 A displays the 18 kDa signals of LAMTOR1 as well as the loading controls GAPDH and TPP1. At the crude liver lysate level, the mean of LAMTOR1 intensities normalized to GAPDH showed a continuous increase in the protein abundances during starvation. The statistical analysis revealed a significant increase of 1.61- and 2.38-fold after 6 and 24 hours of starvation, respectively, compared to control samples. In the same time, the protein level increased by 1.47-fold after 24 hours of starvation in comparison to 6 hours starved samples. In contrast, LAMTOR1 signals at the tritosome level showed a decrease in the abundances beginning from 6 hours of starvation. The unpaired student's t-test of normalized signals to TPP1 indicated a decrease of 3.17- and 2.99-fold after 6 and 24 hours of starvation, respectively, relative to fed mice.

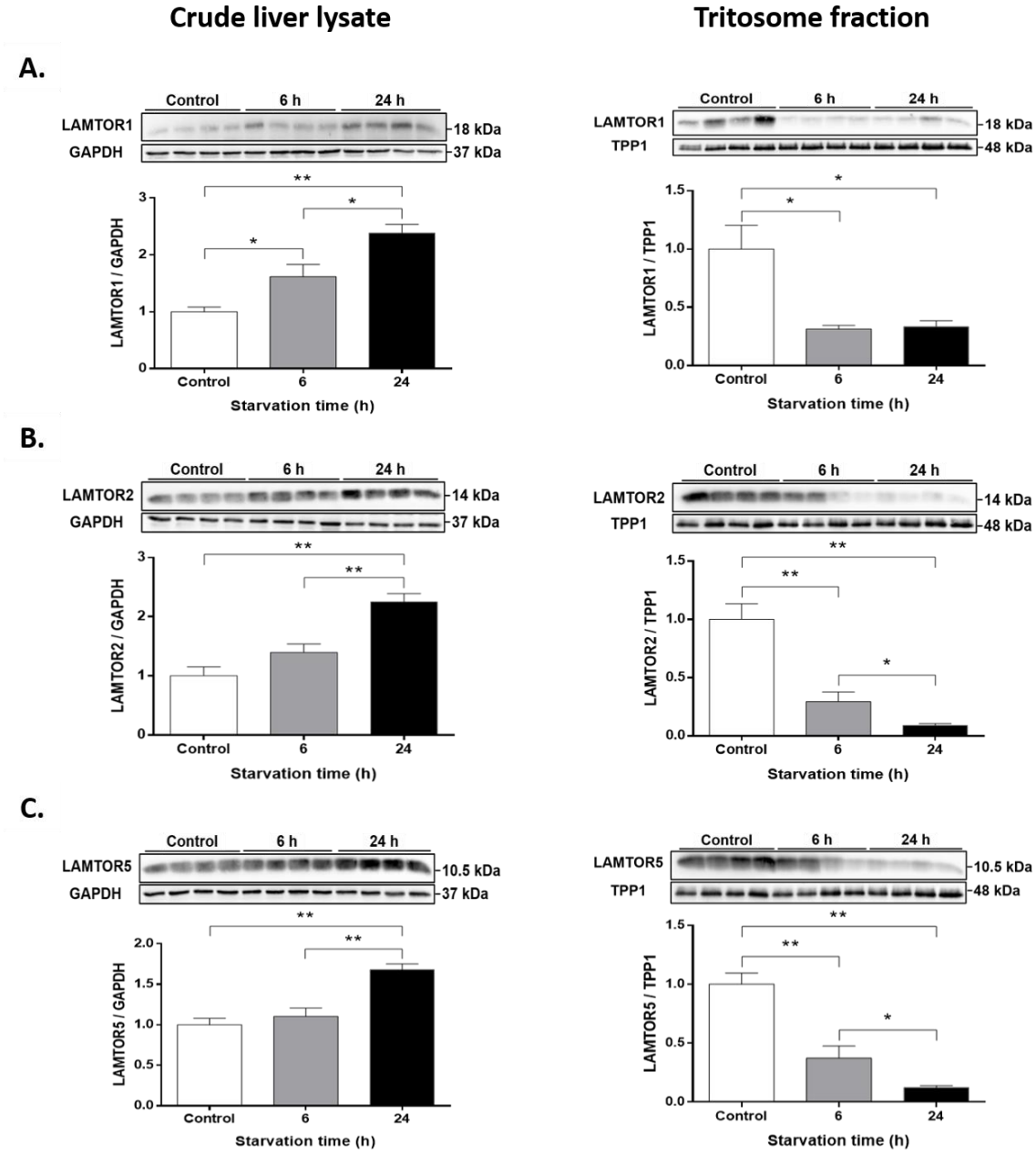

Figure 4.25: Abundances of Ragulator complex components during starvation
Male wild-type mice were injected with Triton WR1339 at the age of 6 months. Following liver isolation from control, 6 and 24 hours starved mice, lysosomes were enriched via sucrose gradient-based separation. 10 µg proteins of crude liver lysate and lysosome 'tritosome' fraction were separated on a 12.5 % SDS-PAGE gel, transferred onto a nitrocellulose membrane and probed with LAMTOR1-, 2- and 5-specific antibodies representing the Ragulator complex components together with GAPDH and TPP1 as loading controls. **A-C.** The detected signals were densitometrically quantified and protein intensities were normalized to their loading control. The average relative intensities of LAMTOR1, 2 and 5 at each condition are shown as bar charts. Displayed signals represent four biological replicates out of eight. Shown are mean + SEM; n=8 and the significance was determined by unpaired student's t-test (*=p<0.05; **=p<0.01). The control samples were set to 1.

In figure 4.25 B, samples were detected using antibodies directed against the 14 kDa-sized LAMTOR2 protein and the loading controls. Opposite to an increase at the crude liver lysate level, LAMTOR2 amounts decreased in tritosome fraction from 6 hours of starvation. The statistical analysis applied to the liver lysate after 24 hours showed that LAMTOR2 amounts increased significantly by 2.25- and 1.61-fold compared to control and 6 hours starved samples, respectively. At the tritosome level, normalized LAMTOR2 intensities were also verified for significance. Compared to control samples, a significant decrease of 3.39- and 10.96-fold after 6 and 24 hours, respectively, was monitored. Furthermore, a 3.23-fold decrease between 6 and 24 hours was also measured.

Moreover, LAMTOR5 detected signals at 10.5 kDa were visualized at the liver lysate and lysosome ‘tritosome’ level along with the corresponding loading control. The average relative intensities are depicted as bar charts in figure 4.25 C. Similar to LAMTOR2, the unpaired student’s t-test of liver whole lysates depicted a significant 1.68- and 1.52-fold increase in LAMTOR5 intensities after 24 hours of starvation, compared to control and 6 hours starved mice, respectively. Contrary to this, a 2.69- and 8.02-fold decrease was calculated in 6 and 24 hours tritosome fraction of starved mice compared to the control mice, respectively. In addition, a 2.98-fold decrease between 6 and 24 hours was also measured.

Western blot validation experiments reveal a significant decrease in the abundances of LAMTOR1, 2 and 5 on the lysosome ‘tritosome’ level during starvation, consistent with the results of proteomic analysis. At the same time, the analysis of Ragulator complex proteins in crude liver lysate displays a continuous increase over the course of starvation.

4.3.2.2.3 Validation of Rag complex regulation after different starvation periods

Essential recruiters of mTORC1 to the lysosomal surface are the Rag GTPases heterodimers, part of the Ragulator-Rag complex, which bind to mTORC1 in their active forms, GTP bound-RagA/B and GDP bound-RagC/D (Reviewed by Kim and Guan 2019). The proteomic analysis of MS data showed a higher downregulation in RagC protein after 6 hours of starvation than after 24 hours. At

the same time, RagA protein was significantly downregulated after short starvation but not after prolonged starvation (Table 4.4). Therefore, the proteomic data of the Rag complex members was verified by western blot analysis. The validation experiment was carried out in eight biological replicates representing control, 6 and 24 hours starved mice. Size-separated proteins of crude liver lysate and lysosome 'tritosome' fraction were probed with RagA- and RagC-specific antibodies. To quantify the detected signals, protein intensities were normalized either to GAPDH or the lysosomal hydrolase TPP1 as a loading control. The sample distribution was measured via the standard error of the mean (SEM) and the control samples were set to 1. The detected signals of four biological replicates are depicted, while the statistical significance of all eight replicates was calculated by unpaired student's t-test.

For control, 6 and 24 hours starved mice, figure 4.26 A shows RagA, GAPDH and TPP1 obtained signals at 30, 37 and 48 kDa, respectively, for liver lysate and lysosome samples. The average relative intensities with the standard error of the mean of normalized RagA are depicted as bar charts. In liver whole lysates, the statistical analysis of RagA showed no significant change in the abundances after short- and long-term starvation in comparison to control. At the lysosomal level, the protein abundance decreased significantly by 1.76-fold after 6 hours of starvation compared to control mice.

The immune detected signals of the 50 kDa-sized RagC protein and the corresponding loading control, GAPDH or TPP1, as well as the normalized intensities are displayed in figure 4.26 B. At the crude liver lysate level, GAPDH-normalized signals depicted an increase in RagC amounts after prolonged starvation. The statistical analysis demonstrated no significant change between control and 6 hours starved mice. In parallel, a significant 1.74- and 1.44-fold increase after 24 hours of starvation was measured compared to control and 6 hours starved mice, respectively. In the lysosomal fraction, the decrease in RagC intensities after 6 hours of starvation was not statistically significant. In contrast, the protein abundance increased significantly by 1.78- and 2.71-fold after 24 hours of starvation relative to control and 6-hour starvation periods, respectively.

By comparing the protein abundances of Ragulator-Rag complex components in the lysosome fraction after immune detection experiments, RagC shows a significant increase after 24 hours of starvation, whereas the abundance of Ragulator complex, LAMTOR1, 2 and 5, decreases significantly at the same starvation period.

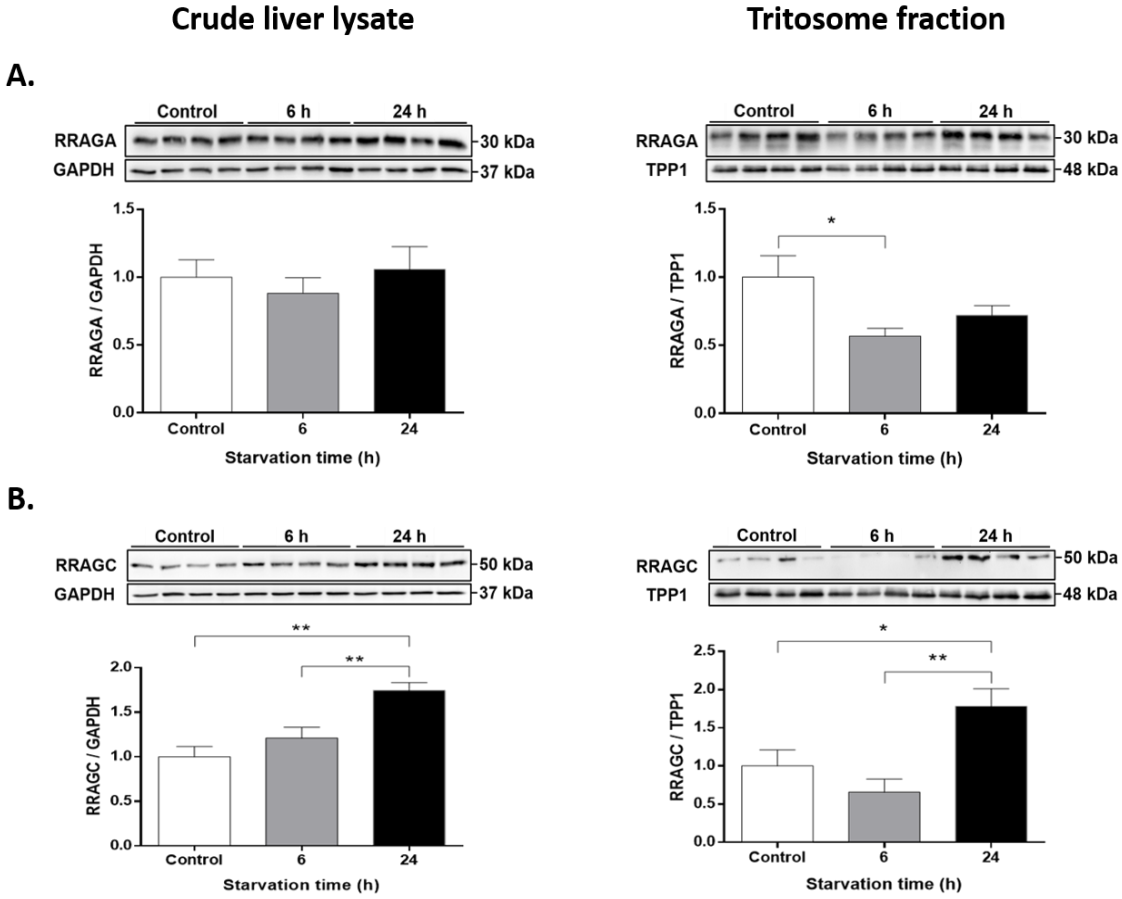

Figure 4.26: Abundances of Rag complex members during starvation
Male wild-type mice were injected with Triton WR1339 at the age of 6 months. Following liver isolation from control, 6 and 24 hours starved mice, lysosomes were enriched via sucrose gradient-based separation. 10 µg proteins of crude liver lysate and lysosome 'tritosome' fraction were separated on a 12.5 % SDS-PAGE gel, transferred onto a nitrocellulose membrane and probed with RagA- and RagC-specific antibodies representing the Rag complex members together with GAPDH and TPP1 as loading controls. **A** and **B.** Western blot signals were visualized and optical densities were quantified. The average relative intensities of RagA and RagC at each condition are depicted as bar charts after normalization. Displayed signals represent four biological replicates out of eight. Shown are mean + SEM; n=8 and the significance was determined by unpaired student's t-test (*=p<0.05; **=p<0.01). The control samples were set to 1.

4.3.2.2.4 Validation of GATOR complex regulation after different starvation periods

The activity of Rag proteins is negatively regulated by the upstream GAP activity towards the Rags complex (GATOR). GATOR consists of eight protein components separated into two subcomplexes based on the affinity of protein-protein interactions (Shaw 2013). GATOR1 regulates the GATOR-Rag interactions and GATOR2 is an upstream inhibitor of GATOR1 (Bar-Peled et al. 2013). The proteomic dataset indicates a significant downregulation of two GATOR1 constituents, DEPDC5 and NPRL2, as well as two GATOR2 components, WDR59 and MIOS, after 24 hours of starvation in the lysosome-enriched samples. In addition, their downregulation after 6 hours was not statistically significant, with the exception of WDR59 (Table 4.4). Therefore, western blot analysis was performed to verify the MS results. Crude liver lysate and lysosome 'tritosome' fractions of eight biological replicates were used and protein abundances were detected by NPRL2-specific antibody. Obtained signals were normalized either to GAPDH or the lysosomal hydrolase TPP1 as a loading control after setting control values to 1. A representative figure of four biological replicates is shown, whereas the statistical analysis of eight biological replicates is depicted as bar charts and standard error of the mean (SEM) was calculated to measure the sample distribution.

Figure 4.27 shows the detected signals of the 41 kDa-sized NPRL2 protein and the corresponding loading controls, namely GAPDH and TPP1. At the crude liver lysate level, the average intensities of normalized NPRL2 and their SEMs depicted a continuous increase in the protein abundance during starvation. Compared to control mice, a significant increase of 1.34- and 1.83-fold was measured after 6 and 24 hours of starvation, respectively. In addition, NPRL2 abundance increased by 1.37-fold between 6 and 24 hours of starvation. At the lysosomal level, NPRL2 abundance showed a continuous decrease after short and long periods of starvation. The unpaired student's t-test revealed a significant 1.46- and 1.88-fold decrease after 6 and 24 hours, compared to control mice, respectively.

In line with the results of proteomic analysis, the western blotting shows a continuous decrease in the level of NPRL2 at the lysosome 'tritosome' during starvation. Meanwhile, the analysis of the GATOR complex protein in crude liver lysate demonstrates a significant increase after 6 and 24 hours of starvation.

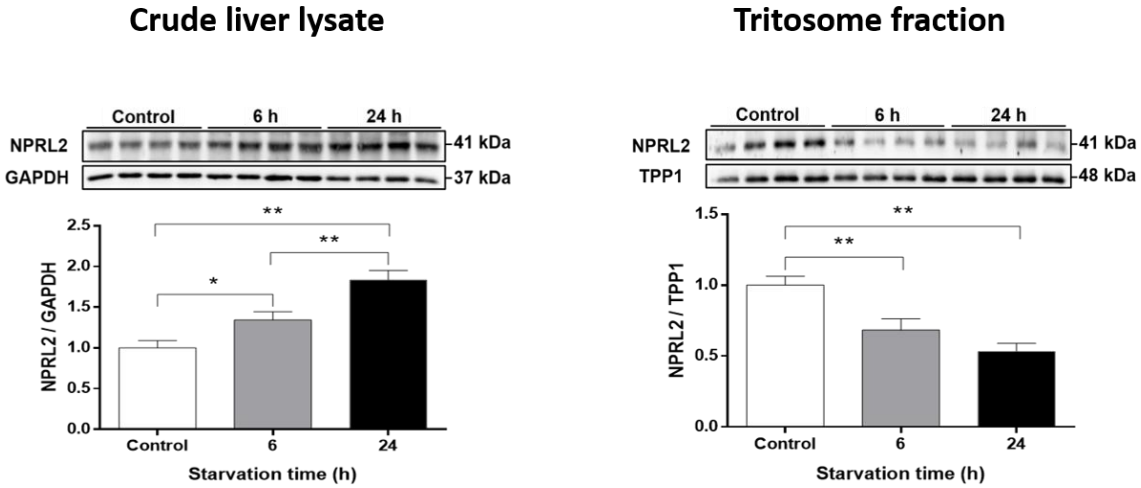

Figure 4.27: Abundances of GATOR complex protein NPRL2 during starvation
Male wild-type mice were injected with Triton WR1339 at the age of 6 months. Following liver isolation from control, 6 and 24 hours starved mice, lysosomes were enriched via sucrose gradient-based separation. 10 µg proteins of crude liver lysate and lysosome 'tritosome' fraction were separated on a 12.5 % SDS-PAGE gel, transferred onto a PVDF membrane and probed with NPRL2-specific antibody representing the GATOR complex together with GAPDH and TPP1 as loading controls. Densitometrically quantified signals were normalized to their loading control. The average relative intensities at each condition are shown as bar charts. Demonstrated signals represent four biological replicates out of eight. Shown are mean + SEM; n=8 and the significance was determined by unpaired student's t-test (*=p<0.05; **=p<0.01). The control samples were set to 1.

4.3.2.3 Identification of differentially regulated non-lysosomal proteins upon short- and long-term starvation in lysosome-enriched fractions

In addition to the lysosomal proteins identified in both starvation datasets, 1492 quantified non-lysosomal proteins were detected as well. To investigate the potential reasons for the presence of these proteins in lysosome-enriched fractions such as their delivery to the lysosome through autophagic pathways after starvation or their interaction with the lysosome, the abundance of the non-lysosomal proteins was evaluated. The proteomic analysis processes applied to non-lysosomal proteins were similar to previously utilized measures on lysosomal proteins, including filtration and normalization steps. For each replicate, starvation to control ratios of 1492 quantified non-lysosomal proteins were

calculated. Fed and 6 hours starved mice were represented by three biological replicates, except for 24 hours starved mice, which were represented by four biological replicates. Adjusted p-values according to the Benjamini-Hochberg method were used to set the significance threshold of 0.05. A volcano plot was used to visualize the results of statistical analysis employing the same standards as those mentioned in section 4.3.2.1. By applying two main parameters, namely adjusted p-value <0.05 and log_2 fold change <-0.75 or >0.75, proteins were considered to be differentially regulated (Figure 4.28).

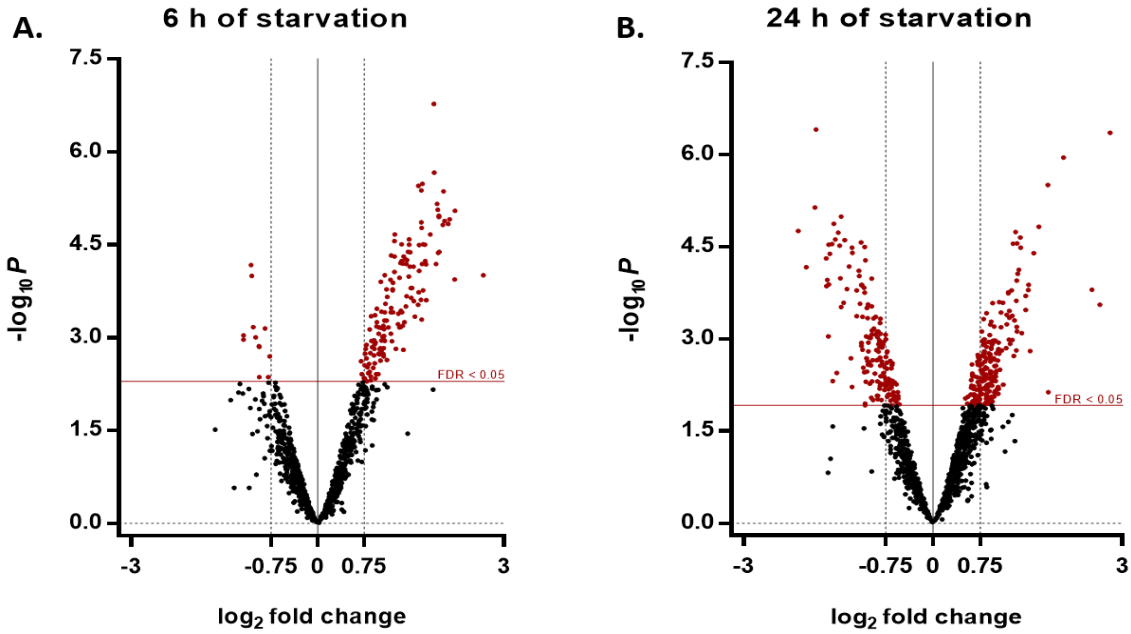

Figure 4.28: Volcano plots of quantified non-lysosomal proteins after 6 and 24 hours of starvation
Enriched lysosomal fractions from control (n=3), 6 (n=3) and 24 (n=4) hours starved mice were tryptic digested. TMT labeled peptides were mixed and fractionated prior to MS measurement. Raw data were searched by proteome discoverer 2.3. Normalized non-lysosomal proteins were statistically analyzed and p-values were corrected by the Benjamini-Hochberg method with a threshold of 0.05. **A** and **B.** The $-log_{10}$ p-values were plotted against log_2 fold change of starved/control. Non-lysosomal proteins with an adjusted p-value <0.05 are marked in red. Among those, proteins with a log_2 fold change <-0.75 or >0.75 are considered differentially regulated. Others are marked in black.

In figure 4.28, the volcano plot analysis of non-lysosomal proteins after 6 hours of starvation showed a significant increase in the upregulated proteins, while 24 hours starved samples demonstrated a comparable distribution in significantly down- and upregulated proteins. 12 and 150 non-lysosomal proteins were detected to be down- and upregulated after 6 hours of starvation, respectively (Figure 4.28 A, table 4.5, table 4.6 and supplementary table 8.3). Furthermore,

the analysis of non-lysosomal proteins after 24 hours of starvation revealed a significant down- and upregulation of 121 and 162 proteins, respectively (Figure 4.28 B, table 4.7, supplementary table 8.4, table 4.8 and supplementary table 8.5). In each table, the log_2 fold change ratios of the non-lysosomal proteins at the starvation period of interest are marked in blue and depicted in a descending order.

Table 4.5: Downregulated non-lysosomal proteins upon 6 hours of starvation
List of the 12 downregulated non-lysosomal proteins identified after short-term starvation in the proteomic dataset. Shown are proteins with more than one unique peptide, p-value <0.05 and log_2 fold change ratios <-0.75. In addition, the log_2 fold change ratios after 24 hours as well as the log_2 fold change ratios of the difference between 6 and 24 hours of starvation are also shown in the table (#: number of unique peptides, blue: starvation period of interest).

Protein name	Gene name	Log_2FC (6h)	Log_2FC (24h)	Log_2FC (24-6h)	#
Serotransferrin	Tf	-1.20	-1.65	-0.46	19
Maspardin	Spg21	-1.19	-1.37	-0.17	8
Synaptosomal-associated protein 29	Snap29	-1.07	-1.08	-0.01	5
Heme oxygenase 1	Hmox1	-1.06	-0.54	0.52	4
Histone H2B type 1-B	Hist1h2bb	-1.04	-0.34	0.70	4
Target of Myb protein 1	Tom1	-1.00	-0.77	0.23	2
Probable low affinity copper uptake protein 2	Slc31a2	-0.95	-0.04	0.91	4
Tyrosine-protein kinase FRK	Frk	-0.94	-0.18	0.76	2
Protein RUFY3	Rufy3	-0.94	-1.05	-0.11	10
Serine/threonine-protein kinase 16	Stk16	-0.85	-0.44	0.40	2
Kelch-like protein 9	Klhl9	-0.79	-1.14	-0.34	3
Histone H4	Hist1h4a	-0.77	-0.53	0.25	2

Next, to evaluate the quantified proteins and to determine the biological pathways to which they belong, kyoto encyclopedia of genes and genomes (KEGG) pathway analysis was conducted on 12 (Table 4.5) and 150 (Supplementary table 8.3) non-lysosomal down- and upregulated proteins after 6 hours of starvation, respectively, using the online software g:Profiler (Raudvere et al. 2019). After protein quantification, significantly enriched pathways were sequenced in a descending order as shown in figure 4.29. Significance threshold was set to 0.05 and p-values were corrected for multiple testing according to the Benjamini-Hochberg method. Pathways were plotted against their $-log_{10}$ of the adjusted p-value. Number of proteins representing each group is given next to the respective bar.

Table 4.6: Top 20 upregulated non-lysosomal proteins upon 6 hours of starvation
List of the top 20 upregulated non-lysosomal proteins identified after short-term starvation in the proteomic dataset. Shown are proteins with more than one unique peptide, p-value <0.05 and log_2 fold change ratios >0.75. In addition, the log_2 fold change ratios after 24 hours as well as the log_2 fold change ratios of the difference between 6 and 24 hours of starvation are also shown in the table (#: number of unique peptides, blue: starvation period of interest).

Protein name	Gene name	Log_2FC (6h)	Log_2FC (24h)	Log_2FC (24-6h)	#
Bile acid-CoA:amino acid N-acyltransferase	Baat	2.67	1.25	-1.42	4
Glycogen [starch] synthase, liver	Gys2	2.21	0.52	-1.69	3
Proteasome subunit alpha type-5	Psma5	2.21	1.26	-0.95	4
Proteasome subunit alpha type-1	Psma1	2.12	1.22	-0.90	5
Proteasome subunit beta type-3	Psmb3	2.10	1.33	-0.77	4
Proteasome subunit alpha type-3	Psma3	2.04	1.20	-0.84	10
2-hydroxyacyl-CoA lyase 1	Hacl1	2.03	0.75	-1.28	10
D-dopachrome decarboxylase	Ddt	2.01	1.16	-0.86	4
Proteasome subunit alpha type-2	Psma2	1.96	1.47	-0.49	2
N-acyl-aromatic-L-amino acid amidohydrolase	Acy3	1.95	0.93	-1.03	2
Sorbitol dehydrogenase	Sord	1.95	1.00	-0.95	10
Proteasome subunit beta type-6	Psmb6	1.94	1.33	-0.61	2
Proteasome subunit beta type-5	Psmb5	1.93	1.21	-0.72	4
Acylamino-acid-releasing enzyme	Apeh	1.92	1.21	-0.71	7
Aldehyde oxidase 3	Aox3	1.90	1.01	-0.89	14
Proteasome subunit alpha type-4	Psma4	1.88	1.11	-0.77	4
Delta-aminolevulinic acid dehydratase	Alad	1.87	0.63	-1.24	2
Proteasome subunit alpha type-7	Psma7	1.81	1.05	-0.77	3
NAD(P)H-hydrate epimerase	Naxe	1.75	1.28	-0.47	3
Alanine aminotransferase 1	Gpt	1.74	0.50	-1.24	5

Figure 4.29 A depicts all 6 KEGG pathways which were significantly enriched from 12 downregulated proteins. Top 3 enriched pathways were found to be ‘Mineral absorption’, ‘Ferroptosis’ and ‘HIF-1 signaling pathway’. Some of these quantified proteins are involved in metal ion homeostasis such as the iron binding transport protein serotransferin (TF) and the probable low affinity copper uptake protein 2, also known as solute carrier family 31 member 2 protein (SLC31A2).
In figure 4.29 B, top 20 enriched pathways from 150 upregulated proteins showed ‘Metabolic pathways’, ‘Proteasome’ and ‘Peroxisomes’ as most enriched pathways. Further analysis of enriched pathways demonstrated 5 are directly linked with amino acid metabolism and 3 are associated with carbohydrate metabolism.

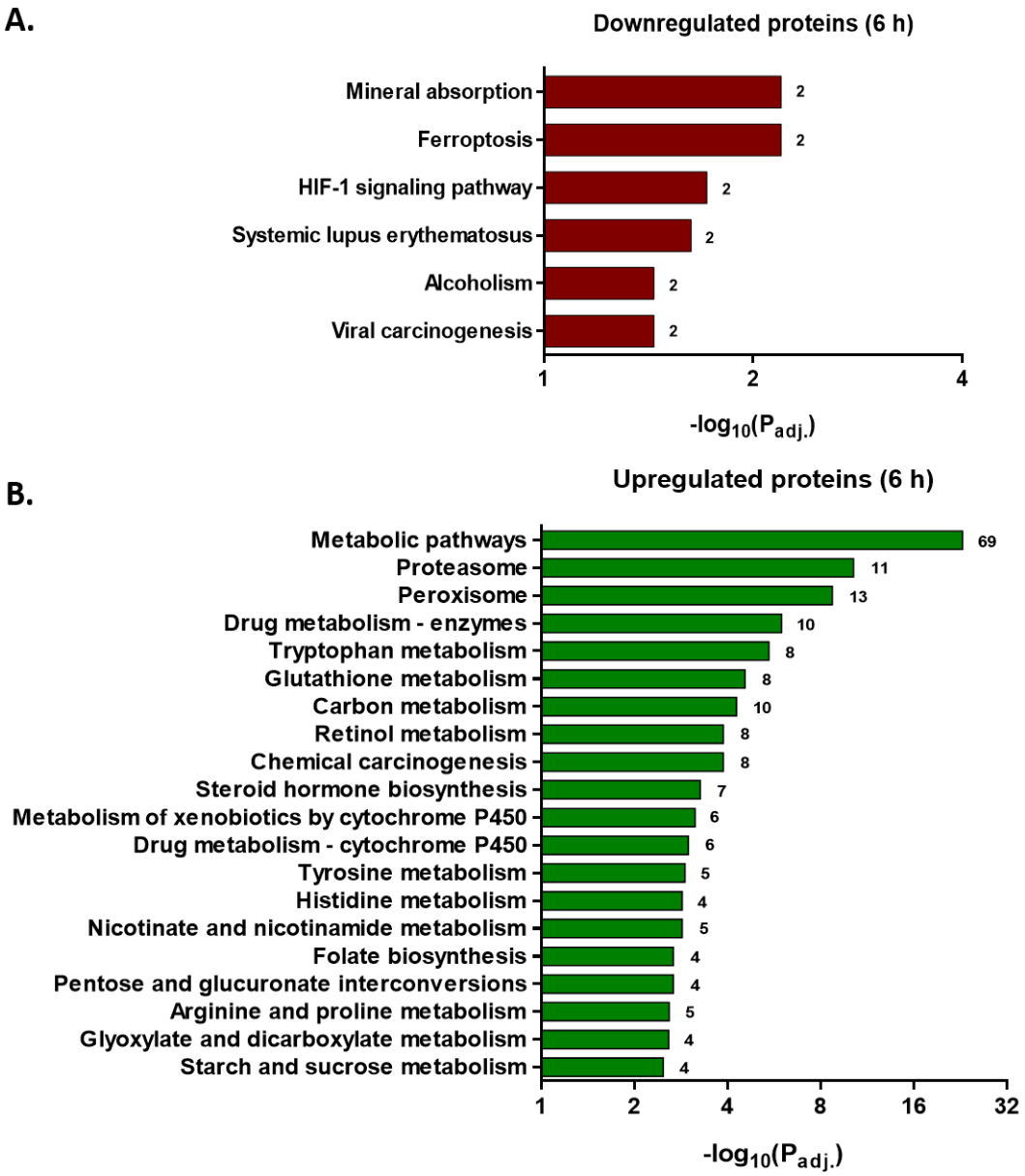

Figure 4.29: KEGG pathway analysis of non-lysosomal down- and upregulated proteins after 6 hours of starvation

KEGG pathway enrichment was performed on 12 (**A**) and 150 (**B**) non-lysosomal down- and upregulated proteins after short starvation period, respectively. Top enriched pathways with an adjusted p-value <0.05 were shown using g:Profiler online software. P-values were corrected based on the Benjamini-Hochberg method. Pathways were plotted against their $-\log_{10}$ of the adjusted p-value and sequenced in a descending order. Number of proteins is given next to the respective bar.

Table 4.7: Top 20 downregulated non-lysosomal proteins upon 24 hours of starvation

List of the top 20 downregulated non-lysosomal proteins identified after long-term starvation in the proteomic dataset. Shown are proteins with more than one unique peptide, p-value <0.05 and log_2 fold change ratios <-0.75. In addition, the log_2 fold change ratios after 6 hours as well as the log_2 fold change ratios of the difference between 6 and 24 hours of starvation are also shown in the table (#: number of unique peptides, blue: starvation period of interest).

Protein name	Gene name	Log_2FC (6h)	Log_2FC (24h)	Log_2FC (24-6h)	#
WASH complex subunit 5	Washc5	-0.75	-2.14	-1.39	15
WASH complex subunit 4	Washc4	-0.77	-2.01	-1.25	13
COMM domain-containing protein 3	Commd3	-0.63	-1.87	-1.24	3
WASH complex subunit 1	Washc1	-0.49	-1.85	-1.36	3
WASH complex subunit 2	Washc2	-0.64	-1.70	-1.06	2
Zinc finger protein-like 1	Zfpl1	-1.11	-1.69	-0.58	3
COMM domain-containing protein 1	Commd1	-0.35	-1.68	-1.32	2
Growth hormone receptor	Ghr	0.19	-1.66	-1.85	4
Serotransferrin	Tf	-1.20	-1.65	-0.46	19
Vacuolar protein sorting-associated protein 26C	Vps26c	-0.41	-1.65	-1.25	4
COMM domain-containing protein 4	Commd4	-0.39	-1.64	-1.25	5
Angiopoietin-related protein 3	Angptl3	-0.39	-1.60	-1.21	6
COMM domain-containing protein 5	Commd5	-0.36	-1.60	-1.24	7
Lipoprotein lipase	Lpl	-0.38	-1.59	-1.20	4
COMM domain-containing protein 8	Commd8	-0.44	-1.57	-1.13	5
COMM domain-containing protein 9	Commd9	-0.57	-1.55	-0.98	2
Golgi-associated PDZ and coiled-coil motif-containing protein	Gopc	-0.85	-1.53	-0.68	2
COMM domain-containing protein 7	Commd7	-0.30	-1.51	-1.21	2
VPS35 endosomal protein sorting factor-like	Vps35l	-0.27	-1.48	-1.22	9
COMM domain-containing protein 10	Commd 10	-0.43	-1.47	-1.05	3

Table 4.8: Top 20 upregulated non-lysosomal proteins upon 24 hours of starvation
List of the top 20 upregulated non-lysosomal proteins identified after long-term starvation in the proteomic dataset. Shown are proteins with more than one unique peptide, p-value <0.05 and log_2 fold change ratios >0.75. In addition, the log_2 fold change ratios after 6 hours as well as the log_2 fold change ratios of the difference between 6 and 24 hours of starvation are also shown in the table (#: number of unique peptides, blue: starvation period of interest).

Protein name	Gene name	Log_2FC (6h)	Log_2FC (24h)	Log_2FC (24-6h)	#
Thioredoxin-dependent peroxide reductase, mitochondrial	Prdx3	0.50	2.81	2.31	13
Copine-3	Cpne3	1.86	2.65	0.78	4
Insulin-like growth factor-binding protein 1	Igfbp1	0.39	2.52	2.13	3
Superoxide dismutase [Cu-Zn]	Sod1	0.8	2.07	1.27	19
Annexin A4	Anxa4	1.45	1.83	0.38	8
Glutathione peroxidase 1	Gpx1	0.77	1.82	1.05	20
Na(+)/H(+) exchange regulatory cofactor NHE-RF2	Slc9a3r2	0.05	1.68	1.63	3
GTP cyclohydrolase 1	Gch1	0.60	1.60	1.00	2
Tyrosine aminotransferase (TAT)	Tat	0.88	1.54	0.66	3
Spectrin beta chain, non-erythrocytic 1	Sptbn1	0.54	1.52	0.98	16
Phosphoenolpyruvate carboxykinase, cytosolic	Pck1	0.87	1.51	0.64	8
Phenazine biosynthesis-like domain-containing protein 1	Pbld1	1.40	1.47	0.07	4
Proteasome subunit alpha type-2	Psma2	1.96	1.47	-0.49	2
Phenazine biosynthesis-like domain-containing protein 2	Pbld2	1.38	1.41	0.02	6
Prolyl endopeptidase	Prep	1.32	1.39	0.07	5
Adhesion G protein-coupled receptor F5	Adgrf5	-0.002	1.38	1.39	2
Amine oxidase [flavin-containing] B	Maob	0.66	1.36	0.70	11
Dysferlin (Dystrophy-associated fer-1-like protein)	Dysf	-0.15	1.34	1.49	4
Annexin A2	Anxa2	0.15	1.33	1.18	15
Proteasome subunit beta type-3	Psmb3	2.10	1.33	-0.77	4

Afterwards, g:Profiler online software was used to conduct KEGG pathway analysis on 121 (Supplementary table 8.4) and 162 (Supplementary table 8.5) non-lysosomal down- and upregulated proteins, respectively, after prolonged starvation. Based on the g:Profiler database, significantly enriched pathways with a corrected p-value <0.05 according to the Benjamini-Hochberg method were represented in a descending order and plotted against their $-log_{10}$ of the adjusted p-value as shown in figure 4.30. Number of proteins representing each group is given next to the respective bar.

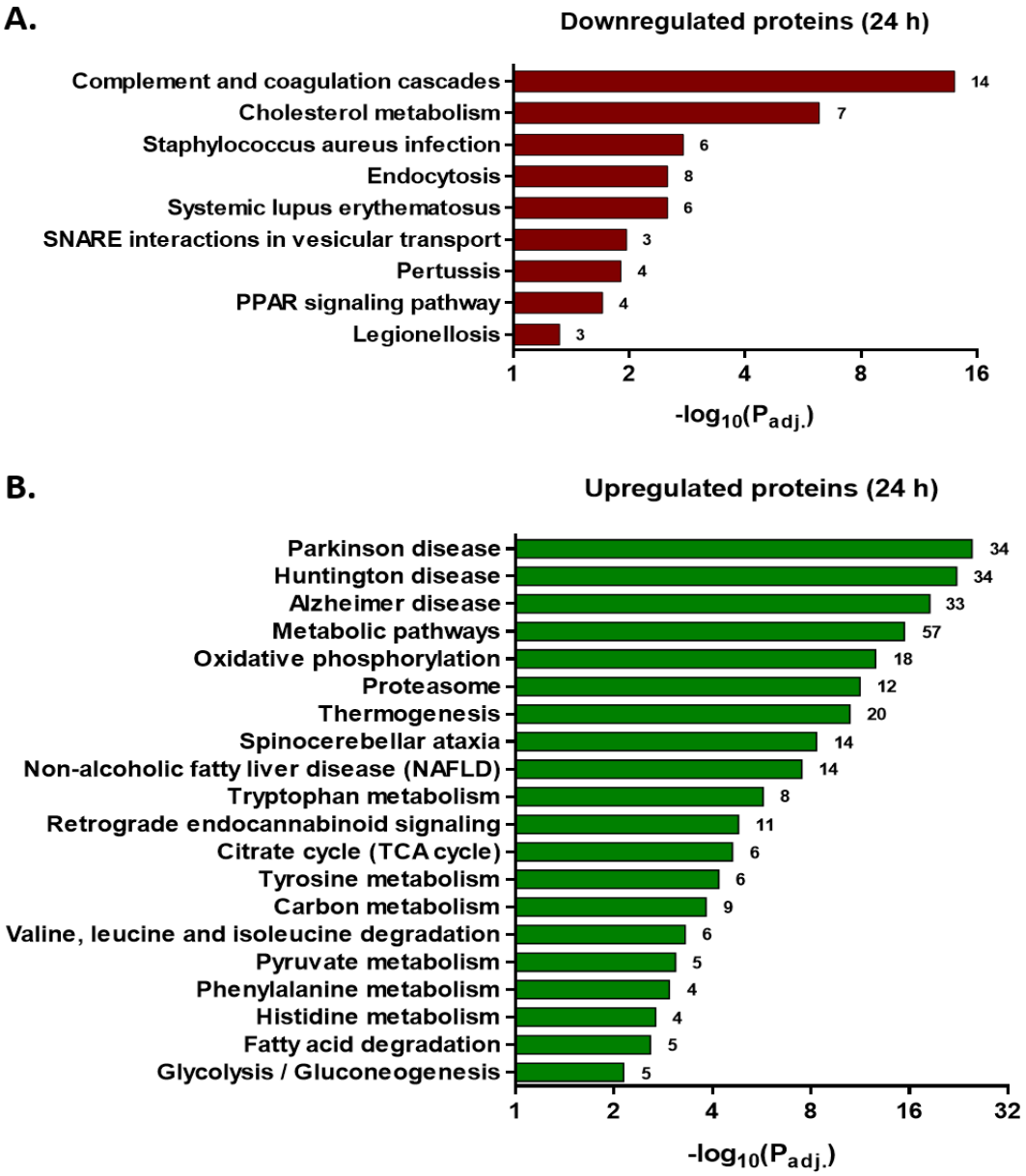

Figure 4.30: KEGG pathway analysis of non-lysosomal down- and upregulated proteins after 24 hours of starvation
KEGG pathway enrichment was performed on 121 (**A**) and 162 (**B**) non-lysosomal down- and upregulated proteins after prolonged starvation period, respectively. Top enriched pathways with an adjusted p-value <0.05 were shown using g:Profiler online software. P-values were corrected based on the Benjamini-Hochberg method. Pathways were plotted against their $-\log_{10}$ of the adjusted p-value and sequenced in a descending order. Number of proteins is given next to the respective bar.

Figure 4.30 A reveals 9 enriched pathways from 121 downregulated proteins where ‘Complement and coagulation cascades’, ‘Cholesterol metabolism’ and ‘Staphylococcus aureus infection’ were described as most enriched pathways. After a manual investigation was performed, the identified proteins are part of several protein complexes such as Wiskott-Aldrich syndrome protein and scar

homolog (WASH), soluble *N*-ethylmaleimide-sensitive factor-attachment protein receptor (SNARE) as shown in the enriched pathways 'Endocytosis' and 'SNARE interactions in vesicular transport', respectively, as well as protein-lipid complexes and copper metabolism gene MURR1 (Comm) domain proteins 1-10. In figure 4.30 B, top 20 enriched pathways from 162 upregulated proteins depicted 'Parkinson disease, 'Huntington disease' and 'Alzheimer disease' as the most enriched pathways. Simultaneously, among the enriched pathways, several pathways are directly correlated with mitochondrial processes such as 'Oxidative phosphorylation', 'Citrate cycle' and 'Fatty acid degradation' and 6 enriched pathways are associated with amino acid metabolism.

Subsequent to the independent analysis of differentially regulated non-lysosomal proteins at each starvation period, a comparative study was conducted using Venn diagrams, generated by Venny online software (Oliveros 2007), between the downregulated proteins after 6 and 24 hours of starvation as well as the upregulated proteins (Figure 4.31). Up- and downregulated proteins after 6 hours of starvation are marked in blue, whereas the orange color represents differentially regulated proteins in 24 hours starved samples.

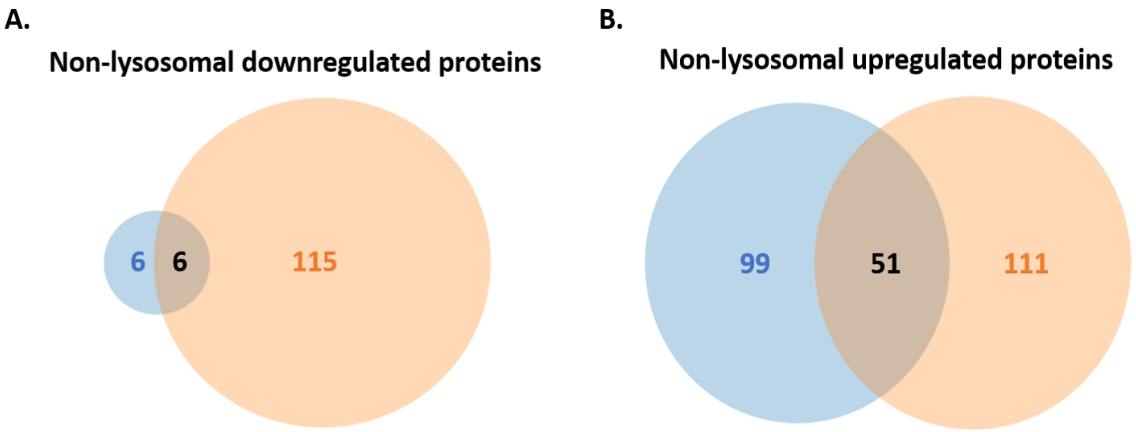

Figure 4.31: Comparative analysis of non-lysosomal differentially regulated proteins after 6 and 24 hours of starvation using Venn diagrams
Non-lysosomal differentially regulated proteins were subjected to a comparative analysis after short and prolonged starvation using Venny online software. **A.** Non-lysosomal downregulated proteins of both starvation datasets were compared and the number of overlapping proteins is shown by Venn diagram in black color. **B.** After 6 and 24 hours of starvation, Venn diagram shows the number of overlapping upregulated proteins. The blue color represents up- and downregulated proteins after 6 hours of starvation, whereas differentially regulated proteins after 24 hours of starvation are shown in orange.

When comparing the downregulated proteins, 6 out of 12 and 121 downregulated proteins after 6 and 24 hours of starvation, respectively, are overlapping between

both datasets (Figure 4.31 A). The overlapping proteins are involved in variable biological pathways. For example, the kelch-like protein 9 (KLHL9) is required for cell cycle regulation, the target of Myb protein 1 (TOM1) is associated with intracellular trafficking and the RUN and FYVE domain containing 3 protein (RUFY3) plays a role in axon growth (Table 4.9).

Table 4.9: Overlapping non-lysosomal downregulated proteins after 6 and 24 hours of starvation

List of the 6 overlapping non-lysosomal downregulated proteins identified after short- and long term starvation in the proteomic dataset. Shown are proteins with more than one unique peptide, p-value <0.05 and log_2 fold change ratios <-0.75. In addition, the log_2 fold change ratios of the difference between 6 and 24 hours of starvation are also shown in the table (#: number of unique peptides).

Protein name	Gene name	Log_2FC (6h)	Log_2FC (24h)	Log_2FC (24-6h)	#
Serotransferrin	Tf	-1.20	-1.65	-0.46	19
Maspardin	Spg21	-1.19	-1.37	-0.17	8
Synaptosomal-associated protein 29	Snap29	-1.07	-1.08	-0.01	5
Target of Myb protein 1	Tom1	-1.00	-0.77	0.23	2
Protein RUFY3	Rufy3	-0.94	-1.05	-0.11	10
Kelch-like protein 9	Klhl9	-0.79	-1.14	-0.34	3

Moreover, 51 proteins are overlapping between 150 and 162 upregulated proteins after short and prolonged starvation, respectively (Figure 4.31 B, supplementary table 8.6). The detected proteins are involved in metabolic processes, specifically catabolic reactions and energy production such as oxidation-reduction and proteolysis reactions according to significantly enriched pathways after applying GO term ‘biological process’. Top 20 overlapping proteins are shown in table 4.10.

Depending on the results acquired from the MS analysis, the lysosome-enriched fractions from mice liver show a change in the regulation of non-lysosomal proteins after 6 hours of starvation compared to a prolonged starvation period.

Table 4.10: Top 20 overlapping non-lysosomal upregulated proteins after 6 and 24 hours of starvation

List of the top 20 overlapping non-lysosomal upregulated proteins identified after short- and long term starvation in the proteomic dataset. Shown are proteins with more than one unique peptide, p-value <0.05 and log_2 fold change ratios >0.75. In addition, the log_2 fold change ratios of the difference between 6 and 24 hours of starvation are also shown in the table (#: number of unique peptides, N/A: not available).

Protein name	Gene name	Log_2FC (6h)	Log_2FC (24h)	Log_2FC (24-6h)	#
Proteasome subunit alpha type-2	Psma2	1.96	1.47	-0.49	2
Phenazine biosynthesis-like domain-containing protein 1	Pbld1	1.40	1.47	0.07	4
Phenazine biosynthesis-like domain-containing protein 2	Pbld2	1.38	1.41	0.02	6
Prolyl endopeptidase	Prep	1.32	1.39	0.07	5
Proteasome subunit beta type-3	Psmb3	2.10	1.33	-0.77	4
Proteasome subunit beta type-6	Psmb6	1.94	1.33	-0.61	2
Thioredoxin reductase 1, cytoplasmic	Txnrd1	1.48	1.32	-0.16	4
Ester hydrolase C11orf54 homolog	N/A	1.51	1.29	-0.22	7
NAD(P)H-hydrate epimerase	Naxe	1.75	1.28	-0.47	3
Proteasome subunit alpha type-5	Psma5	2.21	1.26	-0.95	4
Glutathione S-transferase P 1	Gstp1	1.35	1.26	-0.10	10
Proteasome subunit alpha type-1	Psma1	2.12	1.22	-0.90	5
Proteasome subunit beta type-5	Psmb5	1.93	1.21	-0.72	4
Acylamino-acid-releasing enzyme	Apeh	1.92	1.21	-0.71	7
Proteasome subunit alpha type-3	Psma3	2.04	1.20	-0.84	10
Selenium-binding protein 2; Selenium-binding protein 1	Selenbp2; Selenbp1	0.92	1.19	0.27	20
D-dopachrome decarboxylase	Ddt	2.01	1.16	-0.86	4
Proteasome subunit alpha type-4	Psma4	1.88	1.11	-0.77	4
Glutaredoxin-1	Glrx	1.52	1.09	-0.43	3
Hypoxanthine-guanine phosphoribosyltransferase	Hprt1	1.45	1.08	-0.38	3

4.3.2.4 Starvation influence on the regulation of non-lysosomal candidate proteins based on the proteomic analysis

Since the quantification of the non-lysosomal proteins identified in the MS data revealed a significant change in the abundance of several proteins at the lysosomal level after 6 and 24 hours of starvation, a validation of the results was applied on differentially regulated proteins related to various complexes, organelles and biological processes such as proteasome complex (PSMA7 and PSMB5), WASH complex (WASHC4), gluconeogenesis (PCK1), glycogen metabolism (GYS2 and PYGL) as well as mitochondrial (CPT2, VDAC1, NDUFB7 and NDUFB11) and peroxisomal (LONP2 and NUDT12) proteins (Table 4.11).

Table 4.11: List of the non-lysosomal proteins selected for subsequent validation experiments
Differentially regulated proteins after short and prolonged starvation in the proteomic dataset were analyzed and further investigated. The table displays the candidate proteins, their log_2 fold change ratios after 6 and 24 hours of starvation as well as the log_2 fold change ratios of the difference between 6 and 24 hours of starvation and the corresponding unique peptide number (#: number of unique peptides, *: not significant).

Protein name	Gene name	Log_2FC (6h)	Log_2FC (24h)	Log_2FC (24-6h)	#
Proteasome subunit alpha type-7	Psma7	1.81	1.05	-0.77	3
Proteasome subunit beta type-5	Psmb5	1.93	1.21	-0.72	4
WASH complex subunit 4	Washc4	-0.77*	-2.01	-1.25	13
Glycogen phosphorylase, liver form	Pygl	1.64	0.85	-0.79	11
Glycogen [starch] synthase, liver	Gys2	2.21	0.52*	-1.69	3
Phosphoenolpyruvate carboxykinase, cytosolic	Pck1	0.87*	1.51	0.64	8
Lon protease homolog 2, peroxisomal	Lonp2	1.08	0.02*	-1.06	2
Peroxisomal NADH pyrophosphatase NUDT12	Nudt12	1.37	0.59*	-0.78	4
Carnitine O-palmitoyltransferase 2, mitochondrial	Cpt2	-0.07*	0.79	0.86	11
Voltage-dependent anion-selective channel protein 1	Vdac1	0.01*	0.85	0.84	7
NADH dehydrogenase [ubiquinone] 1 beta subcomplex subunit 7, mitochondrial	Ndufb7	-0.16*	0.90	1.06	2
NADH dehydrogenase [ubiquinone] 1 beta subcomplex subunit 11, mitochondrial	Ndufb11	-0.18*	0.87	1.06	2

The changes in the regulation of the non-lysosomal candidate proteins, shown in the MS results, were further investigated by western blot experiments.

4.3.2.4.1 Validation of proteasome complex regulation after different starvation periods

Besides the lysosomal degradation pathway, the proteasome is responsible for the degradation of intracellular proteins by ubiquitination. It consists of the 20S core complex containing 4 rings, each of which is composed of either seven α or β subunits, and the 19S regulatory complex of ubiquitin (Reviewed by Tanaka 2009). In case of starvation, the large cytosolic protein complex could also be degraded by autophagy (Waite et al. 2016). The proteomic dataset demonstrated a significant upregulation in 12 proteasome subunits after 6 and 24 hours of starvation (Supplementary table 8.3 and 8.5). In addition, the ‘Proteasome’

pathway was also enriched after short- and log-term starvation as shown by KEGG pathway analysis (Figure 4.29 and 4.30).

To verify the upregulation of this large complex in the proteomic data, a western blot experiment was applied with specific antibodies against two significantly upregulated subunits, namely proteasome subunit alpha type-7 (PSMA7) and proteasome subunit beta type-5 (PSMB5) proteins (Table 4.11). Protein signals detected from crude liver lysate and lysosome fractions at each condition were normalized to GAPDH or TPP1 as loading controls. After setting the control values to 1, the standard error of the mean and the statistical significance were determined for eight biological replicates, while the visualized signals for four biological replicates are shown in the following figure.

Figure 4.32 A displays the obtained signals of the 28 kDa-sized PSMA7 protein, 37 kDa GAPDH and 48 kDa TPP1 for control and starved mice. At the crude liver lysate level, PSMA7 amounts did not show a significant change after starvation, while a significant increase in the protein abundance was monitored at the lysosomal level. The unpaired student’s t-test of normalized signals to TPP1 revealed a 4.08- and 3.74-fold increase after 6 and 24 hours of starvation, respectively, compared to control mice.

Furthermore, figure 4.32 B shows the detected signals of PSMB5 at 22 kDa in crude liver lysate and lysosomal fractions together with the corresponding loading control. The average relative intensities indicated no change in PSMB5 abundances at the crude liver lysate level. At the same time, similar to PSMA7, the protein abundance in the lysosomal fraction increased significantly by 2.35- and 2.02-fold after 6 and 24 hours of starvation, respectively, compared to control samples.

Western blot experiments demonstrate a significant increase in the levels of two proteasome complex subunits, namely PSMA7 and PSMB5, at the lysosomal level, in accordance with the proteomic analysis. Moreover, no significant change is detected at the crude liver lysate level.

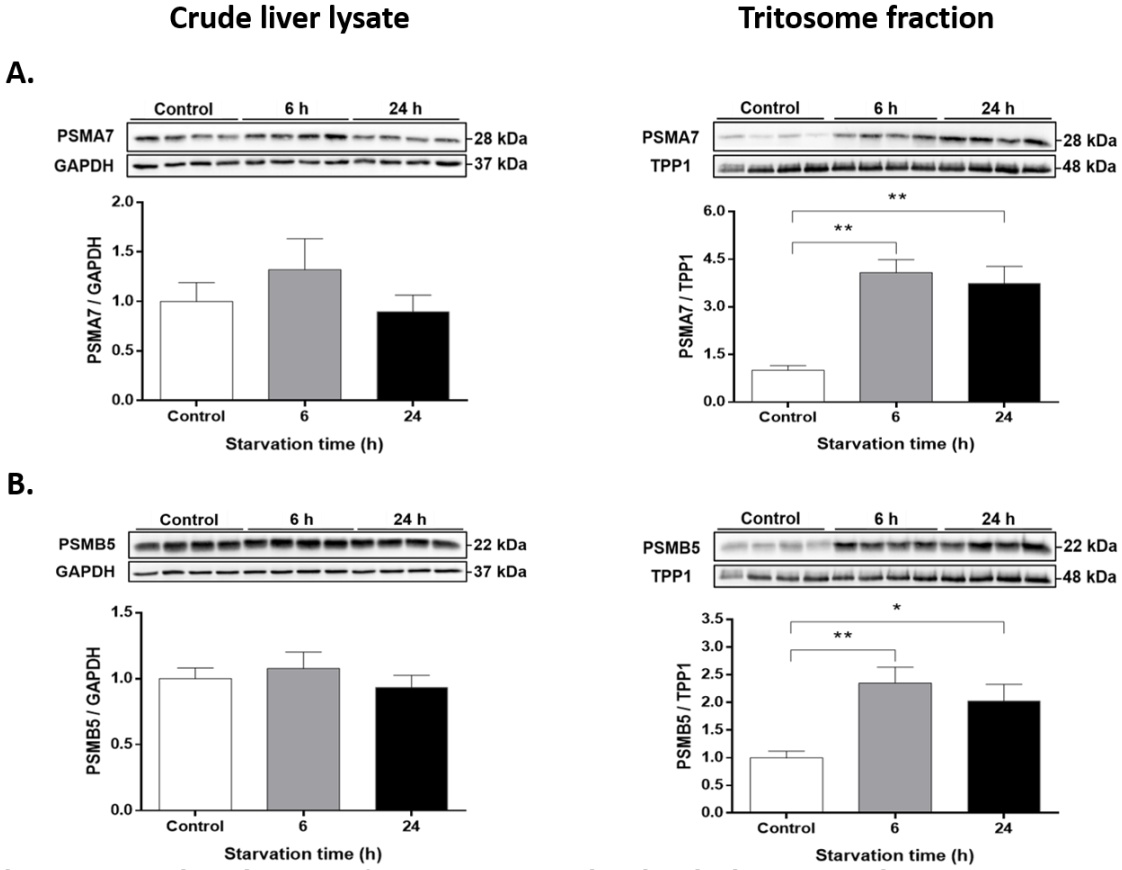

Figure 4.32: Abundances of proteasome subunits during starvation
Male wild-type mice were injected with Triton WR1339 at the age of 6 months. Following liver isolation from control, 6 and 24 hours starved mice, lysosomes were enriched via sucrose gradient-based separation. 10 µg proteins of crude liver lysate and lysosome 'tritosome' fraction were separated on a 12.5 % SDS-PAGE gel, transferred onto a nitrocellulose membrane and probed with PSMA7- and PSMB5-specific antibodies representing proteasome complex subunits together with GAPDH and TPP1 as loading controls. **A** and **B.** Western blot signals were densitometrically quantified, normalized and the average relative intensities of both subunits are depicted as bar charts representing each condition. Displayed signals represent four biological replicates out of eight. Shown are mean + SEM; n=8 and the significance was determined by unpaired student's t-test (*=p<0.05; **=p<0.01). The control samples were set to 1.

4.3.2.4.2 Validation of WASH complex regulation after different starvation periods

The pentameric WASH complex localized on the endosomal surface plays a key role in endosome sorting, by inducing the formation of branched actin network used for cargo trafficking, as well as the autophagy regulation as a response to nutrient starvation (Gomez and Billadeau 2009; Derivery and Gautreau 2010; Dupont and Codogno 2013). In the proteomic dataset, the WASH complex subunits, namely WASH 1, 2, 4 and 5, showed a significant downregulation after 24 hours of starvation, while their downregulation after 6 hours was not

statistically significant (Table 4.7). Similarly, KEGG pathway analysis depicted the downregulation of WASH proteins after prolonged starvation (Figure 30). For this reason, the decline in the abundance after starvation was validated by immune detection using specific antibody against WASH complex subunit 4 (WASHC4). The validation experiment was carried out using eight biological replicates on the crude liver lysate and lysosome 'tritosome' fraction. The protein intensities of control, 6 hours and 24 hours starved samples were normalized either to GAPDH or the lysosomal hydrolase TPP1 as a loading control. After setting the control to 1, the sample distribution was measured by SEM and the statistical significant of eight biological replicates was measured. The detected signals of four biological replicates are depicted in the following figure.

Figure 4.33 represents the detected signals of the 136 kDa-sized WASHC4 protein with the corresponding loading control as well as the average relative intensities of the normalized crude liver lysate and lysosomal samples. In liver whole lysates, no significant changes in WASHC4 amounts were monitored, except for a 1.45-fold increase after 24 hours of starvation compared to 6 hours starved samples. At the lysosomal level, the protein amounts decreased after short as well as prolonged starvation periods. Compared to control samples, the statistical analysis depicted a significant 1.8- and 3.16-fold decrease after 6 and 24 hours of starvation, respectively.

The results obtained from the western blot analysis of lysosomal fractions are consistent with the proteomic analysis, which indicates a downregulation in WASH complex subunits after starvation.

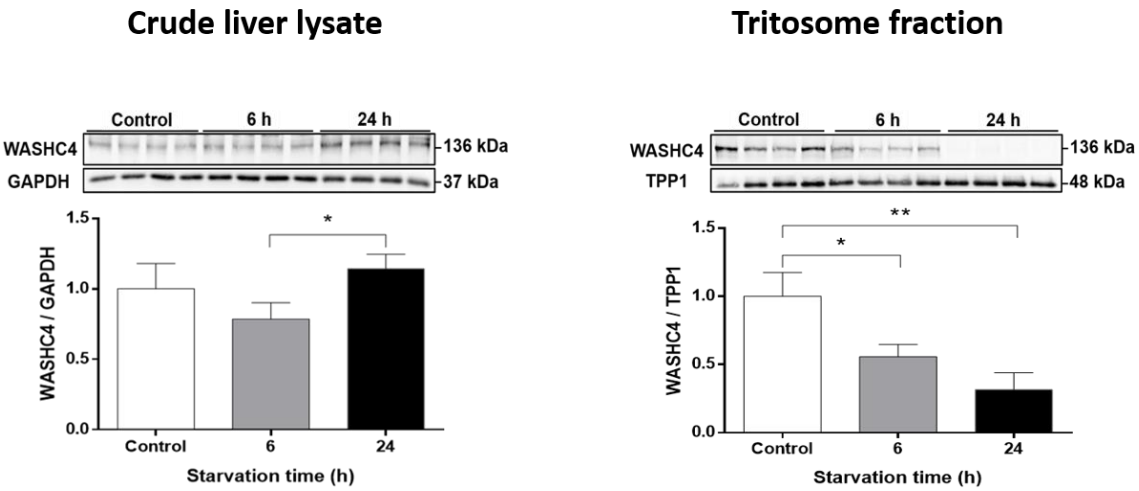

Figure 4.33: Abundances of WASH complex subunit 4 during starvation
Male wild-type mice were injected with Triton WR1339 at the age of 6 months. Following liver isolation from control, 6 and 24 hours starved mice, lysosomes were enriched via sucrose gradient-based separation. 10 µg proteins of crude liver lysate and lysosome 'tritosome' fraction were separated on a 7.5 % SDS-PAGE gel, transferred onto a PVDF membrane and probed with WASHC4-specific antibody representing WASH complex together with GAPDH and TPP1 as loading controls. Protein signals were densitometrically quantified, normalized and the average relative intensities at each condition are shown as bar charts. Demonstrated signals represent four biological replicates out of eight. Shown are mean + SEM; n=8 and the significance was determined by unpaired student's t-test (*=p<0.05; **=p<0.01). The control samples were set to 1.

4.3.2.4.3 Validation of enzymes of glycogen metabolism after different starvation periods

As a branched polymer of glucose, glycogen is synthesized in high circulating glucose levels and serves as a ready glucose source of energy by breaking down when blood glucose levels are diminished (Berg et al. 2002b). One key enzyme needed in the synthesis process is the hepatic glycogen synthase (GYS2), contrarily to the hepatic glycogen phosphorylase (PYGL) which is a decisive factor in the glycogenolysis (Roach et al. 2012; Andersson et al. 2016). The proteomic data indicated a significant upregulation of the two enzymes after 6 hours of starvation, while their level of upregulation was either reduced, PYGL, or not statistically significant, GYS2, after prolonged starvation (Table 4.11). In addition, after the short starvation period, both upregulated proteins were identified in the KEGG enriched pathway 'Starch and sucrose metabolism' (Figure 4.29). Therefore, the MS results were then validated by western blot analysis of crude liver lysate and lysosome fractions of control, 6 and 24 hours

starved mice. Samples from eight biological replicates were probed with PYGL- and GYS2-specific antibodies. The detected signals were normalized to GAPDH or TPP1 loading controls and the control samples were set to 1. The SEM and the unpaired student's t-test were applied to calculate the sample distribution and the statistical significance of eight biological replicates, whereas the depicted signals represent four biological replicates.

The obtained signals of the 97 kDa PYGL and the corresponding loading control, namely GAPDH or TPP1, at each starvation condition are depicted in figure 4.34 A. At the crude liver lysate level, the statistical analysis showed no significant change in the protein abundances after short- and long-term starvation. Meanwhile, at the lysosomal level, the protein amounts increased significantly by 1.97- and 2.23-fold after 6 and 24 hours of starvation, respectively, relative to control samples.

Figure 4.34 B depicts the detected signals of GYS2 and the corresponding loading control. Relative to liver lysate control samples, the abundances of the normalized 81 kDa-sized protein increased by 2.17-fold after 6 hours of starvation. In contrast, a 1.75-fold decrease was demonstrated after 24 hours of starvation comparing to 6 hours starved samples. Similarly, at the lysosomal level, the protein amounts increased by 2.57-fold after short starvation period compared to control samples and decreased by 2.65-fold after prolonged starvation compared to 6 hours starved mice.

These western blot experiments show no change in the amounts of PYGL protein at the crude liver lysate level, but a significant increase is depicted at the lysosomal level after short- and long-term of starvation. Regarding the hepatic glycogen synthase GYS2, the protein intensities pattern is similar in crude liver lysate and lysosome fraction.

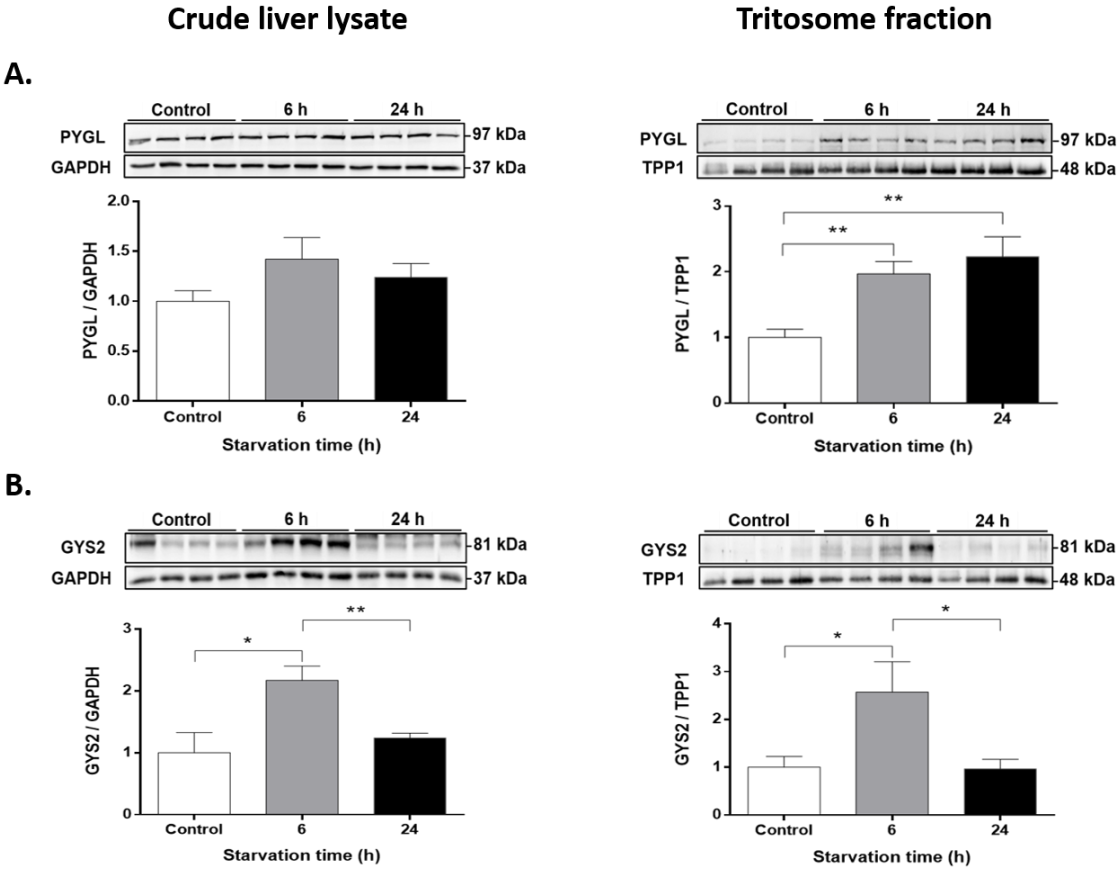

Figure 4.34: Abundances of glycogen-associated proteins during starvation
Male wild-type mice were injected with Triton WR1339 at the age of 6 months. Following liver isolation from control, 6 and 24 hours starved mice, lysosomes were enriched via sucrose gradient-based separation. 10 µg proteins of crude liver lysate and lysosome 'tritosome' fraction were separated on a 12.5 % SDS-PAGE gel, transferred onto a nitrocellulose membrane and probed with PYGL- and GYS2-specific antibodies representing enzymes of glycogen metabolism together with GAPDH and TPP1 as loading controls. **A** and **B.** Abundances of both proteins were densitometrically quantified, normalized and the average relative intensities at each condition are depicted as bar charts. Displayed signals represent four biological replicates out of eight. Shown are mean + SEM; n=8 and the significance was determined by unpaired student's t-test (*=p<0.05; **=p<0.01). The control samples were set to 1.

4.3.2.4.4 Validation of enzymes of gluconeogenesis after different starvation periods

Gluconeogenesis is a metabolic pathway which takes place in the liver or kidney after prolonged starvation and results in the production of glucose from the breakdown of macromolecules such as proteins and lipids (Reviewed by Petersen et al. 2017). Several enzymes are involved in this biological process such as the rate-limiting phosphoenolpyruvate carboxykinase (PCK1), also known as PEPCK, which converts oxaloacetate and GTP into

phosphoenolpyruvate and carbon dioxide (Hanson and Garber 1972; Burgess et al. 2007). The proteomic analysis demonstrated a statistically non-significant upregulation of PCK1 after 6 hours of starvation, while its upregulation after 24 hours was significant (Table 4.11). In parallel, after prolonged starvation, upregulated PCK1 was detected in the KEGG enriched pathway 'Glycolysis/Gluconeogenesis' (Figure 4.30). Therefore, the abundance of PCK1 was validated by western blot analysis using eight biological replicates representing control, 6 and 24 hours starved mice. After antibody detection, PCK1 obtained signals from crude liver lysate and lysosomal fractions were normalized to GAPDH or TPP1 loading controls and control samples were set to 1. The standard error of the mean and the unpaired student's t-test were used to determine the sample distribution and the statistical significance of all eight replicates, respectively, whereas the signals of four replicates are depicted in the following figure.

For control and starved samples, the detected signals of PCK1, GAPDH and TPP1 at 69, 37, 48 kDa, respectively, are shown in figure 4.35. At the crude liver lysate level, no change was displayed in PCK1 levels between control and 6 hours starved mice. GAPDH-normalized intensities of 24 hours starved samples showed a significant increase of 1.55- and 1.82-fold compared to control and 6 hours starved mice, respectively. At the same time, PCK1 abundances in the lysosomal fraction increased significantly by 1.95- and 4.04-fold after 6 and 24 hours of starvation, respectively, compared to control. Furthermore, an increase of 2.07-fold was measured between 6 and 24 hours starved mice.

In line with the proteomic data, PCK1 shows an increase in the abundance after short and prolonged starvation as depicted in the western blot confirmation experiments at the lysosomal level. Furthermore, in liver lysate, PCK1 amount increases after prolonged starvation.

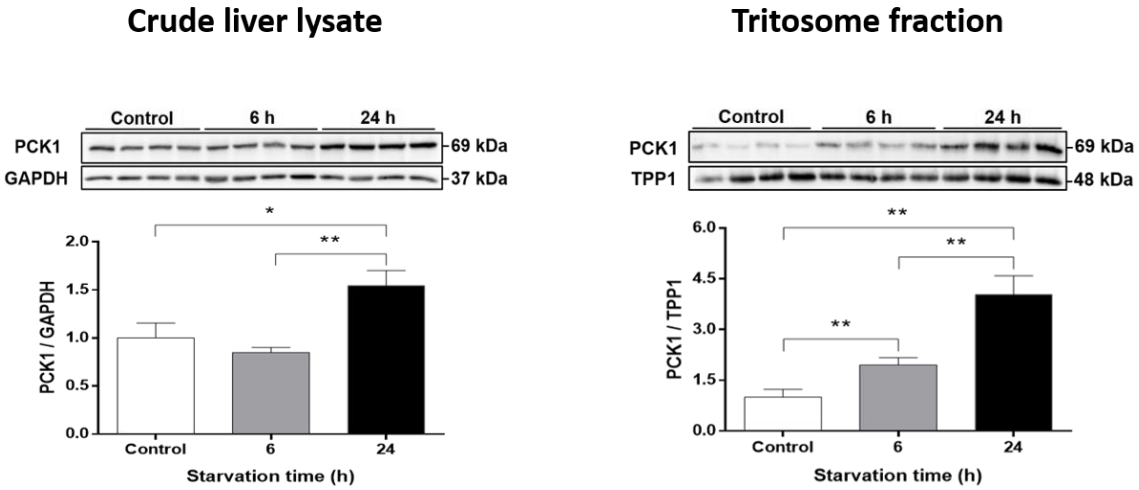

Figure 4.35: Abundances of the gluconeogenic protein PCK1 during starvation
Male wild-type mice were injected with Triton WR1339 at the age of 6 months. Following liver isolation from control, 6 and 24 hours starved mice, lysosomes were enriched via sucrose gradient-based separation. 10 µg proteins of crude liver lysate and lysosome 'tritosome' fraction were separated on a 12.5 % SDS-PAGE gel, transferred onto a PVDF membrane and probed with PCK1-specific antibody representing a gluconeogenic enzyme together with GAPDH and TPP1 as loading controls. Protein signals were visualized, quantified and the average relative intensities of each condition are depicted as bar charts. Displayed signals represent four biological replicates out of eight. Shown are mean + SEM; n=8 and the significance was determined by unpaired student's t-test (*=p<0.05; **=p<0.01). The control samples were set to 1.

4.3.2.4.5 Validation of peroxisomal protein regulation after different starvation periods

As a fundamental organelle for cellular homeostasis maintenance, peroxisomes are involved in several metabolic pathways such as the metabolism of hydrogen peroxide and fatty acid oxidation (Reviewed by Islinger and Schrader 2011). Meanwhile, starvation conditions lead to a decrease in peroxisome abundance in the cell via the autophagic-lysosomal degradation pathways (Sakai et al. 2006). The proteomic data revealed a significant upregulation in a peroxisomal group of 12 proteins after 6 hours of starvation, where no significant change in their regulation was monitored after prolonged starvation (Supplementary table 8.3). These results were also depicted in the KEGG pathway analysis by the enrichment of 'Peroxisome' pathway (Figure 4.29). To clarify whether the increase in the abundance after short starvation is significant, western blot verification experiment was applied to two peroxisomal proteins, namely lon protease homolog 2 (LONP2), an ATP-dependent protease involved in selective degradation of oxidized proteins (Pomatto et al. 2017) and the peroxisomal NADH

pyrophosphatase NUDT12 (NUDT12), a hydrolase regulating the concentrations of independent nucleotides (Abdelraheim et al. 2003) (Table 4.11). The obtained signals of control, 6 and 24 hours starved mice were normalized to GAPDH or TPP1 loading controls and control samples were set to 1. For crude liver lysate and lysosome fractions, the sample distribution and the statistical significance were calculated for eight biological replicates, while the visualized signals represent four biological replicates.

Figure 4.36 A displays the obtained signals from the 95 kDa-sized LONP2 protein as well as GAPDH and TPP1. At the crude liver lysate level, the unpaired student's t-test of LONP2 normalized intensities revealed no change in the protein abundance during starvation. At the lysosomal level, the protein abundances increased significantly by 1.95-fold between control and 6 hours starved mice and a decrease of 1.53-fold was demonstrated after 24 hours of starvation compared to 6 hours starved samples.

Figure 4.36 B represents the detected 52 kDa NUDT12 signals of control, 6 and 24 hours starved mice along with the corresponding loading controls. At the crude liver lysate level, the average relative intensities showed no significant change in the abundances of NUDT12 after starvation, whereas a 1.40-fold increase was measured between control and 6 hours of starvation at the lysosomal level. In parallel, the decrease in NUDT12 levels in the lysosome between 6 and 24 hours of starvation was not statistically significant.

In line with the proteomic data, western bot validation experiments at the lysosomal level depict a significant increase in the levels of peroxisomal proteins after short starvation. Meanwhile, the decrease in the abundances after prolonged starvation is statistically significant in case of LONP2 protein. The analysis on the crude liver lysate level indicates no relevant differences during starvation.

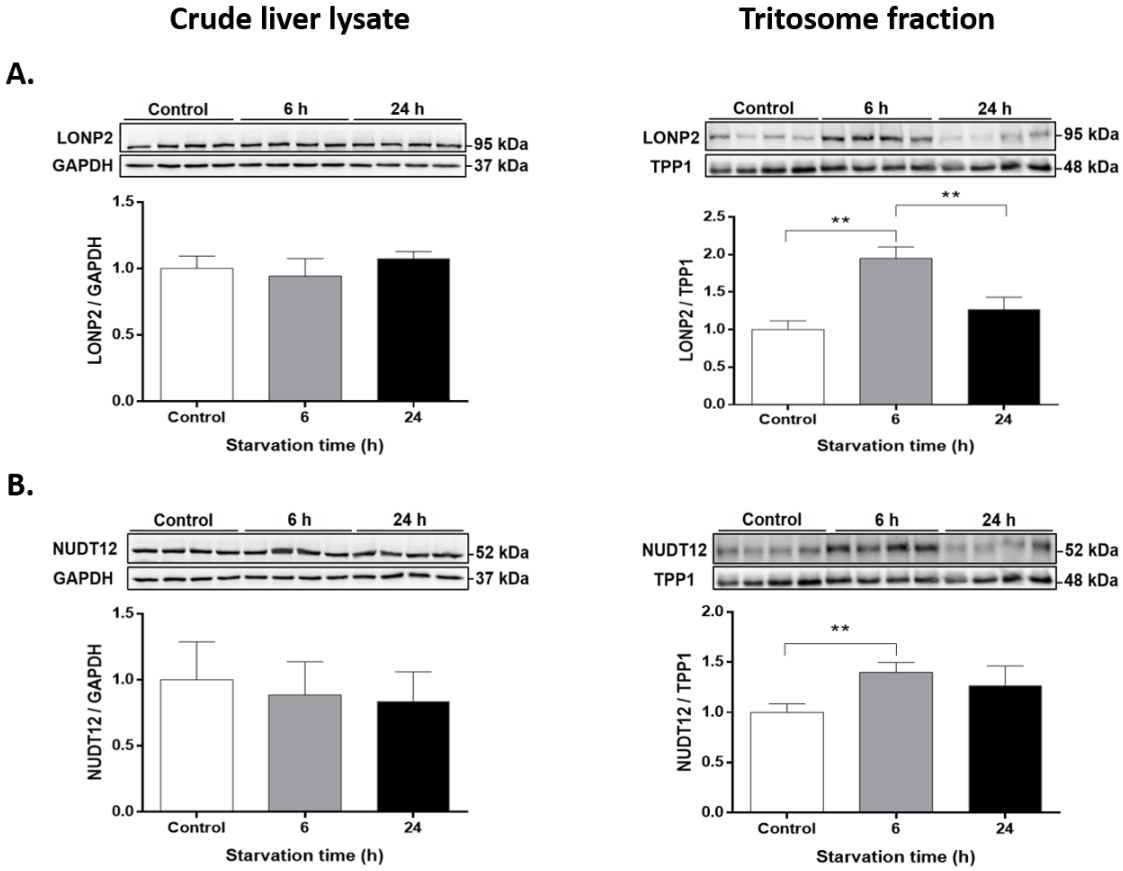

Figure 4.36: Abundances of different peroxisomal proteins during starvation
Male wild-type mice were injected with Triton WR1339 at the age of 6 months. Following liver isolation from control, 6 and 24 hours starved mice, lysosomes were enriched via sucrose gradient-based separation. 10 µg proteins of crude liver lysate and lysosome 'tritosome' fraction were separated on a 7.5 % SDS-PAGE gel, transferred onto a PVDF membrane and probed with LONP2- and NUDT12-specific antibodies representing peroxisomal proteins together with GAPDH and TPP1 as loading controls. **A** and **B.** Densitometrically quantified signals were normalized and the average relative intensities of both proteins are shown as bar charts. Displayed signals represent four biological replicates out of eight. Shown are mean + SEM; n=8 and the significance was determined by unpaired student's t-test (**=p<0.01). The control samples were set to 1.

4.3.2.4.6 Validation of mitochondrial protein regulation after different starvation periods

Mitochondria regulate a wide spectrum of biochemical processes like oxidative phosphorylation and is responsible for cellular energy production. In addition, when mitochondrial metabolism is not required, it is potentially degraded by autophagocytosis to maintain homeostasis (Melser et al. 2015). In this proteomic analysis, the $\log_2$ fold change ratios of 54 mitochondrial proteins, showed a significant upregulation after 24 hours of starvation, while no significant change was monitored after 6 hours (Supplementary table 8.5). These results were also

displayed in the KEGG pathway analysis by the enrichment of several mitochondria-related pathways (Figure 4.30). As another method to verify this observation, western blot confirmation experiment was applied to the carnitine O-palmitoyltransferase 2 (CPT2), which is involved in fatty acid beta-oxidation, the voltage-dependent anion-selective channel protein 1 (VDAC1), which is the most expressed isoform in comparison to VDAC2 and -3 and builds an ion channel through the outer mitochondrial membrane (Hodge and Colombini 1997; Craigen and Graham 2008), as well as two mitochondrial respiratory chain proteins, namely NADH dehydrogenase [ubiquinone] 1 beta subcomplex subunit 7 and 11 (NDUFB7 and -11) (Table 4.11). After antibody detection, acquired signals from crude liver lysate and lysosome fractions were normalized to GAPDH or TPP1 loading controls and control samples were set to 1. The sample distribution and the statistical significance of eight biological replicates were calculated, while the depicted signals represent four biological replicates.

Figure 4.37 A depicts the obtained signals from the 65 kDa-sized CPT2 protein as well as the GAPDH and TPP1 loading controls for control, 6 and 24 hours starved mice. At the crude liver lysate level, the statistical analysis displayed no change in CPT2 amounts between control and 6 hours starved samples. In parallel, the normalized CPT2 intensities showed a 1.35-fold increase in protein levels between 6 and 24 hours starved samples. At the lysosomal level, the protein abundances increased significantly by 2.08- and 1.66-fold after prolonged starvation compared with control and 6 hours starved mice, respectively.

Figure 4.37 B shows the detected signals of the 32 kDa-sized VDAC1 protein with the corresponding loading control as well as the average relative intensities of crude liver lysate and lysosomal fractions. In liver whole lysates, no significant variations in VDAC1 amounts was monitored, except for a 1.72-fold increase after 24 hours of starvation compared to 6 hours starved mice. Meanwhile, the protein amounts in the lysosomal fraction increased after starvation. Compared to control samples, the unpaired student’s t-test displayed an increase of 1.51- and 2.54-fold after 6 and 24 hours of starvation, respectively. Furthermore, between 6 and 24 hours starved samples, a 1.68-fold increase was measured.

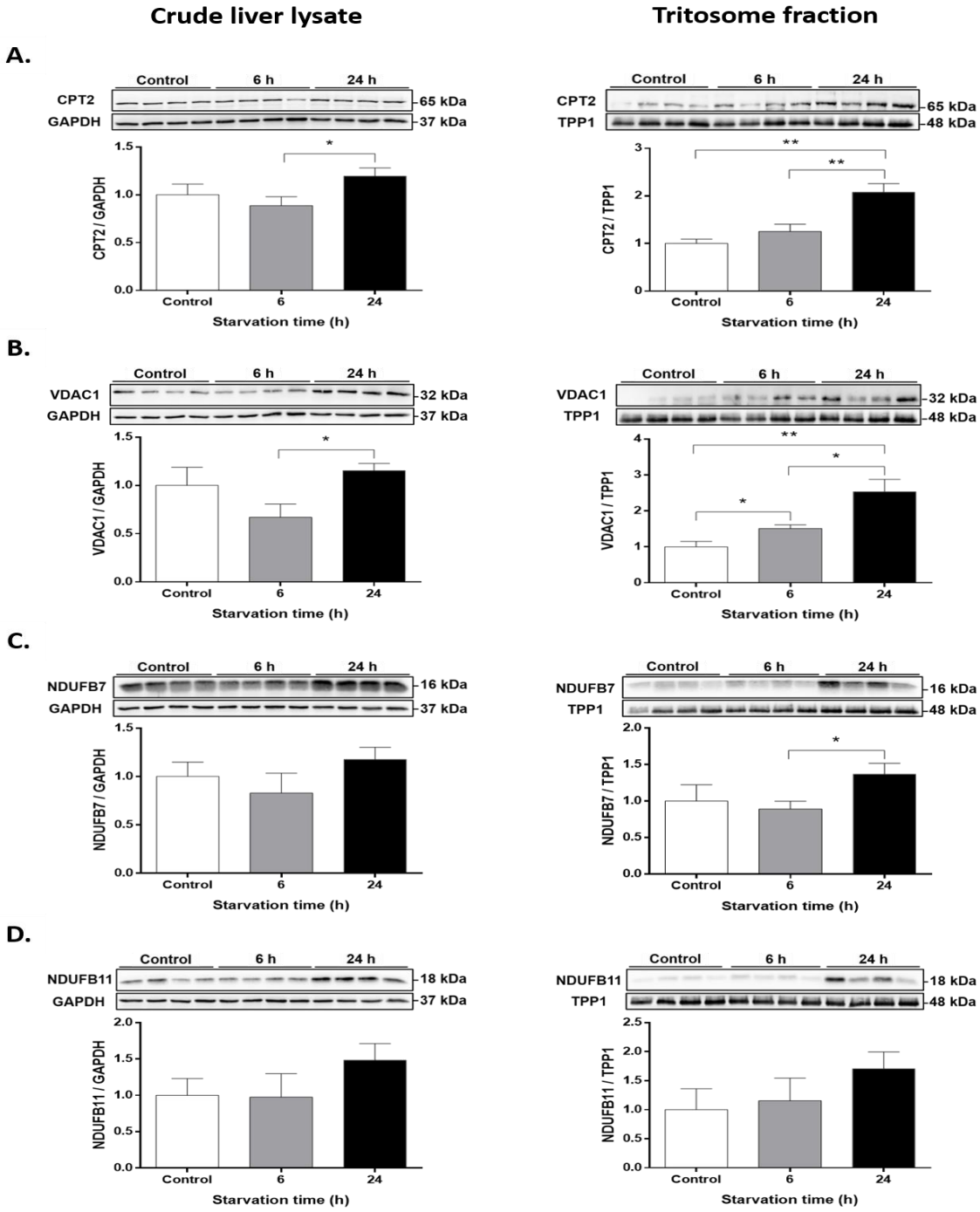

Figure 4.37: Abundances of different mitochondrial proteins during starvation
Male wild-type mice were injected with Triton WR1339 at the age of 6 months. Following liver isolation from control, 6 and 24 hours starved mice, lysosomes were enriched via sucrose gradient-based separation. 10 µg proteins of crude liver lysate and lysosome 'tritosome' fraction were separated on a 12.5 % SDS-PAGE gel, transferred onto a nitrocellulose membrane and probed with CPT2-, VDAC1-, NDUFB7- and NDUFB11-specific antibodies representing mitochondrial proteins together with GAPDH and TPP1 as loading controls. **A-D.** Densitometrically quantified signals were normalized and the average relative intensities of CPT2, VDAC1, NDUFB7 and -11 are shown as bar charts. Displayed signals represent four biological replicates out of eight. Shown are mean + SEM; n=8 and the significance was determined by unpaired student's t-test (*=p<0.05; **=p<0.01). The control samples were set to 1.

The detected 16 kDa NDUFB7 signals at the liver lysate and lysosome level together with the corresponding loading controls are shown in figure 4.37 C. The average relative intensities of each condition are depicted as bar charts. NDUFB7 abundances displayed no change at the crude liver lysate level, whereas a 1.53-fold increase was measured between 6 and 24 hours of starvation at the lysosomal level.

Moreover, figure 4.37 D demonstrates the obtained signals from NDUFB11, GAPDH and TPP1 proteins. The statistical analysis of the normalized 18 kDa-sized protein depicted no change in the intensities after starvation in the liver tissues. Furthermore, in the lysosome fraction, the increase in the protein abundances throughout the starvation time course was not statistically significant.

Western bot validation experiments display a significant increase in the abundances of the mitochondrial proteins CPT2 and VDAC1 on the lysosomal level after prolonged starvation. The analysis on the crude liver lysate level depicts no significant change, except for an increase between 6 and 24 hours starved samples. Furthermore, mitochondrial respiratory chain proteins display no significant changes in liver lysate or lysosome fractions, except for an increase between 6 and 24 hours starved lysosomal samples of NDUFB7.

5 Discussion

Lysosomes are multifunctional organelles that are involved in many molecular processes which regulate cell homeostasis. Beside the degradation of macromolecules in its lumen, the lysosomal surface plays an important role in nutrient sensing and therefore in cell growth via the active mTORC1. In a nutrient deprived state, the kinase mTOR is inactivated and the phosphorylation of its target proteins is reduced (Reviewed by Ballabio and Bonifacino 2020). The precise regulation profile of mTORC1 following different starvation periods and the starvation-induced changes in lysosomal protein amounts are not yet completely understood on the *in vivo* level.

In this thesis several aspects related to cellular metabolism and lysosomal signaling during starvation were studied. The activation of mTORC1 was monitored in different key metabolic organs for different starvation time periods. Subsequently, the lysosomal proteome of the liver was analyzed for alterations in lysosomal/non-lysosomal proteins after two selected starvation periods for short- and long-term starvation. Additionally, the impact of the two starvation periods on the body metabolism was examined.

5.1 mTORC1 activity is differentially regulated in different mouse organs

To investigate the lysosomal proteome under different starvation conditions, it is necessary to determine the starvation time frame in which mTORC1 is the least active. Although some *in vitro* studies have reported on mTORC1 regulation after prolonged starvation (Yu et al. 2010; Rong et al. 2011; Chen et al. 2014; Tan et al. 2017), there is a lack of comprehensive *in vivo* studies to define mTORC1 activity in starved mice. Therefore, liver, skeletal muscle and brain were removed at different starvation time periods (Figure 4.1). In this study, the activity of kinase mTOR was investigated by monitoring the phosphorylation of two downstream targets, 4EBP1 and S6, as part of the protein synthesis pathway (Saxton and Sabatini 2017). The phosphorylation status of both targets is widely accepted as an indicator of mTORC1 activity. T37, T46, S65, T70, S83, S101 and S112 are

the seven 4EBP1 phosphorylation sites identified in humans (Qin et al. 2016). The detected phosphorylation of 4EBP1 at T37/46 works as a precursor to T70 phosphorylation followed by S65 indicating that these phosphorylations are necessary to block 4EPB1 binding to eIF4E protein and therefore to initiate protein synthesis (Gingras et al. 2001). Furthermore, the observed phosphorylation of S6 ribosomal protein, an indirect target of mTOR, at S240/244 is exclusively mediated by p70 ribosomal S6 kinases which enhances mRNA translation initiation (Ferrari et al. 1991; Peterson and Schreiber 1998). In addition to the above described targets, the protein level of LC3, an autophagosome biogenesis marker, was also determined (Hosokawa et al. 2009).

In the liver, starvation was associated with a gradual decrease in mTORC1 activity reaching a significant decrease after 9 and 12 hours of starvation, as depicted by the p-4EBP1 intensities and the gamma isoform levels of total 4EBP1 signals. Following this, a reactivation can be seen after 16 hours (Figure 4.2). The low number of statistically significant changes measured in the phosphorylation of 4EBP1 can be predominantly caused by the uneven abundances in the triplicates of most time periods. Therefore, the activity pattern of mTORC1 was confirmed by western blot analysis of p-S6 ribosomal protein showing a relevant decrease after 6 hours of starvation and a complete reactivation after 20 hours (Figure 4.3). Since the liver plays a key metabolic role in prolonged starvation and provides the body with the necessary energy metabolites (Rui 2014), it is logical to see a reactivation in mTORC1 as a pivotal regulator of liver metabolism in starvation (Reviewed by Liu and Sabatini 2020). In a comparative study of HepG2 and Huh6, two human hepatic cancer cell lines, as well as the human fibroblast cell line LM217, starvation using glucose-free DMEM without fetal bovine serum (FBS) showed a reactivation of mTORC1 in HepG2 and Huh6 cells after 6 and 12 hours of starvation, respectively, but not in LM217 cells (Murata et al. 2015). Another *in vitro* study conducted by Tan and colleagues on amino acid starved HepG2 cells reported a possible reason for mTORC1 reactivation after prolonged starvation. The study suggests that the addition of glutamine alone is sufficient to restore mTORC1 activity after 8 hours of starvation through its role in the production of non-essential amino acids (NEAAs) and the TCA cycle

substrate alpha-ketoglutarate (Tan et al. 2017). Although the starvation time periods at which mTORC1 shows its reactivation are shorter than the *in vivo* results obtained in this study, these variations can possibly be explained due to a change in the biological system used. In other words, *in vitro* experiments are processed in a controlled environment, whereas *in vivo* studies are conducted inside a living organism where many interfering reactions can occur.

In the skeletal muscle, by observing the 4EBP1 phosphorylation and the shift in the protein abundances from gamma isoform, the uppermost phosphorylated isoform, to alpha isoform, the lower and least phosphorylated one in total 4EBP1 blots, a gradual decrease in mTORC1 signaling can be concluded starting from the early starvation periods (Figure 4.4). Although the p-S6 relative quantification results appear to support these findings, there were no statistically significant results, except for a decrease between 12 and 16 hours of starvation, due to variances in the detected signals, mainly the control and 9-hour time period (Figure 4.5). The variation of intensities between the replicates increased the mean abundance and the standard error of the mean leading to a failure in reaching the significance. In addition, after excluding one replicate at the 9-hour starvation period, the statistical analysis using only two values is not accurate and hence it is necessary to increase the number of replicates at this time period.

In 2001, *in vivo* experiments conducted by Bodine et al. demonstrated that mTORC1 activation/deactivation is related to muscle hypertrophy/atrophy (Bodine et al. 2001). In parallel, two separate studies on muscle-specific mTOR knockout mice and muscle-specific Raptor knockout mice showed a severe muscle atrophy phenotype (Bentzinger et al. 2008; Risson et al. 2009). The protein breakdown in the skeletal muscle resulting from mTORC1 deactivation is a direct response to starvation. Many amino acids are released, such as glutamine and alanine, then consumed by the liver as substrates for gluconeogenesis (Felig 1973; Hatazawa et al. 2018).

Western blot analysis of p-4EBP1 and p-S6 in the brain shows no significant alteration in the protein expression after starvation except for a 1.21-fold decrease in the abundance of p-4EBP1 between 9 and 16-hour time periods (Figure 4.6) and a 1.73-fold decrease in the abundance of p-S6 between control

and 12 hours of starvation (Figure 4.7). These reductions are probably not biologically significant. Therefore, the obtained results confirm no relevant change in mTORC1 activity during 20 hours of starvation. The stability in mTORC1 activity is due to the permanent supply of nutrients to the brain either by glucose through the glucose transporter type 3 (GLUT3) or ketone bodies during prolonged starvation, which is then used as the major fuel (Simpson et al. 2008; Watford 2015). This 'nutrition protection' is essential for the regulatory role of mTORC1 in different neurological functions such as neuronal growth and differentiation, circuit formation and synaptic pruning (Park et al. 2008; Tang et al. 2014; Reviewed by Lipton and Sahin 2014).

After monitoring mTORC1 activity through phosphorylation targets within the protein synthesis pathway, the obtained results could be corroborated by analyzing starvation-induced autophagy (Figure 4.8). Autophagosome synthesis or degradation was monitored by measuring the endogenous levels of LC3B marker protein. Since the antibodies affinities can differ between LC3-I and LC3-II and the abundance levels of the forms could be dependent on the tissue type, LC3B-II intensities were normalized to GAPDH as a housekeeping protein (Kimura et al. 2009). However, it is still recommended not to neglect LC3-I abundance levels and its conversion pattern to LC3-II according to Klionsky and colleagues guidelines for monitoring autophagy (Klionsky et al. 2016). Therefore, LC3B-II/LC3B-I ratio was measured as well. For a better understanding of the autophagic process, several starvation studies have also quantified LC3-II accumulation levels as well as LC3B-II/LC3B-I ratio as an indicator of autophagy (Fritzen et al. 2016; Redmann et al. 2017; Raz et al. 2017; Kang and Rhee 2019). Although the lipidated form is larger in molecular mass, it is detected at a lower molecular weight position than LC3B-I. This is probably due to LC3B-II lipidation, which increases the hydrophobicity of the protein, resulting in faster electrophoretic mobility in the SDS-PAGE gel than its actual size (Nath et al. 2014).

In the liver, an analysis of LC3 levels shows a significant increase in lipidated LC3B at the starvation time periods where mTORC1 is least active. This suggests that autophagy occurs mainly after short starvation and reduces after prolonged

starvation. A possible reason for the decrease in the autophagy and for mTORC1 reactivation after prolonged starvation is related to the initiation of autophagy (Yu et al. 2010). Yu and colleagues indicated that the lysosomal degraded components are released into the cytosol as a requirement for lysosome reformation and as nutrient source for mTORC1 activation. In contrast, the amounts of LC3B-II in the skeletal muscle demonstrated no statistical significant change when normalized to GAPDH. Consistent with our results, a separate study on nutrient starved mice for 48 hours showed no significant change in the amounts of actin-normalized LC3-II in the skeletal muscle (Ju et al. 2010). In our study, the conversion of LC3B-I to LC3B-II increased significantly after prolonged starvation. Interestingly, in most studies where LC3-II levels were increased after nutrient starvation (Paolini et al. 2018; Nakai et al. 2020) or after high-intense exercise (Pagano et al. 2014) in the skeletal muscle, LC3B-II/LC3B-I ratio was the method of choice. Since LC3B-II is localized on the inner and outer membrane of the autophagosomes during the autophagy process, the accumulation of LC3B-II could indicate either an enhanced autophagosome formation or an impaired autophagosome degradation (Reviewed by Yoshii and Mizushima 2017). At the same time, this distinct shift to LC3B-II form could be misleading due to the normalization method used as described above. Both normalization methods investigate the steady-state levels of LC3B-II, but not the autophagic flux. Therefore, to monitor the dynamic changes in LC3B-II levels, lysosomal protease inhibitors such as leupeptin, pepstatin and chloroquine (Ahlberg et al. 1985) or lysosomal lumen acidification inhibitors like bafilomycin A1 (Yoshimori et al. 1991), need to be administered. In the presence of the inhibitors, the increase in LC3B-II amounts is an indication of autophagic flux and thus the accumulation of autophagosomes (Reviewed by Loos et al. 2014). In an *in vivo* macroautophagic flux study conducted by Haspel and colleagues on male wild-type mice, an intraperitoneal injection of leupeptin resulted in a high accumulation of LC3-II in different organs reaching its highest in the liver. These amounts increased further after 17-18 hours of starvation (Haspel et al. 2011). Similarly, another *in vivo* autophagic flux study on skeletal muscles of male wild-type mice revealed an augmented LC3-II amounts after an intraperitoneal injection of the

microtubule depolarizing agent colchicine. An additional increase was monitored after applying an autophagic stimulus such as nutrient starvation (Ju et al. 2010). In the brain, both normalization methods depicted a relative stability in LC3B-II levels throughout the course of starvation. In parallel, a strong abundance of cytosolic form LC3B-I signals can be observed compared to LC3B-II. The same observation was shown by Mizushima et al. in a starvation-induced autophagy study on wild-type mice, where distinct intensities of LC3-I were monitored in comparison to LC3-II in brain samples of 24- and 48 hours starved mice (Mizushima et al. 2003). The commonly known high abundance of LC3B-I in brain tissues could be associated with the fast clearance of newly formed autophagosome in neurons (Ariosa and Klionsky 2016; Benito-Cuesta et al. 2017) and the continuous supply of nutrient to the brain (Mizushima et al. 2003; Watford 2015), which probably inhibits the conversion of LC3B-I form to LC3B-II form.

In conclusion, mTORC1 demonstrates different activity patterns during starvation. In the liver, mTORC1 was reactivated after prolonged starvation, while a continuous deactivation in the skeletal muscle was monitored. In contrast, mTORC1 was continuously active in the brain. Monitoring mTORC1 activity and the inverse autophagosome formation after different starvation periods in three key mouse model metabolic organs brings a unique comprehensive overview of the response to nutrient deprivation on the molecular level.

5.2 Short- and long-term starvation have different impacts on body metabolism

The previously obtained findings showed mTORC1 activity varies in different starvation periods. These results at the molecular level did not define the metabolic status of the body, thus requiring additional investigation to determine the changes in the metabolism of the energy sources and the body response to different starvation periods.

5.2.1 Starvation causes weight loss and changes in blood glucose levels

The first investigation to evaluate the general metabolic state of the body after a short and prolonged starvation was to measure the body weight of the mice. Mice were deprived of food, but had access to water. Since starvation is widely correlated with changes in body weight (Strubelt et al. 1981; Claassen 1994; Williams et al. 2002; Sokolović et al. 2007), and while the documentation of weight loss can also be used as a confirmation of starvation, it is mandatory to avoid undetected weight loss >20 % since this is a criterium to end the animal experiment. Starved mice showed a significant decrease in their body weight, starting at 3.18 % and followed by 14.6 % after 6 and 24 hours of starvation, respectively (Figure 4.9). As expected, starvation had a clear physiological effect leading to body weight loss, where the decline was proportional to the starvation period. This decrease can be mainly concluded by the weight loss of adipose tissue (Bronson 1987), skeletal muscle (Donnelly et al. 1991), liver, heart and kidney, whereas the brain weight remains unchanged (Warwick et al. 1985). Compared to this study, other starvation experiments reported a weight loss of 6 % after 6 hours of starvation (Prior et al. 2012) and 11 % after 24 hours (Furner and Feller 1971). Many experimental factors may be the reason for these differences in the measured body weight after starvation between the mentioned studies. For example, the water intake, the possibility of feces or nesting material consumption during starvation periods as well as the differences in housing conditions (Reviewed by Jensen et al. 2013).

Next, the circulating levels of glucose as the main metabolite for energy production was measured. Since age and sex variation can affect the measurement sensitivity of blood glucose concentrations (Carvalho et al. 1996; Macotela et al. 2009), selected wild-type mice were male and 6 months old. Although Tsunseki and colleagues have shown a tendency towards a decrease in the circulating levels after short starvation in mice (Tsuneki et al. 2002), the starved mice in this study depicted no significant change in blood glucose levels after 6 hours (Figure 4.10). At the same time, studies have demonstrated that a significant decrease in blood glucose levels can be first measured after 12 hours of starvation (Geisler et al. 2016; Park et al. 2019). The possible maintenance of

glucose levels in our study in early starvation periods can be attributable to pre-starvation food intake, mice activity and the depletion of hepatic glycogen stores during the transition from fed to fasted state (Izumida et al. 2013). Afterwards, circulating glucose levels show a significant drop after 24 hours of starvation compared to control and 6 hours starved mice, reflecting a strong limitation of carbohydrate intake, in addition to an ongoing transport of glucose to the metabolic organs, mainly the brain, as well as to the red blood cells which are entirely reliant on it (Gelfand and Sherwin 1983). At the same time, the fuel preference starts shifting to ketone bodies, where gluconeogenesis also occurs (Hatting et al. 2018).

5.2.2 Synthesis of ketone bodies increases during starvation

As a metabolic response to the diminished blood glucose levels in starvation, it has been clearly shown that liver ketogenesis increases to replace glucose as an energy source (Dhillon and Gupta 2020). Therefore, as a commonly known rising metabolite in response to starvation (Pan et al. 2001; Rojas-Morales et al. 2016), the synthesis of beta-hydroxybutyrate was investigated. In this study, a continuous increase of 2.04- and 5.01-fold after 6 and 24 hours of starvation, respectively, was monitored (Figure 4.11). In a separate metabolic study performed on 3-month-old male wild-type mice, a persistent increase in serum beta-hydroxybutyrate levels was depicted during 16 hours of starvation, reaching a 5-fold increase compared to control mice (Geisler et al. 2016). The time difference in reaching the same concentrations of beta-hydroxybutyrate in the mentioned studies could be due to different parameters such as the metabolic activity, the age of the animal and the differences in the colorimetric enzyme assays used for the measurement. In another metabolic study conducted by Miyamoto et al. on 7-week-old male wild-type mice, beta-hydroxybutyrate levels elevated by ~11-fold in 48 hours starved mice (Miyamoto et al. 2019). In addition, starvation for 72 hours also showed a significant rise in the amounts of beta-hydroxybutyrate (Hashimoto et al. 2000). The increase after prolonged starvation probably indicates the hepatic export and brain consumption of ketone bodies as they are able to cross the blood-brain barrier (Lopes-Cardozo et al. 1980).

So far, the results show the increase in beta-hydroxybutyrate formation as a final product of ketogenesis. In order to further investigate the influence of starvation on the activation of the ketogenesis process, the expression of two key regulatory genes, Hmgcs2 and Cpt1a, as well as their activator Pparα in liver lysates was verified via qPCR (Figure 4.12). A relative increase in the expression can be observed through the time course of starvation compared to control. Hmgcs2 and Cpt1a displayed a 1.66- and 4.76-fold increase after 6 hours of starvation, respectively, as well as a 10.68- and 19.24-fold increase after 24 hours of starvation, respectively. Compared to our study, Vilà-Brau et al. starvation experiments on 10-week-old male wild-type mice showed that Hmgcs2 and Cpt1a expression increased by ~3- and 2-fold after 6 hours of starvation, respectively (Vilà-Brau et al. 2011). In another study performed by Geisler and colleagues on 3-month-old male wild-type mice, 16 hours of starvation resulted in a ~7.5- and 8-fold increase in the expression of Hmgcs2 and Cpt1a, respectively (Geisler et al. 2016). Since Cpt1a enhances the production of acetyl-CoA, and Hmgcs2 is responsible for its flux into ketogenesis (Reviewed by Grabacka et al. 2016), it is reasonable to monitor a continuous increase in the expression of Hmgcs2 and Cpt1a during starvation as described above. Ketogenesis-related gene Pparα depicts a significant increase of 2.4-fold after 6 hours of starvation. In addition, at 24-hour starvation time period, Pparα shows an increased expression but is not statistically significant due to variations in the measured Ct values between the replicates of the time point. These variations can be observed due to possible contamination during the RNA isolation process or low primer amplification efficiency in one of the replicates. Although the increase was not statistically significant in our study, a ketogenesis-related study on eight-week-old male wild-type mice demonstrated that hepatic Pparα expression increased by 4-fold after 24 hours of starvation (Nakagawa et al. 2016). The same study showed that Pparα-deficient mice ($Ppar\alpha^{-/-}$) display ketogenesis impairment, where the expression of its target genes, Hmgcs2 and Cpt1a, is significantly decreased. This may explain the pivotal role of Pparα in hepatic ketogenesis.

The highly expressed Hmgcs2, Cpt1a and Pparα genes, after starvation, are identified to be involved in fatty acid β-oxidation and ketone body production (Vilà-Brau et al. 2011; Reviewed by Grabacka et al. 2016). Besides the regulation via the genes mentioned above, a detailed study about mTORC1 association with the ketogenesis process shows that mTORC1 inhibition is necessary for starvation-induced Pparα activation (Sengupta et al. 2010a). Based on the acquired data from beta-hydroxybutyrate concentrations and the relative expression of ketogenesis-related genes, it is reasonable to recognize a successful activation of the ketone body synthesis pathway and a progressive increase in ketogenesis throughout the starvation time course.

5.2.3 Concentration of acylcarnitines alters during starvation in a chain-length-dependent manner in whole blood serum

Fatty acids are a main source of body energy stored in adipose tissues in the form of triglycerides (Cohen and Spiegelman 2016). It has been shown that mitochondrial beta-oxidation of long-chain fatty acids is mediated by acylcarnitines, while short-chain fatty acids are carnitine-independent (Schönfeld and Wojtczak 2016; Longo et al. 2016). Prior studies demonstrated that energy production via beta-oxidation increases during starvation (Soeters et al. 2009; Torchon et al. 2016). In this study, no significant change was calculated in the regulation of short- or long-chain acylcarnitines after 6 hours of starvation, except for an increase in tetradecenoyl (C14:1) compared to the control. This result is consistent with a maintained level of glucose in the whole blood serum after 6 hours of starvation (Figure 4.10), reflecting the use of glucose at this time period requiring no shift to fatty acids yet. In a metabolic study conducted by Park and colleagues on 6 hours starved mice, 5 monitored acylcarnitines were also investigated in our study. 3 of which, namely C14, C16:1 and C18, did not show any change in their concentrations after short starvation, while C16 and C18:1 levels elevated in the mouse serum (Park et al. 2019). The increased levels of these two acylcarnitines could be due to their known role as a starvation marker (Reviewed by McCoin et al. 2015).

Moreover, the concentration of circulating acylcarnitines was monitored as a marker of fatty acid beta-oxidation. Compared to the control, the investigation depicts a significant decrease in the concentrations of short-chain acylcarnitines after prolonged starvation (Figure 4.13). Since short-chain acylcarnitines are formed from the catabolism of different metabolites, not only from fatty acids, such as propionyl (C3) and isovaleryl (C5) from amino acids or butyryl (C4) from amino acids and fatty acids (Makrecka-Kuka et al. 2017), the concentrations measured after starvation do not precisely reflect the beta-oxidation of fatty acids. Furthermore, the high abundances of the acetylcarnitine (C2) measured for control and starved samples compared with other short-chain acylcarnitines seem logical, as it is an intermediate metabolite originating from acetyl-CoA, and thus a product involved in most biochemical reactions like beta-oxidation and can be derived from catabolism of amino acids, fatty acids or glucose (Shi and Tu 2015). For free carnitine (C0), the decrease in the concentration after 24 hours potentially represents the highly active transport of long-chain fatty acids to the mitochondria for energy production (Houten et al. 2016).

In contrast, the concentrations of longer acylcarnitines were significantly increased after 24 hours of starvation (Figure 4.14 and 4.15). Consistent with our results, in a separate study conducted by Pomar and colleagues on 3-week-old male and female mice, 8 investigated acylcarnitines were in common with our study. All 8 acylcarnitines, namely C10, C12, C14, C14:1, C16, C16:1, C18 and C18:1, depicted a significant increase in their plasma levels after 12 hours of starvation (Pomar et al. 2019). Since long-chain acylcarnitines are only synthesized in the mitochondria (Berg et al. 2002c) and can be transported back to the cytosol (Violante et al. 2013), the increased concentrations in the whole blood serum samples reveal oxidation of fatty acids and the body probably shifts to fatty acids as primary source of energy during prolonged starvation as previously shown by other studies (Costa et al. 1999; Steinhauser et al. 2018). Since β-oxidation increases during starvation, it is interesting to mention the significant increased expression of three key genes involved in ketogenesis and fatty acid oxidation after prolonged starvation (Figure 4.12), namely Hmgcs2 and Pparα as regulators of hepatic β-oxidation and also Cpt1a as fatty acid

transporter across the outer mitochondrial membrane (Rodríguez et al. 1994; Hsu et al. 2001; Erol et al. 2004). These findings are consistent with two separate studies on Pparα-deficient mice showing a substantial impairment of β-oxidation after prolonged starvation by demonstrating changes in carnitine levels and a decrease in the expression of Pparα target genes (Hashimoto et al. 2000; Makowski et al. 2009).

Most experiments on fatty acid metabolism during starvation were conducted at least after overnight fasting or longer starvation periods, after which changes in acylcarnitine abundance were monitored (Schooneman et al. 2014; Makrecka et al. 2014). The displayed data suggests increased beta-oxidation after prolonged starvation, which is mainly represented by the augmented levels of mitochondrial-specific synthesis of long-chain acylcarnitines.

5.2.4 Starvation is associated with changes in the concentration of circulating amino acids and derivatives

To understand the cellular metabolism after short- and long-term starvation, the concentrations of circulating amino acids and derivatives were measured as essential metabolites in gluconeogenesis, ketogenesis and mTORC1 activation. During starvation, the amino acids and their derivatives displayed differences in regulation that demonstrate the variable responses to food deprivation and protein metabolism (Figure 4.16 and 4.17).

In 2015, Yamamoto and colleagues showed a decrease in the serum levels of 9 amino acids after 24 hours of mice starvation, except for branched-chain amino acids (BCAAs), which are leucine, isoleucine and valine (Yamamoto et al. 2015). After prolonged starvation, 4 of the 9 amino acids, namely alanine, glycine, proline and tryptophan, also decreased significantly in our study. Since the essential amino acids cannot be synthesized due to the lack of the biochemical pathways needed, the absence of food intake might be a reason for the reduction in their concentrations after prolonged starvation (Reviewed by Lopez and Mohiuddin 2020). In contrast, BCAAs demonstrated a significant increased level although they are indispensable amino acids. This increase was also shown previously in other studies (Charkey et al. 1955; Schauder et al. 1985). The

elevated concentrations can either be explained by their important role in nitrogen transport for skeletal muscle synthesis of gluconeogenic amino acids during starvation (Felig 1973; Tom and Nair 2006; Hatazawa et al. 2018), or their diminished transport from the blood due to the decreased insulin that have been shown to modulate BCAA levels in the blood (Shin et al. 2014; Holeček 2018). Additionally, BCAAs are involved in ketogenesis (Holecek et al. 2001) and can activate mTORC1 (Zhenyukh et al. 2017). In an *in vitro* study conducted by Zhenyukh and colleagues, peripheral blood mononuclear cells (PBMCs) exposed to increased BCAAs concentrations demonstrated maximal mTORC1 activation at 10 mmol/l after 1 hour of stimulation (Zhenyukh et al. 2017). As BCAAs levels increased significantly after prolonged starvation (Figure 4.16), this could be a reason for mTORC1 reactivation, as shown in liver tissues (Figure 4.2 and 4.3).
Since methylhistidine, a histidine derivative, is present in muscle proteins such as actin and myosin, and cannot be reused for protein synthesis (Johnson et al. 1967; Vr and Hn 1978), accumulation of circulating methylhistidine was used as an accurate biomarker of muscle protein degradation in starved rodents (Nagasawa et al. 1996; Yoshizawa et al. 1997; Agrawal et al. 2003). In our thesis, the concentrations of 1- and 3-methylhistidine increased significantly after prolonged starvation, indicating a muscle protein breakdown for glucose synthesis. In addition, taurine, a methionine derivative, showed a significant increase after 24 hours of starvation compared to the short starvation period, which could be attributed to its tissue release or circulation before transportation to other tissues (Baba et al. 1981; Lima and Jaffé 1998). Another probable reason was shown by Miyazaki et al., where the increased circulating levels of taurine are explained by its role in binding acetyl-CoA after endurance physical activities (Miyazaki et al. 2015), which could possibly be the case for prolonged starvation. Moreover, in our study the concentrations of 2-aminoadipic acid (2-AAA) and 2-aminobutyric acid (2-ABA) increased significantly after prolonged starvation. The significant increase in 2-AAA, an intermediate in lysine degradation pathway, is associated with the measured decreased levels of lysine or related to insulin resistance, where the accumulation of 2-AAA is shown to be used as a marker for insulin resistance in wild-type mice (Lee et al. 2019). As insulin is reported to

modulate the levels of circulating 2-ABA, similar to BCAAs, and prolonged starvation decreases insulin levels in the blood, elevated 2-ABA concentrations can hence be explained as previously shown in starved human cells (Felig et al. 1969).

Considering the thorough analysis and the results attained after short and long starvation from essential metabolites, namely glucose, ketone bodies, acylcarnitines, amino acids and their derivatives, different characteristics and response mechanisms were revealed at each starvation period. In our study, it is reasonable to claim a stability in glucose concentrations at 6 hours of starvation, where the production of ketone bodies begins to increase. Furthermore, the reduction in glucose levels following 24 hours of starvation is probably accompanied by a significant increase in ketogenesis and beta-oxidation as alternative energy sources. At the same time, the muscle breakdown and release of amino acids for gluconeogenesis starts to occur. In a separate study, where mice starvation was prolonged to 72 hours, it has been shown that the liver metabolism relies predominantly on amino acid-based glucose synthesis (Sokolović et al. 2008), which is consistent with the muscle breakdown seen after 24 hours in this thesis project.

5.3 Proteomic study of altered lysosomal proteome according to the metabolic status

In recent years, several proteomic studies were conducted to identify the proteins of cellular organelles and large-scale analyses were used to determine the changes after various cellular treatments, thus accumulating numerous datasets from different subcellular components such as mitochondria, lysosomes and the endoplasmic reticulum (Reviewed by Andersen and Mann 2006). However, some starvation-related aspects have not yet been examined, especially in the lysosomal research field.

After selecting two time periods, 6 and 24 hours, with distinct molecular response mechanisms and different cellular metabolic status after food deprivation, starvation-dependent changes in the lysosomal proteome regulation were investigated by mass spectrometry (MS)-based proteomics. In this project,

enriched lysosome fractions from starved mice via sucrose gradient-based technique were tryptic digested, mixed and tandem mass tag (TMT) labeled. Fractionated and desalted peptides were analyzed by the MS machine (Figure 4.18). The accurate protein identification, the quantitative proteomic analysis and the utilization of novel bioinformatics methods enabled a reliable proteomic study to define starvation-induced protein alterations on the lysosomal level.

5.3.1 Lysosomes are successfully enriched from mouse liver

Lysosome enrichment is a mandatory step for mass spectrometry-based analysis of lysosomal proteins. Variable approaches were applied to achieve this goal. Some are *in vitro*-specific, such as superparamagnetic iron oxide nanoparticles (SPIONs) delivery into the lysosomes in cell culture (Walker and Lloyd-Evans 2015) and lysosome immunoprecipitation (LysoIP) with tagged transmembrane proteins (Abu-Remaileh et al. 2017), while other methods can be applied for tissues and cultured cells experiments, for example the isolation of lysosomes via density-gradient centrifugation (Graham 2001). Each of these methods has its own advantages and disadvantages, such as the amount of starting material, isolation efficiency, the costs for lysosome isolation and the protein identification numbers obtained after MS analysis (Singh et al. 2020).

In the current study, lysosomes were enriched using a sucrose density-gradient fractionation, where they are present in one of the subfractions. This technique is widely adapted for the enrichment of lysosomes from liver tissues (Aguado et al. 2016). The main difficulty is to purify the lysosomes from other organelles with similar density, namely mitochondria and peroxisomes (Leighton et al. 1968). To improve the purity of the lysosome fraction, an intraperitoneal injection (IP) of Triton WR1339 solution was carried out. Since the solution is taken up by liver hepatocytes and results in the accumulation of lipids in the lysosomes due to lipoprotein lipase inhibition, a lysosomal density shift will be generated in the liver of the animals compared to other organelles (Wattiaux et al. 1963). Therefore, lysosomes treated with Triton WR1339 solution are referred to as liver tritosomes. The purity of the collected fraction depends on many factors including optimal IP injection site, type of tissue homogenizer and the precise formation of a

discontinuous sucrose gradient. In addition, alternative strategies for a successful lysosome enrichment are also available by using other injection solutions like colloidal gold (Henning and Plattner 1974) and dextran (Arai et al. 1991) or applying different density-gradient substances such as percol (Symons and Jonas 1987), metrizamide (Wattiaux et al. 1978) and nycodenz (Graham et al. 1990).

After successful subcellular fractionation, the enrichment of lysosomes was verified by immune detection. Since LAMP-1 is highly enriched in late endosomes/lysosomes and forms an abundant component of lysosomal membrane proteins, it was used as a lysosomal marker protein (Fukuda 1991; Eskelinen et al. 2003). Markmann et al. also performed tritosome isolation from mice liver and displayed LAMP-1 signals obtained from different fractions during the process where the highest abundance of glycosylated membrane protein was in the enriched subfraction (Markmann et al. 2017). Consistently, in this thesis, the collected tritosome fractions from fed, 6- and 24-hour starved mice depicted the most enrichment of lysosomes described by LAMP-1 intensities compared to liver, post-nuclear supernatant and mitochondria/lysosomes fraction (Figure 4.19). Therefore, a successful lysosome enrichment can be concluded. The enriched proteins could be localized at the lysosomal membrane or in the lumen. However, as a result of the lysosome dynamic cellular interaction with other organelles (Pu et al. 2016), the lysosomal degradative function as well as the possible contamination during the enrichment process, numerous non-lysosomal proteins could also be detected.

5.3.2 Proteomic analysis reveals a reliable dataset of quantified proteins in the lysosomal fraction

Quantitative and qualitative proteomics are two powerfully evolving aspects of mass spectrometry-based proteomics (Reviewed by Cox and Mann 2011). Although several large-scale proteomic analyses were conducted, there is still a lack of comprehensive *in vivo* large-scale proteomic studies to investigate the lysosomal proteome after starvation using quantitative mass spectrometry.

In the current project, as the lysosome-enriched samples are obtained from the liver of fed and starved mice, TMT was used as a relative quantitative proteomics technique, where up to 10 peptide samples are chemically labeled with isobaric compounds and combined for MS analysis. This results in a mass shift between the acquired peptide samples from different starvation conditions which helps for an appropriate comparison between the samples (Thompson et al. 2003). Meanwhile, other labeling methods are available, depending on the type of samples, such as SILAC approach for labeling proteins with stable isotopes of amino acids in cell culture (Ong et al. 2002; Thelen et al. 2017), and stable isotope dimethyl labeling of proteins in cultured cells (Hsu et al. 2003).

In this study, 3417 is the overall number of identified proteins in the lysosomal fraction. Since a list of same peptides appears sometimes in two or more identified proteins or some proteins can be identified by only one peptide detected, it is challenging to refer to the proteins in the sample (Nesvizhskii and Aebersold 2005; Huang et al. 2012). Therefore, non-unique peptide and single-hit proteins were excluded resulting in 1725 quantified proteins identified by two or more unique peptides. These included 233 known lysosomal proteins according to the protein center database in PD 2.3 and gene ontology (GO) analysis tool. The lower number of quantified lysosomal proteins compared to 1492 quantified non-lysosomal proteins is due to the degradation of various proteins within the lysosome, the contribution of cytoskeleton and organelle contacts to the spatial distribution of the lysosomes as well as the potential loss of lysosomal proteins and interference of protein contaminants through the purification of lysosomes (Pu et al. 2016; Cohen et al. 2018). Separate studies using the same tritosome isolation technique and TMT-based proteomics of mouse liver showed 904 quantified proteins with 157 lysosomal proteins (Markmann et al. 2017) or 1048 quantified proteins with 169 lysosomal proteins (Massa López et al. 2019) in the lysosome fraction. These differences in the numbers of quantified proteins between the studies could be derived from the quality of sample preparation, the variations in the used MS machines and their sensitivity to detect low abundant peptides after MS scanning (Eriksson and Fenyö 2007).

Before proceeding with statistical analysis, quality control processing of MS data was performed to ensure a good quality of the results. The proteomics quality control aim is to reduce data variations and sample outliers that can influence the outcome due to the usually small number of biological samples in the proteomics experiments (Matzke et al. 2011). Several studies in the lysosomal research field have visualized the quality of their proteomic analysis by depicting sample distribution after normalization using boxplot (Sigloch et al. 2016; Tebani et al. 2020) or visualizing the correlation of replicates belonging to the same treatment by principal component analysis plot (PCA) (Leeman et al. 2018; Hao et al. 2019). In the current research, normalized replicates showed close-to-normal distribution (Figure 4.20) and a high correlation between replicates related to the same nutrient condition (Figure 4.21). Verification of MS data reliability through quality control means that the variability which originates from different steps of the bottom-up proteomics workflow has been decreased, resulting in a reduced bias in the forthcoming statistical analysis (Piehowski et al. 2013).

5.3.2.1 Quantified lysosomal proteins in the lysosomal fractions are differentially regulated after short and prolonged starvation

The proteomic data yielded 1725 quantified proteins, of which 233 were confirmed lysosomal proteins representing 13.5 % of total quantified proteins. These proteins contain luminal soluble acid hydrolases, highly glycosylated membrane proteins, integral-membrane proteins such as ion channels, metabolite transporters and lysosomal fusion proteins, as well as several membrane-associated complexes including members of mTORC1 and its associated complexes, which regulate nutrient signaling (Reviewed by Ballabio and Bonifacino 2020). After determining the significant regulation parameters, corrected p-value <0.05 and $\log_2$ fold change <-0.75 or >0.75, only 11 and 17 proteins were found to be downregulated after 6 and 24 hours of starvation, respectively, and one protein was upregulated after both starvation periods (Figure 4.22). Although a small number of differentially regulated proteins were quantified, which could be attributed to the strict criteria mentioned above, the protein mTOR depicted a significant downregulation after nutrient deprivation as a clear indication of starvation in our data.

Wyant and colleagues also performed a large-scale quantitative proteomic study from lysosome-enriched samples but on amino acid-starved cultured HEK 293T cells using lysosome immunoprecipitation (LysoIP) with tagged transmembrane proteins (Wyant et al. 2018). In their study, 364 UniProt-based lysosomal proteins were quantified when comparing control to starved samples representing 6.8 % of total proteins. In their analysis, 7 proteins were downregulated and 7 were upregulated upon 1 hour of starvation. Between these two studies, 128 detected lysosomal proteins were in common. In addition, from differentially regulated proteins, only mTOR was found to be overlapping as a significantly downregulated protein in amino acid-starved cells and our 6 hours starved mice, which was already shown to be deactivated after starvation in several researches (Sancak et al. 2010; Manifava et al. 2016). The disparity between the two studies could be due to the different biological model systems, the approach and time span of starvation as well as the lysosome-enrichment methods used.

A closer look at the data reveals that 4 out of 11 and 8 out of 17 downregulated proteins after 6 and 24 hours, respectively, are related to the mTOR signaling pathway (Table 4.1 and 4.2). Since nutrient deprivation inhibits mTORC1 as well as Ragulator/Rag signaling and enhances catabolic activities, it was expected that mTOR and its associated proteins to be among the top downregulated proteins after starvation. Moreover, the downregulated mTOR-related proteins at each time period of starvation were changing, except for the overlapping GATOR complex protein WDR59 (Figure 4.23, table 4.3). In parallel, the thiol-specific peroxidase peroxiredoxin-6 (PRDX6) was the only upregulated protein after both starvation periods (Figure 4.22). These alterations in the regulation of the lysosomal proteins upon short and prolonged periods of starvation were further examined.

5.3.2.2 Starvation affects the abundances of candidate lysosomal proteins according to proteomic analysis

Based on the proteomic results indicating changes in the regulation of several lysosomal proteins after starvation, mTOR, RagA, RagC, LAMTOR1, LAMTOR2, LAMTOR5 and NPRL2 were chosen as candidate proteins for further investigation to validate these results (Table 4.4). The proteins share a common

characteristic of being all directly involved in the mTOR signaling pathway. These selected members of the Ragulator-Rag GTPases complex as well as the GATOR complex are part of the mTORC1 activation machinery that recruits it to the lysosomal surface in the presence of nutrients (Bar-Peled and Sabatini 2014). Active mTOR, a subunit of mTORC1 complex, regulates cell growth and proliferation (Laplante and Sabatini 2012).

5.3.2.2.1 Short and long periods of starvation can differently impact mTORC1 abundance

Before showing the influence of starvation on the abundances of regulatory proteins associated with mTORC1 activity, namely the LAMTOR complex, the Rag GTPases and the GATOR complex, the abundance of mTORC1 was investigated. Separate *in vitro* studies showed that mTOR protein interacts with RAPTOR (Kim et al. 2002) and PRAS40 (Sancak et al. 2007) proteins, and these components form the unique part of the mTOR complex 1. Since the subunits are bound together and change their localization as one complex (Reviewed by Liu and Sabatini 2020), the results displayed on these proteins reflect the behavior of the whole complex. When analyzing the proteomic dataset, mTOR protein depicted a greater downregulation after 6 hours of starvation than after 24 hours of starvation (Table 4.4). As the immune detection of the mTOR protein was not successful, RAPTOR and PRAS40 proteins were investigated. Western blot analysis of RAPTOR protein showed a decrease in the abundance after short starvation in the lysosomal samples and an increase after 24 hours. In addition, PRAS40 showed, similarly to RAPTOR protein, a decrease after short starvation and an increase after prolonged starvation, though not statistically significant. In liver whole lysates, a significant decrease after prolonged starvation was demonstrated for PRAS40, while the decreased levels of RAPTOR were not statistically significant (Figure 4.24). Here, the proteomic dataset and western blot results indicate an early dissociation and late repositioning of mTORC1 from and on the lysosomal membrane, consistent with the results regarding mTORC1 reactivation and downstream targets phosphorylation after prolonged starvation in liver (Figure 4.2 and 4.3).

In response to nutrients presence, mTORC1 activation and localization on the lysosome require the binding of two Ras-related small G proteins, Rag- and Rheb-GTPase, in their active forms (Groenewoud and Zwartkruis 2013; Kim and Guan 2019). In addition, the interaction of the Ragulator complex with the Rag GTPases is also mandatory (Colaço and Jäättelä 2017).

After a short period of starvation, the abundance of Rag GTPases and their recruiter LAMTOR complex was significantly decreased (Figure 4.25 and 4.26), which are probably the main causes for mTORC1 release into the cytoplasm as shown in figure 4.24. Furthermore, Demetriades et al. demonstrated that during starvation Rag GTPases are inactivated and the TSC complex is recruited, the Rheb negative regulator, leading to the inhibition of mTORC1 (Demetriades et al. 2014). Based on that, both Ras-related small G proteins are inactivated after short starvation and mTORC1 is relocated into the cytoplasm.

Furthermore, after prolonged starvation, the indicated mTORC1 lysosomal repositioning is probably correlated with the lysosomal localization of its recruiter Rag GTPases as shown in this research (Figure 4.26). Moreover, several *in vitro* studies have reported that mTORC1 reactivation after prolonged starvation is autophagy-dependent, where amino acid uptake is increased by lysosomal degradation and the upregulation of amino acid transporters (Yu et al. 2010; Chen et al. 2014; Tan et al. 2017). In addition, another *in vitro* study on HepG2 and Huh6 cell lines proposes a possible serine/threonine protein kinase Akt activation as a potential reason to promote mTORC1 reactivation under starvation conditions (Murata et al. 2015). This activation is mediated by the phosphorylation of TSC2 and therefore the release of GTPase Rheb (Dan et al. 2014). Subsequently, Vandoorne and colleagues indicated an enhanced mTORC1 activity by the intake of ketone bodies (Vandoorne et al. 2017). In the current research, ketone bodies could be involved in mTORC1 reactivation because ketogenesis increased significantly after prolonged starvation (Figure 4.11 and 4.12).

5.3.2.2.2 Starvation induces a progressive decrease of Ragulator complex levels on the lysosome

The pentameric Ragulator complex is a late endosomal/lysosomal scaffold that consists of two heterodimers, the first contains LAMTOR2-3 and the second contains LAMTOR4-5. In addition, LAMTOR1 protein surrounds and anchors both heterodimers to the lysosomal surface via its palmitoyl and myristoyl groups at the N-terminus (Sancak et al. 2010; Bar-Peled et al. 2012). Several protein crystallography studies have shown a connection of LAMTOR1 to all other Ragulator complex proteins as well as the interaction sites between the proteins of each heterodimer (Araujo et al. 2017; Su et al. 2017; Mu et al. 2017). In the current study, MS data showed significant downregulation of LAMTOR1, 2, 3 and 5 after prolonged starvation (Table 4.4) and the abundances of LAMTOR1 and one protein of each heterodimer, namely LAMTOR2 and LAMTOR5, were monitored after starvation. Immune detection depicts a continuous decrease in the intensities of all investigated proteins after 6 and 24 hours of starvation at the lysosomal level and a significant increase in crude liver lysates (Figure 4.25), which indicates a probable dissociation of the Ragulator complex into the cytosol and thus an inhibition in its function. The reason for its dysfunction could be due to the binding of the p27 protein, a negative regulator of the cell cycle, to LAMTOR1 after starvation. This could lead to Ragulator complex suppression and the blocking of the pentameric complex assembly, as recently shown in a study on amino acid-starved mouse embryonic fibroblast (MEF) cells (Nowosad et al. 2020). As the abundance of Ragulator complex is significantly decreased after starvation and it is known to regulate mTORC1 activity in the presence of amino acids (Bar-Peled et al. 2013), the results obtained from 6 hours starved samples are consistent with our previous results (Figure 4.24) and the literature showing a deactivation and thus dissociation of mTORC1 (Kim et al. 2013). However, mTORC1 was reactivated after prolonged starvation during LAMTOR complex dissociation suggesting a Ragulator-independent mTORC1 reactivation. These results provide novel insights about Ragulator complex localization and its association with mTORC1 regulation after short and prolonged starvation.

Additionally, it has been shown that lysosomal positioning is another important aspect controlled by the LAMTOR pentamer (Pu et al. 2017). The Ragulator complex can either bind to the lysosomal membrane protein SLC38A9 and Rag GTPases to promote mTORC1 activation or to BLOC-1-related complex (BORC) causing lysosomal perinuclear positioning (Filipek et al. 2017). In nutrient-rich conditions, while Ragulator recruits mTORC1, BORC-Arl8b interaction leads to lysosome peripheral movement. In contrast, during starvation, LAMTOR interaction with mTORC1 is abolished and directly switched towards BORC-Arl8b complex causing lysosomes accumulation in the juxtanuclear region (Filipek et al. 2017; Pu et al. 2017). Based on these facts and the downregulation of Ragulator complex after starvation, it is possible that a perinuclear lysosomal localization in the hepatic cells of starved mice assists the fusion with autophagosomes (Li et al. 2016). This could support an mTORC1 reactivation in an autophagy-dependent manner.

5.3.2.2.3 Rag complex abundance differs from its GATOR1 regulating complex after prolonged starvation

The previously described effect of Ragulator in activating mTORC1 is linked to the interaction with Rag GTPases, where LAMTOR1, -2 and -3 bind to Rags C-terminal domains (Araujo et al. 2017). As a guanine nucleotide exchange factor (GEF), the pentameric scaffold Ragulator converts Rag heterodimers into their active forms with GTP bound-RagA/B and GDP bound-RagC/D, which in turn locates mTORC1 onto the lysosomal membrane by binding to its RAPTOR subunit without triggering any conformational changes (Sancak et al. 2010; Bar-Peled et al. 2012; Anandapadamanaban et al. 2019). In this research, the proteomic analysis demonstrated a more prominent decrease in the regulation of Rags after 6 hours of starvation than after prolonged starvation (Table 4.4). At the same time, the abundance of one Ras-related small GTP-binding protein of each heterodimer, namely RagA and -C, was analyzed after short and prolonged starvation. Unlike LAMTOR complex, RagC shows a significant increase in the amounts after prolonged starvation in the lysosomal fraction compared to control and 6 hours starved samples. At the same time, a significant decrease of RagA was measured after short time of starvation, but its increase in the abundance

after 24 hours of starvation was not statistically significant (Figure 4.26). These results suggest a relocation of Rags to the cytoplasm after 6 hours of starvation and a repositioning on the lysosomal membrane after prolonged starvation.

As amino acid-specific regulators of mTORC1 activity, Rag complex inhibition and dissociation after short starvation was probably due to the lack of amino acids turning it into its inactive form, which is consistent with the experiments shown by Sancak and colleagues (Sancak et al. 2008). However, the reanchoring after prolonged starvation may possibly be due to the sensing of the accumulated amino acids in the lysosomal lumen by vacuolar H^+-ATPase, which activates the Ragulator-Rag complex via direct signals as indicated by Zoncu et al. (Zoncu et al. 2011). Furthermore, in the current study, the negative regulator of Rag GTPases, GATOR complex, was also monitored as another potential cause for the high abundances of Rag complex after prolonged starvation. The proteomic analysis of the lysosome-enriched fraction revealed a significant downregulation in 4 quantified protein components of GATOR complex after prolonged starvation (Table 4.4). Meanwhile, the immune detection of GATOR1 complex protein NPRL2 showed a continuous decrease in the abundance during starvation at the lysosomal level and an increase in liver whole lysates (Figure 4.27). The obtained results suggest that the GATOR1 complex dissociates into the cytoplasm and loses its direct interaction with Rags after starvation. Bar-Peled and colleagues proved that GATOR1-deficient cancer cell lines displayed a high activity and a permanent localization of mTORC1 at the lysosomal membrane despite amino acid starvation (Bar-Peled et al. 2013). Since the lysosomal relocalization of mTORC1 after prolonged starvation is linked to Rag GTPases repositioning (Figure 4.24 and 4.26), and mTORC1 activation is firmly related to Rag GTPases binding to the RAPTOR subunit of the complex (Sancak et al. 2008), these findings support our data showing Rags lysosomal repositioning in the absence of GATOR1 complex after prolonged starvation.

As a conclusion from these results, in the presence of nutrients, mTORC1 and its associated protein complexes show an activation of mTORC1 and therefore a localization to the lysosomal surface together with regulatory proteins LAMTOR complex and Rag GTPases. At the same time, the Rag complex is kept active

through the inhibition of GATOR1 by its negative regulator GATOR2 (Panchaud et al. 2013; Bar-Peled et al. 2013). After a short starvation period, all the complexes involved are dissociated into the cytosol. A prolonged starvation period resulted in the repositioning of mTORC1 and Rag complex but not LAMTOR complex (Figure 5.1).

Therefore, our study on the lysosomal proteome changes in the mouse liver provides a new understanding of the possible regulation of mTORC1 and its associated proteins during different starvation periods and suggests potential causes for the reactivation. However, the exact mechanism or activator of the complex, independently of its recruiter LAMTOR complex, is not yet revealed. Therefore, more investigation is needed to specify the activator of Rag complex and thus mTORC1.

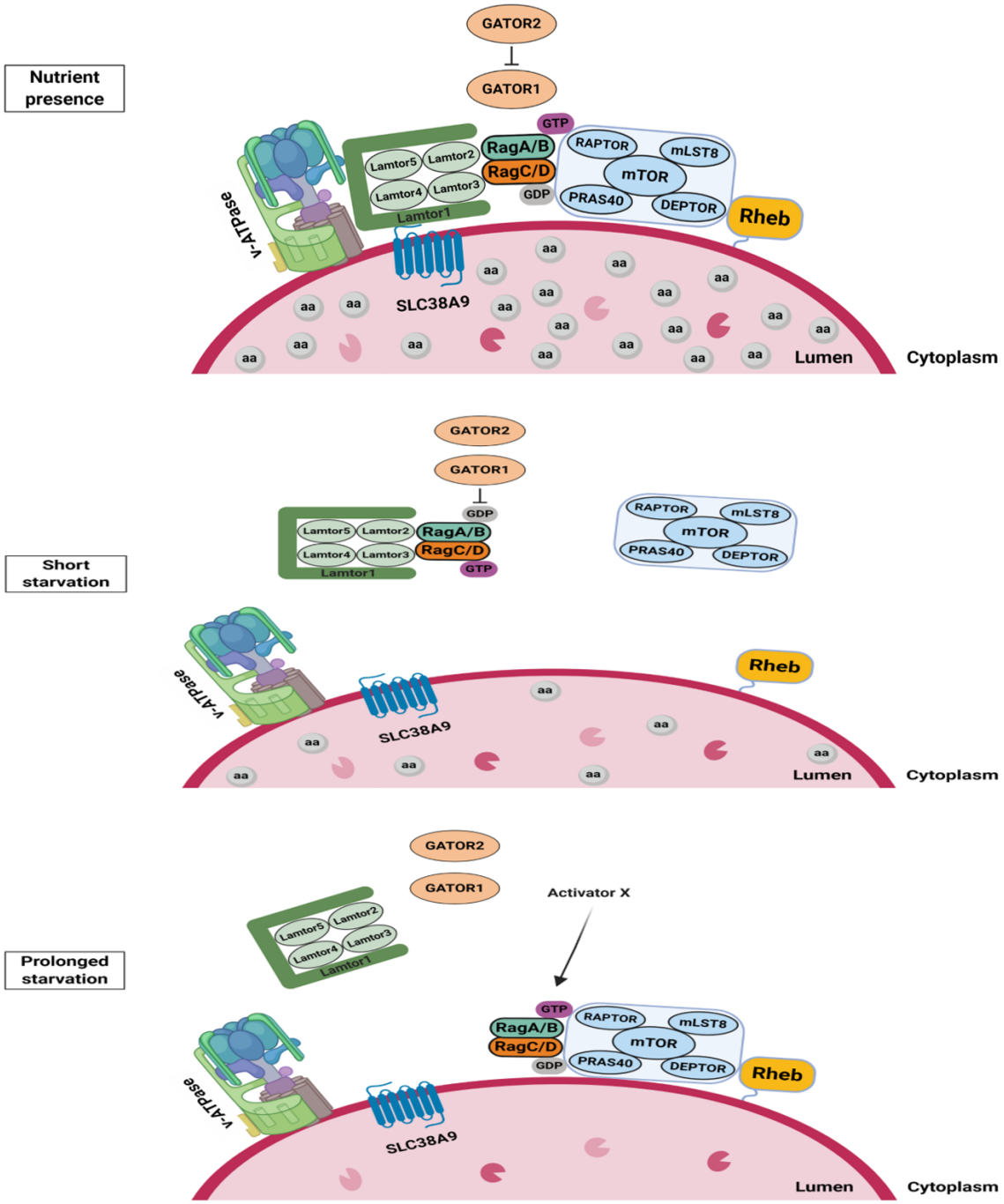

Figure 5.1: Hypothetical model representing the effect of different starvation periods on the activation of mTORC1 and its associated proteins
In the presence of nutrients, mTORC1 and the regulatory proteins LAMTOR complex, Rag GTPases and GATOR complex are active and localized at the lysosomal membrane. These complexes are inactive and relocate into the cytoplasm after short starvation period. After prolonged starvation, Rag GTPases and mTORC1 repositioned at the lysosome by an unknown activator (activator X). (aa: amino acids)

5.3.2.3 Quantified non-lysosomal proteins in the lysosomal fractions are differentially regulated after short and prolonged starvation

Beside the lysosomal proteins, 1492 out of 1725 quantified proteins were identified as non-lysosomal proteins. Only 162 proteins were differentially regulated in 6 hours starved samples representing 10.8 % of the quantified non-lysosomal proteins (Figure 4.28 A). In particular, 12 were downregulated, while the remaining 150 proteins were upregulated in the lysosome fraction (Table 4.5 and supplementary table 8.3). This boost in the numbers of upregulated proteins and decrease in downregulated proteins in the lysosome-enriched samples could be explained by the rise in catabolic processes and the decline of anabolic reactions as a response to starvation in the maintenance of cellular homeostasis (Howell and Manning 2011). Moreover, the upregulation of many proteins can also be interpreted by the increase of the protein transport through the autophagic pathways (Reviewed by Yu et al. 2017).

To evaluate the biological impact of the regulated proteins and their role in the cellular starvation response, KEGG pathway analysis was applied (Figure 4.29). The downregulated proteins were assigned to metabolic processes linked to metal ion homeostasis, which could explain the importance of the metal ions in the activity of many enzymes involved in cytoplasmic metabolic activities (Riordan 1977). Regarding the upregulated proteins, the top KEGG pathways in the dataset were found to be ‘Metabolic pathways’, ‘Proteasome’ and ‘Peroxisome’ which is understandable due to the elevation in the metabolic processes during starvation, particularly the catabolic reactions. In addition, the macroautophagy of organelles is also enhanced such as proteasomes and peroxisomes by proteaphagy (Cuervo et al. 1995) and pexophagy (De Duve and Baudhuin 1966), respectively, for the production of energy and the regulation of cellular homeostasis (Anding and Baehrecke 2017). Furthermore, a possible reason for the enrichment of KEGG pathways related to amino acid and carbohydrate metabolism could be the degradation of enzymes involved in several reactions associated to the metabolism of macromolecules such as proteins and polysaccharides after the initiation of autophagy (Reviewed by Yim and Mizushima 2020). Moreover, Mathew and co-workers performed a

comparative large-scale proteomic study on wild-type and autophagy-deficient ($Atg5^{-/-}$) immortalized baby mouse kidney epithelial (iBMK) cells during starvation using SILAC labeling approach. The research depicts the enrichment of biological pathways associated with protein degradation and demonstrates that induced autophagy is responsible for the breakdown of a significant number of identified proteins after 5 hours of starvation, which implies a pivotal role for autophagy in protein turnover (Mathew et al. 2014). Therefore, it is not surprising that several pathways linked to organelle and macromolecule metabolism are enriched in our MS dataset derived from lysosomal fractions of 6 hours starved samples.

After 24 hours of starvation, 283 proteins were differentially regulated, representing 19 % of the quantified non-lysosomal proteins (Figure 4.28 B). In particular, 121 were downregulated and 162 proteins were upregulated in the lysosome fraction (Supplementary table 8.4 and 8.5). Relative to the short starvation period, downregulated proteins increased by 13.5-folds, while the number of upregulated proteins is still comparable. Since autophagy-degraded metabolites contribute to energy production and several anabolic pathways in the cytoplasm, such as protein synthesis, fatty acid biosynthesis and gluconeogenesis (Reviewed by Kaur and Debnath 2015), it is rational to monitor a significant decrease in the abundance of many proteins in the lysosome after prolonged starvation.

When KEGG pathway analysis was carried out (Figure 4.30), the downregulated proteins were linked to cholesterol metabolism pathway, which supports the switch to fatty acids as a fuel source during prolonged starvation and the increase in mitochondrial β-oxidation (Steinhauser et al. 2018). These results are consistent with our previous findings where long-chain acylcarnitine levels increase in the plasma as a marker for fatty acid oxidation (Figure 4.14 and 4.15). Furthermore, several proteins of the enriched pathways ‘Endocytosis’ and ‘SNARE interactions in vesicular transport’ are related to endosome export pathways and retrograde sorting routes, which are involved in the reuse of metabolites by other organelles in biosynthetic processes explaining their downregulation in the lysosomal fraction (Johannes and Popoff 2008; Huotari and Helenius 2011). The top 3 pathways of upregulated proteins are

neurodegenerative diseases, namely ‘Parkinson disease’, ‘Huntington disease’ and ‘Alzheimer disease’. A thorough examination reveals that the majority of the proteins in these pathways are part of the proteasome or mitochondrial organelles. Since impaired organelles are degraded by selective autophagy and also dysfunctioning proteasomes and mitochondria were implicated as a likely cause for neurodegenerative diseases, the enrichment of these pathways may thereby be explained (Reviewed by Ciechanover and Brundin 2003; Johri and Beal 2012; Anding and Baehrecke 2017). In addition, several enriched pathways are related to mitochondria, proteasome and amino acid metabolism, which validate the well-established hypothesis of mitochondrial and proteasomal macroautophagy via mitophagy (Lemasters 2005) and proteaphagy (Cuervo et al. 1995), respectively, as well as the lysosomal degradation of proteins during starvation (Reviewed by Ciechanover 2005).

Furthermore, the overlapping of differentially regulated proteins after short and prolonged starvation demonstrate the continuous adaptive mechanism of the cell to shift its fuel sources starting already after a short nutrient deprivation time period (Figure 4.31, table 4.9 and supplementary table 8.6).

5.3.2.4 Starvation affects the abundances of candidate non-lysosomal proteins according to proteomic analysis

Based on the proteomic dataset and the KEGG enrichment analysis, protein members of interesting complexes, organelles and biological processes displaying changes in their regulation upon starvation were selected for further validation experiments. The candidates are proteasomal (PSMA7 and PSMB5), mitochondrial (CPT2, VDAC1, NDUFB7 and NDUFB11) and peroxisomal (LONP2 and NUDT12) proteins, as well as WASH complex subunits (WASHC4). In addition, proteins associated with glycogen metabolism (GYS2 and PYGL) and gluconeogenesis (PCK1) biological pathways were also investigated (Table 4.11). The candidate proteins share one feature of being enriched at least in one of the KEGG pathways after short and prolonged starvation periods. Furthermore, the enrichment of non-lysosomal proteins after starvation may imply either their involvement in a lysosome-related biological process or simply their localization in the lysosomal lumen via autophagy (Kaushik et al. 2010).

5.3.2.4.1 Proteaphagy is induced after short and prolonged starvation

As a major proteolytic machinery, the proteasome complex can selectively degrade ubiquitin-tagged proteins (Hershko and Ciechanover 1998). This process eliminates unfolded proteins and provides amino acids for *de novo* protein synthesis (Finley 2009). It has also been shown that autophagy of proteasomes, called proteaphagy, occurs upon starvation in various eukaryotes as a possible source of energy (Marshall et al. 2015; Waite et al. 2016; Cohen-Kaplan et al. 2016).

In this study, MS results show an upregulation in 12 proteasome subunits and the enrichment of 'Proteasome' pathway by KEGG analysis after short and prolonged starvation in the lysosome fraction (Figure 4.29 and 4.30, supplementary table 8.3 and 8.5). In addition, the increase in the abundances was confirmed by western blotting of two proteasomal proteins, namely PSMA7 and PSMB5, while the protein abundances were not significantly decreased in liver whole lysates (Figure 4.32). In line with our results, Cuervo and colleagues demonstrated the accumulation of proteasomes in rat liver lysosomes after nutrient starvation (Cuervo et al. 1995). Moreover, Cohen-Kaplan and co-workers concluded from experiments on HeLa cervical carcinoma cells that starvation-induced autophagy by amino acid depletion leads to the rise in proteasome degradation after its ubiquitination (Cohen-Kaplan et al. 2016). In a large-scale quantitative proteomic study performed by Dengjel et al. on starved MCF7 carcinoma cells using SILAC method, the abundance of proteasomal proteins decreased in whole cell lysates after 12 hours of starvation (Dengjel et al. 2012). Consistent with our results, the above cited studies confirm the induction of proteaphagy after starvation using different models.

5.3.2.4.2 Starvation enhances a continuous decrease of WASH complex levels in the lysosome

Another validated protein is WASHC4, a member of Wiskott-Aldrich syndrome protein and SCAR homologue (WASH) complex, which localizes to endosomes (Reviewed by Alekhina et al. 2017). WASH complex consists of 5 protein subunits and plays an important role in endosomal trafficking via actin polymerization as well as autophagy modulation (Reviewed by Kast and Dominguez 2017).

Separate studies in mammalian cells show that the complex subunits are mutually dependent and the knockdown of one member is accompanied by instability and disruption of the remaining constituents (Gomez and Billadeau 2009; Derivery et al. 2009; Jia et al. 2010). In addition, a research conducted by Gomez and colleagues on MEF cells depicted a significant decrease in the abundance of complex subunits after WASH1 knockout (Gomez et al. 2012). Since the proteins are bound together and function as one complex, the results displayed on WASHC4 would indicate the whole complex behavior.

In the current research, the proteomic analysis demonstrates a significant downregulation in WASH complex components after prolonged starvation in the lysosome (Table 4.7), as also shown by KEGG analysis in 'Endocytosis' enriched pathway (Figure 4.30). Furthermore, the immune detection confirms these results and depicts an additional decrease in the amounts after 6 hours of starvation, while liver whole lysates depict an increase comparing 6 and 24 hours starved samples (Figure 4.33). The change in the abundances in the lysosome and liver lysate could be due to its role in the early steps of the autophagic pathway where WASH proteins were found to be localized at the autophagosomal membrane during starvation according to Xia and colleagues (Xia et al. 2013). Moreover, the same study indicates WASH complex role as an autophagy inhibitor through its interaction with beclin1 protein that is localized at the phagophore and tightly regulates autophagy initiation (Xia et al. 2013). In addition, King et al. comparative starvation study between wild-type and WASH1 knockout cells using *Dictyostelium discoideum* model system demonstrates that WASH complex is required for a correct delivery of lysosomal hydrolases into phagosomes and autophagosomes to attain an effective proteolysis during starvation. Meanwhile, in WASH1 knockout cells, lysosomal enzymes such as cathepsin D were trapped in the late endosomes and an accumulation of phospholipids was monitored in their lysosomes (King et al. 2013). Two separate studies using *Dictyostelium discoideum* (Carnell et al. 2011) and *Drosophila* (Nagel et al. 2017) model systems showed that WASH1 physically interacts with the v-ATPase at the lysosomal surface and can inhibit its acidification function. Nagel and colleagues showed that the loss of WASH1 stimulates the lysosomal acidification during

starvation (Nagel et al. 2017). Since one function of the WASH complex is to negatively regulate autophagy and because low lysosomal acidification is associated with defective autophagy (Reviewed by Colacurcio and Nixon 2016), the decrease in WASH complex abundance at the lysosome in our study could be explained by the initiation of starvation-induced autophagy.

Another potential reason for its regulation pattern could be derived from WASH complex role in endosomal protein sorting. WASH complex is responsible for actin patches formation on endosomal membranes (Derivery et al. 2009), where it is recruited by the retromer complex which consists of VPS35, VPS29 and VPS26 proteins (Harbour et al. 2010). In the current proteomic data, these proteins were also shown to be downregulated in the lysosomal fraction after prolonged starvation (Supplementary table 8.4). Since retromer and WASH complexes are part of the endosome-to-cell surface recycling pathway and also interact with each other (Harbour et al. 2012), the demand for energy production via the recycling endosomes during starvation could clarify the increased WASH complex levels in the liver lysate and the decrease in the lysosome throughout the course of starvation. The above studies on WASH complex roles suggest potential reasons for its abundance levels monitored in our study after starvation.

5.3.2.4.3 Glucose metabolism alters substantially during starvation

The next two investigated proteins are glycogen metabolism-related enzymes GYS2 and PYGL. In nutrient presence, the redundant amounts of glucose are converted to glycogen and stored. The glycogenesis process is mediated by the hepatic glycogen synthase GYS2. Under fasting conditions, the liver produces glucose from the glycogen stores via the activation of PYGL, the key glycogen phosphorylase enzyme in glycogenolysis, and the inhibition of GYS2 (Nordlie et al. 1999). The proteomic dataset and KEGG pathway analysis depict an upregulation of several enzymes, including GYS2, as part of the ‘Starch and sucrose metabolism’ enriched pathway in the lysosomal fraction, after a short period of starvation but not after prolonged starvation (Table 4.6, figure 4.29). The validation via western blot displays the same pattern of regulation, where GYS2 abundances increased after 6 hours of starvation and decreased after 24 hours in liver lysate and lysosome fraction (Figure 4.34). Since the hepatic glycogen

stores are consumed during starvation and no glycogen synthesis is likely to occur (Izumida et al. 2013), the reason for GYS2 increased abundance in the liver lysate after 6 hours of starvation is unclear. To investigate a possible role of GYS2 and thus glycogenesis after short starvation period, more proteins related to the pathway need to be examined. In contrast, the elongation of glycogen chains by GYS2 decreases significantly after prolonged starvation as a reasonable response to the lack of glucose. The analogous enzyme regulation pattern in the lysosome in our data could be due to the higher rate of protein degradation induced by starvation and the glycogenesis absence after prolonged starvation (Jones et al. 2012).

Furthermore, the proteomic dataset and western blot validation experiment show PYGL increased level in the lysosomal samples after short and prolonged starvation (Table 4.11, figure 4.34), at the same time, PYGL did not display a significant increased amount in liver whole lysates. These results suggest a glycogenolysis activity after starvation and therefore an increased amount in PYGL degradation. Within the same context, in addition to the cytosolic glycogen breakdown explained by the blood glucose availability in 6 hours starved mice as shown in our data (Figure 4.10), a lysosomal-autophagy pathway called glycophagy also degrades glycogen via alpha acid glucosidase to provide glucose homeostasis (Kotoulas et al. 2006). However, the exact mechanism of glycogen transport into the lysosome remains elusive. Therefore, it would be interesting to monitor alpha acid glucosidase activity and examine a possible lysosomal interaction with PYGL by co-Immunoprecipitation experiments. This may reveal a potential role for PYGL in the lysosomal glycogen degradation or other lysosomal processes and would further our understanding of the individual enzymes involved in glycogen metabolism.

Related to this, after the depletion of glycogen stores in the liver, non-carbohydrate metabolites are used as a fuel for *de novo* glucose synthesis. Gluconeogenesis takes place mostly in the cytosol and is regulated by the rate-limiting enzyme phosphoenolpyruvate carboxykinase (PCK1), which converts pyruvate to oxaloacetate (Reviewed by Pilkis and Claus 1991). Proteomic dataset demonstrates a continuous upregulation in PCK1 levels after short and prolonged

starvation in the lysosomal fraction and WB confirmation experiment displays a significant increase in the abundance in both lysosome as well as liver lysate (Table 4.11, figure 4.30 and 4.35). During an extended course of starvation, gluconeogenesis is responsible for glucose generation from various precursors such as lactate and glycerol from skeletal muscles and adipose tissues, respectively (Pilkis et al. 1988). For this reason, an increased level of the cytosolic protein PCK1 after food depletion is to be expected. In line with our results, in a glucose-rich environment, Latorre-Muro and colleagues showed a continuous decrease in cytosolic PCK1 activity by increasing glucose concentrations, reaching a reduction of 33 % and 50 % in HEK293T and HepG2 cells, respectively (Latorre-Muro et al. 2018). In parallel, PCK1 abundances also increased in the lysosome but higher than in the liver lysate. Since PCK1 has a destabilized N-terminal proline residue as a primary signal of protein degradation according to N-end rule pathway and a poly ubiquitin chain as a second degradation signal (Varshavsky 2011; Varshavsky 2012; Chen et al. 2017), it is reasonable to have a short intracellular half-life and thus high amounts of accumulated PCK1 in the proteasome. However, proteins could also be degraded through the nonselective starvation-induced autophagy (Kundu and Thompson 2008), which might be another degradation pathway for PCK1 protein. A possible explanation for PCK1 high levels in the lysosome, 4.04-fold increase compared to control, is that the protein gets degraded due to the adaptation of an alternative cellular pathway for energy production, before gluconeogenesis, after prolonged starvation. As this hypothesis is not yet tested and a possible function of the enzyme in the lysosome is not examined, metabolomic studies, an *in vitro* pulse-chase assay as well as a mice refeeding experiment may help to obtain a clearer picture. In addition, a study on PCK1 roles in cellular metabolism using human colon (Colo205) cell line demonstrated that PCK1 has the ability to regulate mTORC1 activity at the lysosome (Montal et al. 2015). Montal and colleagues showed that PCK1-expressing cells have a stronger lysosomal localization and higher activation of mTORC1 than in PCK1 knockdown cells. This could be a second potential reason for PCK1 high levels in the lysosomal fraction in our study, which is consistent with the thesis results regarding

mTORC1 higher abundance levels at the lysosome after prolonged starvation compared to 6 hours starved samples (Figure 4.24).

5.3.2.4.4 Peroxisomal- and mitochondrial autophagocytosis occur at different starvation time periods

Autophagy is a major catabolic pathway that could be induced by starvation and is responsible for the degradation of cytosolic proteins and organelles (Reviewed by Seglen and Bohley 1992). Starvation-induced autophagy experiments conducted by Komatsu et al. on control and Atg7-deficient mice depict an impaired degradation of several cytosolic proteins and organelles in knockout mice (Komatsu et al. 2005). In the current study, the proteomic dataset shows a significant upregulation in a group of 12 peroxisomal proteins after 6 hours of starvation in the lysosome fraction, but not after prolonged starvation (Supplementary table 8.3). These results were also displayed in the KEGG analysis by the enrichment of 'Peroxisome' pathway (Figure 4.29). In addition, the western blotting of two peroxisomal proteins, namely LONP2 and NUDT12, validates these results and also demonstrates no change in the abundance after starvation in liver whole lysates (Figure 4.36). Consequently, the results indicate an early pexophagy. Peroxisomal autophagocytosis has been shown to be induced by PEX2 ligase ubiquitination of peroxisomal membrane proteins and when mTORC1 is inhibited, which suggests the mTORC1 regulation of pexophagy in fed conditions (Sargent et al. 2016). Sargent and co-workers research on amino acid-starved HeLa cells demonstrates an increase in PEX2 levels at the peroxisome surface after 2 hours and a return to initial levels after prolonged starvation. These findings explain the increase in targeting peroxisomes to autophagosomes for degradation after a short starvation, mTORC1 inhibition period, and the reduction after prolonged starvation, mTORC1 reactivation period. In line with Sargent et al. results, in our study, the abundance of several peroxisomal proteins increased when mTORC1 is least active, 6 hours of starvation, and not after its reactivation, prolonged starvation, in the lysosomes of liver tissues. The above mentioned study supports our suggestion of early pexophagy. One of the validated proteins is the peroxisomal matrix protein LONP2, a quality control protein, whose absence or degradation

enhances pexophagy (Bartel et al. 2014). In addition, the increased level of peroxisomal NADH diphosphatase NUDT12 after 6 hours of starvation in the lysosome and its insignificant change in the liver lysate probably suppose active pexophagy after short starvation.

Within the same context of organelle autophagocytosis, mitochondria are also degraded after nutrient depletion but only after prolonged starvation periods due to morphological elongation and the formation of large interconnected networks to prevent sequestration within autophagosomes for several hours (Tondera et al. 2009; Gomes et al. 2011; Rambold et al. 2011). In tested mammalian cell lines such as MEF, HepG2 and HeLa cells, Gomes and colleagues indicated mitochondrial elongation beginning from 1 hour of starvation. In addition, several mitochondrial marker proteins were preserved from degradation in elongated mitochondria of MEF cells and optimal ATP production levels were maintained (Gomes et al. 2011). Furthermore, amino acid starvation experiments on the breast cancer cell line MCF7 demonstrate a major mitochondrial/lysosomal co-localization after 30 hours of starvation in comparison to control and 7 hours starved cells (Kristensen et al. 2008). These studies provide evidence of late mitophagy and show the probable underlying mechanisms. In accordance with the previous results, in the current study, proteomic dataset shows a significant upregulation in a set of 54 mitochondrial proteins after 24 hours of starvation in the lysosome fraction, but not after short starvation (Supplementary table 8.5). These results were also depicted in the KEGG analysis by the enrichment of several mitochondria-related pathways (Figure 4.30). Moreover, four mitochondrial proteins, namely CPT2, VDAC1, NDUFB7 and -11, were validated by WB and three proteins from different biological processes showed a significant increase in the abundances after prolonged starvation in the lysosome, with two depicting a small increase between 6 and 24 hours of starvation in liver whole lysates as well. The findings suggest a late mitophagy (Figure 4.37). Besides mitophagy, the elevated levels of the CPT2 enzyme in the cytoplasm could be related to its involvement in fatty acid beta-oxidation that is increased during starvation (Wolfgang 2020). However, the 1.35-fold increase in CPT2 levels between 6 and 24 hours of starvation in liver lysates is probably not biologically

significant. Furthermore, as a mitochondrial marker protein and a substrate of the mitochondrial ubiquitination enzyme parkin, VDAC1 was displayed to be required for selective mitophagy (Geisler et al. 2010). Therefore, VDAC1 increase could be interpreted as a reason for mitophagy induction. Moreover, NDUFB7 depicted only a small increase between 6 and 24 hours of starvation in the lysosome, while NDUFB11 did not display any significant changes, so further investigation on the respiratory chain proteins is required.

In conclusion, the current *in vivo* research indicates an early pexophagy and a late mitophagy throughout the period of starvation suggesting an ordered organelle degradation and highlights the essential role of autophagy in organelle turnover and cellular homeostasis. In agreement with our outcome, a SILAC-based quantitative proteomic study conducted by Kristensen and colleagues shows that over 36 hours of amino acid starvation of cultured MCF7 cells an autophagic degradation was claimed starting from cytosolic proteins, then ribosomes, and ending with mitochondria based on a bioinformatics cluster analysis of identified proteins. The authors believe that the organelles associated with energy production, such as mitochondria, are degraded last as they help to survive nutrient depletion (Kristensen et al. 2008). This could be an explanation for the degradation order in the present study. However, there is still a gap in our understanding of the mechanism behind the selection of different organelles as well as the biological factors responsible for the shift in degraded organelles during starvation. Our research on the lysosomal proteome changes during different starvation conditions gives novel insights into the degradation time periods of cellular organelles in an *in vivo* mouse model as well as the metabolic changes that accompany it.

6 Conclusion

The conducted study revealed several insights related to lysosomal signaling and cellular metabolism during starvation. In the first part of the thesis, the activity patterns of mTORC1 were successfully determined in three key metabolic organs at various starvation periods. The protein complex indicated unique responses to nutrient starvation. In the liver, mTORC1 was deactivated/reactivated after short/prolonged starvation periods, respectively, while a gradual deactivation in the skeletal muscle and a continuous activation in the brain was monitored. Subsequently, the two selected starvation periods with distinct molecular effects in the liver demonstrated different impacts on cellular metabolism. The levels of the metabolites varied as a response to short- and long-term starvation. Our results showed a stability in glucose levels at 6 hours of starvation, where the synthesis of ketone bodies started to increase. Additionally, the decline in glucose levels after 24 hours of starvation was accompanied with a significant increase in ketogenesis. Other alternative energy sources such as beta-oxidation and gluconeogenesis were also suggested to occur after prolonged starvation.

In the last part, the proteomic analysis of starvation-induced changes in liver lysosomal proteome and the verification experiments indicated a new *in vivo* understanding about the possible localization of mTORC1 and its associated complexes during starvation. The decreased levels of mTORC1 and Rag complex after short starvation and the increase after prolonged starvation, as well as the continuously decreased abundance of Ragulator complex over the course of starvation, suggested a Ragulator-independent mTORC1 reactivation. However, this reactivation mechanism is not yet defined. In addition, the results related to quantified non-lysosomal proteins after starvation showed the abundance levels of gluconeogenesis and glycogen metabolism biomarkers. In addition, the continuous decreased level of WASH complex in the lysosomal fraction was also depicted. In parallel, proteaphagy seemed to be continuously induced during starvation, while in contrast, starvation-induced autophagy suggested an early pexophagy and a late mitophagy indicating an ordered organelle degradation.

7 References

Abdelraheim SR, Spiller DG and McLennan AG (2003) Mammalian NADH diphosphatases of the Nudix family: cloning and characterization of the human peroxisomal NUDT12 protein. Biochem J 374:329–335. doi: 10.1042/BJ20030441

Abu-Remaileh M, Wyant GA, Kim C, Laqtom NN, Abbasi M, Chan SH, Freinkman E and Sabatini DM (2017) Lysosomal metabolomics reveals V-ATPase- and mTOR-dependent regulation of amino acid efflux from lysosomes. Science 358:807–813. doi: 10.1126/science.aan6298

Aebersold R and Mann M (2003) Mass spectrometry-based proteomics. Nature 422:198–207. doi: 10.1038/nature01511

Aebersold R and Mann M (2016) Mass-spectrometric exploration of proteome structure and function. Nature 537:347–355. doi: 10.1038/nature19949

Agrawal S, Thakur P and Katoch SS (2003) Beta adrenoceptor agonists, clenbuterol, and isoproterenol retard denervation atrophy in rat gastrocnemius muscle: use of 3-methylhistidine as a marker of myofibrillar degeneration. Jpn J Physiol 53:229–237. doi: 10.2170/jjphysiol.53.229

Aguado C, Pérez-Jiménez E, Lahuerta M and Knecht E (2016) Isolation of Lysosomes from Mammalian Tissues and Cultured Cells. Methods Mol Biol 1449:299–311. doi: 10.1007/978-1-4939-3756-1_19

Ahlberg J, Berkenstam A, Henell F and Glaumann H (1985) Degradation of short and long lived proteins in isolated rat liver lysosomes. Effects of pH, temperature, and proteolytic inhibitors. J Biol Chem 260:5847–5854.

Alberts B, Johnson A, Lewis J, Raff M, Roberts K and Walter P (2002) How Cells Obtain Energy from Food. Molecular Biology of the Cell. 4th edition

Alekhina O, Burstein E and Billadeau DD (2017) Cellular functions of WASP family proteins at a glance. J Cell Sci 130:2235–2241. doi: 10.1242/jcs.199570

Anandapadamanaban M, Masson GR, Perisic O, Berndt A, Kaufman J, Johnson CM, Santhanam B, Rogala KB, Sabatini DM and Williams RL (2019) Architecture of human Rag GTPase heterodimers and their complex with mTORC1. Science 366:203–210. doi: 10.1126/science.aax3939

Andersen JS and Mann M (2006) Organellar proteomics: turning inventories into insights. EMBO Rep 7:874–879. doi: 10.1038/sj.embor.7400780

Anderson JD, Johansson HJ, Graham CS, Vesterlund M, Pham MT, Bramlett CS, Montgomery EN, Mellema MS, Bardini RL, Contreras Z et al. (2016) Comprehensive Proteomic Analysis of Mesenchymal Stem Cell Exosomes Reveals Modulation of Angiogenesis via Nuclear Factor-KappaB Signaling. STEM CELLS 34:601–613. doi: 10.1002/stem.2298

Anderson NL and Anderson NG (1998) Proteome and proteomics: New technologies, new concepts, and new words. ELECTROPHORESIS 19:1853–1861. doi: 10.1002/elps.1150191103

Andersson LE, Nicholas LM, Filipsson K, Sun J, Medina A, Al-Majdoub M, Fex M, Mulder H and Spégel P (2016) Glycogen metabolism in the glucose-sensing

and supply-driven β-cell. FEBS Letters 590:4242–4251. doi: 10.1002/1873-3468.12460

Anding AL and Baehrecke EH (2017) Cleaning House: Selective Autophagy of Organelles. Dev Cell 41:10–22. doi: 10.1016/j.devcel.2017.02.016

Arai K, Kanaseki T and Ohkuma S (1991) Isolation of highly purified lysosomes from rat liver: identification of electron carrier components on lysosomal membranes. J Biochem 110:541–547. doi: 10.1093/oxfordjournals.jbchem.a123616

Araujo MEG de, Naschberger A, Fürnrohr BG, Stasyk T, Dunzendorfer-Matt T, Lechner S, Welti S, Kremser L, Shivalingaiah G, Offterdinger M et al. (2017) Crystal structure of the human lysosomal mTORC1 scaffold complex and its impact on signaling. Science. doi: 10.1126/science.aao1583

Ariosa AR and Klionsky DJ (2016) Autophagy core machinery: overcoming spatial barriers in neurons. J Mol Med (Berl) 94:1217–1227. doi: 10.1007/s00109-016-1461-9

Awad H, Khamis MM and El-Aneed A (2015) Mass Spectrometry, Review of the Basics: Ionization. Applied Spectroscopy Reviews 50:158–175. doi: 10.1080/05704928.2014.954046

Baba A, Matsuda T, Yamagami S, Mizui T, Maeda S and Iwata H (1981) MECHANISM OF ACCUMULATION OF TAURINE IN THE HEART OF STARVED RATS. Japanese Journal of Pharmacology 31:579–585. doi: 10.1016/S0021-5198(19)52821-9

Ballabio A and Bonifacino JS (2020) Lysosomes as dynamic regulators of cell and organismal homeostasis. Nature Reviews Molecular Cell Biology 21:101–118. doi: 10.1038/s41580-019-0185-4

Ballabio A and Gieselmann V (2009) Lysosomal disorders: From storage to cellular damage. Biochimica et Biophysica Acta (BBA) - Molecular Cell Research 1793:684–696. doi: 10.1016/j.bbamcr.2008.12.001

Bar-Peled L, Chantranupong L, Cherniack AD, Chen WW, Ottina KA, Grabiner BC, Spear ED, Carter SL, Meyerson M and Sabatini DM (2013) A Tumor suppressor complex with GAP activity for the Rag GTPases that signal amino acid sufficiency to mTORC1. Science 340:1100–1106. doi: 10.1126/science.1232044

Bar-Peled L and Sabatini DM (2014) Regulation of mTORC1 by amino acids. Trends in Cell Biology 24:400–406. doi: 10.1016/j.tcb.2014.03.003

Bar-Peled L, Schweitzer LD, Zoncu R and Sabatini DM (2012) Ragulator Is a GEF for the Rag GTPases that Signal Amino Acid Levels to mTORC1. Cell 150:1196–1208. doi: 10.1016/j.cell.2012.07.032

Bartel B, Farmer LM, Rinaldi MA, Young PG, Danan CH and Burkhart SE (2014) Mutation of the Arabidopsis LON2 peroxisomal protease enhances pexophagy. Autophagy 10:518–519. doi: 10.4161/auto.27565

Bartlett K and Eaton S (2004) Mitochondrial β-oxidation. European Journal of Biochemistry 271:462–469. doi: 10.1046/j.1432-1033.2003.03947.x

Baskin KK, Winders BR and Olson EN (2015) Muscle as a “Mediator“ of Systemic Metabolism. Cell Metab 21:237–248. doi: 10.1016/j.cmet.2014.12.021

Benito-Cuesta I, Diez H, Ordoñez L and Wandosell F (2017) Assessment of Autophagy in Neurons and Brain Tissue. Cells. doi: 10.3390/cells6030025

Ben-Sahra I, Hoxhaj G, Ricoult SJH, Asara JM and Manning BD (2016) mTORC1 induces purine synthesis through control of the mitochondrial tetrahydrofolate cycle. Science 351:728–733. doi: 10.1126/science.aad0489

Bentzinger CF, Romanino K, Cloëtta D, Lin S, Mascarenhas JB, Oliveri F, Xia J, Casanova E, Costa CF, Brink M et al. (2008) Skeletal Muscle-Specific Ablation of raptor, but Not of rictor, Causes Metabolic Changes and Results in Muscle Dystrophy. Cell Metabolism 8:411–424. doi: 10.1016/j.cmet.2008.10.002

Berg JM, Tymoczko JL and Stryer L (2003) Biochemistry. Freeman, New York

Berg JM, Tymoczko JL and Stryer L (2002a) Food Intake and Starvation Induce Metabolic Changes. Biochemistry. 5th edition

Berg JM, Tymoczko JL and Stryer L (2002b) Glycogen Metabolism. Biochemistry. 5th edition

Berg JM, Tymoczko JL and Stryer L (2002c) Fatty Acids Are Synthesized and Degraded by Different Pathways. Biochemistry. 5th edition

Bernhardt J (2005) Defining the proteome. Genome Biol 6:360. doi: 10.1186/gb-2005-6-12-360

Bianconi E, Piovesan A, Facchin F, Beraudi A, Casadei R, Frabetti F, Vitale L, Pelleri MC, Tassani S, Piva F et al. (2013) An estimation of the number of cells in the human body. Annals of Human Biology 40:463–471. doi: 10.3109/03014460.2013.807878

Bodine SC, Stitt TN, Gonzalez M, Kline WO, Stover GL, Bauerlein R, Zlotchenko E, Scrimgeour A, Lawrence JC, Glass DJ et al. (2001) Akt/mTOR pathway is a crucial regulator of skeletal muscle hypertrophy and can prevent muscle atrophy in vivo. Nature Cell Biology 3:1014–1019. doi: 10.1038/ncb1101-1014

Bonnefont J-P, Djouadi F, Prip-Buus C, Gobin S, Munnich A and Bastin J (2004) Carnitine palmitoyltransferases 1 and 2: biochemical, molecular and medical aspects. Mol Aspects Med 25:495–520. doi: 10.1016/j.mam.2004.06.004

Bröer S and Bröer A (2017) Amino acid homeostasis and signalling in mammalian cells and organisms. Biochem J 474:1935–1963. doi: 10.1042/BCJ20160822

Bronson FH (1987) Susceptibility of the fat reserves of mice to natural challenges. J Comp Physiol B 157:551–554. doi: 10.1007/BF00700974

Brosnan JT (1999) Comments on metabolic needs for glucose and the role of gluconeogenesis. Eur J Clin Nutr 53 Suppl 1:S107-111. doi: 10.1038/sj.ejcn.1600748

Brunn GJ, Hudson CC, Sekulić A, Williams JM, Hosoi H, Houghton PJ, Lawrence JC and Abraham RT (1997) Phosphorylation of the Translational Repressor PHAS-I by the Mammalian Target of Rapamycin. Science 277:99–101. doi: 10.1126/science.277.5322.99

Buerger C, DeVries B and Stambolic V (2006) Localization of Rheb to the endomembrane is critical for its signaling function. Biochemical and Biophysical Research Communications 344:869–880. doi: 10.1016/j.bbrc.2006.03.220

Burgess SC, He TT, Yan Z, Lindner J, Sherry AD, Malloy CR, Browning JD and Magnuson MA (2007) Cytosolic Phosphoenolpyruvate Carboxykinase Does Not Solely Control the Rate of Hepatic Gluconeogenesis in the Intact Mouse Liver. Cell Metab 5:313–320. doi: 10.1016/j.cmet.2007.03.004

Cahill GF (2006) Fuel Metabolism in Starvation. Annual Review of Nutrition 26:1–22. doi: 10.1146/annurev.nutr.26.061505.111258

Cann GM, Guignabert C, Ying L, Deshpande N, Bekker JM, Wang L, Zhou B and Rabinovitch M (2008) Developmental expression of LC3α and β: Absence of fibronectin or autophagy phenotype in LC3β knockout mice. Developmental Dynamics 237:187–195. doi: 10.1002/dvdy.21392

Carnell M, Zech T, Calaminus SD, Ura S, Hagedorn M, Johnston SA, May RC, Soldati T, Machesky LM and Insall RH (2011) Actin polymerization driven by WASH causes V-ATPase retrieval and vesicle neutralization before exocytosis. J Cell Biol 193:831–839. doi: 10.1083/jcb.201009119

Carvalho CR, Brenelli SL, Silva AC, Nunes AL, Velloso LA and Saad MJ (1996) Effect of aging on insulin receptor, insulin receptor substrate-1, and phosphatidylinositol 3-kinase in liver and muscle of rats. Endocrinology 137:151–159. doi: 10.1210/en.137.1.151

Chait BT (2006) Mass Spectrometry: Bottom-Up or Top-Down? Science 314:65–66. doi: 10.1126/science.1133987

Charkey LW, Kano AK and Hougham DF (1955) Effects of Fasting on Blood Non-Protein Amino Acids in Humans. J Nutr 55:469–480. doi: 10.1093/jn/55.3.469

Chaudhry FA, Reimer RJ and Edwards RH (2002) The glutamine commute. J Cell Biol 157:349–355. doi: 10.1083/jcb.200201070

Chauvin C, Koka V, Nouschi A, Mieulet V, Hoareau-Aveilla C, Dreazen A, Cagnard N, Carpentier W, Kiss T, Meyuhas O et al. (2014) Ribosomal protein S6 kinase activity controls the ribosome biogenesis transcriptional program. Oncogene 33:474–483. doi: 10.1038/onc.2012.606

Chen R, Zou Y, Mao D, Sun D, Gao G, Shi J, Liu X, Zhu C, Yang M, Ye W et al. (2014) The general amino acid control pathway regulates mTOR and autophagy during serum/glutamine starvation. J Cell Biol 206:173–182. doi: 10.1083/jcb.201403009

Chen S-J, Wu X, Wadas B, Oh J-H and Varshavsky A (2017) An N-end rule pathway that recognizes proline and destroys gluconeogenic enzymes. Science. doi: 10.1126/science.aal3655

Chomczynski P and Sacchi N (1987) Single-step method of RNA isolation by acid guanidinium thiocyanate-phenol-chloroform extraction. Analytical Biochemistry 162:156–159. doi: 10.1016/0003-2697(87)90021-2

Ciechanover A (2005) Intracellular protein degradation: from a vague idea thru the lysosome and the ubiquitin–proteasome system and onto human diseases and drug targeting. Cell Death & Differentiation 12:1178–1190. doi: 10.1038/sj.cdd.4401692

Ciechanover A and Brundin P (2003) The Ubiquitin Proteasome System in Neurodegenerative Diseases: Sometimes the Chicken, Sometimes the Egg. Neuron 40:427–446. doi: 10.1016/S0896-6273(03)00606-8

Cigolini M, Cavallo E, Zancanaro C, Micciolo R, Benati D and Bosello O (1985) Starvation-induced insulin resistance: influence on 3-O-methylglucose transport. Acta Diabetol Lat 22:351–355. doi: 10.1007/BF02624754

Claassen V (1994) 13 - Fasting. Techniques in the Behavioral and Neural Sciences. Elsevier, pp 290–320

Clarke DD and Sokoloff L (1999) Regulation of Cerebral Metabolic Rate. Basic Neurochemistry: Molecular, Cellular and Medical Aspects. 6th edition

Coelho M, Oliveira T and Fernandes R (2013) Biochemistry of adipose tissue: an endocrine organ. Arch Med Sci 9:191–200. doi: 10.5114/aoms.2013.33181

Cohen P and Spiegelman BM (2016) Cell biology of fat storage. Mol Biol Cell 27:2523–2527. doi: 10.1091/mbc.E15-10-0749

Cohen S, Valm AM and Lippincott-Schwartz J (2018) Interacting Organelles. Curr Opin Cell Biol 53:84–91. doi: 10.1016/j.ceb.2018.06.003

Cohen-Kaplan V, Livneh I, Avni N, Fabre B, Ziv T, Kwon YT and Ciechanover A (2016) p62- and ubiquitin-dependent stress-induced autophagy of the mammalian 26S proteasome. Proc Natl Acad Sci USA 113:E7490–E7499. doi: 10.1073/pnas.1615455113

Colaço A and Jäättelä M (2017) Ragulator—a multifaceted regulator of lysosomal signaling and trafficking. J Cell Biol 216:3895–3898. doi: 10.1083/jcb.201710039

Colacurcio DJ and Nixon RA (2016) Disorders of lysosomal acidification—The emerging role of v-ATPase in aging and neurodegenerative disease. Ageing Research Reviews 32:75–88. doi: 10.1016/j.arr.2016.05.004

Costa CCG, De Almeida IT, Jakobs C, Poll-The B-T and Duran M (1999) Dynamic Changes of Plasma Acylcarnitine Levels Induced by Fasting and Sunflower Oil Challenge Test in Children. Pediatric Research 46:440–440. doi: 10.1203/00006450-199910000-00013

Cox J, Hein MY, Luber CA, Paron I, Nagaraj N and Mann M (2014) Accurate Proteome-wide Label-free Quantification by Delayed Normalization and Maximal Peptide Ratio Extraction, Termed MaxLFQ. Mol Cell Proteomics 13:2513–2526. doi: 10.1074/mcp.M113.031591

Cox J and Mann M (2011) Quantitative, High-Resolution Proteomics for Data-Driven Systems Biology. Annual Review of Biochemistry 80:273–299. doi: 10.1146/annurev-biochem-061308-093216

Craigen WJ and Graham BH (2008) Genetic strategies for dissecting mammalian and Drosophila voltage-dependent anion channel functions. J Bioenerg Biomembr 40:207–212. doi: 10.1007/s10863-008-9146-x

Cuervo AM, Palmer A, Rivett AJ and Knecht E (1995) Degradation of Proteasomes by Lysosomes in Rat Liver. European Journal of Biochemistry 227:792–800. doi: 10.1111/j.1432-1033.1995.0792p.x

Curi R, Newsholme P, Marzuca-Nassr GN, Takahashi HK, Hirabara SM, Cruzat V, Krause M and de Bittencourt PIH (2016) Regulatory principles in metabolism–then and now. Biochem J 473:1845–1857. doi: 10.1042/BCJ20160103

Dan HC, Ebbs A, Pasparakis M, Van Dyke T, Basseres DS and Baldwin AS (2014) Akt-dependent Activation of mTORC1 Complex Involves Phosphorylation of mTOR (Mammalian Target of Rapamycin) by IκB Kinase α (IKKα). J Biol Chem 289:25227–25240. doi: 10.1074/jbc.M114.554881

De Duve C and Baudhuin P (1966) Peroxisomes (microbodies and related particles). Physiological Reviews 46:323–357. doi: 10.1152/physrev.1966.46.2.323

de Duve C, Pressman BC, Gianetto R, Wattiaux R and Appelmans F (1955) Tissue fractionation studies. 6. Intracellular distribution patterns of enzymes in rat-liver tissue. Biochem J 60:604–617.

DeBerardinis RJ and Thompson CB (2012) Cellular metabolism and disease: what do metabolic outliers teach us? Cell 148:1132–1144. doi: 10.1016/j.cell.2012.02.032

Dedkova EN and Blatter LA (2014) Role of β-hydroxybutyrate, its polymer poly-β-hydroxybutyrate and inorganic polyphosphate in mammalian health and disease. Front Physiol. doi: 10.3389/fphys.2014.00260

Demetriades C, Doumpas N and Teleman AA (2014) Regulation of TORC1 in response to amino acid starvation via lysosomal recruitment of TSC2. Cell 156:786–799. doi: 10.1016/j.cell.2014.01.024

Demine S, Reddy N, Renard P, Raes M and Arnould T (2014) Unraveling Biochemical Pathways Affected by Mitochondrial Dysfunctions Using Metabolomic Approaches. Metabolites 4:831–878. doi: 10.3390/metabo4030831

Dengjel J, Høyer-Hansen M, Nielsen MO, Eisenberg T, Harder LM, Schandorff S, Farkas T, Kirkegaard T, Becker AC, Schroeder S et al. (2012) Identification of Autophagosome-associated Proteins and Regulators by Quantitative Proteomic Analysis and Genetic Screens. Molecular & Cellular Proteomics. doi: 10.1074/mcp.M111.014035

Derivery E and Gautreau A (2010) Evolutionary conservation of the WASH complex, an actin polymerization machine involved in endosomal fission. Commun Integr Biol 3:227–230.

Derivery E, Sousa C, Gautier JJ, Lombard B, Loew D and Gautreau A (2009) The Arp2/3 Activator WASH Controls the Fission of Endosomes through a Large Multiprotein Complex. Developmental Cell 17:712–723. doi: 10.1016/j.devcel.2009.09.010

Dhillon KK and Gupta S (2020) Biochemistry, Ketogenesis. StatPearls

Dibble CC, Elis W, Menon S, Qin W, Klekota J, Asara JM, Finan PM, Kwiatkowski DJ, Murphy LO and Manning BD (2012) TBC1D7 Is a Third Subunit of the TSC1-TSC2 Complex Upstream of mTORC1. Molecular Cell 47:535–546. doi: 10.1016/j.molcel.2012.06.009

Dokken BB and Tsao T-S (2007) The Physiology of Body Weight Regulation: Are We Too Efficient for Our Own Good? Diabetes Spectrum 20:166–170. doi: 10.2337/diaspect.20.3.166

Donnelly JE, Jakicic J and Gunderson S (1991) Diet and Body Composition. Sports Med 12:237–249. doi: 10.2165/00007256-199112040-00003

Dupont N and Codogno P (2013) Autophagy plays a WASHing game. EMBO J 32:2659–2660. doi: 10.1038/emboj.2013.202

Duška F, Anděl M, Kuběna A and Macdonald IA (2005) Effects of acute starvation on insulin resistance in obese patients with and without type 2 diabetes mellitus. Clinical Nutrition 24:1056–1064. doi: 10.1016/j.clnu.2005.08.008

Düvel K, Yecies JL, Menon S, Raman P, Lipovsky AI, Souza AL, Triantafellow E, Ma Q, Gorski R, Cleaver S et al. (2010) Activation of a Metabolic Gene Regulatory Network Downstream of mTOR Complex 1. Molecular Cell 39:171–183. doi: 10.1016/j.molcel.2010.06.022

Eknoyan G (1999) Santorio Sanctorius (1561–1636) – Founding Father of Metabolic Balance Studies. AJN 19:226–233. doi: 10.1159/000013455

Eriksson J and Fenyö D (2007) Improving the success rate of proteome analysis by modeling protein-abundance distributions and experimental designs. Nature Biotechnology 25:651–655. doi: 10.1038/nbt1315

Erkhembaatar M, Gu DR, Lee SH, Yang Y-M, Park S, Muallem S, Shin DM and Kim MS (2017) Lysosomal Ca2+ Signaling is Essential for Osteoclastogenesis and Bone Remodeling. Journal of Bone and Mineral Research 32:385–396. doi: 10.1002/jbmr.2986

Erol E, Kumar LS, Cline GW, Shulman GI, Kelly DP and Binas B (2004) Liver fatty acid binding protein is required for high rates of hepatic fatty acid oxidation but not for the action of PPARalpha in fasting mice. FASEB J 18:347–349. doi: 10.1096/fj.03-0330fje

Eskelinen E-L, Tanaka Y and Saftig P (2003) At the acidic edge: emerging functions for lysosomal membrane proteins. Trends in Cell Biology 13:137–145. doi: 10.1016/S0962-8924(03)00005-9

Felig P (1973) The glucose-alanine cycle. Metabolism 22:179–207. doi: 10.1016/0026-0495(73)90269-2

Felig P, Owen OE, Wahren J and Cahill GF (1969) Amino acid metabolism during prolonged starvation. J Clin Invest 48:584–594.

Fenn JB, Mann M, Meng CK, Wong SF and Whitehouse CM (1989) Electrospray ionization for mass spectrometry of large biomolecules. Science 246:64–71. doi: 10.1126/science.2675315

Ferrari S, Bandi HR, Hofsteenge J, Bussian BM and Thomas G (1991) Mitogen-activated 70K S6 kinase. Identification of in vitro 40 S ribosomal S6 phosphorylation sites. J Biol Chem 266:22770–22775.

Filipek PA, de Araujo MEG, Vogel GF, De Smet CH, Eberharter D, Rebsamen M, Rudashevskaya EL, Kremser L, Yordanov T, Tschaikner P et al. (2017) LAMTOR/Ragulator is a negative regulator of Arl8b- and BORC-dependent late endosomal positioning. J Cell Biol 216:4199–4215. doi: 10.1083/jcb.201703061

Finbow ME and Harrison MA (1997) The vacuolar H+-ATPase: a universal proton pump of eukaryotes. Biochem J 324 (Pt 3):697–712. doi: 10.1042/bj3240697

Finley D (2009) Recognition and processing of ubiquitin-protein conjugates by the proteasome. Annu Rev Biochem 78:477–513. doi: 10.1146/annurev.biochem.78.081507.101607

Foster DW (2004) The role of the carnitine system in human metabolism. Ann N Y Acad Sci 1033:1–16. doi: 10.1196/annals.1320.001

Fritzen AM, Madsen AB, Kleinert M, Treebak JT, Lundsgaard A-M, Jensen TE, Richter EA, Wojtaszewski J, Kiens B and Frøsig C (2016) Regulation of autophagy in human skeletal muscle: effects of exercise, exercise training and insulin stimulation. The Journal of Physiology 594:745–761. doi: https://doi.org/10.1113/JP271405

Fukuda M (1991) Lysosomal membrane glycoproteins. Structure, biosynthesis, and intracellular trafficking. J Biol Chem 266:21327–21330.

Furner RL and Feller DD (1971) The influence of starvation upon hepatic drug metabolism in rats, mice, and guinea pigs. Proc Soc Exp Biol Med 137:816–819. doi: 10.3181/00379727-137-35674

Ge W, Li D, Gao Y and Cao X (2015) The Roles of Lysosomes in Inflammation and Autoimmune Diseases. International Reviews of Immunology 34:415–431. doi: 10.3109/08830185.2014.936587

Geisler CE, Hepler C, Higgins MR and Renquist BJ (2016) Hepatic adaptations to maintain metabolic homeostasis in response to fasting and refeeding in mice. Nutrition & Metabolism 13:62. doi: 10.1186/s12986-016-0122-x

Geisler S, Holmström KM, Skujat D, Fiesel FC, Rothfuss OC, Kahle PJ and Springer W (2010) PINK1/Parkin-mediated mitophagy is dependent on VDAC1 and p62/SQSTM1. Nature Cell Biology 12:119–131. doi: 10.1038/ncb2012

Gelfand RA and Sherwin RS (1983) Glucagon and Starvation. In: Lefebvre PJ (ed) Glucagon II. Springer, Berlin, Heidelberg, pp 223–237

Gersten DM, Kimmerer TW and Bosmann HB (1974) THE LYSOSOME PERIPHERY: BIOCHEMICAL AND ELECTROKINETIC PROPERTIES OF THE TRITOSOME SURFACE. The Journal of Cell Biology 60:764–773. doi: 10.1083/jcb.60.3.764

Gingras A-C, Gygi SP, Raught B, Polakiewicz RD, Abraham RT, Hoekstra MF, Aebersold R and Sonenberg N (1999) Regulation of 4E-BP1 phosphorylation: a novel two-step mechanism. Genes Dev 13:1422–1437.

Gingras AC, Raught B, Gygi SP, Niedzwiecka A, Miron M, Burley SK, Polakiewicz RD, Wyslouch-Cieszynska A, Aebersold R and Sonenberg N (2001) Hierarchical phosphorylation of the translation inhibitor 4E-BP1. Genes Dev 15:2852–2864. doi: 10.1101/gad.912401

Gomes LC, Benedetto GD and Scorrano L (2011) During autophagy mitochondria elongate, are spared from degradation and sustain cell viability. Nature Cell Biology 13:589–598. doi: 10.1038/ncb2220

Gomez TS and Billadeau DD (2009) A FAM21-containing WASH complex regulates retromer-dependent sorting. Dev Cell 17:699–711. doi: 10.1016/j.devcel.2009.09.009

Gomez TS, Gorman JA, Artal-Martinez de Narvajas A, Koenig AO and Billadeau DD (2012) Trafficking defects in WASH-knockout fibroblasts originate from collapsed endosomal and lysosomal networks. MBoC 23:3215–3228. doi: 10.1091/mbc.e12-02-0101

Goodman AD, Fuisz RE and Cahill GF (1966) Renal gluconeogenesis in acidosis, alkalosis, and potassium deficiency: its possible role in regulation of renal ammonia production. J Clin Invest 45:612–619. doi: 10.1172/JCI105375

Grabacka M, Pierzchalska M, Dean M and Reiss K (2016) Regulation of Ketone Body Metabolism and the Role of PPARα. International Journal of Molecular Sciences 17:2093. doi: 10.3390/ijms17122093

Graham JM (2001) Isolation of lysosomes from tissues and cells by differential and density gradient centrifugation. Curr Protoc Cell Biol Chapter 3:Unit 3.6. doi: 10.1002/0471143030.cb0306s07

Graham JM, Ford T and Rickwood D (1990) Isolation of the major subcellular organelles from mouse liver using Nycodenz gradients without the use of an ultracentrifuge. Analytical Biochemistry 187:318–323. doi: 10.1016/0003-2697(90)90463-J

Groenewoud MJ and Zwartkruis FJT (2013) Rheb and Rags come together at the lysosome to activate mTORC1. Biochem Soc Trans 41:951–955. doi: 10.1042/BST20130037

Gu Z, Eils R and Schlesner M (2016) Complex heatmaps reveal patterns and correlations in multidimensional genomic data. Bioinformatics 32:2847–2849. doi: 10.1093/bioinformatics/btw313

Hall KD (2006) Computational model of in vivo human energy metabolism during semistarvation and refeeding. Am J Physiol Endocrinol Metab 291:E23-37. doi: 10.1152/ajpendo.00523.2005

Han H-S, Kang G, Kim JS, Choi BH and Koo S-H (2016) Regulation of glucose metabolism from a liver-centric perspective. Exp Mol Med 48:e218. doi: 10.1038/emm.2015.122

Hanson RW and Garber AJ (1972) Phosphoenolpyruvate carboxykinase. I. Its role in gluconeogenesis. Am J Clin Nutr 25:1010–1021. doi: 10.1093/ajcn/25.10.1010

Hao Y, Kacal M, Ouchida AT, Zhang B, Norberg E and Vakifahmetoglu-Norberg H (2019) Targetome analysis of chaperone-mediated autophagy in cancer cells. Autophagy 15:1558–1571. doi: 10.1080/15548627.2019.1586255

Hara K, Yonezawa K, Kozlowski MT, Sugimoto T, Andrabi K, Weng QP, Kasuga M, Nishimoto I and Avruch J (1997) Regulation of eIF-4E BP1 phosphorylation by mTOR. J Biol Chem 272:26457–26463. doi: 10.1074/jbc.272.42.26457

Harbour ME, Breusegem SY and Seaman MNJ (2012) Recruitment of the endosomal WASH complex is mediated by the extended 'tail' of Fam21 binding to the retromer protein Vps35. Biochem J 442:209–220. doi: 10.1042/BJ20111761

Harbour ME, Breusegem SYA, Antrobus R, Freeman C, Reid E and Seaman MNJ (2010) The cargo-selective retromer complex is a recruiting hub for protein complexes that regulate endosomal tubule dynamics. J Cell Sci 123:3703–3717. doi: 10.1242/jcs.071472

Hashimoto T, Cook WS, Qi C, Yeldandi AV, Reddy JK and Rao MS (2000) Defect in Peroxisome Proliferator-activated Receptor α-inducible Fatty Acid Oxidation

Determines the Severity of Hepatic Steatosis in Response to Fasting. J Biol Chem 275:28918–28928. doi: 10.1074/jbc.M910350199

Haspel J, Shaik RS, Ifedigbo E, Nakahira K, Dolinay T, Englert JA and Choi AMK (2011) Characterization of macroautophagic flux in vivo using a leupeptin-based assay. Autophagy 7:629–642. doi: 10.4161/auto.7.6.15100

Hasselbalch SG, Knudsen GM, Jakobsen J, Hageman LP, Holm S and Paulson OB (1994) Brain metabolism during short-term starvation in humans. J Cereb Blood Flow Metab 14:125–131. doi: 10.1038/jcbfm.1994.17

Hatazawa Y, Qian K, Gong D-W and Kamei Y (2018) PGC-1α regulates alanine metabolism in muscle cells. PLoS One. doi: 10.1371/journal.pone.0190904

Hatting M, Tavares CDJ, Sharabi K, Rines AK and Puigserver P (2018) Insulin regulation of gluconeogenesis. Ann N Y Acad Sci 1411:21–35. doi: 10.1111/nyas.13435

Henning R and Plattner H (1974) Isolation of rat liver lysosomes by loading with colloidal gold. Biochimica et Biophysica Acta (BBA) - General Subjects 354:114–120. doi: 10.1016/0304-4165(74)90059-2

Hershko A and Ciechanover A (1998) The Ubiquitin System. Annual Review of Biochemistry 67:425–479. doi: 10.1146/annurev.biochem.67.1.425

Hodge T and Colombini M (1997) Regulation of metabolite flux through voltage-gating of VDAC channels. J Membr Biol 157:271–279. doi: 10.1007/s002329900235

Holeček M (2018) Branched-chain amino acids in health and disease: metabolism, alterations in blood plasma, and as supplements. Nutr Metab (Lond). doi: 10.1186/s12986-018-0271-1

Holecek M, Sprongl L and Tilser I (2001) Metabolism of branched-chain amino acids in starved rats: the role of hepatic tissue. Physiol Res 50:25–33.

Hosokawa N, Hara T, Kaizuka T, Kishi C, Takamura A, Miura Y, Iemura S, Natsume T, Takehana K, Yamada N et al. (2009) Nutrient-dependent mTORC1 association with the ULK1-Atg13-FIP200 complex required for autophagy. Mol Biol Cell 20:1981–1991. doi: 10.1091/mbc.e08-12-1248

Houten SM, Violante S, Ventura FV and Wanders RJA (2016) The Biochemistry and Physiology of Mitochondrial Fatty Acid β-Oxidation and Its Genetic Disorders. Annual Review of Physiology 78:23–44. doi: 10.1146/annurev-physiol-021115-105045

Houten SM and Wanders RJA (2010) A general introduction to the biochemistry of mitochondrial fatty acid β-oxidation. Journal of Inherited Metabolic Disease 33:469–477. doi: 10.1007/s10545-010-9061-2

Howell JJ and Manning BD (2011) mTOR couples cellular nutrient sensing to organismal metabolic homeostasis. Trends in Endocrinology & Metabolism 22:94–102. doi: 10.1016/j.tem.2010.12.003

Hsu J-L, Huang S-Y, Chow N-H and Chen S-H (2003) Stable-isotope dimethyl labeling for quantitative proteomics. Anal Chem 75:6843–6852. doi: 10.1021/ac0348625

Hsu MH, Savas U, Griffin KJ and Johnson EF (2001) Identification of peroxisome proliferator-responsive human genes by elevated expression of the peroxisome proliferator-activated receptor alpha in HepG2 cells. J Biol Chem 276:27950–27958. doi: 10.1074/jbc.M100258200

Huang T, Wang J, Yu W and He Z (2012) Protein inference: a review. Brief Bioinform 13:586–614. doi: 10.1093/bib/bbs004

Huber W, von Heydebreck A, Sültmann H, Poustka A and Vingron M (2002) Variance stabilization applied to microarray data calibration and to the quantification of differential expression. Bioinformatics 18:S96–S104. doi: 10.1093/bioinformatics/18.suppl_1.S96

Huotari J and Helenius A (2011) Endosome maturation. The EMBO Journal 30:3481–3500. doi: 10.1038/emboj.2011.286

Huynh KK, Eskelinen E-L, Scott CC, Malevanets A, Saftig P and Grinstein S (2007) LAMP proteins are required for fusion of lysosomes with phagosomes. The EMBO Journal 26:313–324. doi: 10.1038/sj.emboj.7601511

Islinger M and Schrader M (2011) Peroxisomes. Current Biology 21:R800–R801. doi: 10.1016/j.cub.2011.07.024

Izumida Y, Yahagi N, Takeuchi Y, Nishi M, Shikama A, Takarada A, Masuda Y, Kubota M, Matsuzaka T, Nakagawa Y et al. (2013) Glycogen shortage during fasting triggers liver–brain–adipose neurocircuitry to facilitate fat utilization. Nature Communications 4:2316. doi: 10.1038/ncomms3316

Jelen S, Wacker S, Aponte-Santamaría C, Skott M, Rojek A, Johanson U, Kjellbom P, Nielsen S, Groot BL de and Rützler M (2011) Aquaporin-9 Protein Is the Primary Route of Hepatocyte Glycerol Uptake for Glycerol Gluconeogenesis in Mice. J Biol Chem 286:44319–44325. doi: 10.1074/jbc.M111.297002

Jensen T, Kiersgaard M, Sørensen D and Mikkelsen L (2013) Fasting of mice: a review. Lab Anim 47:225–240. doi: 10.1177/0023677213501659

Jia D, Gomez TS, Metlagel Z, Umetani J, Otwinowski Z, Rosen MK and Billadeau DD (2010) WASH and WAVE actin regulators of the Wiskott–Aldrich syndrome protein (WASP) family are controlled by analogous structurally related complexes. PNAS 107:10442–10447. doi: 10.1073/pnas.0913293107

Johannes L and Popoff V (2008) Tracing the Retrograde Route in Protein Trafficking. Cell 135:1175–1187. doi: 10.1016/j.cell.2008.12.009

Johnson P, Harris CI and Perry SV (1967) 3-Methylhistidine in actin and other muscle proteins. Biochem J 105:361–370.

Johri A and Beal MF (2012) Mitochondrial Dysfunction in Neurodegenerative Diseases. J Pharmacol Exp Ther 342:619–630. doi: 10.1124/jpet.112.192138

Jones CB, Ott EM, Keener JM, Curtiss M, Sandrin V and Babst M (2012) Regulation of membrane protein degradation by starvation-response pathways. Traffic 13:468–482. doi: 10.1111/j.1600-0854.2011.01314.x

Ju J-S, Varadhachary AS, Miller SE and Weihl CC (2010) Quantitation of “autophagic flux” in mature skeletal muscle. Autophagy 6:929–935. doi: 10.4161/auto.6.7.12785

Kabeya Y, Mizushima N, Ueno T, Yamamoto A, Kirisako T, Noda T, Kominami E, Ohsumi Y and Yoshimori T (2000) LC3, a mammalian homologue of yeast Apg8p, is localized in autophagosome membranes after processing. EMBO J 19:5720–5728. doi: 10.1093/emboj/19.21.5720

Kabeya Y, Mizushima N, Yamamoto A, Oshitani-Okamoto S, Ohsumi Y and Yoshimori T (2004) LC3, GABARAP and GATE16 localize to autophagosomal membrane depending on form-II formation. J Cell Sci 117:2805–2812. doi: 10.1242/jcs.01131

Käll L, Storey JD, MacCoss MJ and Noble WS (2008) Assigning significance to peptides identified by tandem mass spectrometry using decoy databases. J Proteome Res 7:29–34. doi: 10.1021/pr700600n

Kang SJ and Rhee WJ (2019) Silkworm Storage Protein 1 Inhibits Autophagy-Mediated Apoptosis. International Journal of Molecular Sciences 20:318. doi: 10.3390/ijms20020318

Kast DJ and Dominguez R (2017) The Cytoskeleton-Autophagy Connection. Curr Biol 27:R318–R326. doi: 10.1016/j.cub.2017.02.061

Kaur J and Debnath J (2015) Autophagy at the crossroads of catabolism and anabolism. Nature Reviews Molecular Cell Biology 16:461–472. doi: 10.1038/nrm4024

Kaushik S, Singh R and Cuervo AM (2010) Autophagic pathways and metabolic stress. Diabetes Obes Metab 12:4–14. doi: 10.1111/j.1463-1326.2010.01263.x

Kerner J and Hoppel C (2000) Fatty acid import into mitochondria. Biochimica et Biophysica Acta (BBA) - Molecular and Cell Biology of Lipids 1486:1–17. doi: 10.1016/S1388-1981(00)00044-5

Kim D-H, Sarbassov DD, Ali SM, King JE, Latek RR, Erdjument-Bromage H, Tempst P and Sabatini DM (2002) mTOR Interacts with Raptor to Form a Nutrient-Sensitive Complex that Signals to the Cell Growth Machinery. Cell 110:163–175. doi: 10.1016/S0092-8674(02)00808-5

Kim J and Guan K-L (2019) mTOR as a central hub of nutrient signalling and cell growth. Nat Cell Biol 21:63–71. doi: 10.1038/s41556-018-0205-1

Kim J, Kundu M, Viollet B and Guan K-L (2011) AMPK and mTOR regulate autophagy through direct phosphorylation of Ulk1. Nature Cell Biology 13:132–141. doi: 10.1038/ncb2152

Kim J, Saidel GM and Cabrera ME (2007) Multi-scale computational model of fuel homeostasis during exercise: effect of hormonal control. Ann Biomed Eng 35:69–90. doi: 10.1007/s10439-006-9201-x

Kim SG, Buel GR and Blenis J (2013) Nutrient Regulation of the mTOR Complex 1 Signaling Pathway. Mol Cells 35:463–473. doi: 10.1007/s10059-013-0138-2

Kimura S, Fujita N, Noda T and Yoshimori T (2009) Chapter 1 Monitoring Autophagy in Mammalian Cultured Cells through the Dynamics of LC3. Methods in Enzymology. Academic Press, pp 1–12

King JS, Gueho A, Hagedorn M, Gopaldass N, Leuba F, Soldati T and Insall RH (2013) WASH is required for lysosomal recycling and efficient autophagic and phagocytic digestion. MBoC 24:2714–2726. doi: 10.1091/mbc.e13-02-0092

Klionsky DJ, Abdelmohsen K, Abe A, Abedin MJ, Abeliovich H, Acevedo Arozena A, Adachi H, Adams CM, Adams PD, Adeli K et al. (2016) Guidelines for the use and interpretation of assays for monitoring autophagy (3rd edition). Autophagy 12:1–222. doi: 10.1080/15548627.2015.1100356

Komatsu M, Waguri S, Ueno T, Iwata J, Murata S, Tanida I, Ezaki J, Mizushima N, Ohsumi Y, Uchiyama Y et al. (2005) Impairment of starvation-induced and constitutive autophagy in Atg7-deficient mice. J Cell Biol 169:425–434. doi: 10.1083/jcb.200412022

Korolchuk VI and Rubinsztein DC (2011) Regulation of autophagy by lysosomal positioning. Autophagy 7:927–928. doi: 10.4161/auto.7.8.15862

Kotoulas OB, Kalamidas SA and Kondomerkos DJ (2006) Glycogen autophagy in glucose homeostasis. Pathology - Research and Practice 202:631–638. doi: 10.1016/j.prp.2006.04.001

Kristensen AR, Schandorff S, Høyer-Hansen M, Nielsen MO, Jäättelä M, Dengjel J and Andersen JS (2008) Ordered Organelle Degradation during Starvation-induced Autophagy. Molecular & Cellular Proteomics 7:2419–2428. doi: 10.1074/mcp.M800184-MCP200

Ktistakis NT and Tooze SA (2016) Digesting the Expanding Mechanisms of Autophagy. Trends in Cell Biology 26:624–635. doi: 10.1016/j.tcb.2016.03.006

Kundu M and Thompson CB (2008) Autophagy: basic principles and relevance to disease. Annu Rev Pathol 3:427–455. doi: 10.1146/annurev.pathmechdis.2.010506.091842

Kuo CJ, Chung J, Fiorentino DF, Flanagan WM, Blenis J and Crabtree GR (1992) Rapamycin selectively inhibits interleukin-2 activation of p70 S6 kinase. Nature 358:70–73. doi: 10.1038/358070a0

Laemmli UK (1970) Cleavage of Structural Proteins during the Assembly of the Head of Bacteriophage T4. Nature 227:680–685. doi: 10.1038/227680a0

Laffel L (1999) Ketone bodies: a review of physiology, pathophysiology and application of monitoring to diabetes. Diabetes Metab Res Rev 15:412–426. doi: 10.1002/(sici)1520-7560(199911/12)15:6<412::aid-dmrr72>3.0.co;2-8

Lamming DW and Bar-Peled L (2019) Lysosome: The metabolic signaling hub. Traffic 20:27–38. doi: 10.1111/tra.12617

Laplante M and Sabatini DM (2012) mTOR signaling in growth control and disease. Cell 149:274–293. doi: 10.1016/j.cell.2012.03.017

Latorre-Muro P, Baeza J, Armstrong EA, Hurtado-Guerrero R, Corzana F, Wu LE, Sinclair DA, López-Buesa P, Carrodeguas JA and Denu JM (2018) Dynamic Acetylation of Phosphoenolpyruvate Carboxykinase Toggles Enzyme Activity between Gluconeogenic and Anaplerotic Reactions. Molecular Cell 71:718-732.e9. doi: 10.1016/j.molcel.2018.07.031

Lê S, Josse J and Husson F (2008) FactoMineR: An R Package for Multivariate Analysis. Journal of Statistical Software 25:1–18. doi: 10.18637/jss.v025.i01

Lee HJ, Jang HB, Kim W-H, Park KJ, Kim KY, Park SI and Lee H-J (2019) 2-Aminoadipic acid (2-AAA) as a potential biomarker for insulin resistance in childhood obesity. Scientific Reports 9:13610. doi: 10.1038/s41598-019-49578-z

Leeman DS, Hebestreit K, Ruetz T, Webb AE, McKay A, Pollina EA, Dulken BW, Zhao X, Yeo RW, Ho TT et al. (2018) Lysosome activation clears aggregates and enhances quiescent neural stem cell activation during aging. Science 359:1277–1283. doi: 10.1126/science.aag3048

Leighton F, Poole B, Beaufay H, Baudhuin P, Coffey JW, Fowler S and De Duve C (1968) THE LARGE-SCALE SEPARATION OF PEROXISOMES, MITOCHONDRIA, AND LYSOSOMES FROM THE LIVERS OF RATS INJECTED WITH TRITON WR-1339 Improved Isolation Procedures, Automated Analysis, Biochemical and Morphological Properties of Fractions. J Cell Biol 37:482–513. doi: 10.1083/jcb.37.2.482

Lemasters JJ (2005) Selective Mitochondrial Autophagy, or Mitophagy, as a Targeted Defense Against Oxidative Stress, Mitochondrial Dysfunction, and Aging. Rejuvenation Research 8:3–5. doi: 10.1089/rej.2005.8.3

León IR, Schwämmle V, Jensen ON and Sprenger RR (2013) Quantitative assessment of in-solution digestion efficiency identifies optimal protocols for unbiased protein analysis. Mol Cell Proteomics 12:2992–3005. doi: 10.1074/mcp.M112.025585

Li X, Rydzewski N, Hider A, Zhang X, Yang J, Wang W, Gao Q, Cheng X and Xu H (2016) A molecular mechanism to regulate lysosome motility for lysosome positioning and tubulation. Nature Cell Biology 18:404–417. doi: 10.1038/ncb3324

Lima L and Jaffé E (1998) Plasma Concentration of Taurine is Higher in Malnourished than Control Children: Differences between Kwashiorkor and Marasmus. In: Schaffer S, Lombardini JB and Huxtable RJ (eds) Taurine 3: Cellular and Regulatory Mechanisms. Springer US, Boston, MA, pp 487–494

Lipton JO and Sahin M (2014) The Neurology of mTOR. Neuron 84:275–291. doi: 10.1016/j.neuron.2014.09.034

Liu GY and Sabatini DM (2020) mTOR at the nexus of nutrition, growth, ageing and disease. Nature Reviews Molecular Cell Biology 21:183–203. doi: 10.1038/s41580-019-0199-y

Livak KJ and Schmittgen TD (2001) Analysis of Relative Gene Expression Data Using Real-Time Quantitative PCR and the 2−ΔΔCT Method. Methods 25:402–408. doi: 10.1006/meth.2001.1262

Longo N, Frigeni M and Pasquali M (2016) CARNITINE TRANSPORT AND FATTY ACID OXIDATION. Biochim Biophys Acta 1863:2422–2435. doi: 10.1016/j.bbamcr.2016.01.023

Loos B, Toit A du and Hofmeyr J-HS (2014) Defining and measuring autophagosome flux—concept and reality. Autophagy 10:2087–2096. doi: 10.4161/15548627.2014.973338

Lopes-Cardozo M, Klein W and Jager JE (1980) UTILISATION OF KETONE BODIES BY RAT BRAIN HOMOGENATES. In: Brzin M, Sket D and Bachelard H (eds) Synaptic Constituents in Health and Disease. Pergamon, p 622

Lopez MJ and Mohiuddin SS (2020) Biochemistry, Essential Amino Acids. StatPearls

Lowry OH, Rosebrough NJ, Farr AL and Randall RJ (1951) Protein measurement with the Folin phenol reagent. J Biol Chem 193:265–275.

Lübke T, Lobel P and Sleat DE (2009) Proteomics of the lysosome. Biochim Biophys Acta 1793:625–635. doi: 10.1016/j.bbamcr.2008.09.018

Luzio JP, Pryor PR and Bright NA (2007) Lysosomes: fusion and function. Nature Reviews Molecular Cell Biology 8:622–632. doi: 10.1038/nrm2217

Macotela Y, Boucher J, Tran TT and Kahn CR (2009) Sex and Depot Differences in Adipocyte Insulin Sensitivity and Glucose Metabolism. Diabetes 58:803–812. doi: 10.2337/db08-1054

Makowski L, Noland RC, Koves TR, Xing W, Ilkayeva OR, Muehlbauer MJ, Stevens RD and Muoio DM (2009) Metabolic profiling of PPARα−/− mice reveals defects in carnitine and amino acid homeostasis that are partially reversed by oral carnitine supplementation. FASEB J 23:586–604. doi: 10.1096/fj.08-119420

Makrecka M, Kuka J, Volska K, Antone U, Sevostjanovs E, Cirule H, Grinberga S, Pugovics O, Dambrova M and Liepinsh E (2014) Long-chain acylcarnitine content determines the pattern of energy metabolism in cardiac mitochondria. Mol Cell Biochem 395:1–10. doi: 10.1007/s11010-014-2106-3

Makrecka-Kuka M, Sevostjanovs E, Vilks K, Volska K, Antone U, Kuka J, Makarova E, Pugovics O, Dambrova M and Liepinsh E (2017) Plasma acylcarnitine concentrations reflect the acylcarnitine profile in cardiac tissues. Scientific Reports 7:17528. doi: 10.1038/s41598-017-17797-x

Manifava M, Smith M, Rotondo S, Walker S, Niewczas I, Zoncu R, Clark J and Ktistakis NT (2016) Dynamics of mTORC1 activation in response to amino acids. eLife 5:e19960. doi: 10.7554/eLife.19960

Manza LL, Stamer SL, Ham A-JL, Codreanu SG and Liebler DC (2005) Sample preparation and digestion for proteomic analyses using spin filters. PROTEOMICS 5:1742–1745. doi: 10.1002/pmic.200401063

Markmann S, Krambeck S, Hughes CJ, Mirzaian M, Aerts JMFG, Saftig P, Schweizer M, Vissers JPC, Braulke T and Damme M (2017) Quantitative Proteome Analysis of Mouse Liver Lysosomes Provides Evidence for Mannose 6-phosphate-independent Targeting Mechanisms of Acid Hydrolases in Mucolipidosis II. Molecular & Cellular Proteomics 16:438–450. doi: 10.1074/mcp.M116.063636

Marshall RS, Li F, Gemperline DC, Book AJ and Vierstra RD (2015) Autophagic Degradation of the 26S Proteasome Is Mediated by the Dual ATG8/Ubiquitin Receptor RPN10 in Arabidopsis. Mol Cell 58:1053–1066. doi: 10.1016/j.molcel.2015.04.023

Massa López D, Thelen M, Stahl F, Thiel C, Linhorst A, Sylvester M, Hermanns-Borgmeyer I, Lüllmann-Rauch R, Eskild W, Saftig P et al. (2019) The lysosomal transporter MFSD1 is essential for liver homeostasis and critically depends on its accessory subunit GLMP. eLife 8:e50025. doi: 10.7554/eLife.50025

Mathew R, Khor S, Hackett SR, Rabinowitz JD, Perlman DH and White E (2014) Functional Role of Autophagy-Mediated Proteome Remodeling in Cell Survival

Signaling and Innate Immunity. Molecular Cell 55:916–930. doi: 10.1016/j.molcel.2014.07.019

Matzke MM, Waters KM, Metz TO, Jacobs JM, Sims AC, Baric RS, Pounds JG and Webb-Robertson B-JM (2011) Improved quality control processing of peptide-centric LC-MS proteomics data. Bioinformatics 27:2866–2872. doi: 10.1093/bioinformatics/btr479

McCoin CS, Knotts TA and Adams SH (2015) Acylcarnitines--old actors auditioning for new roles in metabolic physiology. Nat Rev Endocrinol 11:617–625. doi: 10.1038/nrendo.2015.129

Melser S, Lavie J and Bénard G (2015) Mitochondrial degradation and energy metabolism. Biochimica et Biophysica Acta (BBA) - Molecular Cell Research 1853:2812–2821. doi: 10.1016/j.bbamcr.2015.05.010

Melzer K (2011) Carbohydrate and fat utilization during rest and physical activity. European e-Journal of Clinical Nutrition and Metabolism 6:e45–e52. doi: 10.1016/j.eclnm.2011.01.005

Miyamoto J, Ohue-Kitano R, Mukouyama H, Nishida A, Watanabe K, Igarashi M, Irie J, Tsujimoto G, Satoh-Asahara N, Itoh H et al. (2019) Ketone body receptor GPR43 regulates lipid metabolism under ketogenic conditions. PNAS 116:23813–23821. doi: 10.1073/pnas.1912573116

Miyazaki T, Ishikura K, Honda A, Ra S-G, Komine S, Miyamoto Y, Ohmori H and Matsuzaki Y (2015) Increased N-Acetyltaurine in Serum and Urine After Endurance Exercise in Human. In: Marcinkiewicz J and Schaffer SW (eds) Taurine 9. Springer International Publishing, Cham, pp 53–62

Mizushima N, Yamamoto A, Matsui M, Yoshimori T and Ohsumi Y (2003) In Vivo Analysis of Autophagy in Response to Nutrient Starvation Using Transgenic Mice Expressing a Fluorescent Autophagosome Marker. MBoC 15:1101–1111. doi: 10.1091/mbc.e03-09-0704

Montal ED, Dewi R, Bhalla K, Ou L, Hwang BJ, Ropell AE, Gordon C, Liu W-J, DeBerardinis RJ, Sudderth J et al. (2015) PEPCK Coordinates the Regulation of Central Carbon Metabolism to Promote Cancer Cell Growth. Molecular Cell 60:571–583. doi: 10.1016/j.molcel.2015.09.025

Mosteller F and Tukey JW (1977) Data Analysis and Regression: A Second Course in Statistics, 1st ed. Pearson, Reading, Mass

Mu Z, Wang L, Deng W, Wang J and Wu G (2017) Structural insight into the Ragulator complex which anchors mTORC1 to the lysosomal membrane. Cell Discov 3:17049. doi: 10.1038/celldisc.2017.49

Murata Y, Uehara Y and Hosoi Y (2015) Activation of mTORC1 under nutrient starvation conditions increases cellular radiosensitivity in human liver cancer cell lines, HepG2 and HuH6. Biochemical and Biophysical Research Communications 468:684–690. doi: 10.1016/j.bbrc.2015.11.016

Nagasawa T, Yoshizawa F and Nishizawa N (1996) Plasma Nτ-Methylhistidine Concentration Is a Sensitive Index of Myofibrillar Protein Degradation during Starvation in Rats. Bioscience, Biotechnology, and Biochemistry 60:501–502. doi: 10.1271/bbb.60.501

Nagel BM, Bechtold M, Rodriguez LG and Bogdan S (2017) Drosophila WASH is required for integrin-mediated cell adhesion, cell motility and lysosomal neutralization. J Cell Sci 130:344–359. doi: 10.1242/jcs.193086

Nakagawa Y, Satoh A, Tezuka H, Han S, Takei K, Iwasaki H, Yatoh S, Yahagi N, Suzuki H, Iwasaki Y et al. (2016) CREB3L3 controls fatty acid oxidation and ketogenesis in synergy with PPARα. Scientific Reports 6:39182. doi: 10.1038/srep39182

Nakai N, Kitai S, Iida N, Inoue S, Nakata K, Murakami T and Higashida K (2020) Induction of Autophagy and Changes in Cellular Metabolism in Glucose Starved C2C12 Myotubes. J Nutr Sci Vitaminol 66:41–47. doi: 10.3177/jnsv.66.41

Nath S, Dancourt J, Shteyn V, Puente G, Fong WM, Nag S, Bewersdorf J, Yamamoto A, Antonny B and Melia. TJ (2014) Lipidation of the LC3/GABARAP family of autophagy proteins relies upon a membrane curvature-sensing domain in Atg3. Nat Cell Biol 16:415–424. doi: 10.1038/ncb2940

Nesvizhskii AI and Aebersold R (2005) Interpretation of Shotgun Proteomic Data: The Protein Inference Problem. Molecular & Cellular Proteomics 4:1419–1440. doi: 10.1074/mcp.R500012-MCP200

Newman JC and Verdin E (2017) β-Hydroxybutyrate. Annu Rev Nutr 37:51–76. doi: 10.1146/annurev-nutr-071816-064916

Newman JC and Verdin E (2014) Ketone bodies as signaling metabolites. Trends in Endocrinology & Metabolism 25:42–52. doi: 10.1016/j.tem.2013.09.002

Nguyen TN, Padman BS, Usher J, Oorschot V, Ramm G and Lazarou M (2016) Atg8 family LC3/GABARAP proteins are crucial for autophagosome–lysosome fusion but not autophagosome formation during PINK1/Parkin mitophagy and starvation. J Cell Biol 215:857–874. doi: 10.1083/jcb.201607039

Nicholson JK, Lindon JC and Holmes E (1999) “Metabonomics”: understanding the metabolic responses of living systems to pathophysiological stimuli via multivariate statistical analysis of biological NMR spectroscopic data. Xenobiotica 29:1181–1189. doi: 10.1080/004982599238047

Nordlie RC, Foster JD and Lange AJ (1999) Regulation of Glucose Production by the Liver. Annual Review of Nutrition 19:379–406. doi: 10.1146/annurev.nutr.19.1.379

Novikoff AB, Beaufay H and de Duve C (1956) ELECTRON MICROSCOPY OF LYSOSOME-RICH FRACTIONS FROM RAT LIVER. J Biophys Biochem Cytol 2:179–184.

Nowosad A, Jeannot P, Callot C, Creff J, Perchey RT, Joffre C, Codogno P, Manenti S and Besson A (2020) p27 regulates the autophagy-lysosomal pathway via the control of Ragulator and mTOR activity in amino acid deprived cells. bioRxiv 2020.01.07.896860. doi: 10.1101/2020.01.07.896860

Oliveros JC (2007) VENNY. An interactive tool for comparing lists with Venn diagrams. http://bioinfogp.cnb.csic.es/tools/venny/index.html

Ong S-E, Blagoev B, Kratchmarova I, Kristensen DB, Steen H, Pandey A and Mann M (2002) Stable isotope labeling by amino acids in cell culture, SILAC, as a simple and accurate approach to expression proteomics. Mol Cell Proteomics 1:376–386. doi: 10.1074/mcp.m200025-mcp200

Owen OE, Morgan AP, Kemp HG, Sullivan JM, Herrera MG and Cahill GF (1967) Brain Metabolism during Fasting*. J Clin Invest 46:1589–1595.

Pagano AF, Py G, Bernardi H, Candau RB and Sanchez AMJ (2014) Autophagy and protein turnover signaling in slow-twitch muscle during exercise. Med Sci Sports Exerc 46:1314–1325. doi: 10.1249/MSS.0000000000000237

Pan JW, Telang FW, Lee JH, de Graaf RA, Rothman DL, Stein DT and Hetherington HP (2001) Measurement of beta-hydroxybutyrate in acute hyperketonemia in human brain. J Neurochem 79:539–544. doi: 10.1046/j.1471-4159.2001.00575.x

Panchaud N, Péli-Gulli M-P and Virgilio CD (2013) Amino Acid Deprivation Inhibits TORC1 Through a GTPase-Activating Protein Complex for the Rag Family GTPase Gtr1. Sci Signal 6:ra42–ra42. doi: 10.1126/scisignal.2004112

Panuwet P, Hunter RE, D'Souza PE, Chen X, Radford SA, Cohen JR, Marder ME, Kartavenka K, Ryan PB and Barr DB (2016) Biological Matrix Effects in Quantitative Tandem Mass Spectrometry-Based Analytical Methods: Advancing Biomonitoring. Crit Rev Anal Chem 46:93–105. doi: 10.1080/10408347.2014.980775

Paolini A, Omairi S, Mitchell R, Vaughan D, Matsakas A, Vaiyapuri S, Ricketts T, Rubinsztein DC and Patel K (2018) Attenuation of autophagy impacts on muscle fibre development, starvation induced stress and fibre regeneration following acute injury. Scientific Reports 8:9062. doi: 10.1038/s41598-018-27429-7

Park KK, Liu K, Hu Y, Smith PD, Wang C, Cai B, Xu B, Connolly L, Kramvis I, Sahin M et al. (2008) Promoting Axon Regeneration in the Adult CNS by Modulation of the PTEN/mTOR Pathway. Science 322:963–966. doi: 10.1126/science.1161566

Park S, Oh TS, Kim S and Kim E-K (2019) Palmitate-induced autophagy liberates monounsaturated fatty acids and increases Agrp expression in hypothalamic cells. Animal Cells and Systems 23:384–391. doi: 10.1080/19768354.2019.1696407

Pause A, Belsham GJ, Gingras A-C, Donzé O, Lin T-A, Lawrence JC and Sonenberg N (1994) Insulin-dependent stimulation of protein synthesis by phosphorylation of a regulator of 5'-cap function. Nature 371:762–767. doi: 10.1038/371762a0

Perera RM and Zoncu R (2016) The Lysosome as a Regulatory Hub. Annu Rev Cell Dev Biol 32:223–253. doi: 10.1146/annurev-cellbio-111315-125125

Petersen MC, Vatner DF and Shulman GI (2017) Regulation of hepatic glucose metabolism in health and disease. Nature Reviews Endocrinology 13:572–587. doi: 10.1038/nrendo.2017.80

Peterson RT and Schreiber SL (1998) Translation control: connecting mitogens and the ribosome. Curr Biol 8:R248-250. doi: 10.1016/s0960-9822(98)70152-6

Peterson TR, Sengupta SS, Harris TE, Carmack AE, Kang SA, Balderas E, Guertin DA, Madden KL, Carpenter AE, Finck BN et al. (2011) mTOR Complex 1 Regulates Lipin 1 Localization to Control the SREBP Pathway. Cell 146:408–420. doi: 10.1016/j.cell.2011.06.034

Piehowski PD, Petyuk VA, Orton DJ, Xie F, Moore RJ, Ramirez-Restrepo M, Engel A, Lieberman AP, Albin RL, Camp DG et al. (2013) Sources of Technical Variability in Quantitative LC–MS Proteomics: Human Brain Tissue Sample Analysis. J Proteome Res 12:2128–2137. doi: 10.1021/pr301146m

Pilkis SJ and Claus TH (1991) Hepatic Gluconeogenesis/Glycolysis: Regulation and Structure/Function Relationships of Substrate Cycle Enzymes. Annual Review of Nutrition 11:465–515. doi: 10.1146/annurev.nu.11.070191.002341

Pilkis SJ, El-Maghrabi MR and Claus TH (1988) Hormonal Regulation of Hepatic Gluconeogenesis and Glycolysis. Annual Review of Biochemistry 57:755–783. doi: 10.1146/annurev.bi.57.070188.003543

Pomar CA, Kuda O, Kopecky J, Rombaldova M, Castro H, Picó C, Sánchez J and Palou A (2019) Alterations in plasma acylcarnitine and amino acid profiles may indicate poor nutrition during the suckling period due to maternal intake of an unbalanced diet and may predict later metabolic dysfunction. FASEB J 33:796–807. doi: 10.1096/fj.201800327RR

Pomatto LCD, Raynes R and Davies KJA (2017) The peroxisomal Lon protease LonP2 in aging and disease: functions and comparisons with mitochondrial Lon protease LonP1. Biol Rev Camb Philos Soc 92:739–753. doi: 10.1111/brv.12253

Porstmann T, Santos CR, Griffiths B, Cully M, Wu M, Leevers S, Griffiths JR, Chung Y-L and Schulze A (2008) SREBP activity is regulated by mTORC1 and contributes to Akt-dependent cell growth. Cell Metab 8:224–236. doi: 10.1016/j.cmet.2008.07.007

Prior H, Ewart L, Bright J and Valentin J-P (2012) Refinement of the Charcoal Meal Study by Reduction of the Fasting Period: Alternatives to Laboratory Animals. doi: 10.1177/026119291204000209

Pu J, Guardia CM, Keren-Kaplan T and Bonifacino JS (2016) Mechanisms and functions of lysosome positioning. J Cell Sci 129:4329–4339. doi: 10.1242/jcs.196287

Pu J, Keren-Kaplan T and Bonifacino JS (2017) A Ragulator–BORC interaction controls lysosome positioning in response to amino acid availability. J Cell Biol 216:4183–4197. doi: 10.1083/jcb.201703094

Puchalska P and Crawford PA (2017) Multi-dimensional roles of ketone bodies in fuel metabolism, signaling, and therapeutics. Cell Metab 25:262–284. doi: 10.1016/j.cmet.2016.12.022

Qin X, Jiang B and Zhang Y (2016) 4E-BP1, a multifactor regulated multifunctional protein. Cell Cycle 15:781–786. doi: 10.1080/15384101.2016.1151581

R Core Team (2018) R: A language and environment for statistical computing. R Foundation for Statistical Computing, Vienna, Austria. URL https://www.R-project.org/.

Rambold AS, Kostelecky B, Elia N and Lippincott-Schwartz J (2011) Tubular network formation protects mitochondria from autophagosomal degradation during nutrient starvation. PNAS 108:10190–10195. doi: 10.1073/pnas.1107402108

Ramsay RR, Gandour RD and van der Leij FR (2001) Molecular enzymology of carnitine transfer and transport. Biochim Biophys Acta 1546:21–43. doi: 10.1016/s0167-4838(01)00147-9

Rappsilber J, Mann M and Ishihama Y (2007) Protocol for micro-purification, enrichment, pre-fractionation and storage of peptides for proteomics using StageTips. Nature Protocols 2:1896–1906. doi: 10.1038/nprot.2007.261

Raudvere U, Kolberg L, Kuzmin I, Arak T, Adler P, Peterson H and Vilo J (2019) g:Profiler: a web server for functional enrichment analysis and conversions of gene lists (2019 update). Nucleic Acids Res 47:W191–W198. doi: 10.1093/nar/gkz369

Raz V, Dickson G and ’t Hoen PAC (2017) Dysfunctional transcripts are formed by alternative polyadenylation in OPMD. Oncotarget 8:73516–73528. doi: 10.18632/oncotarget.20640

Redmann M, Benavides GA, Berryhill TF, Wani WY, Ouyang X, Johnson MS, Ravi S, Barnes S, Darley-Usmar VM and Zhang J (2017) Inhibition of autophagy with bafilomycin and chloroquine decreases mitochondrial quality and bioenergetic function in primary neurons. Redox Biology 11:73–81. doi: 10.1016/j.redox.2016.11.004

Riordan JF (1977) The role of metals in enzyme activity. Ann Clin Lab Sci 7:119–129.

Risson V, Mazelin L, Roceri M, Sanchez H, Moncollin V, Corneloup C, Richard-Bulteau H, Vignaud A, Baas D, Defour A et al. (2009) Muscle inactivation of mTOR causes metabolic and dystrophin defects leading to severe myopathy. J Cell Biol 187:859–874. doi: 10.1083/jcb.200903131

Ritchie ME, Phipson B, Wu D, Hu Y, Law CW, Shi W and Smyth GK (2015) limma powers differential expression analyses for RNA-sequencing and microarray studies. Nucleic Acids Res 43:e47. doi: 10.1093/nar/gkv007

Roach PJ, Depaoli-Roach AA, Hurley TD and Tagliabracci VS (2012) Glycogen and its metabolism: some new developments and old themes. Biochem J 441:763–787. doi: 10.1042/BJ20111416

Robinson AM and Williamson DH (1980) Physiological roles of ketone bodies as substrates and signals in mammalian tissues. Physiological Reviews 60:143–187. doi: 10.1152/physrev.1980.60.1.143

Roczniak-Ferguson A, Petit CS, Froehlich F, Qian S, Ky J, Angarola B, Walther TC and Ferguson SM (2012) The Transcription Factor TFEB Links mTORC1 Signaling to Transcriptional Control of Lysosome Homeostasis. Sci Signal 5:ra42–ra42. doi: 10.1126/scisignal.2002790

Rodríguez JC, Gil-Gómez G, Hegardt FG and Haro D (1994) Peroxisome proliferator-activated receptor mediates induction of the mitochondrial 3-hydroxy-3-methylglutaryl-CoA synthase gene by fatty acids. J Biol Chem 269:18767–18772.

Rojas-Morales P, Tapia E and Pedraza-Chaverri J (2016) β-Hydroxybutyrate: A signaling metabolite in starvation response? Cell Signal 28:917–923. doi: 10.1016/j.cellsig.2016.04.005

Rong Y, McPhee CK, Deng S, Huang L, Chen L, Liu M, Tracy K, Baehrecke EH, Yu L and Lenardo MJ (2011) Spinster is required for autophagic lysosome reformation and mTOR reactivation following starvation. PNAS 108:7826–7831. doi: 10.1073/pnas.1013800108

Rui L (2014) Energy Metabolism in the Liver. Compr Physiol 4:177–197. doi: 10.1002/cphy.c130024

Ruivo R, Anne C, Sagné C and Gasnier B (2009) Molecular and cellular basis of lysosomal transmembrane protein dysfunction. Biochimica et Biophysica Acta (BBA) - Molecular Cell Research 1793:636–649. doi: 10.1016/j.bbamcr.2008.12.008

Saftig P (2005) Lysosomal Membrane Proteins. In: Saftig P (ed) Lysosomes. Springer US, Boston, MA, pp 37–49

Saito K, Araki Y, Kontani K, Nishina H and Katada T (2005) Novel role of the small GTPase Rheb: its implication in endocytic pathway independent of the activation of mammalian target of rapamycin. J Biochem 137:423–430. doi: 10.1093/jb/mvi046

Sakai Y, Oku M, van der Klei IJ and Kiel JAKW (2006) Pexophagy: Autophagic degradation of peroxisomes. Biochimica et Biophysica Acta (BBA) - Molecular Cell Research 1763:1767–1775. doi: 10.1016/j.bbamcr.2006.08.023

Sancak Y, Bar-Peled L, Zoncu R, Markhard AL, Nada S and Sabatini DM (2010) Ragulator-Rag complex targets mTORC1 to the lysosomal surface and is necessary for its activation by amino acids. Cell 141:290–303. doi: 10.1016/j.cell.2010.02.024

Sancak Y, Peterson TR, Shaul YD, Lindquist RA, Thoreen CC, Bar-Peled L and Sabatini DM (2008) The Rag GTPases Bind Raptor and Mediate Amino Acid Signaling to mTORC1. Science 320:1496–1501. doi: 10.1126/science.1157535

Sancak Y, Thoreen CC, Peterson TR, Lindquist RA, Kang SA, Spooner E, Carr SA and Sabatini DM (2007) PRAS40 Is an Insulin-Regulated Inhibitor of the mTORC1 Protein Kinase. Molecular Cell 25:903–915. doi: 10.1016/j.molcel.2007.03.003

Sapir DG and Owen OE (1975) Renal conservation of ketone bodies during starvation. Metab Clin Exp 24:23–33. doi: 10.1016/0026-0495(75)90004-9

Sargent G, van Zutphen T, Shatseva T, Zhang L, Di Giovanni V, Bandsma R and Kim PK (2016) PEX2 is the E3 ubiquitin ligase required for pexophagy during starvation. J Cell Biol 214:677–690. doi: 10.1083/jcb.201511034

Saxton RA and Sabatini DM (2017) mTOR Signaling in Growth, Metabolism, and Disease. Cell 169:361–371. doi: 10.1016/j.cell.2017.03.035

Schauder P, Herbertz L and Langenbeck U (1985) Serum branched chain amino and keto acid response to fasting in humans. Metab Clin Exp 34:58–61. doi: 10.1016/0026-0495(85)90061-7

Schönfeld P and Wojtczak L (2016) Short- and medium-chain fatty acids in energy metabolism: the cellular perspective. J Lipid Res 57:943–954. doi: 10.1194/jlr.R067629

Schooneman MG, Achterkamp N, Argmann CA, Soeters MR and Houten SM (2014) Plasma acylcarnitines inadequately reflect tissue acylcarnitine

metabolism. Biochimica et Biophysica Acta (BBA) - Molecular and Cell Biology of Lipids 1841:987–994. doi: 10.1016/j.bbalip.2014.04.001

Schultz E (2005) A guided discovery approach for learning metabolic pathways. Biochemistry and Molecular Biology Education 33:1–7. doi: 10.1002/bmb.2005.494033010433

Schwake M, Schröder B and Saftig P (2013) Lysosomal Membrane Proteins and Their Central Role in Physiology. Traffic 14:739–748. doi: 10.1111/tra.12056

Seglen PO and Bohley P (1992) Autophagy and other vacuolar protein degradation mechanisms. Experientia 48:158–172. doi: 10.1007/BF01923509

Sengupta S, Peterson TR, Laplante M, Oh S and Sabatini DM (2010a) mTORC1 controls fasting-induced ketogenesis and its modulation by ageing. Nature 468:1100–1104. doi: 10.1038/nature09584

Sengupta S, Peterson TR and Sabatini DM (2010b) Regulation of the mTOR complex 1 pathway by nutrients, growth factors, and stress. Mol Cell 40:310–322. doi: 10.1016/j.molcel.2010.09.026

Settembre C and Ballabio A (2014) Lysosomal Adaptation: How the Lysosome Responds to External Cues. Cold Spring Harb Perspect Biol. doi: 10.1101/cshperspect.a016907

Settembre C, Fraldi A, Medina DL and Ballabio A (2013) Signals for the lysosome: a control center for cellular clearance and energy metabolism. Nat Rev Mol Cell Biol 14:283–296. doi: 10.1038/nrm3565

Settembre C, Zoncu R, Medina DL, Vetrini F, Erdin S, Erdin S, Huynh T, Ferron M, Karsenty G, Vellard MC et al. (2012) A lysosome-to-nucleus signalling mechanism senses and regulates the lysosome via mTOR and TFEB. The EMBO Journal 31:1095–1108. doi: 10.1038/emboj.2012.32

Sharabi K, Tavares CDJ, Rines AK and Puigserver P (2015) Molecular Pathophysiology of Hepatic Glucose Production. Mol Aspects Med 46:21–33. doi: 10.1016/j.mam.2015.09.003

Shaw RJ (2013) GATORs Take a Bite Out of mTOR. Science 340:1056–1057. doi: 10.1126/science.1240315

Shen H-M and Mizushima N (2014) At the end of the autophagic road: an emerging understanding of lysosomal functions in autophagy. Trends in Biochemical Sciences 39:61–71. doi: 10.1016/j.tibs.2013.12.001

Shi L and Tu BP (2015) Acetyl-CoA and the Regulation of Metabolism: Mechanisms and Consequences. Curr Opin Cell Biol 33:125–131. doi: 10.1016/j.ceb.2015.02.003

Shin AC, Fasshauer M, Filatova N, Grundell LA, Zielinski E, Zhou J-Y, Scherer T, Lindtner C, White PJ, Lapworth AL et al. (2014) Brain insulin lowers circulating BCAA levels by inducing hepatic BCAA catabolism. Cell Metab 20:898–909. doi: 10.1016/j.cmet.2014.09.003

Sigloch FC, Knopf JD, Weißer J, Gomez-Auli A, Biniossek ML, Petrera A and Schilling O (2016) Proteomic analysis of silenced cathepsin B expression suggests non-proteolytic cathepsin B functionality. Biochimica et Biophysica Acta (BBA) - Molecular Cell Research 1863:2700–2709. doi: 10.1016/j.bbamcr.2016.08.005

Simpson IA, Dwyer D, Malide D, Moley KH, Travis A and Vannucci SJ (2008) The facilitative glucose transporter GLUT3: 20 years of distinction. Am J Physiol Endocrinol Metab 295:E242–E253. doi: 10.1152/ajpendo.90388.2008

Singh J, Kaade E, Muntel J, Bruderer R, Reiter L, Thelen M and Winter D (2020) Systematic Comparison of Strategies for the Enrichment of Lysosomes by Data Independent Acquisition. J Proteome Res 19:371–381. doi: 10.1021/acs.jproteome.9b00580

Singh R and Cuervo AM (2011) Autophagy in the Cellular Energetic Balance. Cell Metab 13:495–504. doi: 10.1016/j.cmet.2011.04.004

Smith BJ, Martins-de-Souza D and Fioramonte M (2019) A Guide to Mass Spectrometry-Based Quantitative Proteomics. In: Guest PC (ed) Pre-Clinical Models: Techniques and Protocols. Springer, New York, NY, pp 3–39

Soeters MR, Sauerwein HP, Duran M, Wanders RJ, Ackermans MT, Fliers E, Houten SM and Serlie MJ (2009) Muscle acylcarnitines during short-term fasting in lean healthy men. Clin Sci (Lond) 116:585–592. doi: 10.1042/CS20080433

Sokolović M, Sokolović A, Wehkamp D, van Themaat EVL, de Waart DR, Gilhuijs-Pederson LA, Nikolsky Y, van Kampen AH, Hakvoort TB and Lamers WH (2008) The transcriptomic signature of fasting murine liver. BMC Genomics 9:528. doi: 10.1186/1471-2164-9-528

Sokolović M, Wehkamp D, Sokolović A, Vermeulen J, Gilhuijs-Pederson LA, van Haaften RI, Nikolsky Y, Evelo CT, van Kampen AH, Hakvoort TB et al. (2007) Fasting induces a biphasic adaptive metabolic response in murine small intestine. BMC Genomics 8:361. doi: 10.1186/1471-2164-8-361

Song S, Attia RR, Connaughton S, Niesen MI, Ness GC, Elam MB, Hori RT, Cook GA and Park EA (2010) Peroxisome proliferator activated receptor α (PPARα) and PPAR gamma coactivator (PGC-1α) induce carnitine palmitoyltransferase IA (CPT-1A) via independent gene elements. Mol Cell Endocrinol 325:54–63. doi: 10.1016/j.mce.2010.05.019

Steinhauser ML, Olenchock BA, O'Keefe J, Lun M, Pierce KA, Lee H, Pantano L, Klibanski A, Shulman GI, Clish CB et al. (2018) The circulating metabolome of human starvation. JCI Insight. doi: 10.1172/jci.insight.121434

Strubelt O, Dost-Kempf E, Siegers C-P, Younes M, Völpel M, Preuss U and Dreckmann JG (1981) The influence of fasting on the susceptibility of mice to hepatotoxic injury. Toxicology and Applied Pharmacology 60:66–77. doi: 10.1016/0041-008X(81)90136-8

Stumvoll M, Perriello G, Meyer C and Gerich J (1999) Role of glutamine in human carbohydrate metabolism in kidney and other tissues. Kidney Int 55:778–792. doi: 10.1046/j.1523-1755.1999.055003778.x

Su M-Y, Morris KL, Kim DJ, Fu Y, Lawrence R, Stjepanovic G, Zoncu R and Hurley JH (2017) Hybrid Structure of the RagA/C-Ragulator mTORC1 Activation Complex. Molecular Cell 68:835-846.e3. doi: 10.1016/j.molcel.2017.10.016

Symons LJ and Jonas AJ (1987) Isolation of highly purified rat liver lysosomal membranes using two Percoll gradients. Anal Biochem 164:382–390. doi: 10.1016/0003-2697(87)90508-2

Tan HWS, Sim AYL and Long YC (2017) Glutamine metabolism regulates autophagy-dependent mTORC1 reactivation during amino acid starvation. Nature Communications 8:1–10. doi: 10.1038/s41467-017-00369-y

Tanaka K (2009) The proteasome: Overview of structure and functions. Proc Jpn Acad Ser B Phys Biol Sci 85:12–36. doi: 10.2183/pjab.85.12

Tanaka K, Waki H, Ido Y, Akita S, Yoshida Y, Yoshida T and Matsuo T (1988) Protein and polymer analyses up to m/z 100 000 by laser ionization time-of-flight mass spectrometry. Rapid Communications in Mass Spectrometry 2:151–153. doi: 10.1002/rcm.1290020802

Tang G, Gudsnuk K, Kuo S-H, Cotrina ML, Rosoklija G, Sosunov A, Sonders MS, Kanter E, Castagna C, Yamamoto A et al. (2014) Loss of mTOR-Dependent Macroautophagy Causes Autistic-like Synaptic Pruning Deficits. Neuron 83:1131–1143. doi: 10.1016/j.neuron.2014.07.040

Tanida I, Minematsu-Ikeguchi N, Ueno T and Kominami E (2005) Lysosomal turnover, but not a cellular level, of endogenous LC3 is a marker for autophagy. Autophagy 1:84–91. doi: 10.4161/auto.1.2.1697

Tebani A, Mauhin W, Abily-Donval L, Lesueur C, Berger MG, Nadjar Y, Berger J, Benveniste O, Lamari F, Laforêt P et al. (2020) A Proteomics-Based Analysis Reveals Predictive Biological Patterns in Fabry Disease. Journal of Clinical Medicine 9:1325. doi: 10.3390/jcm9051325

Thelen M, Winter D, Braulke T and Gieselmann V (2017) SILAC-Based Comparative Proteomic Analysis of Lysosomes from Mammalian Cells Using LC-MS/MS. In: Öllinger K and Appelqvist H (eds) Lysosomes: Methods and Protocols. Springer, New York, NY, pp 1–18

Thompson A, Schäfer J, Kuhn K, Kienle S, Schwarz J, Schmidt G, Neumann T and Hamon C (2003) Tandem Mass Tags: A Novel Quantification Strategy for Comparative Analysis of Complex Protein Mixtures by MS/MS. Anal Chem 75:1895–1904. doi: 10.1021/ac0262560

Todkar K, Ilamathi HS and Germain M (2017) Mitochondria and Lysosomes: Discovering Bonds. Front Cell Dev Biol. doi: 10.3389/fcell.2017.00106

Tom A and Nair KS (2006) Assessment of Branched-Chain Amino Acid Status and Potential for Biomarkers. J Nutr 136:324S-330S. doi: 10.1093/jn/136.1.324S

Tondera D, Grandemange S, Jourdain A, Karbowski M, Mattenberger Y, Herzig S, Da Cruz S, Clerc P, Raschke I, Merkwirth C et al. (2009) SLP-2 is required for stress-induced mitochondrial hyperfusion. The EMBO Journal 28:1589–1600. doi: 10.1038/emboj.2009.89

Torchon E, Ray R, Hulver MW, McMillan RP and Voy BH (2016) Fasting rapidly increases fatty acid oxidation in white adipose tissue of young broiler chickens. Adipocyte 6:33–39. doi: 10.1080/21623945.2016.1263777

Towbin H, Staehelin T and Gordon J (1979) Electrophoretic transfer of proteins from polyacrylamide gels to nitrocellulose sheets: procedure and some applications. Proc Natl Acad Sci U S A 76:4350–4354.

Tsun Z-Y, Bar-Peled L, Chantranupong L, Zoncu R, Wang T, Kim C, Spooner E and Sabatini DM (2013) The folliculin tumor suppressor is a GAP for the RagC/D

GTPases that signal amino acid levels to mTORC1. Mol Cell 52:495–505. doi: 10.1016/j.molcel.2013.09.016

Tsuneki H, Sugihara Y, Honda R, Wada T, Sasaoka T and Kimura I (2002) Reduction of blood glucose level by orexins in fasting normal and streptozotocin-diabetic mice. European Journal of Pharmacology 448:245–252. doi: 10.1016/S0014-2999(02)01936-2

Unger RH, Eisentraut AM and Madison LL (1963) THE EFFECTS OF TOTAL STARVATION UPON THE LEVELS OF CIRCULATING GLUCAGON AND INSULIN IN MAN. J Clin Invest 42:1031–1039. doi: 10.1172/JCI104788

van Vlies N, Ferdinandusse S, Turkenburg M, Wanders RJA and Vaz FM (2007) PPAR alpha-activation results in enhanced carnitine biosynthesis and OCTN2-mediated hepatic carnitine accumulation. Biochim Biophys Acta 1767:1134–1142. doi: 10.1016/j.bbabio.2007.07.001

Vandoorne T, De Smet S, Ramaekers M, Van Thienen R, De Bock K, Clarke K and Hespel P (2017) Intake of a Ketone Ester Drink during Recovery from Exercise Promotes mTORC1 Signaling but Not Glycogen Resynthesis in Human Muscle. Front Physiol. doi: 10.3389/fphys.2017.00310

Varshavsky A (2011) The N-end rule pathway and regulation by proteolysis. Protein Sci 20:1298–1345. doi: 10.1002/pro.666

Varshavsky A (2012) The ubiquitin system, an immense realm. Annu Rev Biochem 81:167–176. doi: 10.1146/annurev-biochem-051910-094049

Vilà-Brau A, De Sousa-Coelho AL, Mayordomo C, Haro D and Marrero PF (2011) Human HMGCS2 regulates mitochondrial fatty acid oxidation and FGF21 expression in HepG2 cell line. J Biol Chem 286:20423–20430. doi: 10.1074/jbc.M111.235044

Violante S, Ijlst L, Te Brinke H, Tavares de Almeida I, Wanders RJA, Ventura FV and Houten SM (2013) Carnitine palmitoyltransferase 2 and carnitine/acylcarnitine translocase are involved in the mitochondrial synthesis and export of acylcarnitines. FASEB J 27:2039–2044. doi: 10.1096/fj.12-216689

von Morze C, Chang G-Y, Larson PEZ, Shang H, Allu PKR, Bok RA, Crane JC, Olson MP, Tan CT, Marco-Rius I et al. (2017) Detection of Localized Changes in the Metabolism of Hyperpolarized Gluconeogenic Precursors 13C-Lactate and 13C-Pyruvate in Kidney and Liver. Magn Reson Med 77:1429–1437. doi: 10.1002/mrm.26245

Vr Y and Hn M (1978) Ntau-methylhistidine (3-methylhistidine) and muscle protein turnover: an overview. Fed Proc 37:2291–2300.

Waite KA, Mota-Peynado AD-L, Vontz G and Roelofs J (2016) Starvation Induces Proteasome Autophagy with Different Pathways for Core and Regulatory Particles. J Biol Chem 291:3239–3253. doi: 10.1074/jbc.M115.699124

Walker MW and Lloyd-Evans E (2015) A rapid method for the preparation of ultrapure, functional lysosomes using functionalized superparamagnetic iron oxide nanoparticles. Methods Cell Biol 126:21–43. doi: 10.1016/bs.mcb.2014.10.019

Wang F, Gómez-Sintes R and Boya P (2018) Lysosomal membrane permeabilization and cell death. Traffic 19:918–931. doi: 10.1111/tra.12613

Wang S, Tsun Z-Y, Wolfson RL, Shen K, Wyant GA, Plovanich ME, Yuan ED, Jones TD, Chantranupong L, Comb W et al. (2015) Lysosomal amino acid transporter SLC38A9 signals arginine sufficiency to mTORC1. Science 347:188–194. doi: 10.1126/science.1257132

Warwick RO, Smith MP, Graffy MA and Lage GL (1985) Altered distribution and toxicity of digitoxigenin in fasted mice. Life Sci 37:775–782. doi: 10.1016/0024-3205(85)90548-x

Watford M (2015) Starvation: Metabolic Changes. eLS. American Cancer Society, pp 1–7

Wattiaux R, Wattiaux-De Coninck S, Ronveaux-dupal MF and Dubois F (1978) Isolation of rat liver lysosomes by isopycnic centrifugation in a metrizamide gradient. J Cell Biol 78:349–368. doi: 10.1083/jcb.78.2.349

Wattiaux R, Wibo M and Baudhuin P (1963) [Effect of the injection of Triton WR 1339 on the hepatic lysosomes of the rat.]. Arch Int Physiol Biochim 71:140–142.

Wickham H (2016) ggplot2: Elegant Graphics for Data Analysis. Springer-book, New York.

Wiese S, Reidegeld KA, Meyer HE and Warscheid B (2007) Protein labeling by iTRAQ: A new tool for quantitative mass spectrometry in proteome research. PROTEOMICS 7:340–350. doi: 10.1002/pmic.200600422

Williams TD, Chambers JB, Henderson RP, Rashotte ME and Overton JM (2002) Cardiovascular responses to caloric restriction and thermoneutrality in C57BL/6J mice. American Journal of Physiology-Regulatory, Integrative and Comparative Physiology 282:R1459–R1467. doi: 10.1152/ajpregu.00612.2001

Wolfgang MJ (2020) Local and systemic actions of hepatic fatty acid oxidation. The FASEB Journal 34:1–1. doi: 10.1096/fasebj.2020.34.s1.00211

Wolfson RL, Chantranupong L, Wyant GA, Gu X, Orozco JM, Shen K, Condon KJ, Petri S, Kedir J, Scaria SM et al. (2017) KICSTOR recruits GATOR1 to the lysosome and is necessary for nutrients to regulate mTORC1. Nature 543:438–442. doi: 10.1038/nature21423

Wolfson RL and Sabatini DM (2017) The dawn of the age of amino acid sensors for the mTORC1 pathway. Cell Metab 26:301–309. doi: 10.1016/j.cmet.2017.07.001

Wong YC, Kim S, Peng W and Krainc D (2019) Regulation and Function of Mitochondria–Lysosome Membrane Contact Sites in Cellular Homeostasis. Trends in Cell Biology 29:500–513. doi: 10.1016/j.tcb.2019.02.004

Woods SC and Ramsay DS (2011) Food Intake, Metabolism and Homeostasis. Physiol Behav 104:4–7. doi: 10.1016/j.physbeh.2011.04.026

Wu Y, Wu M, He G, Zhang X, Li W, Gao Y, Li Z, Wang Z and Zhang C (2012) Glyceraldehyde-3-phosphate dehydrogenase: A universal internal control for Western blots in prokaryotic and eukaryotic cells. Analytical Biochemistry 423:15–22. doi: 10.1016/j.ab.2012.01.012

Wyant GA, Abu-Remaileh M, Frenkel EM, Laqtom NN, Dharamdasani V, Lewis CA, Chan SH, Heinze I, Ori A and Sabatini DM (2018) NUFIP1 is a ribosome

receptor for starvation-induced ribophagy. Science 360:751–758. doi: 10.1126/science.aar2663

Xia P, Wang S, Du Y, Zhao Z, Shi L, Sun L, Huang G, Ye B, Li C, Dai Z et al. (2013) WASH inhibits autophagy through suppression of Beclin 1 ubiquitination. The EMBO Journal 32:2685–2696. doi: 10.1038/emboj.2013.189

Xiong J (2018) Fatty Acid Oxidation in Cell Fate Determination. Trends in Biochemical Sciences 43:854–857. doi: 10.1016/j.tibs.2018.04.006

Yamamoto J, Kamata S, Miura A, Nagata T, Kainuma R and Ishii I (2015) Differential adaptive responses to 1- or 2-day fasting in various mouse tissues revealed by quantitative PCR analysis. FEBS Open Bio 5:357–368. doi: 10.1016/j.fob.2015.04.012

Yim WW-Y and Mizushima N (2020) Lysosome biology in autophagy. Cell Discovery 6:1–12. doi: 10.1038/s41421-020-0141-7

Yoshii SR and Mizushima N (2017) Monitoring and Measuring Autophagy. Int J Mol Sci. doi: 10.3390/ijms18091865

Yoshimori T, Yamamoto A, Moriyama Y, Futai M and Tashiro Y (1991) Bafilomycin A1, a specific inhibitor of vacuolar-type H(+)-ATPase, inhibits acidification and protein degradation in lysosomes of cultured cells. J Biol Chem 266:17707–17712.

Yoshizawa F, Nagasawa T, Nishizawa N and Funabiki R (1997) Protein Synthesis and Degradation Change Rapidly in Response to Food Intake in Muscle of Food-Deprived Mice. J Nutr 127:1156–1159. doi: 10.1093/jn/127.6.1156

Yu L, Chen Y and Tooze SA (2017) Autophagy pathway: Cellular and molecular mechanisms. Autophagy 14:207–215. doi: 10.1080/15548627.2017.1378838

Yu L, McPhee CK, Zheng L, Mardones GA, Rong Y, Peng J, Mi N, Zhao Y, Liu Z, Wan F et al. (2010) Termination of autophagy and reformation of lysosomes regulated by mTOR. Nature 465:942–946. doi: 10.1038/nature09076

Zhang Y, Fonslow BR, Shan B, Baek M-C and Yates JR (2013) Protein analysis by shotgun/bottom-up proteomics. Chem Rev 113:2343–2394. doi: 10.1021/cr3003533

Zhao J and Goldberg AL (2016) Coordinate regulation of autophagy and the ubiquitin proteasome system by MTOR. Autophagy 12:1967–1970. doi: 10.1080/15548627.2016.1205770

Zhenyukh O, Civantos E, Ruiz-Ortega M, Sánchez MS, Vázquez C, Peiró C, Egido J and Mas S (2017) High concentration of branched-chain amino acids promotes oxidative stress, inflammation and migration of human peripheral blood mononuclear cells via mTORC1 activation. Free Radic Biol Med 104:165–177. doi: 10.1016/j.freeradbiomed.2017.01.009

Zoncu R, Bar-Peled L, Efeyan A, Wang S, Sancak Y and Sabatini DM (2011) mTORC1 senses lysosomal amino acids through an inside-out mechanism that requires the vacuolar H(+)-ATPase. Science 334:678–683. doi: 10.1126/science.1207056

8 Appendix

8.1 Metabolic analysis (Acylcarnitines and amino acids)

Supplementary table 8.1: List of serum acylcarnitine and amino acid concentrations

6-month-old male wild-type mice were starved for 6 or 24 hours and control mice were fed *ad libitum* before sacrifice. Blood serum was collected from each group and the average concentrations (µmol/l) of acylcarnitines and amino acids were measured using ESI-MS/MS and LC-MS/MS, respectively. Shown are mean + SEM (N/A: not available).

Acylcarnitine (µmol/l)	**Fed *ad libitum***	**6 hours starvation**	**24 hours starvation**
3OH-butyryl (C4OH)	0.458 + 0.094	0.502 + 0.095	0.397 + 0.060
3OH-hexadecenoyl (C16:1OH)	0.013 + 0.002	0.011 + 0.001	0.063 + 0.007
3OH-isovaleryl (C5OH)	0.156 + 0.031	0.17 + 0.022	0.1 + 0.017
3OH-linoleoyl (C18:2OH)	0.014 + 0.002	0.01 + 0.001	0.06 + 0.012
3OH-oleoyl (C18:1OH)	0.012 + 0.002	0.011 + 0.002	0.083 + 0.019
3OH-palmitoyl (C16OH)	0.01 + 0.001	0.012 + 0.002	0.039 + 0.006
3OH-stearoyl (C18OH)	0.015 + 0.003	0.01 + 0.002	0.044 + 0.010
3OH-tetradecanoyl (C14OH)	0.01 + 0.001	0.01 + 0.002	0.016 + 0.003
Acetyl (C2)	24.616 + 1.936	29.287 + 2.727	17.4 + 1.649
Butyryl (C4)	2.629 + 0.404	2.139 + 0.818	0.699 + 0.099
Free carnitine (C0)	24.391 + 2.609	25.787 + 2.151	13.43 + 1.483
Decenoyl (C10:1)	0.02 + 0.004	0.022 + 0.003	0.036 + 0.005
Decanoyl (C10)	0.016 + 0.003	0.026 + 0.005	0.030 + 0.004
Dodecanoyl (C12)	0.039 + 0.004	0.036 + 0.006	0.08 + 0.011
Glutaryl (C5DC)	0.08 + 0.021	0.061 + 0.010	0.232 + 0.077
Hexanoyl (C6)	0.296 + 0.060	0.311 + 0.146	0.079 + 0.011
Isovaleryl (C5)	0.200 + 0.028	0.162 + 0.020	0.092 + 0.011
Malonyl (C3DC)	0.180 + 0.038	0.172 + 0.021	0.205 + 0.025
Methylmalonyl (C4DC)	21.012 + 9.053	0.175 + 0.026	12.93 + 5.489
Octadecanoyl (C18)	0.076 + 0.016	0.045 + 0.008	0.659 + 0.138
Octanoyl (C8)	0.028 + 0.005	0.034 + 0.010	0.032 + 0.005
Octenoyl (C8:1)	0.013 + 0.002	0.015 + 0.004	0.014 + 0.002
Oleoyl (C18:1)	0.166 + 0.024	0.215 + 0.024	1.241 + 0.199
Palmitoleyl (C16:1)	0.058 + 0.009	0.081 + 0.012	0.192 + 0.026
Palmitoyl (C16)	0.274 + 0.036	0.303 + 0.030	0.935 + 0.107
Propionyl (C3)	1.043 + 0.146	0.789 + 0.131	0.531 + 0.085
Tetradecadienoyl (C14:2)	0.019 + 0.003	0.025 + 0.004	0.065 + 0.011
Tetradecanoyl (C14)	0.048 + 0.006	0.072 + 0.013	0.178 + 0.024
Tetradecenoyl (C14:1)	0.039 + 0.005	0.067 + 0.010	0.163 + 0.019
Tiglyl (C5:1)	0.015 + 0.001	0.012 + 0.001	0.015 + 0.003
Amino acid (µmol/l)	**Fed *ad libitum***	**6 hours starvation**	**24 hours starvation**
1-Methylhistidine	3.04 + 0.361	3.4 + 0.624	3.925 + 0.360
3-Methylhistidine	3.5 + 0.539	4.437 + 0.481	9.2 + 0.922

2-Aminoadipic acid	10.7 + 1.182	8.437 + 0.838	53.983 + 11.513
2-Aminobutyric acid	4.95 + 0.406	4.687 + 0.371	19.333 + 1.967
Alanine	449.416 + 42.844	392.25 + 37.535	290.333 + 37.341
Arginine	85.95 + 17.203	61.3 + 14.776	90.441 + 20.937
Asparagine	42.941 + 2.185	43.812 + 8.334	44.908 + 3.219
Aspartic acid	44.558 + 6.168	51.975 + 7.778	52.667 + 8.875
β-Alanine	6.208 + 0.593	6.737 + 0.357	6.472 + 1.028
Carnosine	8.158 + 2.277	6.875 + 1.262	5.808 + 1.258
Citrulline	66.717 + 5.490	58.875 + 8.054	66.433 + 6.835
Cystathionine	2.2 + 0.290	2.7 + 0.452	3.95 + 0.682
Cystine	3.111 + 0.497	2.933 + 0.549	7.65 + 2.297
Ethanolamine	32.933 + 3.288	36.575 + 2.547	34.458 + 3.312
γ-Aminobutyric acid	3.05 + 0.355	2.22 + 0.412	2.775 + 0.417
Glutamine	800.333 + 31.155	815.25 + 38.856	747.833 + 33.645
Glutamic acid	161.767 + 30.537	136.237 + 15.962	135.981 + 25.852
Glycine	373.25 + 31.289	448.375 + 56.430	305.333 + 26.087
Histidine	66.058 + 3.477	70.587 + 11.431	72.133 + 7.627
Hydroxylysine	N/A	N/A	4.033 + 0.633
Hydroxyproline	11.525 + 1.122	11.925 + 0.950	6.763 + 1.112
Isoleucine	94.625 + 6.113	84.225 + 6.364	133.55 + 10.100
Leucine	146.875 + 9.790	145 + 10.587	277.5 + 35.543
Lysine	251.917 + 10.157	220.125 + 9.709	229 + 24.614
Methionine	31.672 + 10.148	42.275 + 2.083	24.02 + 7.752
Ornithine	145.95 + 19.251	221.587 + 75.418	133.45 + 17.177
Phenylalanine	92.65 + 3.772	89.75 + 5.495	110.35 + 6.288
Phosphoethanolamine	18.617 + 6.845	18.925 + 2.878	21.675 + 4.534
Proline	113.108 + 8.277	81.337 + 11.368	77.217 + 4.792
Sarcosine	3.488 + 0.515	3.317 + 0.598	2.487 + 0.372
Serine	116.5 + 9.930	178.25 + 74.115	106.675 + 7.463
Taurine	1172.833 + 100.879	996.875 + 58.236	1423.833 + 144.397
Threonine	131.1 + 7.080	131.925 + 16.505	140 + 7.566
Tryptophan	80.673 + 8.226	81.725 + 7.217	62.383 + 6.618
Tyrosine	95.137 + 3.706	79 + 8.076	68.587 + 9.638
Valine	243.25 + 12.185	211.75 + 9.842	361.875 + 43.413

8.2 Proteomics

Supplementary table 8.2: List of 233 lysosomal annotated proteins in lysosome-enriched fractions from control, 6 and 24 hours starved mice according to the protein center database in Proteome Discoverer 2.3

Uniprot ID	Gene	Uniprot ID	Gene	Uniprot ID	Gene
P41234	Abca2	P54818	Galc	Q62086	Pon2
Q8R4P9	Abcc10	Q571E4	Galns	O88531	Ppt1
P09470	Ace	P17439	Gba	O35448	Ppt2
Q05117	Acp5	Q9DBL2	Gdap2	Q7TMR0	Prcp

Q64191	Aga	Q9Z0L8	Ggh	O08709	Prdx6
P45376	Akr1b1	Q8BWF2	Gimap5	Q61207	Psap
Q91Y97	Aldob	P51569	Gla	P49769	Psen1
Q810B6	Ankfy1	P23780	Glb1	Q61144	Psen2
Q3UMR0	Ankrd27	Q60648	Gm2a	Q91V41	Rab14
P97449	Anpep	P21278	Gna11	P53994	Rab2a
Q9Z1T1	Ap3b1	P21279	Gnaq	P35278	Rab5c
O54774	Ap3d1	P62874	Gnb1	P51150	Rab7a
Q9JKC8	Ap3m1	P62880	Gnb2	Q9R0M6	Rab9a
P08226	Apoe	Q8BFR4	Gns	Q9ERI6	Rdh14
Q8VEH3	Arl8a	O70362	Gpld1	Q8VC42	Rmc1
Q9CQW2	Arl8b	P28798	Grn	C0HKG5	Rnaset2a
P50428	Arsa	P12265	Gusb	O54965	Rnf13
P50429	Arsb	P14438	H2-Aa	Q80X95	Rraga
Q3TYD4	Arsg	P29416	Hexa	Q99K70	Rragc
Q9WV54	Asah1	P20060	Hexb	Q61009	Scarb1
P16460	Ass1	Q3UDW8	Hgsnat	O35114	Scarb2
P98197	Atp11a	Q6YGZ1	Hpse	Q8R2U0	Seh1l
Q9QZW0	Atp11c	Q9ESB3	Hrg	P70665	Siae
Q9CTG6	Atp13a2	P11499	Hsp90ab1	Q8CIF6	Sidt2
P15920	Atp6v0a2	P63017	Hspa8	P49282	Slc11a2
P51863	Atp6v0d1	P48441	Idua	Q9JIS8	Slc12a4
Q80SY3	Atp6v0d2	Q9ESY9	Ifi30	Q8BPX9	Slc15a3
P50516	Atp6v1a	Q9CQW9	Ifitm3	Q8BN82	Slc17a5
P62814	Atp6v1b2	Q07113	Igf2r	Q80ZD3	Slc26a11
Q9Z1G3	Atp6v1c1	O09046	Il4i1	Q9JIF3	Slc2a8
P57746	Atp6v1d	Q60766	Irgm1	Q8VE96	Slc35f6
P50518	Atp6v1e1	Q80XH1	Kxd1	Q8BGD6	Slc38a9
Q9CR51	Atp6v1g1	P11438	Lamp1	Q9D8M3	Slc48a1
Q8BVE3	Atp6v1h	P17047	Lamp2	Q04519	Smpd1
O55102	Bloc1s1	Q9CQ22	Lamtor1	O09044	Snap23
Q9CWG9	Bloc1s2	Q9JHS3	Lamtor2	Q9Z266	Snapin
Q9D920	Borcs5	O88653	Lamtor3	Q9WV80	Snx1
Q9D6W8	Borcs6	Q9D1L9	Lamtor5	Q9CWK8	Snx2
Q9CRC6	Borcs7	P35951	Ldlr	Q6P8X1	Snx6
Q9D6Y4	Borcs8	O89017	Lgmn	Q3UHA3	Spg11
P24270	Cat	Q9Z0M5	Lipa	Q8R0G7	Spns1
Q8C1Y8	Ccz1	Q8K0B2	Lmbrd1	Q9JJF9	Sppl2a
P11609	Cd1d1	Q8C129	Lnpep	Q61542	Stard3
P31996	Cd68	Q91ZX7	Lrp1	Q9DCI3	Stard3nl
P04441	Cd74	P25911	Lyn	Q3TAA7	Stk11ip
O70496	Clcn7	P24668	M6pr	O70439	Stx7
Q3UMW8	Cln5	O09159	Man2b1	O88983	Stx8
Q68FD5	Cltc	O54782	Man2b2	Q64324	Stxbp2
Q61147	Cp	Q8K2I4	Manba	A2A9C3	Szt2
Q9WVJ3	Cpq	Q99J21	Mcoln1	Q99MB1	Tlr3
P21460	Cst3	Q8BH31	Mfsd8	P58681	Tlr7
Q8R242	Ctbs	Q8VE19	Mios	Q9EQU3	Tlr9
P16675	Ctsa	P11247	Mpo	Q9DBU0	Tm9sf1
P10605	Ctsb	P27573	Mpz	Q80X71	Tmem106b
P97821	Ctsc	Q9JLN9	Mtor	P52875	Tmem165

P18242	Ctsd	Q9D7V9	Naaa	Q9CXT7	Tmem192
Q9R013	Ctsf	Q9QWR8	Naga	Q9QY73	Tmem59
P49935	Ctsh	Q9CWZ7	Napg	Q91YT8	Tmem63a
P55097	Ctsk	O09043	Napsa	Q9EQJ0	Tpcn1
P06797	Ctsl	P57716	Ncstn	O89023	Tpp1
Q8BM88	Ctso	O35657	Neu1	Q02053	Uba1
O70370	Ctss	O35604	Npc1	P70280	Vamp7
Q9WUU7	Ctsz	Q9Z0J0	Npc2	O70404	Vamp8
Q91WC9	Daglb	Q9WUE4	Nprl2	Q91W86	Vps11
P61460	Depdc5	Q8VIJ8	Nprl3	Q920Q4	Vps16
P60904	Dnajc5	P46460	Nsf	Q8R307	Vps18
P56542	Dnase2	Q8BGT0	Ostm1	P40336	Vps26a
P28843	Dpp4	Q9JJX6	P2rx4	Q9D2N9	Vps33a
Q9ET22	Dpp7	Q80W65	Pcsk9	Q9EQH3	Vps35
Q9CR48	Dram2	Q9CQF9	Pcyox1	Q8R5L3	Vps39
Q4PZA2	Ece1	Q2TBE6	Pi4k2a	Q5KU39	Vps41
P16406	Enpep	Q8CBQ5	Pi4k2b	O88384	Vti1b
O08917	Flot1	Q3TWL2	Pip4p1	Q8CFJ9	Wdr24
P09528	Fth1	Q9CZX7	Pip4p2	Q3UDP0	Wdr41
P29391	Ftl1	Q8VEB4	Pla2g15	Q8C0M0	Wdr59
Q99LJ1	Fuca1	Q8VCI0	Plbd1	Q5ND34	Wdr81
P70699	Gaa	Q3TCN2	Plbd2	Q3UPF5	Zc3hav1
Q9DCD6	Gabarap	Q9Z280	Pld1		

Supplementary table 8.3: Upregulated non-lysosomal proteins upon 6 hours of starvation

List of the 150 upregulated non-lysosomal proteins identified after short-term starvation in the proteomic dataset. Shown are proteins with more than one unique peptide, p-value <0.05 and log_2 fold change ratios >0.75. In addition, the log_2 fold change ratios after 24 hours as well as the log_2 fold change ratios of the difference between 6 and 24 hours of starvation are also shown in the table (#: number of unique peptides, blue: starvation period of interest, green: proteasome complex subunits, yellow: peroxisomal proteins, N/A: not available).

Protein name	Gene name	Log_2FC (6h)	Log_2FC (24h)	Log_2FC (24-6h)	#
Bile acid-CoA:amino acid N-acyltransferase	Baat	2.67	1.25	-1.42	4
Glycogen [starch] synthase, liver	Gys2	2.21	0.52	-1.69	3
Proteasome subunit alpha type-5	Psma5	2.21	1.26	-0.95	4
Proteasome subunit alpha type-1	Psma1	2.12	1.22	-0.90	5
Proteasome subunit beta type-3	Psmb3	2.10	1.33	-0.77	4
Proteasome subunit alpha type-3	Psma3	2.04	1.20	-0.84	10
2-hydroxyacyl-CoA lyase 1	Hacl1	2.03	0.75	-1.28	10
D-dopachrome decarboxylase	Ddt	2.01	1.16	-0.86	4
Proteasome subunit alpha type-2	Psma2	1.96	1.47	-0.49	2
N-acyl-aromatic-L-amino acid amidohydrolase	Acy3	1.95	0.93	-1.03	2
Sorbitol dehydrogenase	Sord	1.95	1.00	-0.95	10
Proteasome subunit beta type-6	Psmb6	1.94	1.33	-0.61	2
Proteasome subunit beta type-5	Psmb5	1.93	1.21	-0.72	4
Acylamino-acid-releasing enzyme	Apeh	1.92	1.21	-0.71	7

Aldehyde oxidase 3	Aox3	1.90	1.01	-0.89	14
Proteasome subunit alpha type-4	Psma4	1.88	1.11	-0.77	4
Delta-aminolevulinic acid dehydratase	Alad	1.87	0.63	-1.24	2
Proteasome subunit alpha type-7	Psma7	1.81	1.05	-0.77	3
NAD(P)H-hydrate epimerase	Naxe	1.75	1.28	-0.47	3
Alanine aminotransferase 1	Gpt	1.74	0.50	-1.24	5
Aldehyde oxidase 3;1	Aox3;Aox1	1.73	0.54	-1.19	2
Aldo-keto reductase family 1 member D1	Akr1d1	1.73	0.86	-0.87	4
Glyceraldehyde-3-phosphate dehydrogenase	Gapdh	1.70	0.98	-0.72	9
Aldehyde oxidase 1	Aox1	1.70	1.04	-0.66	6
Fructose-1,6-bisphosphatase 1	Fbp1	1.68	0.73	-0.95	13
Retinol dehydrogenase 16	Rdh16	1.68	0.78	-0.91	2
Proteasome subunit beta type-7	Psmb7	1.68	0.91	-0.77	2
Hydroxyacid oxidase 1	Hao1	1.67	0.25	-1.42	2
17-beta-hydroxysteroid dehydrogenase type 6; Retinol dehydrogenase 7;16	Hsd17b6;Rdh7;Rdh16	1.67	0.66	-1.01	3
Proteasome subunit beta type-1	Psmb1	1.67	0.82	-0.85	2
Aspartate aminotransferase	Got1	1.66	1.03	-0.63	6
Dihydropyrimidine dehydrogenase [NADP(+)]	Dpyd	1.64	0.43	-1.20	9
Glycogen phosphorylase, liver form	Pygl	1.64	0.85	-0.79	11
Kynurenine--oxoglutarate transaminase 1	Kyat1	1.63	0.63	-1.00	2
Peroxiredoxin-4	Prdx4	1.62	0.92	-0.70	3
Tripeptidyl-peptidase 2	Tpp2	1.62	0.97	-0.65	3
17-beta-hydroxysteroid dehydrogenase type 6	Hsd17b6	1.57	0.77	-0.79	6
Alpha-aminoadipic semialdehyde dehydrogenase	Aldh7a1	1.55	1.06	-0.48	12
Proteasome subunit alpha type-6	Psma6	1.54	0.97	-0.57	4
Glutaredoxin-1	Glrx	1.52	1.09	-0.43	3
Ester hydrolase C11orf54 homolog	N/A	1.51	1.29	-0.22	7
Cytosolic 10-formyltetrahydrofolate dehydrogenase	Aldh1l1	1.50	0.32	-1.19	17
Glutathione reductase, mitochondrial	Gsr	1.49	0.90	-0.59	5
Thioredoxin reductase 1, cytoplasmic	Txnrd1	1.48	1.32	-0.16	4
Carboxylesterase 1F	Ces1f	1.47	0.36	-1.11	9
Carnitine O-octanoyltransferase	Crot	1.47	0.83	-0.64	3
Inositol monophosphatase 1	Impa1	1.47	0.94	-0.54	2
Hypoxanthine-guanine phosphoribosyltransferase	Hprt1	1.45	1.08	-0.38	3
Glutathione S-transferase Mu 2	Gstm2	1.44	0.97	-0.47	2
Peroxisomal coenzyme A diphosphatase NUDT7	Nudt7	1.43	-0.15	-1.59	2
Gephyrin	Gphn	1.43	0.51	-0.92	6
Urocanate hydratase (Urocanase)	Uroc1	1.42	0.81	-0.61	4
Cytochrome P450 2D9	Cyp2d9	1.41	0.43	-0.99	5

Phenazine biosynthesis-like domain-containing protein 1	Pbld1	1.40	1.47	0.07	4
Alanine--tRNA ligase, cytoplasmic	Aars	1.39	0.67	-0.72	4
Phenazine biosynthesis-like domain-containing protein 2	Pbld2	1.38	1.41	0.02	6
Argininosuccinate lyase	Asl	1.37	0.38	-1.00	7
Peroxisomal NADH pyrophosphatase NUDT12	Nudt12	1.37	0.59	-0.78	4
Alpha-methylacyl-CoA racemase	Amacr	1.35	0.39	-0.96	4
4-trimethylaminobutyraldehyde dehydrogenase	Aldh9a1	1.35	0.48	-0.87	6
Glutathione S-transferase P 1	Gstp1	1.35	1.26	-0.10	10
Bleomycin hydrolase	Blmh	1.34	0.87	-0.47	6
Histidine ammonia-lyase	Hal	1.33	0.40	-0.93	10
Ribosyldihydronicotinamide dehydrogenase	Nqo2	1.33	0.75	-0.58	3
Threonine--tRNA ligase 1, cytoplasmic	Tars	1.32	0.65	-0.67	3
Prolyl endopeptidase	Prep	1.32	1.39	0.07	5
60 kDa heat shock protein, mitochondrial	Hspd1	1.30	0.72	-0.58	16
Inosine-5'-monophosphate dehydrogenase 2	Impdh2	1.30	1.03	-0.27	2
Acyl-coenzyme A amino acid N-acyltransferase 1	Acnat1	1.26	0.40	-0.86	4
Cytochrome P450 2D26	Cyp2d26	1.24	0.24	-0.99	7
Carboxymethylenebutenolidase homolog	Cmbl	1.24	0.65	-0.59	2
Glutathione synthetase	Gss	1.24	0.69	-0.56	4
1,4-alpha-glucan-branching enzyme	Gbe1	1.23	0.52	-0.71	2
Peroxisomal trans-2-enoyl-CoA reductase	Pecr	1.21	-0.02	-1.23	5
Bifunctional epoxide hydrolase 2	Ephx2	1.21	0.19	-1.02	8
Epoxide hydrolase 1	Ephx1	1.21	0.85	-0.36	11
Xanthine dehydrogenase/oxidase	Xdh	1.21	0.97	-0.24	11
Regucalcin	Rgn	1.20	0.85	-0.35	6
Cytochrome P450 2C29	Cyp2c29	1.19	0.30	-0.89	10
Peroxisomal 2,4-dienoyl-CoA reductase	Decr2	1.18	-0.08	-1.26	3
Glyoxylate reductase/hydroxypyruvate reductase	Grhpr	1.18	0.57	-0.61	4
Thioredoxin domain-containing protein 17	Txndc17	1.18	0.63	-0.56	2
Retinol dehydrogenase 7;16	Rdh7;Rdh16	1.17	0.64	-0.53	2
Regulator of nonsense transcripts 1	Upf1	1.14	0.31	-0.83	2
ATP-dependent (S)-NAD(P)H-hydrate dehydratase	Naxd	1.12	0.50	-0.62	3

Serine--pyruvate aminotransferase, Mitochondrial	Agxt	1.11	0.30	-0.81	2
Serine--tRNA ligase, cytoplasmic	Sars	1.11	0.74	-0.37	2
Purine nucleoside phosphorylase	Pnp	1.11	0.75	-0.36	2
Tetratricopeptide repeat protein 38	Ttc38	1.10	0.63	-0.47	2
UTP--glucose-1-phosphate uridylyltransferase	Ugp2	1.09	0.63	-0.46	12
Lon protease homolog 2, peroxisomal	Lonp2	1.08	0.02	-1.06	2
DNA damage-binding protein 1	Ddb1	1.08	0.39	-0.69	6
Thioredoxin	Txn	1.08	0.61	-0.48	4
Galactose mutarotase	Galm	1.08	0.67	-0.41	3
Fumarylacetoacetase	Fah	1.07	0.37	-0.70	4
Adenosylhomocysteinase	Ahcy	1.07	0.57	-0.50	9
N-fatty-acyl-amino acid synthase/hydrolase	Pm20d1	1.07	0.69	-0.38	8
GDH/6PGL endoplasmic bifunctional protein	H6pd	1.06	0.44	-0.62	6
Isochorismatase domain-containing protein 1	Isoc1	1.06	0.73	-0.34	3
2-iminobutanoate/2-iminopropanoate deaminase	Rida	1.06	0.84	-0.23	8
Sepiapterin reductase	Spr	1.06	0.85	-0.20	3
Glutathione S-transferase Mu 1;2;3;6;7	Gstm1; Gstm2; Gstm3; Gstm6; Gstm7	1.05	0.55	-0.49	4
2-aminomuconic semialdehyde dehydrogenase	Aldh8a1	1.03	0.27	-0.76	10
Retinol dehydrogenase 7	Rdh7	1.03	0.56	-0.47	5
Cholinesterase	Bche	1.03	0.91	-0.11	3
Cytosol aminopeptidase	Lap3	1.02	0.41	-0.60	7
Isoleucine--tRNA ligase, cytoplasmic	Iars	1.02	0.77	-0.25	2
2,4-dienoyl-CoA reductase, mitochondrial	Decr1	1.01	0.64	-0.38	6
Glutathione S-transferase A4	Gsta4	1.01	0.66	-0.35	4
Formimidoyltransferase-cyclodeaminase	Ftcd	1.00	0.47	-0.53	3
Indolethylamine N-methyltransferase	Inmt	1.00	0.65	-0.35	5
Phenylalanine-4-hydroxylase	Pah	0.99	0.51	-0.47	11
Cytochrome P450 2C70	Cyp2c70	0.98	-0.85	-1.82	7
26S proteasome non-ATPase regulatory subunit 2	Psmd2	0.98	0.62	-0.36	2
Malate dehydrogenase, cytoplasmic	Mdh1	0.98	0.70	-0.28	4
von Willebrand factor A domain-containing protein 8	Vwa8	0.95	0.35	-0.60	4
Estradiol 17 beta-dehydrogenase 5	Akr1c6	0.95	0.37	-0.58	10
Trans-1,2-dihydrobenzene-1,2-diol dehydrogenase	Dhdh	0.95	0.43	-0.52	2

Aldehyde dehydrogenase, cytosolic 1; Aldehyde dehydrogenase, mitochondrial; Retinal dehydrogenase 1; Aldehyde dehydrogenase X, mitochondrial	Aldh1a7;Aldh2;Aldh1a1;Aldh1b1	0.95	0.47	-0.48	2
3-hydroxyisobutyrate dehydrogenase	Hibadh	0.94	0.31	-0.64	7
Agmatinase, mitochondrial	Agmat	0.93	0.26	-0.67	2
Glutathione S-transferase omega-1	Gsto1	0.93	0.65	-0.28	5
Endoplasmic reticulum aminopeptidase 1	Erap1	0.92	0.22	-0.70	7
26S proteasome non-ATPase regulatory subunit 12	Psmd12	0.92	0.61	-0.31	2
Selenium-binding protein 2; Selenium-binding protein 1	Selenbp2;Selenbp1	0.92	1.19	0.27	20
4-hydroxyphenylpyruvate dioxygenase	Hpd	0.91	0.12	-0.79	8
Cytochrome P450 2D10	Cyp2d10	0.91	0.29	-0.62	2
Dihydropteridine reductase	Qdpr	0.91	0.48	-0.44	4
Aldo-keto reductase family 1 member C13	Akr1c13	0.89	0.78	-0.11	3
Ketohexokinase	Khk	0.88	0.33	-0.54	4
Kynureninase	Kynu	0.88	0.34	-0.54	4
T-complex protein 1 subunit theta	Cct8	0.86	0.34	-0.52	7
Carboxylesterase 1D	Ces1d	0.86	0.36	-0.50	9
Alpha-enolase	Eno1	0.86	0.46	-0.40	11
Carboxylesterase 3B	Ces3b	0.85	-0.12	-0.98	2
Phytanoyl-CoA dioxygenase, peroxisomal	Phyh	0.85	0.09	-0.76	3
Nicotinate-nucleotide pyrophosphorylase	Qprt	0.85	0.60	-0.25	2
Retinal dehydrogenase 1	Aldh1a1	0.84	0.47	-0.37	10
Aldehyde dehydrogenase family 3 member A2	Aldh3a2	0.84	0.73	-0.11	9
Glutathione S-transferase Mu 1	Gstm1	0.82	0.31	-0.51	6
Peroxiredoxin-2	Prdx2	0.82	0.54	-0.28	5
Carbonyl reductase [NADPH] 1	Cbr1	0.81	0.53	-0.28	2
Phosphatidylethanolamine-binding protein 1	Pebp1	0.80	0.59	-0.21	2
Eukaryotic translation initiation factor 6	Eif6	0.79	0.11	-0.68	2
Plastin-3	Pls3	0.79	0.45	-0.33	3
Glycerol kinase	Gk	0.78	0.46	-0.32	5
Xylulose kinase	Xylb	0.77	0.47	-0.30	2
Acyl-CoA dehydrogenase family member 11	Acad11	0.76	0.07	-0.69	5
5-oxoprolinase	Oplah	0.76	0.37	-0.39	3
Triokinase/FMN cyclase	Tkfc	0.76	0.38	-0.38	11

Supplementary table 8.4: Downregulated non-lysosomal proteins upon 24 hours of starvation

List of the 121 downregulated non-lysosomal proteins identified after long-term starvation in the proteomic dataset. Shown are proteins with more than one unique peptide, p-value <0.05 and log_2 fold change ratios <-0.75. In addition, the log_2 fold change ratios after 6 hours as well as the log_2 fold change ratios of the difference between 6 and 24 hours of starvation are also shown in the table (#: number of unique peptides, blue: starvation period of interest).

Protein name	Gene name	Log_2FC (6h)	Log_2FC (24h)	Log_2FC (24-6h)	#
WASH complex subunit 5	Washc5	-0.75	-2.14	-1.39	15
WASH complex subunit 4	Washc4	-0.77	-2.01	-1.25	13
COMM domain-containing protein 3	Commd3	-0.63	-1.87	-1.24	3
WASH complex subunit 1	Washc1	-0.49	-1.85	-1.36	3
WASH complex subunit 2	Washc2	-0.64	-1.70	-1.06	2
Zinc finger protein-like 1	Zfpl1	-1.11	-1.69	-0.58	3
COMM domain-containing protein 1	Commd1	-0.35	-1.68	-1.32	2
Growth hormone receptor	Ghr	0.19	-1.66	-1.85	4
Serotransferrin	Tf	-1.20	-1.65	-0.46	19
Vacuolar protein sorting-associated protein 26C	Vps26c	-0.41	-1.65	-1.25	4
COMM domain-containing protein 4	Commd4	-0.39	-1.64	-1.25	5
Angiopoietin-related protein 3	Angptl3	-0.39	-1.60	-1.21	6
COMM domain-containing protein 5	Commd5	-0.36	-1.60	-1.24	7
Lipoprotein lipase	Lpl	-0.38	-1.59	-1.20	4
COMM domain-containing protein 8	Commd8	-0.44	-1.57	-1.13	5
COMM domain-containing protein 9	Commd9	-0.57	-1.55	-0.98	2
Golgi-associated PDZ and coiled-coil motif-containing protein	Gopc	-0.85	-1.53	-0.68	2
COMM domain-containing protein 7	Commd7	-0.30	-1.51	-1.21	2
VPS35 endosomal protein sorting factor-like	Vps35l	-0.27	-1.48	-1.22	9
COMM domain-containing protein 10	Commd 10	-0.43	-1.47	-1.05	3
Coiled-coil domain-containing protein 93	Ccdc93	-0.25	-1.46	-1.21	10
COMM domain-containing protein 6	Commd6	-0.49	-1.45	-0.96	2
COMM domain-containing protein 2	Commd2	-0.16	-1.42	-1.26	2
Coiled-coil domain-containing protein 22	Ccdc22	-0.40	-1.40	-1.00	11
Maspardin	Spg21	-1.19	-1.37	-0.17	8
Complement factor B	Cfb	-0.46	-1.33	-0.87	12
Transmembrane protein 176B	Tmem176b	-0.29	-1.30	-1.01	5
Vacuolar protein sorting-associated protein 29	Vps29	-0.42	-1.29	-0.86	8
Apolipoprotein F	Apof	-0.54	-1.28	-0.74	2
Gamma-secretase-activating protein	Gsap	-0.05	-1.28	-1.24	2
Vesicle-trafficking protein SEC22b	Sec22b	-0.68	-1.21	-0.53	4
Haptoglobin	Hp	-0.46	-1.21	-0.75	14
Apolipoprotein A-I	Apoa1	-0.71	-1.17	-0.47	10

Pigment epithelium-derived factor	Serpinf1	-0.18	-1.17	-1.00	5
Integral membrane protein 2B	Itm2b	-0.22	-1.16	-0.93	8
Kelch-like protein 9	Klhl9	-0.79	-1.14	-0.34	3
Apolipoprotein C-III	Apoc3	-0.42	-1.14	-0.73	4
Hemopexin	Hpx	-0.89	-1.13	-0.24	15
Vacuolar protein sorting-associated protein 26B	Vps26b	-0.15	-1.13	-0.98	3
Apolipoprotein C-I	Apoc1	0.24	-1.13	-1.37	5
Fibulin-1	Fbln1	0.35	-1.12	-1.47	2
Protein AMBP	Ambp	-0.81	-1.11	-0.29	3
Tripartite motif-containing protein 14	Trim14	-0.28	-1.11	-0.84	9
Melanoregulin	Mreg	-0.28	-1.09	-0.80	2
Sodium-coupled neutral amino acid transporter 3	Slc38a3	-0.27	-1.09	-0.82	5
Synaptosomal-associated protein 29	Snap29	-1.07	-1.08	-0.01	5
ADP-ribosylation factor-like protein 5A	Arl5a	-0.46	-1.08	-0.62	2
Major urinary protein 3	Mup3	-0.27	-1.08	-0.81	3
Protein ERGIC-53	Lman1	-0.67	-1.07	-0.40	7
Kininogen-1	Kng1	-0.37	-1.07	-0.70	9
Protein transport protein Sec23A;Sec23B	Sec23a; Sec23b	-0.49	-1.06	-0.57	2
Beta-galactoside alpha-2,6-sialyltransferase 1	St6gal1	-0.13	-1.06	-0.93	15
Protein RUFY3	Rufy3	-0.94	-1.05	-0.11	10
Vesicular integral-membrane protein VIP36	Lman2	-0.63	-1.05	-0.42	6
Plasma kallikrein	Klkb1	-0.39	-1.05	-0.67	2
Alpha-1-acid glycoprotein 1	Orm1	-0.79	-1.04	-0.25	6
Alpha-1-antitrypsin 1-1;1-2;1-5;1-4	Serpina1a;Serpina1b;Serpina1e;Serpina1d	-0.68	-1.03	-0.36	7
Ribonuclease 4	Rnase4	-0.38	-1.03	-0.65	2
Proteoglycan 4	Prg4	-0.13	-1.03	-0.89	2
Hepatic triacylglycerol lipase	Lipc	0.10	-1.03	-1.14	4
Albumin	Alb	-0.72	-1.02	-0.30	30
Alpha-1-antitrypsin 1-1;1-4	Serpina1a;Serpina1d	-0.63	-1.02	-0.40	2
Extracellular serine/threonine protein kinase FAM20C	Fam20c	0.08	-1.02	-1.09	2
Sorting nexin-3	Snx3	-0.38	-1.00	-0.62	2
Insulin-like growth factor-binding protein 4	Igfbp4	-0.30	-0.99	-0.69	2
Syndecan-2	Sdc2	-0.04	-0.99	-0.96	3
Beta-1,4-glucuronyltransferase 1	B4gat1	-0.65	-0.98	-0.32	2
Follistatin-related protein 1	Fstl1	0.08	-0.98	-1.07	2
Casein kinase II subunit alpha	Csnk2a1	-0.63	-0.97	-0.34	3
Protein transport protein Sec23A	Sec23a	-0.44	-0.97	-0.53	15

Carboxypeptidase B2	Cpb2	-0.24	-0.97	-0.74	3
Chloride channel protein 2	Clcn2	-0.21	-0.97	-0.76	3
Vacuolar protein sorting-associated protein 8	Vps8	-0.10	-0.97	-0.88	4
Alpha-2-HS-glycoprotein	Ahsg	-0.38	-0.95	-0.58	5
Serum paraoxonase/arylesterase 1	Pon1	-0.23	-0.95	-0.71	5
Corticosteroid-binding globulin	Serpina6	0.17	-0.95	-1.13	2
Sulfhydryl oxidase 1	Qsox1	-0.36	-0.94	-0.58	8
Insulin-like growth factor-binding protein 7	Igfbp7	-0.26	-0.92	-0.66	3
Vitamin K-dependent protein C	Proc	-0.11	-0.92	-0.81	3
Sec1 family domain-containing protein 1	Scfd1	-0.19	-0.91	-0.72	3
Sorting nexin-27	Snx27	-0.13	-0.90	-0.76	8
Tsukushin	Tsku	-0.40	-0.89	-0.49	3
Protein transport protein Sec24A	Sec24a	-0.31	-0.89	-0.58	9
Protein PRRC1	Prrc1	-0.29	-0.89	-0.60	4
Inter-alpha-trypsin inhibitor heavy chain H3	Itih3	-0.63	-0.88	-0.24	14
Sorting nexin-17	Snx17	-0.17	-0.88	-0.71	3
Receptor-type tyrosine-protein phosphatase F	Ptprf	0.08	-0.88	-0.96	3
Vitamin D-binding protein	Gc	-0.48	-0.87	-0.39	14
Sodium/bile acid cotransporter 5	Slc10a5	-0.33	-0.87	-0.54	3
Syntaxin-5	Stx5	-0.33	-0.86	-0.53	5
Complement C4-B	C4b	-0.26	-0.86	-0.60	20
Complement factor H	Cfh	-0.09	-0.86	-0.77	19
Protein dopey-2	Dop1b	-0.29	-0.85	-0.56	3
Complement component C9	C9	-0.14	-0.85	-0.72	5
Complement C1r-A subcomponent	C1ra	0.11	-0.85	-0.96	4
Cytochrome P450 2C70	Cyp2c70	0.98	-0.85	-1.82	7
Serine protease inhibitor A3K	Serpina3k	-0.65	-0.84	-0.19	6
Transforming growth factor-beta receptor-associated protein 1	Tgfbrap1	-0.59	-0.84	-0.24	2
Apolipoprotein A-II	Apoa2	-0.46	-0.84	-0.38	3
Transmembrane 9 superfamily member 2	Tm9sf2	-0.41	-0.84	-0.43	10
Prothrombin	F2	-0.30	-0.84	-0.53	8
Asialoglycoprotein receptor 2	Asgr2	-0.38	-0.83	-0.45	3
Alpha-mannosidase 2	Man2a1	-0.30	-0.83	-0.54	22
Complement component C8 gamma chain	C8g	0.11	-0.83	-0.94	4
Probable C-mannosyltransferase DPY19L1	Dpy19l1	-0.20	-0.82	-0.63	2
Conserved oligomeric Golgi complex subunit 7	Cog7	-0.11	-0.82	-0.71	5
Serine protease inhibitor A3K;A3M	Serpina3k;Serpina3m	-0.71	-0.81	-0.10	2
Ras-related protein Rab-1A	Rab1A	-0.32	-0.81	-0.48	4

Afamin	Afm	-0.19	-0.80	-0.61	6
Armadillo-like helical domain-containing protein 3	Armh3	-0.41	-0.79	-0.38	6
Complement C2	C2	0.09	-0.79	-0.88	2
Complement C3	C3	-0.79	-0.78	0.01	53
Golgin subfamily A member 3	Golga3	0.13	-0.78	-0.91	7
Target of Myb protein 1	Tom1	-1.00	-0.77	0.23	2
Extracellular matrix protein 1	Ecm1	-0.03	-0.77	-0.74	2
Retinol dehydrogenase 10	Rdh10	0.07	-0.77	-0.84	2
Heparin cofactor 2	Serpind1	-0.32	-0.76	-0.43	3
Solute carrier family 35 member E1	Slc35e1	-0.30	-0.76	-0.46	2
Stimulated by retinoic acid gene 6 protein-like	Stra6l	-0.30	-0.76	-0.46	5
Transmembrane protease serine 6	Tmprss6	0.25	-0.75	-1.01	5
Major urinary protein 17;2	Mup17;Mup2	-0.51	-0.52	-0.52	10

Supplementary table 8.5: Upregulated non-lysosomal proteins upon 24 hours of starvation

List of the 162 upregulated non-lysosomal proteins identified after long-term starvation in the proteomic dataset. Shown are proteins with more than one unique peptide, p-value <0.05 and log_2 fold change ratios >0.75. In addition, the log_2 fold change ratios after 6 hours as well as the log_2 fold change ratios of the difference between 6 and 24 hours of starvation are also shown in the table (#: number of unique peptides, blue: starvation period of interest, green: proteasome complex subunits, orange: mitochondrial proteins, N/A: not available).

Protein name	**Gene name**	**Log_2FC (6h)**	**Log_2FC (24h)**	**Log_2FC (24-6h)**	**#**
Thioredoxin-dependent peroxide reductase, mitochondrial	Prdx3	0.50	2.81	2.31	13
Copine-3	Cpne3	1.86	2.65	0.78	4
Insulin-like growth factor-binding protein 1	Igfbp1	0.39	2.52	2.13	3
Superoxide dismutase [Cu-Zn]	Sod1	0.8	2.07	1.27	19
Annexin A4	Anxa4	1.45	1.83	0.38	8
Glutathione peroxidase 1	Gpx1	0.77	1.82	1.05	20
Na(+)/H(+) exchange regulatory cofactor NHE-RF2	Slc9a3r2	0.05	1.68	1.63	3
GTP cyclohydrolase 1	Gch1	0.60	1.60	1.00	2
Tyrosine aminotransferase (TAT)	Tat	0.88	1.54	0.66	3
Spectrin beta chain, non-erythrocytic 1	Sptbn1	0.54	1.52	0.98	16
Phosphoenolpyruvate carboxykinase, cytosolic	Pck1	0.87	1.51	0.64	8
Phenazine biosynthesis-like domain-containing protein 1	Pbld1	1.40	1.47	0.07	4
Proteasome subunit alpha type-2	Psma2	1.96	1.47	-0.49	2
Phenazine biosynthesis-like domain-containing protein 2	Pbld2	1.38	1.41	0.02	6
Prolyl endopeptidase	Prep	1.32	1.39	0.07	5

Adhesion G protein-coupled receptor F5	Adgrf5	-0.002	1.38	1.39	2
Amine oxidase [flavin-containing] B	Maob	0.66	1.36	0.70	11
Dysferlin (Dystrophy-associated fer-1-like protein)	Dysf	-0.15	1.34	1.49	4
Annexin A2	Anxa2	0.15	1.33	1.18	15
Proteasome subunit beta type-3	Psmb3	2.10	1.33	-0.77	4
Proteasome subunit beta type-6	Psmb6	1.94	1.33	-0.61	2
Cell adhesion molecule 3	Cadm3	0.11	1.32	1.21	2
Spectrin alpha chain, non-erythrocytic 1	Sptan1	0.41	1.32	0.91	27
Thioredoxin reductase 1, cytoplasmic	Txnrd1	1.48	1.32	-0.16	4
GMP reductase 2	Gmpr2	0.43	1.31	0.88	4
Ester hydrolase C11orf54 homolog	N/A	1.51	1.29	-0.22	7
NAD(P)H-hydrate epimerase	Naxe	1.75	1.28	-0.47	3
Steryl-sulfatase	Sts	0.44	1.27	0.83	5
Glutathione S-transferase P 1	Gstp1	1.35	1.26	-0.10	10
Proteasome subunit alpha type-5	Psma5	2.21	1.26	-0.95	4
Kynurenine 3-monooxygenase	Kmo	0.75	1.24	0.49	7
Proteasome subunit alpha type-1	Psma1	2.12	1.22	-0.90	5
Acylamino-acid-releasing enzyme	Apeh	1.92	1.21	-0.71	7
Proteasome subunit beta type-5	Psmb5	1.93	1.21	-0.72	4
Band 4,1-like protein 2	Epb41l2	0.11	1.20	1.09	4
Proteasome subunit alpha type-3	Psma3	2.04	1.20	-0.84	10
Selenium-binding protein 2; Selenium-binding protein 1	Selenbp 2;Selenb p1	0.92	1.19	0.27	20
Cell surface hyaluronidase	Cemip2	-0.14	1.17	1.31	3
Protein S100-A10 (Calpactin I light chain)	S100a10	-0.36	1.17	1.53	3
D-dopachrome decarboxylase	Ddt	2.01	1.16	-0.86	4
Annexin A11	Anxa11	0.65	1.11	0.47	6
Proteasome subunit alpha type-4	Psma4	1.88	1.11	-0.77	4
Glutaredoxin-1	Glrx	1.52	1.09	-0.43	3
Hypoxanthine-guanine phosphoribosyltransferase	Hprt1	1.45	1.08	-0.38	3
Mitochondrial pyruvate carrier 2	Mpc2	0.33	1.08	0.75	2
Filamin-A	Flna	0.44	1.07	0.63	13
Alpha-aminoadipic semialdehyde dehydrogenase	Aldh7a1	1.55	1.06	-0.48	12
7-alpha-hydroxycholest-4-en-3-one 12-alpha-hydroxylase	Cyp8b1	0.15	1.05	0.90	2
Proteasome subunit alpha type-7	Psma7	1.81	1.05	-0.77	3
Aldehyde oxidase 1	Aox1	1.70	1.04	-0.66	6
24-hydroxycholesterol 7-alpha-hydroxylase	Cyp39a1	0.47	1.04	0.57	2
Mitochondrial glutamate carrier 1	Slc25a22	-0.04	1.04	1.08	3
Aspartate aminotransferase	Got1	1.66	1.03	-0.63	6
Transmembrane glycoprotein NMB	Gpnmb	-0.19	1.03	1.23	3

Inosine-5'-monophosphate dehydrogenase 2	Impdh2	1.30	1.03	-0.27	2
Amine oxidase [flavin-containing] A	Maoa	0.39	1.02	0.63	4
Aldehyde oxidase 3	Aox3	1.90	1.01	-0.89	14
Ferrochelatase, mitochondrial	Fech	0.39	1.00	0.62	5
OCIA domain-containing protein 2	Ociad2	-0.07	1.00	1.07	2
Sorbitol dehydrogenase	Sord	1.95	1.00	-0.95	10
AFG3-like protein 2	Afg3l2	0.28	0.99	0.71	2
Cytochrome c oxidase subunit 5B, mitochondrial	Cox5b	-0.26	0.99	1.25	4
Phenazine biosynthesis-like domain-containing protein 1;2	Pbld1;Pbld2	0.69	0.99	0.31	2
Platelet endothelial cell adhesion molecule	Pecam1	-0.06	0.99	1.05	3
Glyceraldehyde-3-phosphate dehydrogenase	Gapdh	1.70	0.98	-0.72	9
Stabilin-2	Stab2	-0.24	0.98	1.22	3
Glutathione S-transferase Mu 2	Gstm2	1.44	0.97	-0.47	2
Trifunctional enzyme subunit alpha, mitochondrial	Hadha	0.16	0.97	0.81	10
NADH dehydrogenase [ubiquinone] 1 beta subcomplex subunit 5, mitochondrial	Ndufb5	-0.19	0.97	1.16	2
Proteasome subunit alpha type-6	Psma6	1.54	0.97	-0.57	4
Selenium-binding protein 2	Selenbp2	0.71	0.97	0.26	2
Tripeptidyl-peptidase 2	Tpp2	1.62	0.97	-0.65	3
Xanthine dehydrogenase/oxidase	Xdh	1.21	0.97	-0.24	11
Dihydrolipoyl dehydrogenase, mitochondrial	Dld	0.88	0.96	0.09	10
DnaJ homolog subfamily C member 11	Dnajc11	0.08	0.96	0.88	2
CDGSH iron-sulfur domain-containing protein 1	Cisd1	-0.11	0.95	1.06	2
Apoptosis-inducing factor 1, mitochondrial	Aifm1	0.25	0.94	0.68	8
Inositol monophosphatase 1	Impa1	1.47	0.94	-0.54	2
Integrin alpha-9	Itga9	-0.39	0.94	1.33	2
55 kDa erythrocyte membrane protein	Mpp1	-0.18	0.94	1.13	3
NADH dehydrogenase [ubiquinone] 1 alpha subcomplex subunit 8	Ndufa8	-0.004	0.94	0.94	3
Voltage-dependent anion-selective channel protein 2	Vdac2	0.10	0.94	0.84	8
N-acyl-aromatic-L-amino acid amidohydrolase	Acy3	1.95	0.93	-1.03	2
Glutathione hydrolase 5 proenzyme	Ggt5	-0.14	0.93	1.08	3
Isocitrate dehydrogenase [NADP], mitochondrial	Idh2	0.16	0.93	0.77	9

Alpha-1-antitrypsin 1-1;1-2;1-4	Serpina1a;Serpina1b;Serpina1d	-0.04	0.93	0.97	2
Very long-chain specific acyl-CoA dehydrogenase, mitochondrial	Acadvl	0.19	0.92	0.73	18
NADH dehydrogenase [ubiquinone] iron-sulfur protein 4, mitochondrial	Ndufs4	0.22	0.92	0.71	3
Peroxiredoxin-4	Prdx4	1.62	0.92	-0.70	3
Sideroflexin-5	Sfxn5	0.26	0.92	0.66	2
Mitochondrial 2-oxodicarboxylate carrier	Slc25a21	0.29	0.92	0.63	2
ADP/ATP translocase 1;2	Slc25a4;Slc25a5	0.33	0.92	0.59	6
Acyl-coenzyme A thioesterase 13	Acot13	0.64	0.91	0.28	2
Cholinesterase	Bche	1.03	0.91	-0.11	3
FERM, ARHGEF and pleckstrin domain-containing protein 2	Farp2	-0.32	0.91	1.23	2
NADH dehydrogenase [ubiquinone] iron-sulfur protein 3, mitochondrial	Ndufs3	0.16	0.91	0.75	3
Programmed cell death protein 6	Pdcd6	0.27	0.91	0.64	2
Proteasome subunit beta type-7	Psmb7	1.68	0.91	-0.77	2
Cytochrome b-c1 complex subunit 9	Uqcr10	-0.34	0.91	1.25	2
Plasma membrane calcium-transporting ATPase 4; Plasma membrane calcium-transporting ATPase 1	Atp2b4;Atp2b1	-0.07	0.90	0.97	2
Glutathione reductase, mitochondrial	Gsr	1.49	0.90	-0.59	5
Integrin alpha-1	Itga1	-0.16	0.90	1.06	11
Major urinary protein 20	Mup20	1.08	0.90	-0.18	4
NADH dehydrogenase [ubiquinone] 1 alpha subcomplex subunit 5	Ndufa5	0.44	0.90	0.47	4
NADH dehydrogenase [ubiquinone] 1 beta subcomplex subunit 7	Ndufb7	-0.16	0.90	1.06	2
Mitochondrial carnitine/acylcarnitine carrier protein	Slc25a20	0.10	0.90	0.80	6
Trifunctional enzyme subunit beta, mitochondrial	Hadhb	0.31	0.89	0.58	8
Pyruvate dehydrogenase E1 component subunit alpha, somatic form, mitochondrial	Pdha1	0.54	0.89	0.35	2
Mitochondrial 2-oxoglutarate	Slc25a11	0.44	0.89	0.45	2
ADP/ATP translocase 4;1;2	Slc25a31;Slc25a4;Slc25a5	0.29	0.89	0.61	2
Tricarboxylate transport protein, mitochondrial	Slc25a1	0.08	0.88	0.80	2
Bleomycin hydrolase	Blmh	1.34	0.87	-0.47	6
NADH dehydrogenase [ubiquinone] 1 beta subcomplex subunit 11, mitochondrial	Ndufb11	-0.18	0.87	1.06	2

NADH dehydrogenase [ubiquinone] flavoprotein 1, mitochondrial	Ndufv1	0.35	0.87	0.52	6
Sulfite oxidase, mitochondrial	Suox	0.34	0.87	0.53	3
Aldo-keto reductase family 1 member D1	Akr1d1	1.73	0.86	-0.87	4
NADH dehydrogenase [ubiquinone] 1 alpha subcomplex subunit 10, mitochondrial	Ndufa10	0.13	0.86	0.73	3
NADH dehydrogenase [ubiquinone] 1 alpha subcomplex subunit 9, mitochondrial	Ndufa9	0.01	0.86	0.85	3
NADH dehydrogenase [ubiquinone] 1 beta subcomplex subunit 4	Ndufb4	-0.11	0.86	0.96	2
Mitochondrial ornithine transporter 1	Slc25a15	0.26	0.86	0.60	2
Sushi domain-containing protein 2	Susd2	-0.12	0.86	0.98	2
Catenin alpha-1; Catenin alpha-2	Ctnna1; Ctnna2	0.01	0.85	0.83	3
Epoxide hydrolase 1	Ephx1	1.21	0.85	-0.36	11
Unconventional myosin-Id	Myo1d	-0.01	0.85	0.86	4
Glycogen phosphorylase, liver form	Pygl	1.64	0.85	-0.79	11
Regucalcin	Rgn	1.20	0.85	-0.35	6
Sepiapterin reductase	Spr	1.06	0.85	-0.20	3
Voltage-dependent anion-selective channel protein 1	Vdac1	0.01	0.85	0.85	7
ATP synthase subunit gamma, mitochondrial	Atp5f1c	0.05	0.84	0.79	5
Integrin beta-3	Itgb3	0.04	0.84	0.80	5
2-iminobutanoate/2-iminopropanoate deaminase	Rida	1.06	0.84	-0.23	8
ATP synthase F(0) complex subunit B1, mitochondrial	Atp5pb	0.04	0.83	0.79	4
Carnitine O-octanoyltransferase	Crot	1.47	0.83	-0.64	3
Malate dehydrogenase, mitochondrial	Mdh2	0.76	0.83	0.08	7
Radixin; Moesin	Rdx;Msn	-0.24	0.83	1.06	7
Heat shock protein beta-1	Hspb1	0.56	0.82	0.26	2
Proteasome subunit beta type-1	Psmb1	1.67	0.82	-0.85	2
Regulator of microtubule dynamics protein 1	Rmdn1	0.25	0.82	0.56	5
Sideroflexin-2	Sfxn2	0.15	0.82	0.68	2
ATP synthase subunit beta, mitochondrial	Atp5f1b	0.06	0.81	0.75	12
Cytochrome c oxidase assembly protein COX15 homolog	Cox15	0.14	0.81	0.67	2
Dynamin-like 120 kDa protein, mitochondrial	Opa1	-0.01	0.81	0.82	8
Calcium-binding mitochondrial carrier protein Aralar2	Slc25a13	0.10	0.81	0.71	14
Urocanate hydratase (Urocanase)	Uroc1	1.42	0.81	-0.61	4
Annexin A5	Anxa5	0.73	0.80	0.07	9
Citrate synthase, mitochondrial	Cs	0.36	0.80	0.44	3

Glycerol-3-phosphate dehydrogenase, mitochondrial	Gpd2	0.12	0.80	0.68	5
Myosin light polypeptide 6	Myl6	0.13	0.80	0.67	3
Carnitine O-palmitoyltransferase 2, mitochondrial	Cpt2	-0.07	0.79	0.86	11
Cytochrome c, somatic	Cycs	0.36	0.79	0.43	3
Neuroplastin (Stromal cell-derived receptor 1)	Nptn	0.07	0.79	0.72	3
Aldo-keto reductase family 1 member C13	Akr1c13	0.89	0.78	-0.11	3
Plasma membrane calcium-transporting ATPase 1	Atp2b1	-0.10	0.78	0.87	2
Prohibitin (B-cell receptor-associated protein 32)	Phb	0.24	0.78	0.54	10
Retinol dehydrogenase 16	Rdh16	1.68	0.78	-0.91	2
Cytochrome b-c1 complex subunit 2	Uqcrc2	0.34	0.78	0.43	7
Vascular cell adhesion protein 1	Vcam1	-0.37	0.78	1.16	4
Voltage-dependent anion-selective channel protein 3	Vdac3	0.05	0.78	0.73	8
Isoleucine--tRNA ligase, cytoplasmic	Iars	1.02	0.77	-0.25	2
Myosin-9	Myh9	0.31	0.77	0.46	23
Acyl carrier protein, mitochondrial	Ndufab1	-0.21	0.75	0.96	3
Vinculin	Vcl	0.38	0.75	0.38	3

Supplementary table 8.6: Overlapping upregulated non-lysosomal proteins after 6 and 24 hours of starvation

List of the 51 overlapping non-lysosomal upregulated proteins identified after short- and long term starvation in the proteomic dataset. Shown are proteins with more than one unique peptide, p-value <0.05 and log_2 fold change ratios >0.75. In addition, the log_2 fold change ratios of the difference between 6 and 24 hours of starvation are also shown in the table (#: number of unique peptides, N/A: not available).

Protein name	Gene name	Log_2FC (6h)	Log_2FC (24h)	Log_2FC (24-6h)	#
Proteasome subunit alpha type-2	Psma2	1.96	1.47	-0.49	2
Phenazine biosynthesis-like domain-containing protein 1	Pbld1	1.40	1.47	0.07	4
Phenazine biosynthesis-like domain-containing protein 2	Pbld2	1.38	1.41	0.02	6
Prolyl endopeptidase	Prep	1.32	1.39	0.07	5
Proteasome subunit beta type-3	Psmb3	2.10	1.33	-0.77	4
Proteasome subunit beta type-6	Psmb6	1.94	1.33	-0.61	2
Thioredoxin reductase 1, cytoplasmic	Txnrd1	1.48	1.32	-0.16	4
Ester hydrolase C11orf54 homolog	N/A	1.51	1.29	-0.22	7
NAD(P)H-hydrate epimerase	Naxe	1.75	1.28	-0.47	3
Proteasome subunit alpha type-5	Psma5	2.21	1.26	-0.95	4
Glutathione S-transferase P 1	Gstp1	1.35	1.26	-0.10	10
Proteasome subunit alpha type-1	Psma1	2.12	1.22	-0.90	5
Proteasome subunit beta type-5	Psmb5	1.93	1.21	-0.72	4
Acylamino-acid-releasing enzyme	Apeh	1.92	1.21	-0.71	7
Proteasome subunit alpha type-3	Psma3	2.04	1.20	-0.84	10

Selenium-binding protein 2; Selenium-binding protein 1	Selenbp2; Selenbp1	0.92	1.19	0.27	20
D-dopachrome decarboxylase	Ddt	2.01	1.16	-0.86	4
Proteasome subunit alpha type-4	Psma4	1.88	1.11	-0.77	4
Glutaredoxin-1	Glrx	1.52	1.09	-0.43	3
Hypoxanthine-guanine phosphoribosyltransferase	Hprt1	1.45	1.08	-0.38	3
Alpha-aminoadipic semialdehyde dehydrogenase	Aldh7a1	1.55	1.06	-0.48	12
Proteasome subunit alpha type-7	Psma7	1.81	1.05	-0.77	3
Aldehyde oxidase 1	Aox1	1.70	1.04	-0.66	6
Aspartate aminotransferase	Got1	1.66	1.03	-0.63	6
Inosine-5'-monophosphate dehydrogenase 2	Impdh2	1.30	1.03	-0.27	2
Aldehyde oxidase 3	Aox3	1.90	1.01	-0.89	14
Sorbitol dehydrogenase	Sord	1.95	1.00	-0.95	10
Glyceraldehyde-3-phosphate dehydrogenase	Gapdh	1.70	0.98	-0.72	9
Tripeptidyl-peptidase 2	Tpp2	1.62	0.97	-0.65	3
Proteasome subunit alpha type-6	Psma6	1.54	0.97	-0.57	4
Glutathione S-transferase Mu 2	Gstm2	1.44	0.97	-0.47	2
Xanthine dehydrogenase/oxidase	Xdh	1.21	0.97	-0.24	11
Inositol monophosphatase 1	Impa1	1.47	0.94	-0.54	2
N-acyl-aromatic-L-amino acid amidohydrolase	Acy3	1.95	0.93	-1.03	2
Peroxiredoxin-4	Prdx4	1.62	0.92	-0.70	3
Proteasome subunit beta type-7	Psmb7	1.68	0.91	-0.77	2
Cholinesterase	Bche	1.03	0.91	-0.11	3
Glutathione reductase, mitochondrial	Gsr	1.49	0.90	-0.59	5
Bleomycin hydrolase	Blmh	1.34	0.87	-0.47	6
Aldo-keto reductase family 1 member D1	Akr1d1	1.73	0.86	-0.87	4
Glycogen phosphorylase, liver form	Pygl	1.64	0.85	-0.79	11
Epoxide hydrolase 1	Ephx1	1.21	0.85	-0.36	11
Regucalcin	Rgn	1.20	0.85	-0.35	6
Sepiapterin reductase	Spr	1.06	0.85	-0.20	3
2-iminobutanoate/2-iminopropanoate deaminase	Rida	1.06	0.84	-0.23	8
Carnitine O-octanoyltransferase	Crot	1.47	0.83	-0.64	3
Proteasome subunit beta type-1	Psmb1	1.67	0.82	-0.85	2
Urocanate hydratase (Urocanase)	Uroc1	1.42	0.81	-0.61	4
Retinol dehydrogenase 16	Rdh16	1.68	0.78	-0.91	2
Aldo-keto reductase family 1 member C13	Akr1c13	0.89	0.78	-0.11	3
Isoleucine--tRNA ligase, cytoplasmic	Iars	1.02	0.77	-0.25	2

9 List of Figures

10 List of Tables

11 List of Supplementary Tables

12 Acknowledgment

It is a pleasure to thank those who made this work possible. I would like to express my thankfulness to Prof. Dr. Volkmar Gieselmann for giving me the opportunity to work in his group and for being the first referee of my thesis. Furthermore, I especially thank him for his valuable support, advices and experiences which helped me a lot to improve my project.

I'm also grateful to Prof. Dr. Walter Witke for accepting to be the second referee, as well as Prof. Dr. Benjamin Odermatt and Prof. Dr. Pavel Kroupa for being the 'fachnahes' and the 'fachfremdes' member of the committee, respectively.

Special appreciation goes to Dr. Melanie Thelen for being always available for any arising questions, offering her assistance and guidance throughout the whole project. I thank her a lot for the fruitful discussions and valuable suggestions which positively contributed to my research.

Furthermore, I would like to express my gratitude to the past and present lab members as well as the whole team at the institute of Biochemistry and Molecular Biology for the pleasant working atmosphere and nice time we spent during the past years. I would like to deeply thank our technical assistants for sharing their experiences with me, especially Simone Mausbach who assisted me solving any problem I faced during my time working in the lab. Moreover, I would like to acknowledge the administrative assistants for their support and the cleaning workers for keeping our institute hygienic and tidy.

My full gratitude shall be expressed to every person who stood by my side and gave me strength and support over the years.

Finally, I owe my deepest gratefulness to my beloved father, mother and brother for their understanding and endless assistance throughout the duration of my research and writing the thesis. Thank you!

Edgar Kaade

13 Publications and Conference Presentations

Publications

- Singh, Jasjot; **Kaade, Edgar**; Muntel, Jan; Bruderer, Roland; Reiter, Lukas; Thelen, Melanie; Winter, Dominic (2020). Systematic Comparison of Strategies for the Enrichment of Lysosomes by Data Independent Acquisition. Journal of Proteome Research 19:371–381. Doi: 10.1021/acs.jproteome.9b00580

Oral Presentations

- Variable Nutrient Conditions and their Impact on the Lysosomal Proteome in Different Mouse Tissues. 5th Bonn International Graduate School (BIGS) Neuroscience Symposium. Aachen, Germany (2019)

Poster Presentations (Selected)

- **Kaade, Edgar**; Gieselmann, Volkmar; Thelen, Melanie. Investigation of the Lysosomal Proteome in Different Nutrient Conditions. 4th International Symposium on Protein Trafficking in Health and Disease. Hamburg, Germany (2017)
- **Kaade, Edgar**; Gieselmann, Volkmar; Thelen, Melanie. Investigation of the Lysosomal Proteome in Different Nutrient Conditions. 21st European Study Group for Lysosomal Diseases (ESGLD) Workshop. Lyon, France (2017)
- **Kaade, Edgar**; Mausbach, Simone; Gieselmann, Volkmar; Thelen, Melanie. Effect of Starvation on Lysosomal Protein Composition in Liver and *in vivo* mTORC1 Activity in Different Mouse Tissues. 22nd European Study Group for Lysosomal Diseases (ESGLD). Barcelona, Spain (2019)
- Mosen, Peter; **Kaade, Edgar**; Sakson, Roman; Ruppert, Thomas; Gieselmann, Volkmar; Winter, Dominic. Targeted Absolute Quantification of the Lysosomal Proteome using Stable Isotope Labeled Engineered Recombinant Standard Proteins and Mass Spectrometry. The 4th Gordon Research Conference on Lysosomal Diseases. Lucca, Italy (2017)
- Mosen, Peter; **Kaade, Edgar**; Sakson, Roman; Ruppert, Thomas; Gieselmann, Volkmar; Winter, Dominic. Absolute Quantification of Lysosomal Proteins by Mass Spectrometry. The 4th Gordon Research Conference on Lysosomal Diseases. Galveston, USA (2019)
- Mosen, Peter; Sakson, Roman; **Kaade, Edgar**; Ruppert, Thomas; Gieselmann, Volkmar; Winter, Dominic. QConCat-based Absolute Quantification of the Lysosomal Proteome by Multiple Reaction monitoring. 22nd International Mass Spectrometry Conference (IMSC). Florence, Italy (2018)
- Mosen, Peter; Sakson, Roman; **Kaade, Edgar**; Ruppert, Thomas; Gieselmann, Volkmar; Winter, Dominic. Absolute Quantification of the Lysosomal Proteome by Multiple Reaction Monitoring and QconCAT Protein Standards. 67th Conference on Mass Spectrometry and Allied Topics. Atlanta, USA (2019)
- Singh, Jasjot; Ponnaiyan, Srigayatri; Akter, Fatema; **Kaade, Edgar**; Winter, Dominic. Analysis of the Lysosomal Membrane Interactome via Cross-linking Mass-spectrometry. 67th Conference on Mass Spectrometry and Allied Topics. Atlanta, USA (2019)